Development of a tailings simulation model using System Dynamics

by

Xiaochuan Zheng

A thesis submitted in partial fulfillment of the requirements for the degree of

Master of Science

in

Geotechnical Engineering

Department of Civil and Environmental Engineering
University of Alberta

ABSTRACT

This thesis aims to demonstrate the feasibility of using System Dynamics (SD) techniques to develop a transparent, open-source and reproducible model capable of simulating long-term soil water dynamics in a tailings-cap system subject to upward flux from a consolidating tailings substrate. The developed model, which consists of a consolidation sub-model and an un-saturated flow sub-model, explores various feedback mechanisms in the self-weight consolidation process and unsaturated soil water movement under climatic influence. The tailings simulation model uses Causal Loop Diagramming (CLD) techniques to identify key feedback structures, promote system thinking and facilitate shared understanding of the inter-related behaviour between the reclamation cap and the tailings substrate.

The model is implemented in the GoldSim simulation environment. The consolidation sub-model uses an explicit finite difference method to calculate the void ratio at each time step. Through various validation cases, the consolidation sub-model demonstrates its capability in carrying out both deterministic and stochastic simulations. The un-saturated flow sub-model is based on a previously developed infiltration-drainage model. This research improves the original model by adding capabilities of handling dynamic boundary conditions and inter-layer overflow mechanisms. Additional validation cases are conducted to build confidence in the modified model.

The integrated model simulated a case study involving a 3 m thick coarse sand tailings (CST) cap on top of a 50 m thick thickened tailings (TT) deposit. Simulation results show that soil water dynamics in the CST cap is highly sensitive to the water release from the TT settlement. An increase in the initial solids contents of TT by 10% can delay the daylighting of the consolidation flux at the cap surface by one to two years. In order to prevent the daylighting of consolidation release water at the surface, the initial solids content of TT needs to be above 60%. The simulation also shows that the local behaviour of soil water storage in the CST cap is sensitive to changes in saturated hydraulic conductivity while the global behaviour is less sensitive to such changes.

Supplemental material related to this thesis is available at
https://era.library.ca/collections/7p88ck40x

Preface

The work in this thesis was completed by Tony Zheng. Part of Chapter 2 in this thesis has been published in the 2018 Tailings and Mine Waste Conference. Part of Chapter 3 in this thesis has been published in the 71st Canadian Geotechnical Conference in 2018. Co-authors provided editing comments only.

References:

Chapter 2:

Zheng,T. and Beier, N. (2018). System Dynamics Approach to Tailings Management Simulation. Tailings and Mine Waste Conference, Keystone, Colorado, USA, September 30 – October 2, 2018. pp 95-108.

Chapter 3:

Zheng,T. and Beier, N. (2018). Stochastic Simulation of Tailings Consolidation Process. 71st Canadian Geotechnical Conference, Edmonton, Alberta, September 23 – 26, 2018.

Acknowledgments

Table of Contents

List of Tables

List of Figures

List of Symbols and Acronyms

A, Af	Compressibility consolidation curve-fitting parameter
a, alph	van Genuchten fitting parameter
B, Bf	Compressibility consolidation curve-fitting parameter
C, Cf	Permeability consolidation curve-fitting parameter
D, Df	Permeability consolidation curve-fitting parameter
AE	Actual Evaporation Rate
AER	Alberta Energy Regulator
Beta-PERT	Beta Program Evaluation and Review Technique Distribution
CCDF	Complementary Cumulative Distribution Function
CDF	Cumulative Distribution Function
CFF	Cross Flow Filtration
CNRL	Canadian Natural Resources Limited
COF	Cyclone Overflow
COSIA	Canada Oil Sands Innovation Alliance
CPU	Central Processing Unit
CLD	Causal Loop Diagram
e	Void ratio defined as the volume of voids over the volume of solids
e_{fines}	Fines void ratio
e_0	Initial void ratio prior to consolidation
e_{0_1}, e_{0_0}	Fictitious void ratio for Layer 0 in the consolidation sub-model
$e_{0\_fictitious}$	User-input fictitious void ratio for the impermeable foundation
ETF	External Tailings Facility
f	Inter-layer transmission rate
FC	Fines Content
FFT	Fluid Fine Tailings
g	Gravitational acceleration at 9.81 m/s2
G_s	Specific gravity of solids
G_{coarse}	Specific gravity of coarse mineral grains
G_{fines}	Specific gravity of fines mineral grains
H_0	Static initial total height of the entire tailings deposit
h	Dynamic height of individual tailings layer
h_0	Static initial height of individual tailings layer
h_T	Dynamic total height of the consolidating tailings deposit
h_a	Relative humidity of the air above the soil surface
h_r	Relative humidity of the soil voids
i	Layer numbers ranging from 0 to 18
JPM	Jackpine Mine
K	Saturated-unsaturated hydraulic conductivity
Ks	Saturated hydraulic conductivity
m	van Genuchten fitting parameter; m=1-1/n
MFT	Mature Fine Tailings
MRE	Mean Relative Error
N	Discretization factor for the fictitious layer

n	van Genuchten fitting parameter
OSPW	Oil Sands Process-Affected Water
PAW	Process Affected Water
Ph	Soil suction head in positive values
PE	Potential Evaporation Rate
PV	Previous Value element in GoldSim
Q, q	Volumetric water content
Qs	Saturated volumetric water content
Qr	Residual volumetric water content
R	Universal gas constant at 8.314 J/mol.K
R^2	Coefficient of determination
RMSE	Root Mean Square Error
S	Soil water storage of the individual layer
St	Total soil water storage of the soil cover
Sat	Degree of saturation
Se	Normalized or effective degree of saturation
SC	Solids content by mass
SD	System Dynamics
SFD	Stock and Flow Diagram
SWCC	Soil Water Characteristic Curve
Δt	Time step
Thk	Individual layer thickness
TSF	Tailings Storage Facility
TMS	Tailings Management System
Ta	Mean air temperature above the soil surface
TT	Thickened tailings
UDF	User Defined Function
Δu	Excess pore pressure
w	Water content as % (mass of water divided by mass of solids (sand, fines and bitumen)
Wv	Molecular weight of water at 0.018 kg/mol
Δz	Layer thickness in material coordinates
ε	Strain
γ_b	Buoyant unit weight
γ_s	Unit weight of solids
γ_w	Unit weight of water
ρ_w	Water density
ρ_d	Dry density of soil
ρ_s	Solids density
σ'_v, σ'	Vertical effective stress
ψ	Total matric suction expressed in metres taken as positive

1 INTRODUCTION

1.1 BACKGROUND

In Alberta, tailings storage facilities at several oil sands mines are due for closure in the next decade. Closure strategies can be classified into wet and dry reclamation. To support construction equipment and future vegetation, closure activities after the end of tailings deposition typically involve the placement of an intermediate capping material on top of the tailings deposit. Some oil sands operators have proposed using coarse sand tailings (CST) as the intermediate capping material between the thickened tailings (TT) deposit and the vegetation cover in their regulatory applications (Imperial 2016, Shell 2016 and Suncor 2017). However, there has been no successful precedents in using CST to cap deep fines-dominated deposits such as TT.

Due to the absence of compaction by construction equipment and its greater overall thickness, tailings deposit may generate more consolidation-induced process-affected water (PAW) than overburden waste. Survival of future vegetation cover on top of capping material is highly sensitive to the salinity distribution of the released PAW (Cilia 2018). Most studies of the reclamation cover system in the oil sands have focused on the water and contaminant transport between overburden waste and capping material. Few studies have focused on reclamation scenarios that consist of tailings deposits. Therefore, the effect of upward migration of PAW on the long-term soil water storage of the capping material needs to be further investigated.

Numerical models of mass transport often relied on commercial software that use black-box, proprietary finite element and finite difference codes. These numerical models output flux quantities and pressure head distributions by solving complex, coupled differential equations. Significant effort has been directed toward improving the accuracy of numerical prediction. Little effort has been directed toward improving the communication and understanding of the water transport process in the reclamation landscape. Therefore, one of the objectives of this thesis is to develop a transparent, physically-based simulation tool sophisticated enough to capture key physical processes yet simple enough to foster shared understandings between technical and non-technical stakeholders.

One of the key challenges at the beginning is to select an appropriate modelling methodology capable of explicitly modelling key physical processes without the need to simultaneously solve

differential equations. In the end, a lumped dynamic modeling method called System Dynamics (SD) was chosen SD uses causal loop diagrams (CLD) as the transitional tool between the qualitative and quantitative models. The process of drawing CLD, which requires no specialized software or tools, helps modelers and users to visually identify key feedback mechanisms within the system. CLD can also be used as a visual check to maintain the right level of complexity in relations to the model objectives.

1.2 OBJECTIVES

In light of the above, the overall objectives of the thesis are three-fold as follows:

- Use the SD method to develop a qualitative model of soil water movement within the tailings reclamation cover; specifically, transfer learnings from other disciplines and develop Causal Loop Diagrams (CLD).
- Transform the CLD-based qualitative model developed above into a transparent quantitative model intended for shared understanding and inter-disciplinary collaboration; manage the model's complexity through iterative revisions of CLDs, the Bull's Eye diagram and visual design of model organization and user interface.
- Use the quantitative model to simulate a case study involving advective water transport between a CST capping layer and a TT deposit undergoing consolidation; gain insights on the long-term dynamics of soil water storage within the CST cap under various boundary conditions and external influences.

1.3 OUTLINE OF THESIS

This thesis consists of six chapters. The research project was developed in sequence of these chapters. The introduction below describes the motivation behind the development of each chapter.

Chapter 2 introduces SD within for the scope of the thesis. It starts with the history of development and its applications outside tailings management and then uses qualitative models and CLDs to demonstrate how the SD methodology can be applied in tailings management and geotechnical engineering in general.

An earlier tailings management simulation model called TMSim (Beier 2015) uses output from a black-box third party software to calculate consolidation of tailings deposits. Instead, Chapter 3

developed a transparent consolidation sub-model without the need to use external tools and software. Calibration effort is also kept to a minimum level. The conceptualization of the consolidation sub-model adopted a bottom-up approach. Numerical solution to the governing equation was formulated first. CLDs and feedback loops were were constructed to describe and communicate the formulated numerical solution.

Chapter 4 replicated a previously developed unsaturated flow model by Huang et al (2011) with several modifications in the handling of boundary conditions, additional validation cases, improved user interfaces and enhanced visualization design to emphasize feedback structures.

Chapter 5 combined sub-models developed in Chapter 3 and Chapter 4 into a single model. The combined model simulated a case study involving advective water transport between a 3 m thick coarse sand tailings (CST) cap and a 50 m high thickened tailings (TT) deposit under climatic conditions in Fort McMurray, Alberta.

Chapter 6 provides a summary of conclusions and recommendations for future work.

2 TAILINGS MANAGEMENT: A SYSTEM DYNAMICS APPROACH

2.1 INTRODUCTION

Tailings Management System (TMS) consists of inter-related sub-systems across disciplinary and organizational boundaries. Conventional predictive models simulate physical processes in each discipline with great details. In contrast, simulation based on System Dynamics (SD) focuses on overall behavior of the system over time rather than the typical mechanistic predictions seen in conventional numerical models. SD technique has been widely used to simulate problems in business, ecology, public health, and environmental studies but rarelypracticed in tailings management.

SD is well suited for modeling integrated social-economic-environmental systems. Whilte social and economic factors are integral parts of tailings management (McKenna, 2002), this thesis limits the scope to the environmental system and focuses on physical-based problems regarding soil water dynamics between the atmosphere and the tailings cap system. Additionally, the thesis attempts to demonstrate the transparency and flexibility of SD models in the context of tailings management. The thesis builds on the foundation of a previously developed dynamic simulation tool, Tailings Management Simulator (TMSim) to demonstrate how SD can be used as a Advantages and limitations of SD-based modeling approach will also be discussed.

The descriptions of SD in this and the following chapters are sufficient for the development of the consolidation and unsaturated flow sub-models. These descriptions serve as a mere introduction to SD. For a more comprehensive coverage, abundant literature is available from social sciences and environmental engineering. To highlight a few examples, Sterman (2004) and Maani and Cavana (2007) provided a theoretical coverage of SD with a heavy emphasis on applications in business and social sciences. Ford (2010) adopted a more practical approach by demonstrating the application of SD in environmental and ecological modelling. Meadows (2008) focused on system thinking instead at a more general and philosophical level.

2.2 SYSTEM DYNAMICS MODELING APPROACH

2.2.1 Introduction

This chapter provides an overview of the SD philosophy and how it can be applied in the tailings management context. The SD modelling process consists of two major parts: qualitative stage and quantitative stage. This chapter will introduce the qualitative stage of SD modeling while serving as a companion chapter to the modeling of soil water dynamics between reclamation covers and underlying tailings substrate in Chapter 4 and Chapter 5.

2.2.2 History of System Dynamics

Originated from the development of feedback control mechanisms for military radars and gun mounts during World War II (Forrester, 1994), System Dynamics is a modelling technique that deals with complex inter-relationships between components within a system or multiple systems. Jay Forrester first applied the methodology in the mid-1950s to the field of business and operations research at the newly created Sloan School of Management at MIT. The first application of SD was a dynamic model, created in late 1950s, to explain poor business performance at General Electric where the employment instability was later discovered to come from internal structures rather than external forces such as economic cycles. In the 1970s, the use of SD gradually shifted from business modelling to urban planning due to the proliferation of low-cost housing initiatives. Over the years, the application of SD has found its way into a variety of fields such as public health, ecology and engineering (Lane and Sterman, 2017). SD has become a full-fledged academic field that an association named System Dynamics Society and its affiliated academic journal, System Dynamics Review, are solely dedicated to its advancement and promotion.

2.2.3 System Dynamics in Tailings Management

Despite its wide applications in business and social sciences, SD has not been widely used in tailings management and mine closure planning. Based on a preliminary keyword review of the bibliography database in System Dynamics Journal, Table 2-1 showed that only 12% of the total articles in the bibliography database from System Dynamics Society is related to technical fields most relevant to the mining industry. A preliminary keyword search of "System Dynamics Tailings" in Scorpus, a online search engine for peer reviewed literature, has also yielded very few papers directly related to tailings management. Examples of SD models in water resource

management include Li and Simonovic (2002) who modeled hydrological processes in groundwater flow, Elshorbagy and Ormsbee (2006) who proposed using object-oriented SD to model surface water quality, Davies and Simonovic (2011) who studied social-economic and environmental aspects of water resource management and more recently, King et al (2017) who adopted SD in the evaluation of hydro-power dam safety from a system perspective. Examples directly related to oil sands tailings management include Elshorbagy et al (2005), Julta (2006) and Huang et al (2011a and 2011b) who used SD to simulate advective flow in un-saturated soil cover. The mining industry at large and sub-fields like tailings and closure management have benefited very little from this modelling method.

The lack of case studies in SD-based tailings management simulation can be attributed to the unique gap between conventional numerical models and our mental models. Conventional numerical models are based on extensive experimental and empirical evidence. In contrast, mental models are built upon heuristics and intuition. In Figure 2-1, different types of models are located inside an inverted triangle formed by three axes of scale. The diagram puts the traditional numerical models at the bottom since they provide the foundation on which other types of models are built. At the top of the inverted triangle are the mental and conceptual models, which strive for simplicity and maximum degree of horizontal integration. In the middle of the graph, the intermediate models strive for balance between breadth and comprehensiveness.

Ford (2010) argued that SD models are the most powerful when designed to fit in the conceptual model category near the top of the inverted triangle in Figure 2-1. For broad topics like climate change and evolutionary ecology, maximum horizontal integration across different disciplines is not only productive but sometimes necessary. However, over-simplification and absence of key physical processes in a model will inevitably pose challenges during calibration and validation process. Furthermore, endogenous variables in climate systems such as precipitation and daily temperatures become exogenous in a tailings management context due to the much smaller system boundary. Therefore, SD-based models in tailings management should aim for the middle ground between conceptual models and traditional numerical models.

Table 2-1 Keyword search of System Dynamics Review bibliography database.

Keyword	Number of Articles	Proportion*
Mining	88	<1%
Water	972	8%
Construction	500	4%
Dam	17	<1%

*Based on a total number of 12,412 articles
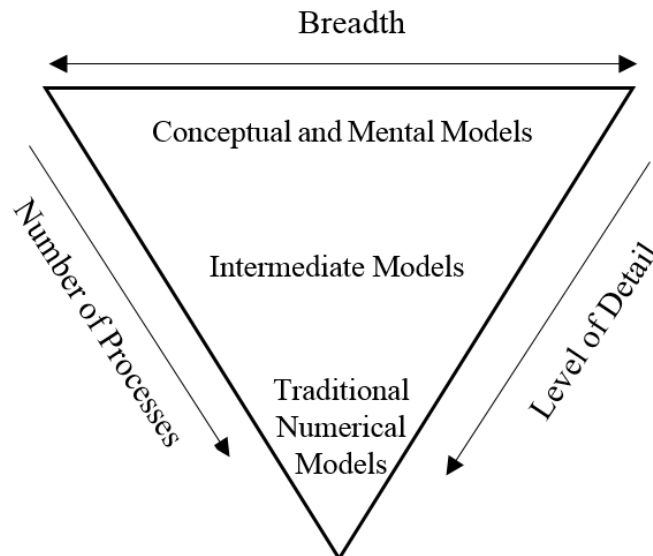
Figure 2-1 Hierarchy of models

2.3 SYSTEM DYNAMICS MODELLING PROCESS

2.3.1 Qualitative Stage

Stocks and flows, delays, and feedback structures are the four basic building blocks of any SD-based models. Stocks are state variables that track accumulation of quantities at any given time. Flows are variables that add or subtract quantities from stock variables per unit of time step. Delays

are variables that describe the time lagging of output behind input. Feedback structures are closed-form relationships that either reinforce or balance each other. Auxiliary variables in the form of mathematical equations are often needed to explain flow variables.

According to Ford (2010), the qualitative stage of model development involves the following steps: i) familiarization with the system and background studies; ii) construction of specific questions that need to be answered by the model; iii) identification of variables, stocks and flows; iv) formulation of causal loop diagrams; and v) iterative revision of causal loop diagrams through learning, debate and discussion. It should be noted that, though anything qualitative tends to be perceived as being conceptual, the qualitative stage in SD modelling is a rigorous process with its own set of syntax, clear-defined rules and best practices. During this stage of model development, general patterns are more important than exact numbers (Ford 2010).

Feedback structures are represented by causal loop diagrams which are drawn by the Vensim software in this thesis. Figure 2-2 is a popular case study used in many SD literature to explain the basics of causal loop diagrams. Here, population is a stock element. Variables are connected by one-way arrows which represent causal relationships. Either positive (+) or negative (-) polarity is assigned to the arrowhead based on how the dependent variable changes in response to changes in the independent variables. Positive causal link means that the variables change in the same direction. All else being equal, a higher birth rate will increase population which in turn drives up the birth rate. Negative causal link means that variables change in the opposite direction. Likewise, in Figure 2-3, a higher death rate will decrease population which in turn reduces death rate. It should be noted that, as a good practice, polarity is assigned by testing the effect of positive polarity on variables at the arrowhead. If the number of negative polarities in a loop is odd, the feedback loop is classified as negative or balancing. If the number of negative polarities is even, the feedback loop is identified as positive or reinforcing. Negative feedback loop balances the system while positive feedback loop gives rise to run-away behavior or amplified system response to any changes in variables (Richardson 1997).

In Figure 2-2, the parallel lines at the top and bottom of the loop denote the concept of delay. There are two types of delay: material delay and information delay. The reason behind the material delay is that the effect of increasing population will not be reflected in the birth rate since family formation and pregnancy take time. The reason behind the information delay is that even though

the rising birth rate is instantaneously reflected in the population, modelers will not be aware of this information due to time interval between population censuses. The same rationale can also be applied to the delay effect shown in Figure 2-3.

"Fractional Growth" and "Fractional Decay" in Figure 2-2 and Figure 2-3 are called converters or auxiliary variables whose primary function is to explain flow variables. They are also called exogenous variables, which are any variables not part of a feedback loop or outside the system. Similarly, any variables part of a feedback loop or inside the system can be classified as endogenous variables. In this case, "Birth Rate" and "Population" are considered endogenous. It is the endogenous variables that give rise to interesting behaviors in the system (Richardson 2011).

Note that typically the box symbol of stock elements is visible in the Stock Flow Diagram (SFD) but absent in the CLD (Sterman 2004). However, Ford (2010) suggested identifying stock elements as the starting point to create CLDs. Ford (2010) also prefers the plus and minus sign for labelling reinforcing and balancing feedback loops due to their neutrality and wide coverage of different contexts. To facilitate the transition from CLD to SFD, all the CLDs in this thesis will have stock elements explicitly labelled by a rectangular box icon; all the feedback loops in the thesis will be labelled as either positive or negative feedback.
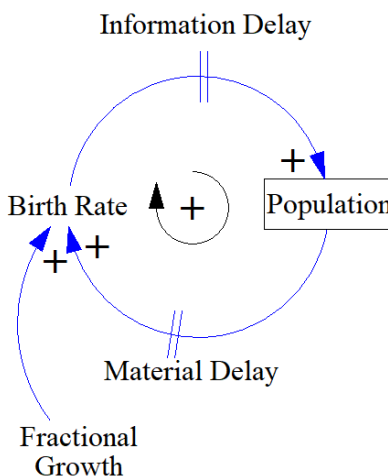
Figure 2-2. Causal loop diagram for population growth
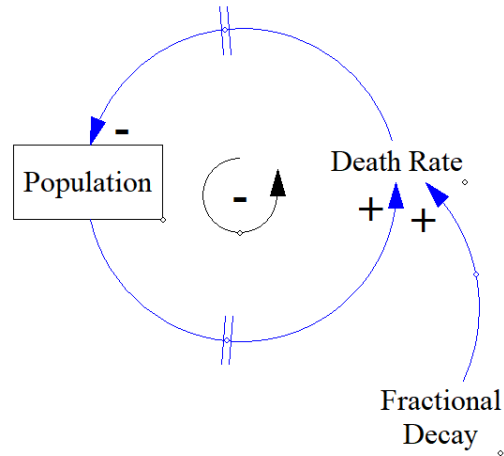
Figure 2-3 Causal loop diagram for population decay

The CLD diagramming method can be applied to problems in tailings mangement. Geomorphological process is an important consideration in the landform design of tailings storage facilities during closure (Slingerland et al. 2018). Feedback relationships are also evident in many geomorphological processes (Chorley et al. 1984). For example, the fluvial erosion process is dominated by negative feedback mechanisms in the short term (King 1970). The CLD in Figure 2-4, based on similar diagrams by King (1970), describes those negative feedback mechanisms. The following narrative can be derived from the CLD. Greater stream discharge increases stream velocity, assuming the geometry of the channel is constant. Greater stream velocity accelerates erosion, which in turn enlarges the cross section of the channel, as represented by depth and breadth. The geometry of the channel closes the feedback loop by regulating the stream velocity.

Feedback mechanisms and CLD can also describe one-dimensional consolidation behavior of foundation soil under a rising tailings storage facility. Excess pore pressure is modelled as a stock element with construction rate as inflow and dissipation rate as outflow (Figure 2-5). Assuming that Darcy's Law is valid and that the principle stress in the foundation soil can be approximated by the vertical stress, an increase in construction rate will trigger a series of chain reactions and lead to a negative feedback structure, which makes sense since the consolidation process brings the system back into balance. The counter-clockwise loop symbol is also given a name to communicate the major theme of the feedback structure. Alternatively, a numeric value can be assigned to keep track of multiple feedback loops.

"Construction Rate", "Hydrostatic Pore Pressure" and "Existing Total Stress" are all considered exogenous to the system or outside of any feedback structures. Exogenous variables can become endogenous and vice versa depending on how the boundary of the system is defined. For example, construction rate becomes endogenous when additional feedback loops such as performance monitoring measures are added to expand the system boundary (Figure 2-6). However, the modeler needs to critically assess whether such expansion of system boundary is warranted in light of modelling objectives and practical limitations (i.e. budget and schedule). As part of the participatory modelling process, modelers, users, and stakeholders often take active roles to define the appropriate boundary of the model, and consequently the number and extent of feedback structures (Ford 2010).

The CLD in Figure 2-5 may not contain enough information for quantitative modelling since its primary function is mental mapping at a conceptual level. Spatial arrangement, level of confining stress, principle stress rotation, and in-situ soil properties are also not considered. However, the systematic process of creating the CLD diagram builds a robust foundation on which further revision of the model can be communicated across disciplinary boundaries (Ford 2010).
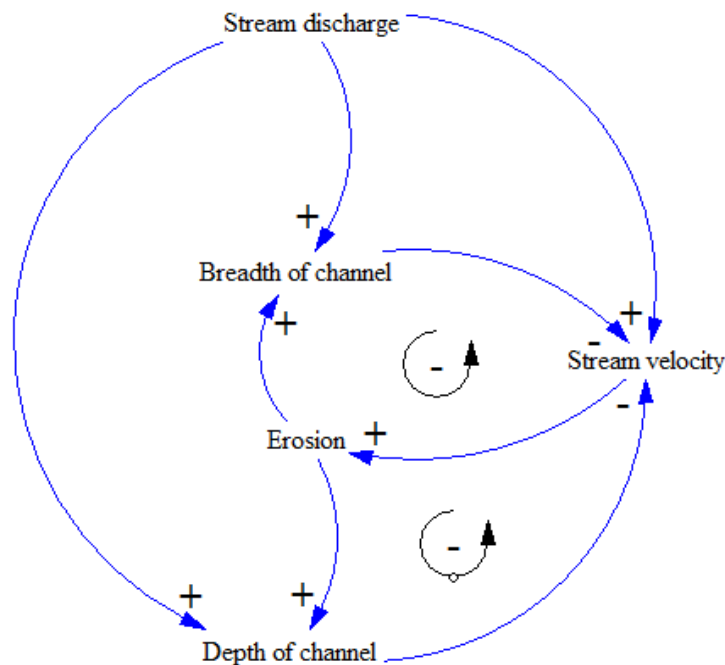
Figure 2-4. CLD description of the fluvial erosion process
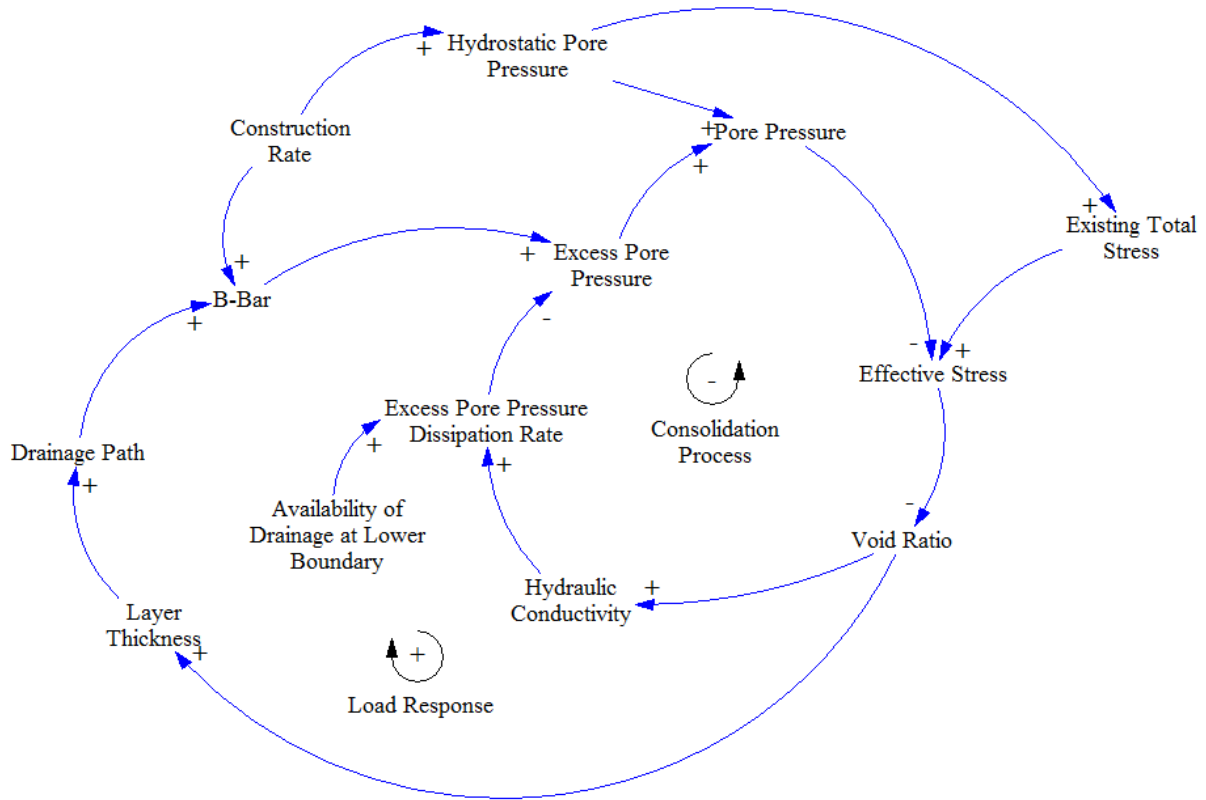
Figure 2-5 Causal loop diagram for consolidation of foundation layer under fully saturated condition (Zheng and Beier 2018)
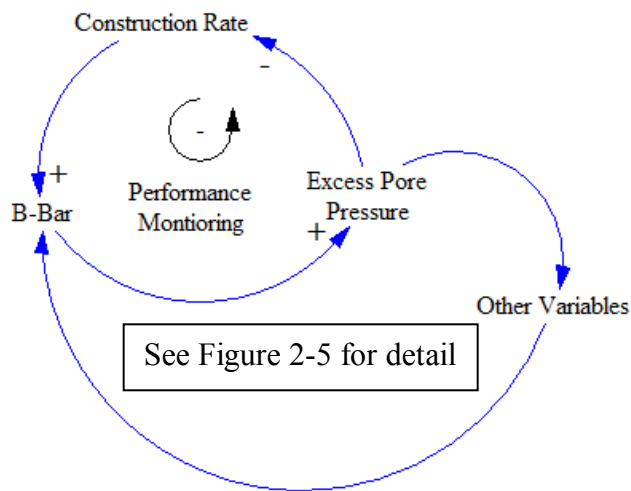
Figure 2-6 Expanded CLD where "Construction Rate" becomes an endogenous variable.

2.3.2 Quantitative Stage

The quantitative stage of SD consists of the following major steps: i) conversion of causal loop diagrams to executable models; ii) parameter estimation; iii) model validation; iv) sensitivity analysis; v) analysis of varying parameter input and model structures; and vi) continued model maintenance based on new information and insights. Once CLDs are set up along with necessary auxiliary variables, the next step is to convert CLDs to a Stock-Flow Diagram (SFD). Stock elements are identified first in a SFD followed by the flow elements into and out of the stock. Converters and auxiliary variables that explain the flow elements connect to each other and flow elements through one-way arrows. Variables at the head of the one-way arrow are functions of variables at the tail end of the one-way arrow. This logic applies to every variable and their calculations in CLDs.

Parameter estimation involves specifying initial values and boundary conditions. Sources of parameter estimation can range from soft to hard (Ford 2010). Hard sources are typically based on experimental and field data, statistical information, and empirical evidence from case studies. Soft sources are typically based on on expert opinions, tentative knowledge, stakeholder participation, engineering judgement and intuition. Uncertainties exist in both soft and hard sources of parameter input.

Model validation is similar to that of a conventional numerical model. A combination of experimental and simulation data is used to establish basic validity of the model. Stress tests, such as extreme condition and family member testing, help to identify limitation and weakness of the model. Section 2.4.2 b) describes some of the challenges associated with model validation in a SD environment.

Sensitivity analysis can be both numerical and structural. Numerical sensitivity analysis tests numeric differences in output under a range of expected input values. SD models are most powerful in structural sensitivity analysis, which instead focuses on the behavioural differences under a range of expected input values (Sterman 2004). The absolute numerical values of the output are given less importance if the objective is to gain insights on changes in system behaviour. For example, there could be significant implications in system performance and policy interventions if simulation output changes from a sustained oscillatory behaviour to a damped oscillatory behavior over time.

SD models are not pre-made packages off the shelf. Building models from scratch is the norm rather than the exception in SD modelling (Homer 1996). Since it is possible to incorporate tentative knowledge and assumptions in SD models, continuous improvement of the model is necessary, especially when key parameters transition from being soft to hard as a result of new data becoming available.

Mine plans and tailings plans continue to evolve through multiple feedback structures. At the beginning of mine development, mine planners provide input parameters to tailings planners in a one-way manner. Over time, the mine plan is continuously adjusted as the performance of tailings system becomes available and lessons-learned are shared. This dynamic nature of planning cycles requires constant questioning of underlying assumptions in SD models.

2.3.3   Model Software
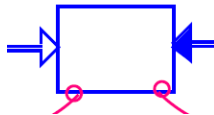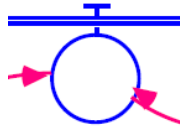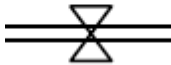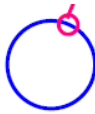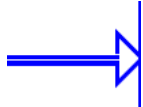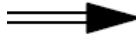
A wide range of simulation software is available for building SD models. This thesis uses the GoldSim software as the simulation engine and Vensim software as the sketch tool for drawing CLDs. The way GoldSim simulates stocks and flows is similar to other SD simulation tools (i.e. Stella and Vensim), which are more familiar to the SD community. Like Stella and Vensim, GoldSim allows the modeler and user to manipulate and visualize data and equations through highly graphical user-interface and object-oriented programming environment.

Similar to other SD tools, GoldSim also supports stock, flow, converter and delay variables. However, GoldSim uses different graphical icons to represent stocks, flow and delay variables (see Table 2-2). Appendix 4 provides a detailed description of GoldSim elements used in this thesis. Note that converters are simply expressed as text in Vensim. Converters and delay elements are functionally linked to each other and to stock and flow elements by one-way influence arrows in which mathematical relationships are embedded.

GoldSim is advantageous in Monte Carlo simulation due to its user-friendliness and graphical interface (GoldSim 2018). GoldSim also offers more element types than classical SD software such as "Selector" and "Previous Value", which graphically represent multiple "if" logical statements and time-dependent variables respectively (GoldSim 2018). However, GoldSim is not

designed to create standard CLDs and SFDs. Therefore, in this thesis, Vensim is used to draw CLDs instead.

Table 2-2. Comparison of icons between GoldSim and traditional SD software

Variable Type	SD icon in GoldSim	SD icon in Stella	SD icon in Vensim
Stock			
Flow			
Converters			Text
Inflow / Outflow Arrow			
Influence Arrow			

2.4 WHY SYSTEM DYNAMICS?

2.4.1 Advantages and Benefits

a) Transparency

In a SD simulation environment, all elements and functional relationships are exposed, visual and transparent through causal loop diagrams and stock-and-flow figures. Modelers and users can also explore the underlying empirical relationships and numerical schemes that are used to explain

inter-relationships between elements. There should be no black boxes and hidden components in a SD simulation environment (Nicolson et al. 2002). In **Figure 2-7**, additional visualization is used in GoldSim to enhance clarity for dynamically simulating volumes of Fluid Fine Tailings (FFT), further demonstrating the communicative power of SD.
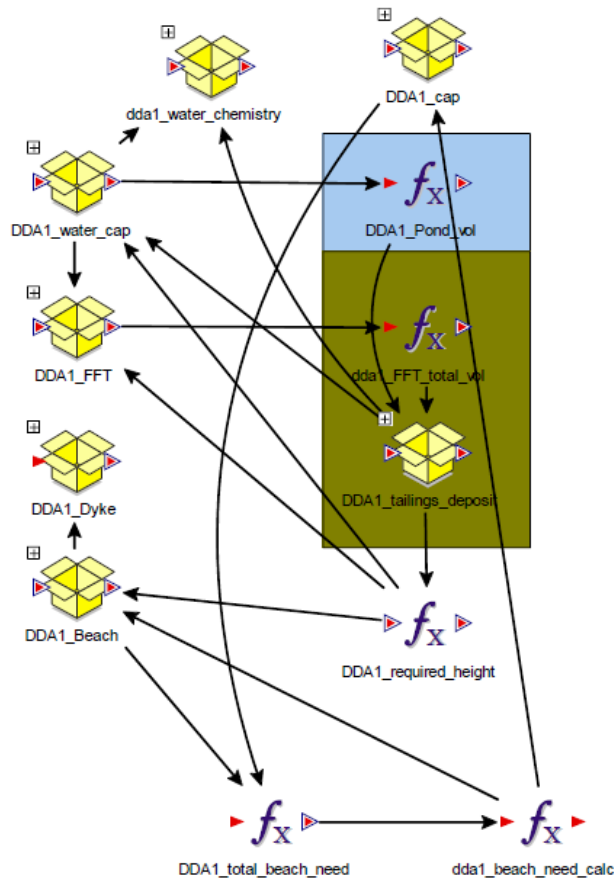
Figure 2-7 Elements of a sub-model in GoldSim (after Beier, 2015)

b) Expandability and Transparency

As part of the object-oriented approach, simplified "child" models can first be developed prior to creating time-consuming larger models. The nature of object-oriented programming facilitates scalability and replicability of those "child" model elements, saving time and preventing accumulation of errors. This is particularly useful since SD-based tools are not intended to model spatial variables. Additional "child" models can be easily added provided that elements in each "child" models follow the same data structure and naming convention.

Model transparency in the GoldSim software is demonstrated in Figure 2-8 and Figure 2-9. All elements of the calculation process and their respective influence directions are exposed and visible to the user. The numerical scheme is linearized based on an explicit, non-iterative finite difference method. Figure 2-8 shows the inside view of a "child" model for consolidation of tailings deposits. As shown in Figure 2-9, each box container denotes a discretized layer. The arrows linking each box container denote functional relationships between elements within each container. To discretize the tailings deposit into 12 layers, the model uses a total of 12 containers that contain elements of identical functional relationships and naming conventions. However, should greater accuracy be needed, the user can easily add more containers by duplication without creating new mathematical relationships.
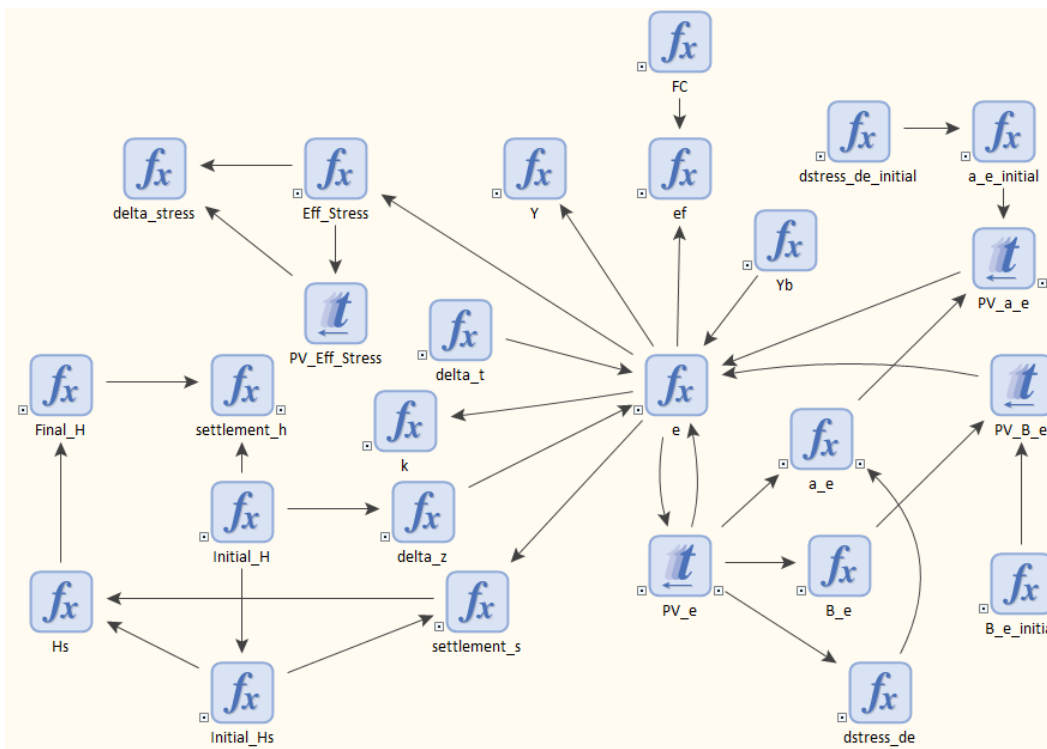
Figure 2-8 Exposed components of the "child" consolidation module (Zheng and Beier 2018)
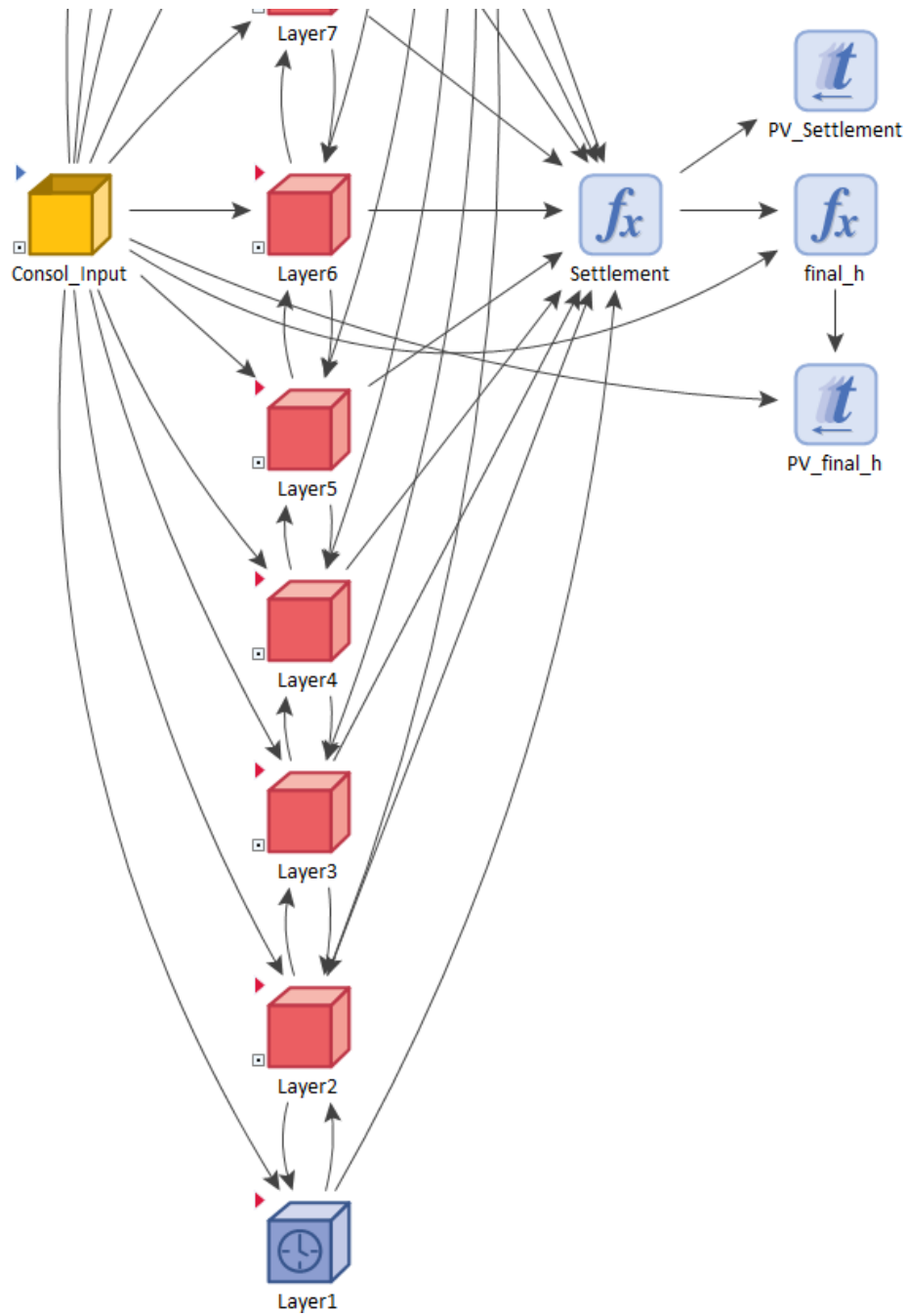
Figure 2-9 Parental setup of all the "child" consolidation modules with 6 spatial layers visible (Zheng and Beier 2018)

The CLD in Figure 2-10 is constructed using the methodology described in Section 2.1. As the name of the feedback loop suggests, the CLD describes the un-saturated flow mechanism in a soil layer. Any effect from rainfall or snowmelt on the water storage will be amplified through the positive feedback loop. The CLD in Figure 2-10 may be sufficient if the goal is to understand the run-away behavior of the system under climatic forces. However, if the objective of the model is to evaluate the state of water storage and soil water content over time, the CLD in Figure 2-10 needs to be expanded to include additional physical processes such as evaporation and run-off.

As shown in Figure 2-11, the expandability of CLD allows for the incorporation of evapotranspiration (ET) process and the volume change process to the unsaturated flow mechanism. The feedback loops for ET and volume change are negative, regulating the run-away behavior of the unsaturated flow loop. The rate of change in soil water content due to both ET and volume change is the greatest when the soil water storage is abundant, decreases as the soil water storage becomes depleted and eventually becomes insignificant once the soil reaches past its residual water content (Fredlund et al. 2012).
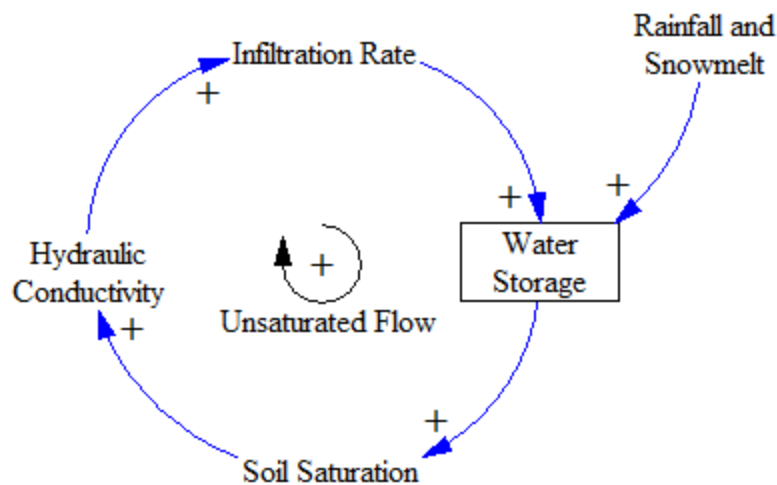
Figure 2-10 Causal loop diagram for un-saturated flow in soil cover (Modified from Elshorbagy et al. 2005).
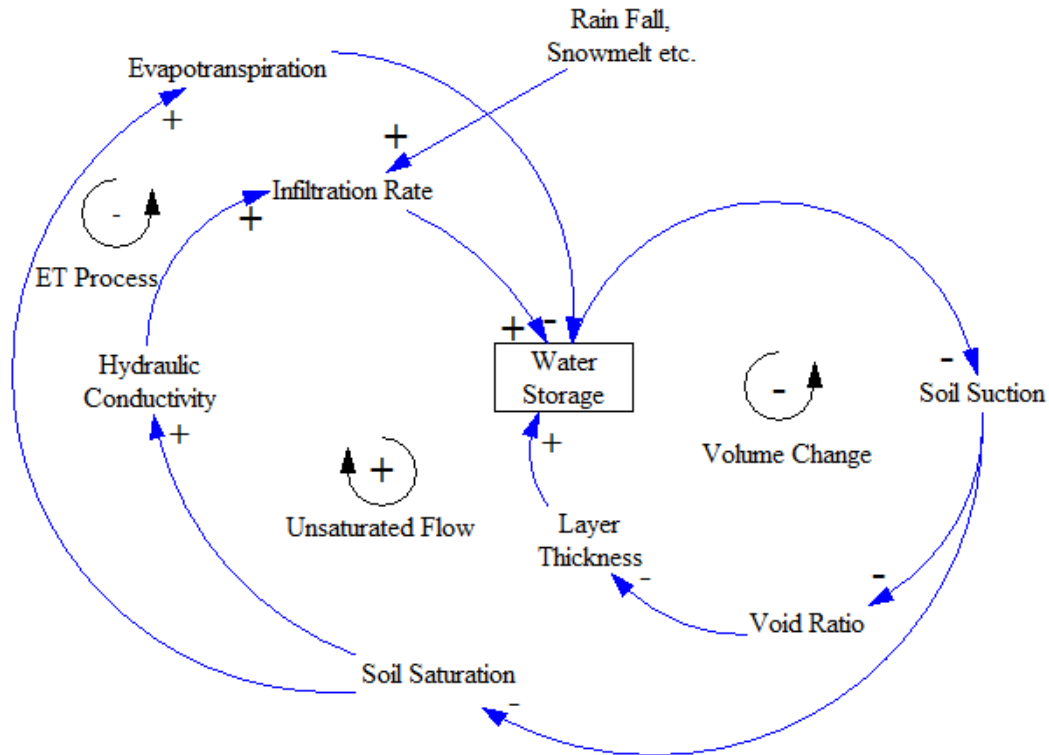
Figure 2-11 Expanded causal loop diagram from Figure 2-10.

c) Stakeholder Participation

Due to the extensive qualitative process required for SD models, the modelling process itself, rather than the end-product, offers the greatest insights. This view is supported by publications on the philosophy of SD modelling (Richmond 1993, Forrestoer 1994, Sternman 1994 and Meadows 2008) as well as on case histories of SD (Hovmand 2014 and ElSawah et al. 2017). Beier (2015) also shared the same view that failed simulation runs and the process of gathering input data itself provided insights into underlying mine planning assumptions.

Hovmand (2014) showed that stakeholders without in-depth knowledge of differential equations are able to contribute to model conceptualization, formulation and simulation through causal loop diagramming exercises in a group workshop setting. Minimum expertise in coding is required for participants to actively engage in the modelling process. In fact, this type of modelling workshop is feasible even without any basic knowledge of SD from the participants.

Hager et al (2015) described a case study where researchers attempted to use qualitative measures from SD to equip small-scale village farmers in Zambia with short-term and long-term strategies to increase their food security and economic stability. In addition to the tactical objectives, a more strategic goal of the study was to improve the shared learning experiences in preparation for changing environment and adaptive policies. In Figure 2-12, stock and flow elements were represented by tangible objects familiar to the village farmers. Variable names were simply written on the white board. Model facilitators used water glasses to show effects of changing variables and devised intuitive terms such as "draining the glasses" and "filling the glasses". The end results were encouraging, according to Hager et al (2015), despite participants' lack of formal training.

Figure 2-12 Community-based modelling workshop in Zambia (Hager et al, 2015)

d) Structural Sensitivity

Numerical sensitivity analysis studies the impact of varying specific parameter input with other parameters being held constant. In contrast, the emphasis of structural sensitivity is no longer the variation of numerical values but instead the variation of structural and behavioral assumptions of the model. As Ford (2010) pointed out, both input and output can change if the fundamental

structure of the model is altered. For example, a different model time step is required if the dominant groundwater transport mechanism changes from advection-based to diffusion-based process. Sterman (2004) also recommends the modeler to examine the sensitivity of results to alternative structural assumptions, such as changing key performance indicators and how boundary conditions of the system are treated.

e) The "Intangibles"

The use of CLD in the SD method provides opportunities for integration between the construction side and design aspects of TMS. TMS is a complex system of inter-related "intangible" components outside the technical realms. Primary organizational and human components of TMS consist of in-house operation staff, Engineer-of-Records, Independent Technical Review Board, consultants, research institutes, advisory associations, regulatory bodies and community stakeholders (Mining Association of Canada 2017). In addition to the adoption of Best Available Technology (BAT) and Best Available Practice (BAP), understanding the dynamic interaction between those organizational and human components plays an equally important role in successfully managing TMS.

Figure 2-13 demonstrates how CLDs can be used to create qualitative models of tailings management in the context of construction Quality Control and Quality Assurance (QA/QC) of a tailings storage facility. For simplicity, only three feedback structures most critical to the process were shown, and they only offered a partial picture of the construction QA/QC process. Each feedback loop is classified as either positive or negative and given a name to reflect its major theme.

For large-scale tailings dams that stretch over several kilometers in length, it is not uncommon to open multiple work fronts far apart and construct the dam structure simultaneously from different locations. It is also desirable, from a financial perspective, to maintain high rate of construction to meet aggressive deadlines and save on equipment and labor costs.

In Figure 2-13, the original student-assignment model from Sterman (2004) was revised to better fit in the context of tailings dam construction. At a fixed staffing level, backlogs are created by an increase in the number of work fronts and construction rate. Mathematically, "Tasks Backlog" is equal to rate of new tasks subtracted by "Task Completion Rate". Work pressure depends on the

number of backlogged tasks and inspection interval assigned to each task. The shorter the time interval between inspection, the longer work hours are required to complete all the QA/QC tasks.

For management, the first intuitive reaction to increasing backlogs is to demand overtime and longer work hours. The positive feedback loop "QA/QC Staff Burnout" operates as a vicious cycle – increasing work hours to combat backlogs leads to more backlogs being generated.

The negative loop in "Staff Feedback" balances the vicious cycle in "Staff Burnout". As work pressure is increased, QA/QC staff may submit additional requests for extension of time between each inspection. In response, construction managers will extend inspection intervals based on the frequency of requests from QA/QC staff. With more time to travel between each work front, QA/QC staff now has less pressure to rush inspections at each site, causing reduced influence of the "QA/QC Staff Burnout" and "Corner Cutting" feedback loops.

The negative feedback loop of "Corner Cutting" also balances the vicious cycle in "Staff Burnout". One way to reduce backlogs is to spend less effort on each task, which in turn increases task completion rate. Since both "Productivity" and "Efforts Devoted to Each Task" work together to affect "Task Completion Rate", their combined effect on "Tasks Backlog" depends on which feedback loop structure would dominate the other over time.

Elements from both design and construction can be combined into a single CLD through shared variables (i.e. construction rate). A more extensive causal loop diagram is possible by incorporating more feedback processes such as the observational method (Figure 2-6) and budget control. The combination of causal loop diagrams from different perspectives promotes inter-disciplinary understanding. However, as causal loops are combined and expanded, it is important to strike the right balance between over-simplification and over-complication of the system boundary.
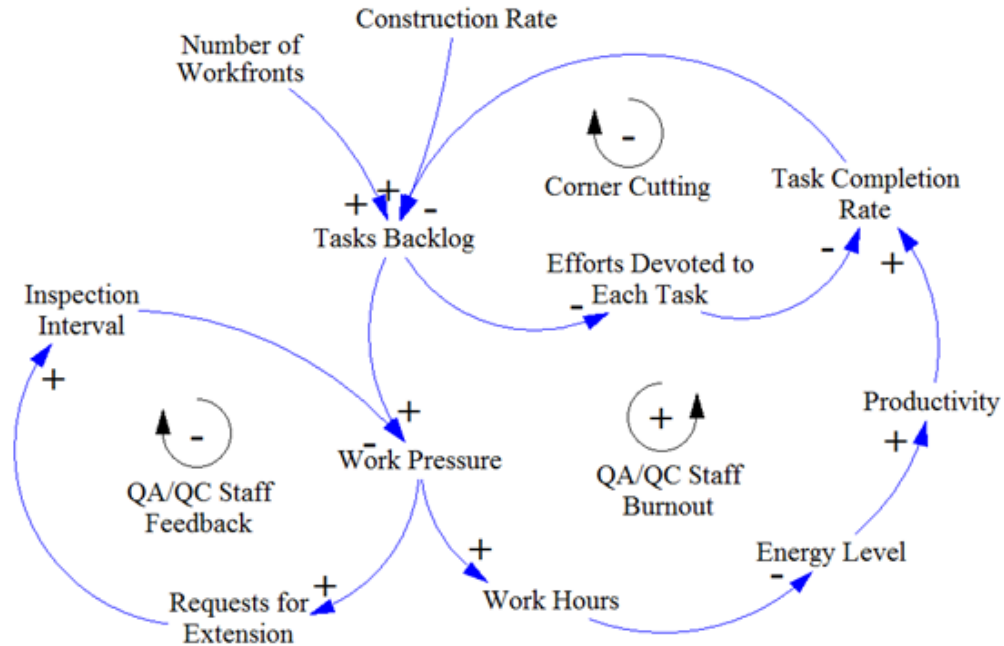
Figure 2-13 Causal loop diagram for staff fatigue and burnout (Modified from Sterman, 2004)

2.4.2 Limitations

a) **Predictive Power**

SD models are constructed to help us gain a big-picture understanding of system behaviors and why they follow certain patterns (Lane and Sterman 2017). The process of simplification and linearization of key physical processes inevitably reduce their predictive powers in terms of absolute numeric values. SD models may provide satisfactory prediction in exchange for larger model size and increased computational time. However, at a macro level, SD models are lumped models that only output the average, aggregated state of the system. At a micro level, traditional numerical models are better suited for predicting disaggregated, spatial variables over time.

On the other hand, predictive models focus on a singular objective that is to provide the most accurate forecast of the future state of the system. Reconciling the difference between predictive models and SD-based models continues to be a challenge partly due to heavy emphasis on discipline-based, narrowly-defined numerical modelling methods taught in the engineering curriculum (Haraldsson et al. 2006). Furthermore, SD models are often misunderstood as

predictive models, further deepening the suspicion from end users (Ford 2010). While SD models may lack predictive power in the absolute numeric sense, they can still be useful comparative tools as long as the model is able to produce correct behaviours under various conditions.

b) Model Validation

Validation of predictive models is straightforward. Matching model results with historical and experimental data gives confidence in the model provided that the same underlying assumptions and boundary conditions are used during the validation process (Ford 2010).

Validation of SD-based models is similar to that of predictive models based on matching historical behavior and measured data if available (Elshorbagy et al. 2005 and Huang et al. 2011a). Difficulties arise when little to no measured data exists, as in the case of farm villagers in Zambia in Figure 2-12 and staff fatigue and burnout model in Figure 9. In this case, alternative validation approaches must be adopted. Various practitioners and theorists of SD have advocated for a soft approach to validation: building confidence in the model through debate, education, critique and qualitatively matching behaviors based on expert opinion and well-established fundament physical processes.

Sterman (2004) noted that validation in a SD context is an iterative process where modelers and users continuously question the model's ability to qualitatively replicate expected behavior based on critiques, discussion, known empirical relationships, tentative knowledge and expert opinions. These un-settled validation techniques have become a point of contention and heavy criticisms for the SD modelling paradigm.

c) Causality vs Correlation

Causality should not be confused with correlation. Sterman (2004) discussed the difference between causality and correlation. Causality is the causal relationship between variables underlying the observed behavior. Correlation reflects historical behavior of the system without the support of physical processes and empirical evidence. If variables or boundary conditions change, causality remains unchanged while correlation may break down. CLD represents causal

relationships only. Therefore, the arrow linking variables and stocks in CLD must represent strong causal relationships without ambiguity.

Sometimes, the difference between causality and correlation is obvious. For example, in Alberta, the amount of precipitation correlates well with the level of construction activities. However, higher rate of construction activities is not caused by greater amount of precipitation during summer but instead by the availability of favorable weather condition.

Modelers need to pay close attention to differences between causality and correlation. In tailings dam construction, for instance, it can be tempting to draw a causal link between frequency of dam foundation movement and number of construction workforce. The modeler must critically debate the strength of the causal link by asking what other factors stand in between foundation movement and number of construction workforce. As shown in Figure 2-14 and Figure 2-15, causality is improved by reversing the original link and adding another variable that has stronger causal relationship to the other two variables.
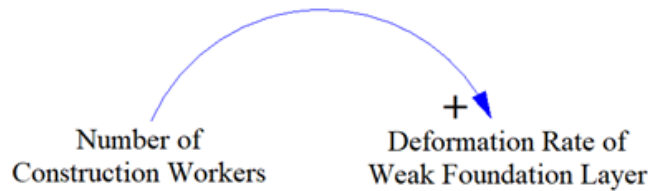
Figure 2-14 Weak causality
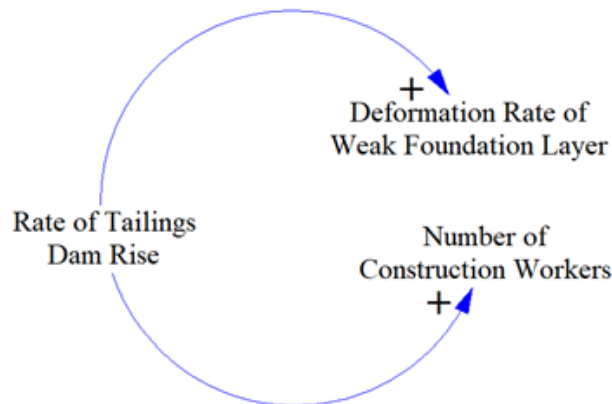
Figure 2-15 Improved causality

d) Resistance vs Over-reliance

When SD is employed in a participatory modeling environment, resistance to adopting SD can come from specialists who tend to concentrate on the detail with which they are most familiar. (Nicolson et al. 2002). To be successful in inter-disciplinary modelling exercises, Cockerill et al (2007) suggested that participants need to have a sense of humility and accept the fact that they need to learn new languages and concepts from other disciplines as well as general principles of SD modeling. Nicolson et al. (2002) further warned that there will be steep learning curves for participants even though they may be experts in their respective fields.

At the other end of the spectrum is over-reliance on SD models which seem to have the ability of integrating multiple disciplines. Limitations in the predictive power of SD models cannot be ignored. Over-emphasis on CLD can also erode sound scientific basis and exaggerate the usefulness of conceptual models. Homer (1996) argued that the ease with which CLD can be created may have exacerbated the belief that SD is mainly conceptual instead of empirical, and that creativity takes precedence over thoroughness. Kelly et al (2013) expressed similar views that the user friendliness of SD modeling software allows modelers to create large and overly complex models that lack clear focuses and obscure key mechanisms.

2.5   CONCLUSIONS

Traditionally, multi-disciplinary modelling involves one discipline mechanistically using the output from a black-box model developed by another discipline. System Dynamics (SD) allows for coupling of multiple processes and systems across disciplinary boundaries. Different views and ideas from multiple disciplines can be expressed by the process of creating causal loop diagrams (CLD) and subsequent conversion of CLDs into quantitative models. Underlying assumptions of the model are made explicit by the presence and absence of feedback structures.

Furthermore, the qualitative stage of the SD modeling is a rigorous process with its own syntax, well-established rules, and best practices.   The qualitative stage of SD modeling process also emphasizes transparency, simplicity and flexibility. The process of constructing CLD provides further insights into the tailings management process and serves as a vehicle for inter-disciplinary communication.

However, CLD constructed in this chapter may not contain enough information for subsequent quantitative modeling exercises. As research and stakeholder participation progress, additional causal loop diagrams, variables and processes need to be identified and incorporated. At the same time, redundant components and insignificant processes may be discarded.

3   SIMULATION OF TAILINGS SELF-WEIGHT CONSOLIDATION PROCESS

3.1   INTRODUCTION

In the oil sands mining industry, the Tailings Management System (TMS) is a complex process that involves dynamic interaction among distinct but inter-related sub-systems. Various research has focused, in isolation, on the individual components of TMS at a micro-scale (Beier et al. 2014). Therefore, a system dynamic simulation tool, TMSim, was developed to address this lack of integration and bring together different disciplines on a common platform (Beier 2015). GoldSim software was chosen as the primary simulation engine for its graphical user-friendly interface, object-oriented programming environment and ability to provide insights in system behavior under data-poor scenarios frequently encountered in mining operations.

Current tailings regulatory framework (Directive 085) in Alberta emphasizes the importance of fluid tailings management through volumetric reduction of both legacy Mature Fine Tailings (MFT) and future growth of fluid fine tailings. The implementation of new dewatering technologies, some borrowed from metals mining industry while others still in the pilot stage, poses significant risks when the life of mine in the oil sands is taken into consideration. Significant uncertainties exist in time-dependent properties of tailings material and depositional environment. As part of a simulation-based approach to modeling uncertainties, Baecher and Christian (2003) discussed the classification of uncertainties into two separate categories: those due to lack of knowledge or ignorance (epistemic) and those due to inherent variabilities (aleatory). The usefulness of separating uncertainties in geotechnical engineering is still debatable and highly dependent on project-specific requirement (Vick 2002). Therefore, the stochastic simulation of the consolidation sub-model aims only at demonstrating the use of nested Monte Carlo techniques to simulate the two uncertainties together.

The development of the consolidation sub-model involves first building and validating the deterministic model and then converting the deterministic model to a stochastic model in GoldSim. For the deterministic model, a simplified quiescent or self-weight consolidation module was created in GoldSim based on an explicit finite difference numerical scheme described in Section 3.2.3. To facilitate understanding and communication beyond disciplinary borders, the modeler

also created a series of causal loop diagrams (CLD) to describe the numerical scheme in a non-mathematical manner. For the stochastic model, compressibility (e-σ') and permeability (e-k) relationships are assigned probabilistic distributions. Nested Monte Carlo technique is used to explicitly model epistemic and aleatory uncertainties. For stochastic simulation, a simple case study based on deposition of phosphate tailings is demonstrated here.

3.1.1   Model Objective

The objectives of this chapter are summarized as follow: 1) create a consolidation sub-model in a SD-based environment that is open-box, transparent and easy to use for technical and non-technical stakeholders; 2) create CLDs to facilitate communication and understanding of the large-strain consolidation process underlying the sub-model; and 3) using the base case model developed in 1), demonstrate the capability of explicitly modelling uncertainties due to lack of knowledge and those due to inherent variabilities using nested Monte Carlo techniques. Finally, the developed sub-model will provide input to the unsaturated flow model in Chapter 4 as part of the integrated modelling exercise.

3.1.2   Model Conceptualization

The first step in SD-based model formulation is to identify feedback loop structures by creating a causal loop diagram. Causal loop diagram is an effective tool of communication during early conceptual development stage (Richardson 1997). In this modelling exercise, CLD is used for conceptualization and communication purposes only.

The dynamics of consolidation process is conceptualized as a causal loop diagram based on stock-flow relationships (Figure 3-1). Stock variables are represented by labels inside a rectangle. Flow rate and converters that explain the flow rates are simply labelled in plain text. The positive sign at the arrow head indicates a positive relationship, that is an increase in one variable will cause increases in another. The negative sign denotes a negative or inverse relationship, that is an increase in one variable will cause decreases in another. In a closed loop, odd number of negative signs indicate negative feedback structure while even number of negative signs indicate positive feedback structure. Negative feedback brings the system to equilibrium state while positive feedback amplifies growth and cause run-away behaviors (Ford 2010).

In Figure 3-1, excess pore pressure is modelled as a stock element with construction rate as inflow and dissipation rate as outflow. Assuming the validity of Darcy's Law and ability of vertical stress to approximate principle stress in the foundation soil (i.e. no principle stress rotation), an increase in construction rate will trigger a series of chain reactions and lead to a negative feedback structure through the dissipation mechanism, which makes sense since the consolidation process brings the system back into balance. The counter-clockwise loop symbol is also assigned a name "Consolidation Process" to communicate the major theme of the feedback structure. In contrast, high rate of construction may cause sustained generation of excess pore pressure through reduced layer thickness and soil response to changes in vertical effective stress. Again, counting the number of negative signs indicates that the load response is a positive feedback loop that amplifies any changes in construction rate. The behavior of excess pore pressure is governed by whichever is the more dominant process between "Consolidation Process" and "Load Response" feedback loops.

With a conceptual understanding of the consolidation process in place, the next step is to develop mathematical relationships hidden behind the one-way arrows. To convert the CLD in Figure 3-1 to a functioning numerical model, two approaches can be taken: top-down and bottom-up. The top-down approach builds directly on the CLD from Figure 3-1 and incorporates empirical relationships to describe the dissipation rate. Additional calibration effort with experimental data may be required prior to predictive simulation.

The bottom-up approach is based on an explicit finite difference solution described by Cargill (1982) to the governing equation. The CLD in a top-down approach can be directly transformed into a SFD. In the bottom-up approach, CLD helps explain the solution to governing equations without clear identifications of stock and flow variables. Minimal effort of calibration is required since there is less empiricism in the bottom-up approach. The top-down approach can be easily understood by non-technical stakeholders while the bottom-up approach is numerically more rigorous. To minimize calibration effort, the bottom-up approach is chosen as the conceptual framework for the consolidation sub-model. "Bottom-up" refers to the perspective from which the modeler views and analyzes the problem. Thus, the model building process should always be top-down. The modeler should start from the simplest form of models and only add complexity after gaining enough confidence in the simple model.

From a bottom-up perspective, the CLDs serve as mere communication tools to understand the inner workings of the numerical scheme (see Figure 3-2 and Figure 3-3). The finite difference solution at each time step solves for the void ratio from which settlement height, excess pore pressure, effective stress and solids content are derived. The remaining sections of the chapter will describe how the consolidation model is created in GoldSim.
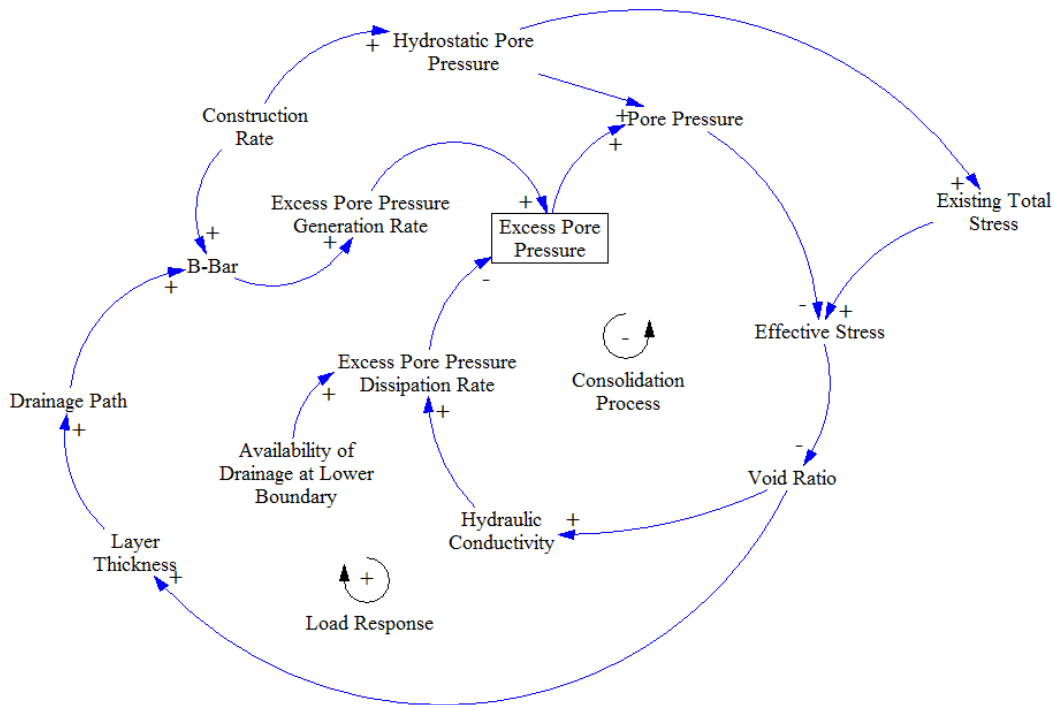
Figure 3-1 Conceptual stock-flow based CLD (modified after Zheng and Beier, 2018)

3.2 DETERMINISTIC MODEL SETUP IN GOLDSIM

3.2.1 Compressibility and Permeability

Before solving the governing equation of large-strain consolidation, two key relationships are required: compressibility or effective stress-void ratio relationship and saturated hydraulic conductivity-void ratio relationship (Jeeravilpoolvarn 2010). Constitutive relationships are derived from experimental data and most commonly curve-fitted to a power law function below:

$$e = A\sigma'^B \qquad\qquad (3.1)$$

$$K = Ce^D \qquad\qquad (3.2)$$

Where σ' is the effective stress; e is the average void ratio of the soil layer and K is the saturated hydraulic conductivity of the soil in m/day; A, B, C, and D are curve-fitting parameters.

Other forms of equations, such as Weibull functions for K-e relationship, have been proposed to handle different types of tailings and deposition conditions. For demonstration purposes and simplicity, the power law functions are used in the GoldSim module. If required, users can easily define customary constitutive relationships in the software.

3.2.2   Governing Equation for Large Strain Consolidation

The one-dimensional finite strain consolidation theory (Gibson et al. 1967) has been the theoretical basis for modelling consolidation behavior of soft soil and tailing slurry. The theory assumes that Darcy's Law is valid, properties of soil skeleton are not time-dependent and there is no lateral consolidation strain or flow. The governing equation is derived from satisfying both material equilibrium and fluid continuity equations and expressed in terms of void ratio below:

$$\left(\frac{\rho_s}{\rho_f} - 1 \right) \left(\frac{d\left[\frac{K(e)}{1+e} \right]}{de} \right) \left(\frac{\partial e}{\partial z} \right) + \frac{\partial}{\partial z}\left[\frac{K(e)}{\rho_f(1+e)} \frac{d\sigma'}{dz} \frac{\partial e}{\partial z} \right] + \frac{\partial e}{\partial t} = 0 \qquad (3.3)$$

where ρ_s and ρ_f are the density of solids and fluid respectively; e is the void ratio; K is the saturated hydraulic conductivity expressed as a function of void ratio; σ' is the effective stress also expressed as a function of void ratio; t is the time step; and z is the material coordinate. In this model, the density of fluid is assumed to equal to that of water.

3.2.3   Numerical Solution to the Governing Equation

Analytical solution to Equation 3.3 is not possible due to non-linearity of its coefficients. An explicit finite difference method developed by Cargill (1982) is used to solve Equation 3.3. At each time step, void ratio is calculated as the dependent variable. The explicit numerical scheme computes output at the current time step based on output at the previous time step while the implicit numerical scheme computes output at the current time step based on the current time output itself

and future time output. Bromwell (1984) and Pollock (1988) showed that the explicit approach produced similar and sometimes better results than the implicit approach provided that numerical stability issues such as number of layers and time step are properly addressed. Additionally, the implicit approach requires solvers to iteratively solve systems of equations at each time step. However, built-in matrix solvers must be externally attached since they are not available in GoldSim. Therefore, the explicit approach is chosen for its simplicity, non-iterative nature and ease of implementation in a SD environment.

Cargill (1982) provided detailed accounts of assumptions, derivation and case studies using this method. Only key information will be repeated here. Equation 3.3 is solved by a backward time and central difference space numerical scheme, as follows:

$$
e_{i,j+1} = e_{i,j} - \left(\frac{\Delta t}{\gamma_w}\right) \left[\left(\gamma_b \beta(e_{i,j}) + \frac{a(e_{i+1,j}) - a(e_{i-1,j)})}{2\Delta z} \right) \times \left(\frac{e_{i+1,j} - e_{i-1,j}}{2\Delta z} \right) \right.
$$
$$
\left. + a(e_{i,j}) \times \left(\frac{e_{i+1,j} - 2e_{i,j} + e_{i-1,j}}{\Delta z^2} \right) \right] \tag{3.4}
$$

where γ_w and γ_b are the unit weight of water and buoyant unit weight of solids respectively; γ_s is the unit weight of solids; all unit weights are expressed in kN/m³; i is the spatial node; j is the time increment whose range depends on the resolution of time step and total simulation duration specified by the user; Δz in m is the spatial discretization in material coordinate (see Equation 3.10); and Δt is the simulation time step. The maximum value of i depends on the number of discretized layers for the deposit. In this case, the deposit is discretized into 10 equal layers as a compromise between model complexity and numerical accuracy. Validation cases in Section 3.2.12 showed that a 10-layer discretization satisfactorily replicated experimental and simulated behaviour. Therefore, i varies from 1 to 10 in Equation 3.4. γ_b, γ_s, $a(e)$ and $\beta(e)$ are defined as follows:

$$a(e) = \frac{K(e)}{1 + e} \frac{d\sigma'}{de} \tag{3.5}$$

$$\beta(e) = \frac{d}{de}\left(\frac{K(e)}{1 + e}\right) \tag{3.6}$$

$$\gamma_b = \gamma_s - \gamma_w \tag{3.7}$$

$$\gamma_s = \rho_s g \tag{3.8}$$

Where γ_w is the unit weight of water; ρ_s is the density of solids with its magnitude taken from specific gravity of solids G_s; and g is the gravitational acceleration. Using rules of differentiation, Equation 3.5 and 3.6 can be re-formulated analytically in terms of void ratio and the power law relationships (see Equation 3.1 and 3.2):

$$\frac{d\sigma'}{de} = \left(\frac{1}{A}\right)^{\frac{1}{B}}\left(\frac{1}{B}\right)e^{\frac{1}{B}-1} \tag{3.9}$$

$$a(e) = \left(\frac{Ce^D}{1 + e}\right) \times \left[\left(\frac{1}{A}\right)^{\frac{1}{B}}\left(\frac{1}{B}\right)e^{\frac{1}{B}-1}\right] \tag{3.10}$$

$$\beta(e) = \frac{CDe^{D-1}}{1 + e} - \frac{Ce^D}{(1 + e)^2} \tag{3.11}$$

It is assumed that the initial conditions of the tailings deposit are at a uniform void ratio and zero effective stress over the entire depth of the deposit. The individual thickness of each layer is converted to material coordinates as:

$$\Delta z = \frac{h_0}{1 + e_0} \tag{3.12}$$

$$h_0 = \frac{H_0}{10} \qquad\qquad (3.13)$$

where h_0 in m is the initial discretized height of each layer; H_0 is the total height of the entire deposit prior to any consolidation. As the basis of measurement, Δz focuses on the height of solids, which remains fixed over time while height of water is changing due to consolidation release of water. This way, the simulation does not need to update geometry at each time step. Once the new void ratio is calculated for each time step, settlement in the material coordinate can be converted back to the Eulerian coordinate as follows:

$$\varepsilon = \frac{e_0 - e}{1 + e_0} \qquad\qquad (3.14)$$

$$h = h_0 - h_0 \varepsilon \qquad\qquad (3.15)$$

where e_0 is the user-defined initial void ratio of the tailings deposit prior to consolidation; e is the void ratio at current time step i and spatial node j; ε is the strain of the system as defined by Monte and Krizek (1976); and h is the current interface height of the layer in m. The amount of settlement in each layer given by $h_0 \varepsilon$. The interface height for the entire deposit h_T is given by summing individual layer height:

$$h_T = \sum_{i=1}^{10} h_i \qquad\qquad (3.16)$$

where h_i is the current interface height of the layer "i" calculated by Equation 3.14 and Equation 3.15.

3.2.4 Re-interpretation of the Numerical Solution using CLD

Equation 3.4 in Section 3.2.3 can also be interpreted from a different angle by constructing causal loop diagrams (CLD) in the same manner described in Chapter 2. The CLDs shown in Figure 3-2 and Figure 3-3 provide only partial coverage of Equation 3.4 as exogenous variables and additional layers are omitted. It is important to note that only the techniques of constructing CLD are used to re-construct and re-interpret the numerical solution. There is no clear cause and effect in the functional relationships.

Figure 3-2 illustrates the temporal feedback structures for the void ratio calculation. In GoldSim, the Previous Value (PV) element is used to calculate temporal advancement for each variable. The PV element allows the user to reference an output at a previous time step (GoldSim 2018). Over time, changes in void ratio tend to drive the system to equilibrium due to the presence of three negative feedback loops. There are two negative feedback loops going through hydraulic conductivity and only one through dStress_de or the compressibility relationship described in Equation 3.9. From the perspective of this numerical method, the rate and magnitude of self-weight consolidation are more dependent on the hydraulic conductivity than on the compressibility relationship, though both relationships contribute to the rate of consolidation.

Figure 3-3 describes the spatial feedback structures for the void ratio in Layer 2. There are seven negative and two positive feedback loops. The self-weight consolidation process, from a spatial perspective, is still predominantly balancing in nature due to the presence of more negative feedback loops than positive ones.
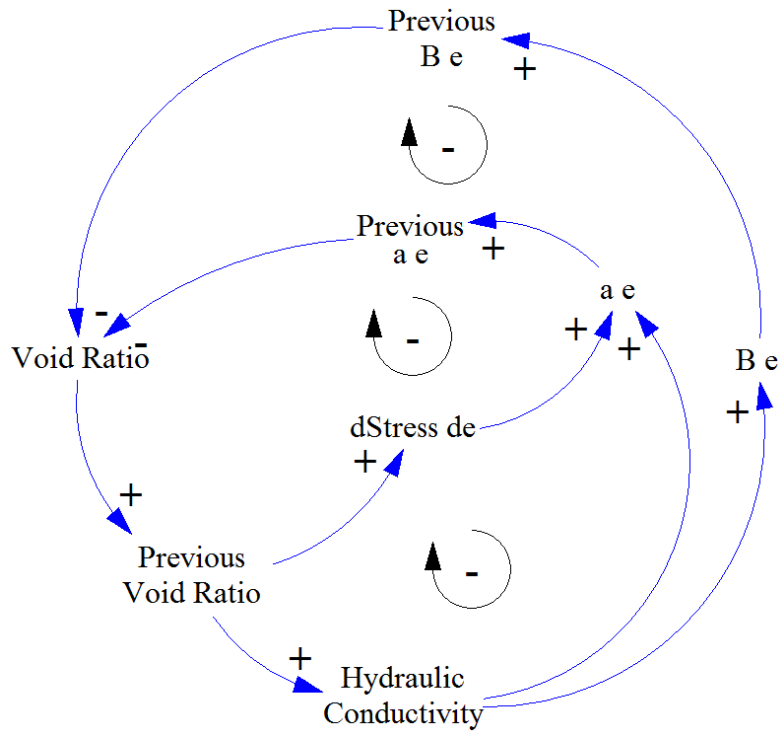
Figure 3-2 Temporal re-interpretation of Equation 3.4 using CLDs
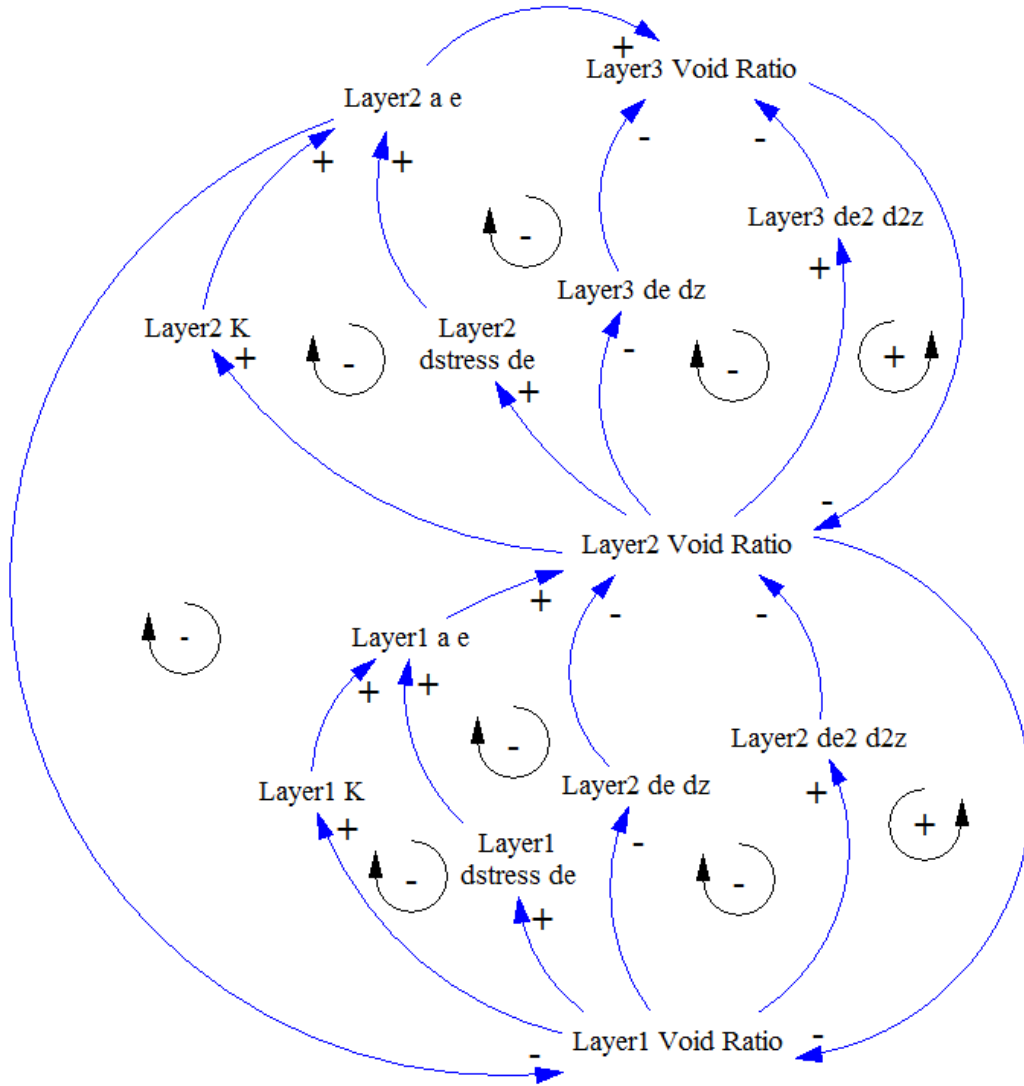
Figure 3-3 Spatial re-interpretation of Equation 3.4 using CLDs

3.2.5   Excess Pore Pressure and Effective Stress

At each time step, the model will calculate the void ratio $e_{i,j}$ using Equation 3.4. The effective stress of each layer is calculated by re-arranging the power-law relationship from the compressibility curve:

$$\sigma' = \left(\frac{e_{i,j}}{A}\right)^{\frac{1}{B}} \tag{3.16}$$

A stock element in GoldSim represents excess pore pressure Δu in kPa, with its initial value set to the effective stress expected at the end of consolidation. The initial value of excess pore pressure $\Delta u_{initial}$ in the excess pore pressure stock element is calculated as follows:

$$\Delta u_{initial} = \frac{\gamma_w(G_s - 1)}{1 + e_0} \times \left(H_0 - \frac{(i-1) \times H_0}{10}\right) \tag{3.17}$$

Where i in this case varies from 1 to 10; H_0 is the initial deposit height based on user-input; $\frac{\gamma_w(G_s-1)}{1+e_0}$ is the buoyant bulk density. The inflow rate (kPa/day) to this stock element is assumed to be the change in effective stress $\Delta\sigma'$ between each time step. In GoldSim, this is handled by subtraction between a PV element of σ' and the current value of σ'.

3.2.6   Upward Consolidation Flux

The surface upward flux v in m/day is expressed by Equation 3.18 and 3.19 based on Darcy's Law. Layer 10 is considered the surface layer of the deposit. The hydraulic gradient is dependent on the excess pore pressure available within the layer and the thickness of the layer at a given time step

"j". The saturated hydraulic conductivity $K_{10,j}$ is calculated by the power law relationship. Void ratio $e_{10,j}$ is calculated by Equation 3.4.

$$v = \frac{K_{10,j}\Delta u}{\gamma_w h} \qquad (3.18)$$

$$K_{10,j} = C\left(e_{10,j}\right)^D \qquad (3.19)$$

3.2.7   Upper Boundary Conditions

Boundary conditions in this model are specified as the value of initial void ratio or solids content (SC). In GoldSim, the upper boundary condition is handled by an imaginary layer (Layer 11) where the void ratio is equal to the initial void ratio in Layer 10. The purpose of the fictitious layers is numerical convenience and stability. To ensure numerical stability, the void ratio in Layer 11 is fixed to the initial void ratio of the deposit.

The effect of surcharge loadings is ignored. Surcharge loadings are assumed to come from a sandy cap which does not impede the release of consolidation water. Any surcharge loadings are likely placed gradually over time, thus will unlikely induce any significant excess pore pressure during construction. A sand cap may accelerate the rate of consolidation in the tailings substrate. However, the effect of surcharge loading on the upward flux is considered minimal in the long term since it is confined to the upper part of a deep fines-dominated deposit (COSIA 2012).

3.2.8   Lower Boundary Conditions

Like the upper boundary, the bottom boundary condition is also handled by an imaginary, non-contributing layer (Layer 0) outside the real boundary. The purpose of the fictitious layers is numerical convenience and stability. Figure 3-4 illustrates, at a conceptual level, how the variables in the bottom layer are spatially arranged in relation to the fictitious Layer 0. Mathematical treatment of Layer 0 is described by Equation 3.20 to 3.23, which are graphically represented by GoldSim elements and functional relationships as shown in Figure 3-5 and Figure 3-6.

Because this thesis uses deep fines-dominated deposits as the case study, the bottom boundary assumes an impermeable, thus single-drained condition. The fictitious void ratio e_{0_0} and $e_{0\_1,j}$ below the bottom of Layer 0 are calculated below:

$$e_{0\_0,j} = e_{0\_1,j} + \frac{2\Delta z}{N}\left(\frac{de}{d\sigma'}\right)_{Layer_0}(\gamma_s - \gamma_w) \tag{3.20}$$

$$e_{0\_1,j} = e_{0,j} + \left(\frac{\Delta z}{N}\right)\left(\frac{e_{1,j} - e_{0,j}}{\Delta z}\right) \tag{3.21}$$

Where N is the spatial discretization for numerical stability (see Equation 3.23); $e_{0\_1,j}$ is linearly interpolated between $e_{0,j}$ in Layer 0 and $e_{1,j}$ in Layer 1 (see Equation 3.21 and Figure 3-4); $\left(\frac{de}{d\sigma'}\right)_{Layer_0}$ is the slope of the compressibility curve associated with Layer 0. Note that $e_{0,j}$ is handled by a PV element in GoldSim (Figure 3-6) and calculated by Equation 3.4 in the same way as the rest of layer void ratios. The linear interpolation of $e_{0\_1,j}$ is calculated by Equation 3.21.

Equation 3.4 is used to calculate $e_{0,j}$ in Layer 0 with the exception that the Δz in Equation 3.4 is replaced by $\frac{\Delta z}{N}$ in Equation 3.22. $e_{0,j}$ is initialized by a PV element whose initial value is specified by the user as the initial solids content. Once the fictitious void ratio is calculated at $j = 0$, Equation 3.20 and 3.21 will advance the void ratio along the compressibility curve and repeat the same calculation at each time step.

$$e_{0,j+1} = e_{0,j} - \left(\frac{\Delta t}{\gamma_w}\right)\left[\left(\gamma_b\beta(e_{0,j}) + \frac{a(e_{0\_1,j}) - a(e_{0\_0,j)})}{2\left(\frac{\Delta z}{N}\right)}\right) \times \left(\frac{e_{0\_1,j} - e_{0\_0,j}}{2\left(\frac{\Delta z}{N}\right)}\right)\right.$$
$$\left. + a(e_{0,j}) \times \left(\frac{e_{0\_1,j} - 2e_{0,j} + e_{0\_0,j}}{(\Delta z/N)^2}\right)\right] \tag{3.22}$$

At the beginning of the simulation, the steepness of the compressibility curve $\frac{de}{d\sigma'}$ can drive $e_{0\_0,j}$ into negative values, especially if the time step Δt and layer thickness Δz are not small enough. Therefore, Δz for the bottom layer is further discretized by a factor of N (see Figure 3-4). For the same reason, the model ignores any contributions in interface height from Layer 0 since inclusion of void ratio $e_{0,j+1}$ from Layer 0 in the calculation of interface height would cause an abrupt, unrealistic drop in interface heights at the beginning of the simulation. However, Layer 0 still contributes to the flux calculation at the surface. In GoldSim, instead of specifying a value for N, the user is required to specify a fictitious void ratio, $e_{0\_fictitious}$, for the impermeable foundation. The value of N is then back calculated from $e_{0\_fictitious}$, which is set to 0.1 by default (see Equation 3.23). The value of $e_{0\_fictitious}$ shall be as small as possible. However, the user can adjust the value if numerical instability occurs during simulation.

$$
N = \frac{2\Delta z(\gamma_s - \gamma_w)\left(\dfrac{1}{\left((A)^{-\frac{1}{B}}\right) * \left(\dfrac{1}{B}\right) * (e_{initial})^{\frac{1}{B}-1}}\right)}{e_{0\_fictitious} - e_{initial}}
\tag{3.23}
$$

where $e_{initial}$ is the user-specified initial void ratio for the tailings deposit; A and B are curve-fitting parameters for the compressibility curve. Note that N does not have to be an integer and does not vary over time.
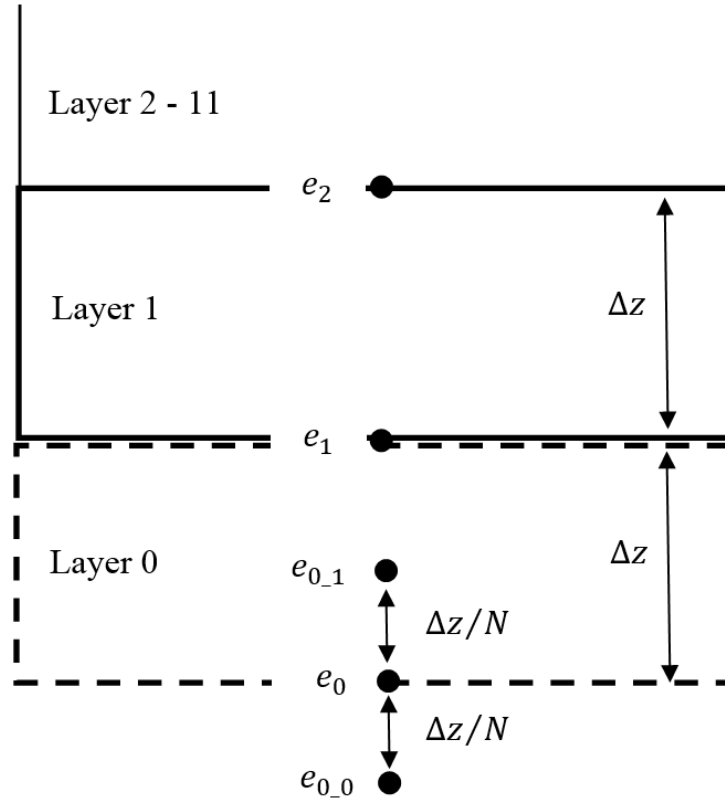
Figure 3-4 Spatial setup of the fictitious bottom layer in dashed rectangular box (Layer 0)

Figure 3-5 GoldSim setup of the fictitious bottom layer (Layer 0)

Figure 3-6 GoldSim setup inside the Fictitious_Boundary container based on Equation 3.19 and 3.20.

3.2.9   Time Step

The resolution of time step in SD models should be carefully considered due to its importance in the accuracy and numerical stability of the finite difference equations and the level of stock at any given time. Ideally, for the greatest accuracy, the time step should be as small as possible. However, a time step too fine may increase model run-time and reduce efficiency. On the other hand, a time step too coarse may fill up or drain out the stock prematurely as the amount of inflow and outflow is integrated over a longer time interval.

A smaller time step is required during the early stages of simulation when the slope of the compressibility curve is steep. As a result, a time step too large would force $e_{0,j+1}$ into negative values (see Equation 3.16). The GoldSim model uses dynamic time stepping for run-time efficiency. After trials and errors, the following setup is deemed optimal for the consolidation sub-model. The bottom fictitious Layer 0 adopts an internal clock with a time step of one minute. However, the model will only save results at the main time interval of one day, not at the internal clock time interval of one minute. Results from Layer 0 will simply be aggregated and exported at the main time interval. The simulation model outside Layer 0 runs on a daily basic time step with hourly dynamic updates. The size of the model is kept to a manageable level since the saving frequency of the model results is only daily and the hourly dynamic updates are not saved at each time step.

3.2.10   Model Organization

Conceptually the model is divided into 12 layers of equal thickness. Layer 1 to 10 are active layers that contribute to total settlement and consolidation flux. Layer 0 and Layer 11 are imaginary layers, which handle boundary conditions (see Figure 3-7) but do not contribute to total settlement. The organization of the model in Goldsim takes advantage of the object-oriented programming environment. In the model, each discretized layer is organized in containers (Figure 3-8). The top and bottom container store the fictitious layers. All elements of the numerical solution are exposed and visible to the user (Figure 3-9), facilitating communication of the finite difference numerical process. Container elements in Figure 3-8 are used to group and organize different categories and functionalities, minimizing visual congestion and enhancing clarities. Except the top and bottom layer container, elements in all other containers share the same functional relationships and naming

conventions. Container elements with the top closed are localized containers, which allows identical naming of variables inside. Therefore, additional containers or layers can be easily added or removed with minimum amount of work. This modeling practice saves time and effort when SD models become large and complex.

Figure 3-8 represents the GoldSim implementation of the spatial CLDs from Figure 3-3 and Figure 3-4. The temporal CLDs in Figure 3-2 corresponds to the GoldSim setup shown in Figure 3-9. In GoldSim, any influence arrows associated with the feedback structures are bolded and coloured to emphasize and distinguish different feedback loops. In Figure 3-9, negative feedback loop #1 and #2, coloured in black and red, are related to permeability, and negative feedback loop #3, coloured in blue, is related to compressibility. Mathematical relationships and the solution to the governing equation are embedded in the one-way arrows. Elements at the head of an influence arrow are expressed as functions of elements at the tail end of an influence arrow. The user can click on each element to see how it is calculated. Right-clicking an element and choosing "Function Of" or "Effects" allows the user to see dependency relationships with other elements in the model.

Consolidation Flux

Top Fictitious Boundary Layer (i=11)

Inter-Layer
(10 Layers; i varies from 1 to 10)

Bottom Fictitious Boundary Layer (i=0)

Impermeable Foundation
(Single Drainage)
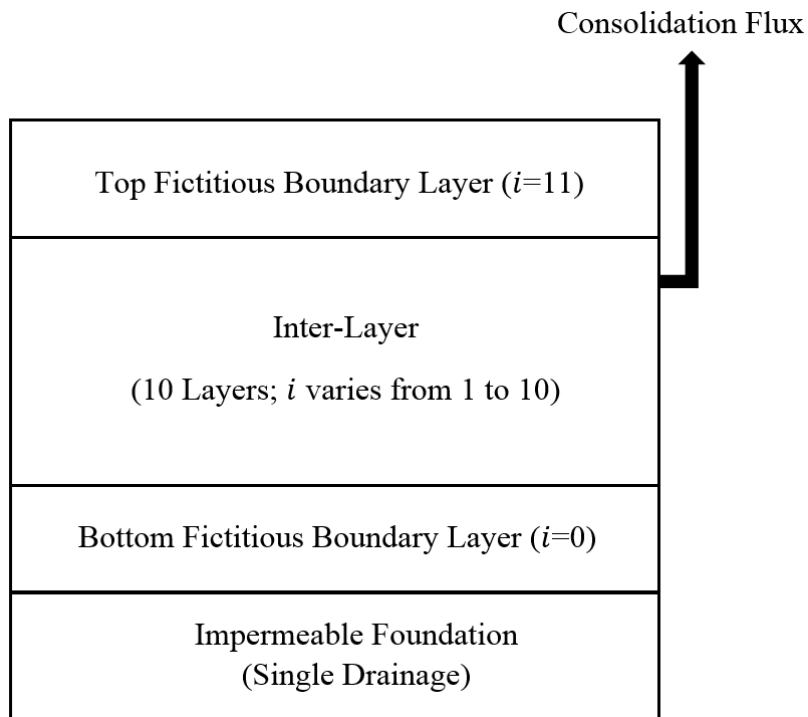
Figure 3-7 Conceptual setup in GoldSim
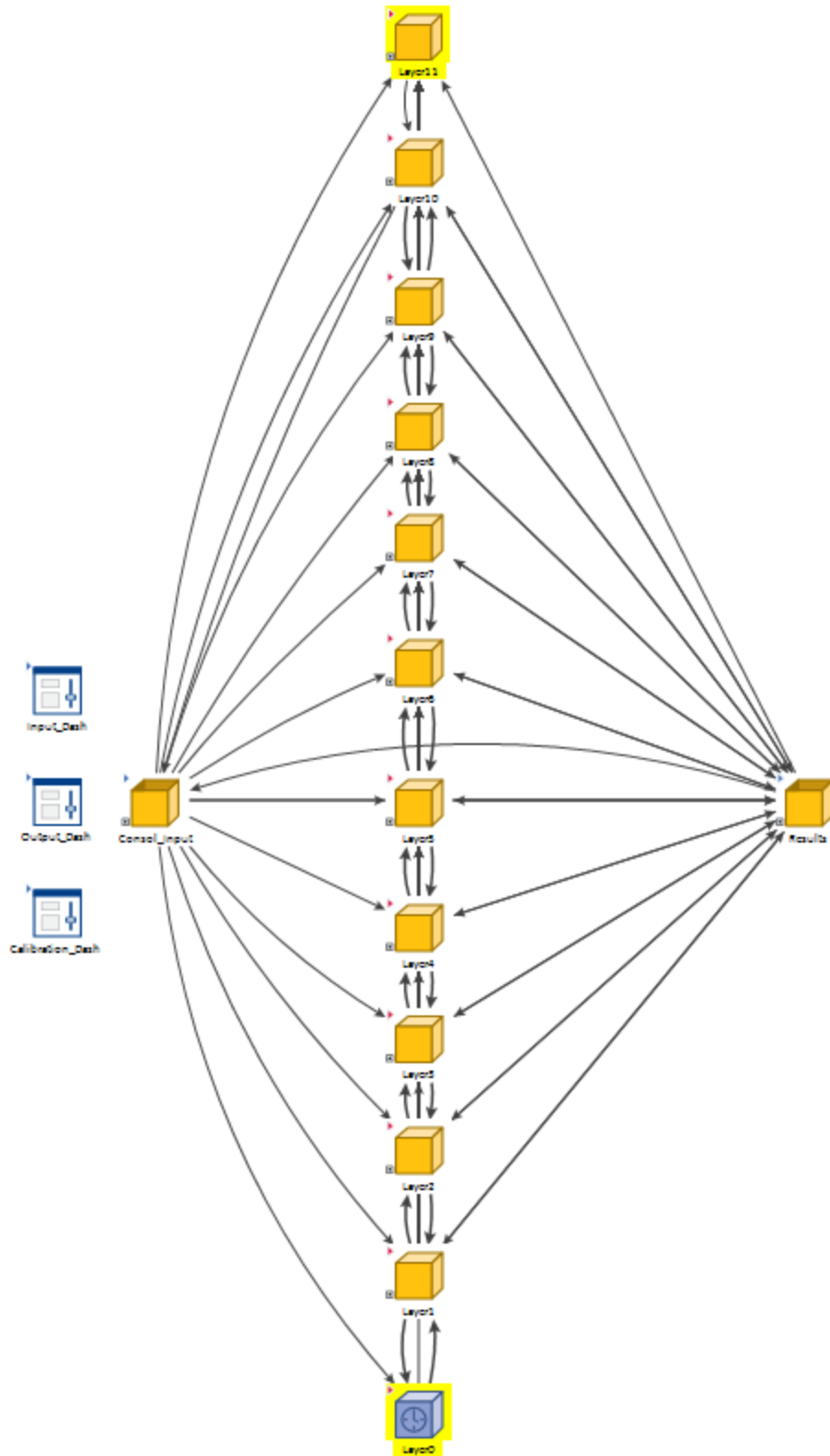
Figure 3-8 Layer container setup in GoldSim; the containers with background highlighted in yellow represent fictitious boundary layers
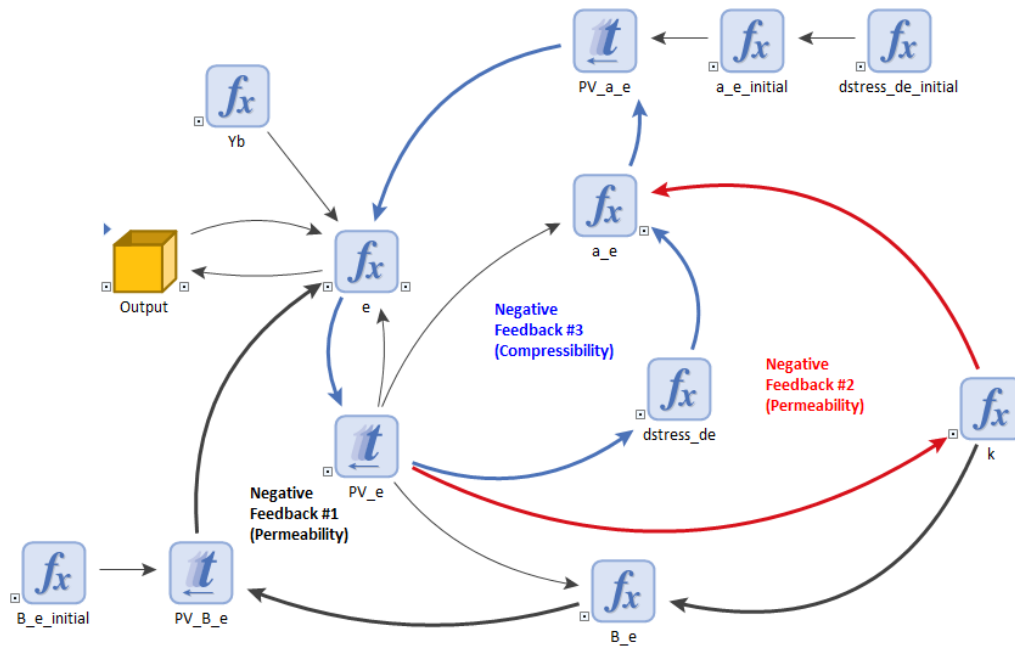
Figure 3-9 Model elements and influence diagrams inside one of the layer containers from Figure 3-8.

3.2.11 User Input Interface

The panel named "Step 1" in Figure 3-10 lists the required parameter inputs prior to running the simulation. For simulation of real-world cases, the power-law curve-fitting coefficients (A, B, C, D) and specific gravity of the solids are experimentally determined material properties. Initial solids content and deposit height are values typically measured in the field.
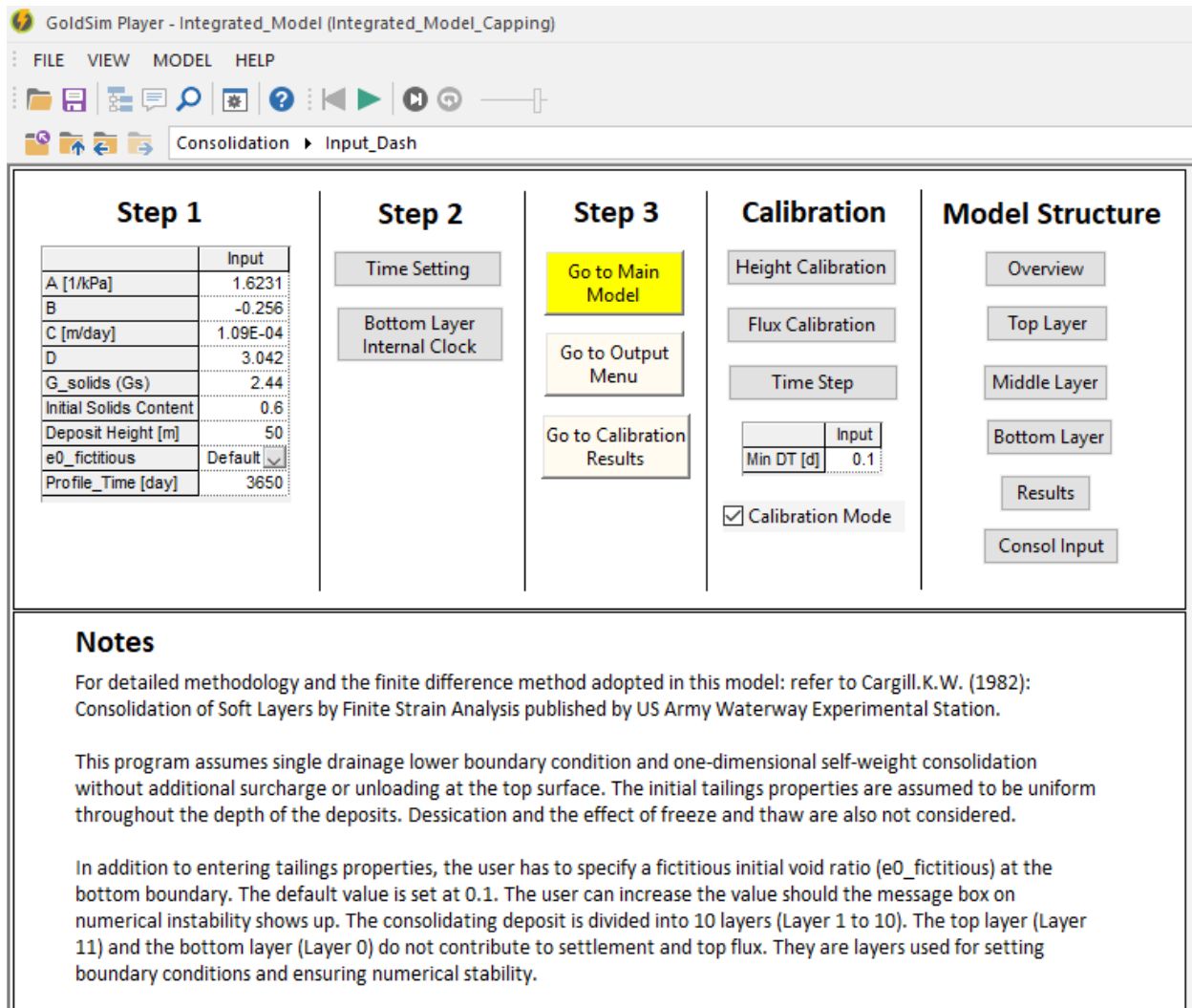
Figure 3-10 Consolidation module user input interface.

3.2.12 Model Validation

The validation cases were carefully chosen to cover three key aspects: behaviour reproduction, extreme condition; and family member tests, as suggested by Sterman (2004). First, the behaviour reproduction test focuses on whether the system is capable of reproducing behaviours exhibited by measured data, both quantitatively and qualitatively. For this test, past experimental and simulated datasets were used. Second, the extreme condition test focuses on whether the system can obey basic physical laws and produce reasonable output under extreme parameter input. For this type of tests, properties from mature fine tailings (MFT) and thickened tailings (TT) were used as their solids contents are at the opposite end of the tailings property spectrum (BGC 2012). The

extreme condition is also reflected in the experimental set up of the selected validation cases. The MFT was tested in a 1 m standpipe over a period of two years while the TT case is tested under the assumption of a 50 m high deposit over a period of 50 years. And lastly the family member test focuses on the ability of the model to simulate behaviours from a wide range of materials. To this end, tailings produced by different commodities, extraction and dewatering technologies were selected for validation.

Table 3-1 outlines parameter input for all validation cases tested for the GoldSim model. For all the cases, global $\Delta t = 1$ day, local $\Delta t = 1$ minute and a dynamic time step of 1 hour were specified. In the absence of experimentally measured data, results from FSCA, a commercial software based on Jeeravipoolvarn (2010), are compared against GoldSim results. Figure 3-11 to 3-14 and Figure 3-15 to 3-18 present validation results for caustic and non-caustic MFT respectively based on the work from Jeeravipoolvarn et al (2017). Figure 3-19 to 3-24 present validation results for phosphate tailings from Florida based on the numerical modeling work of Townsend and McVay (1990) and FSCA. Figure 3-25 to 3-28 present a hypothetical scenario involving self-weight consolidation of cyclone overflow (COF) tailings stream. Figure 3-29 to 3-32 compare FSCA results with GoldSim simulation for a hypothetical 50 m high TT deposit as there is no field measurement available for TT deposits at this thickness.

In general, interface height results from GoldSim qualitatively and quantitatively agreed well with FSCA and experimental data. GoldSim tends to over-estimate excess pore pressure and under-estimate solids content profile when compared to FSCA. However, GoldSim seems to produce slightly better results in terms of solids content than FSCA when compared to experimental data (see Figure 3-12 and Figure 3-16). The GoldSim model also tends to underestimate the amount of upward flux after the primary consolidation phase. If the number of spatial discretization nodes in FSCA was reduced from 200 nodes to the minimally allowed 24 nodes in the software, the end of primary consolidation will align better between GoldSim and FSCA (see Figure 3-14 and Figure 3-18). Finer discretization also creates additional hydraulic gradient that dissipates more excess pore pressure and produces additional upward flux. Therefore, one of the reasons for this discrepancy is the limited spatial discretization in GoldSim. Discrepancies could also be attributed to limited temporal increment, the use of fictitious layers and numerical instability from the use of explicit finite difference method. McVay et al (1986) showed that regardless of coordinates,

methods and numerical schemes, all solutions to the governing equations from Gibson et al (1967) are identical, satisfying the same equilibrium and constitutive equations. Therefore, any observed discrepancies are due to differences in the numerical schemes such as spatial discretization, time step, and choice of dependent variables (Townsend and McVay 1990).

Table 3-1 Parameter input for validation cases.

Validation Case	A (kPa)	B	C (m/day)	D	G_s	Initial SC
1 m Caustic MFT	3.12	-0.219	2.00E-11	3.90	2.48	0.22
1 m Non-Caustic MFT	3.00	-0.234	6.94E-11	3.70	2.45	0.22
9.6 m Phosphate Tailings	7.72	-0.220	2.50E-07	4.65	2.82	0.16
1.284 m Cycloned Over Flow (COF)	3.18	-0.196	3.52E-06	4.23	2.52	0.20
50 m Total TT	1.62	-0.256	8.64E-05	3.40	2.44	0.60
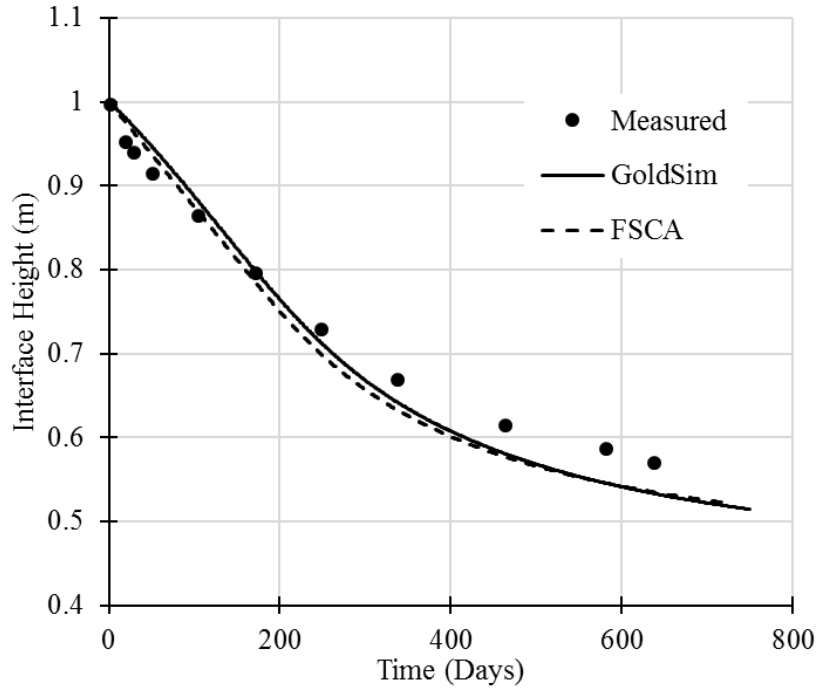
Figure 3-11 Inter-face height comparison for caustic MFT.
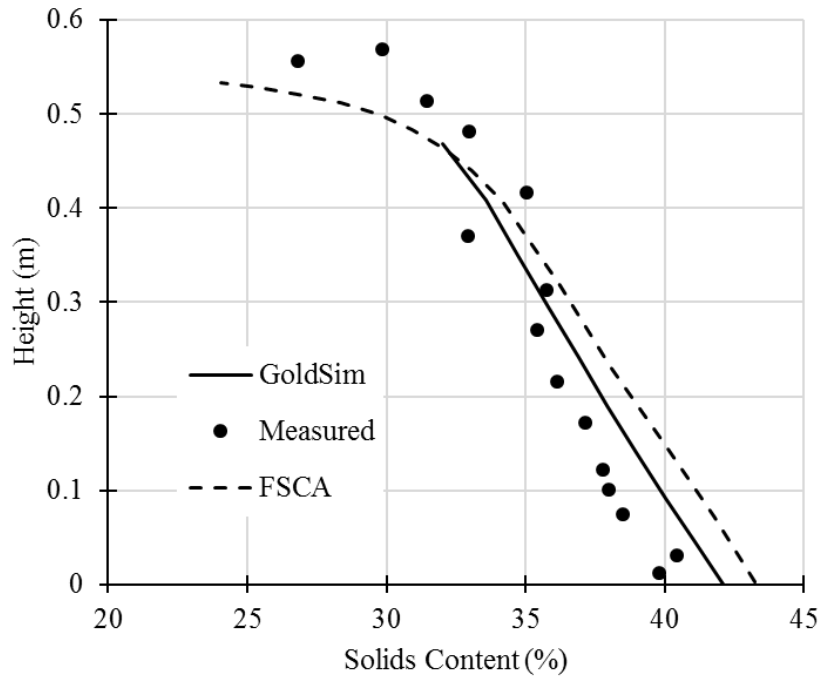
Figure 3-12 Solids content profile comparison at 641-day for caustic MFT.
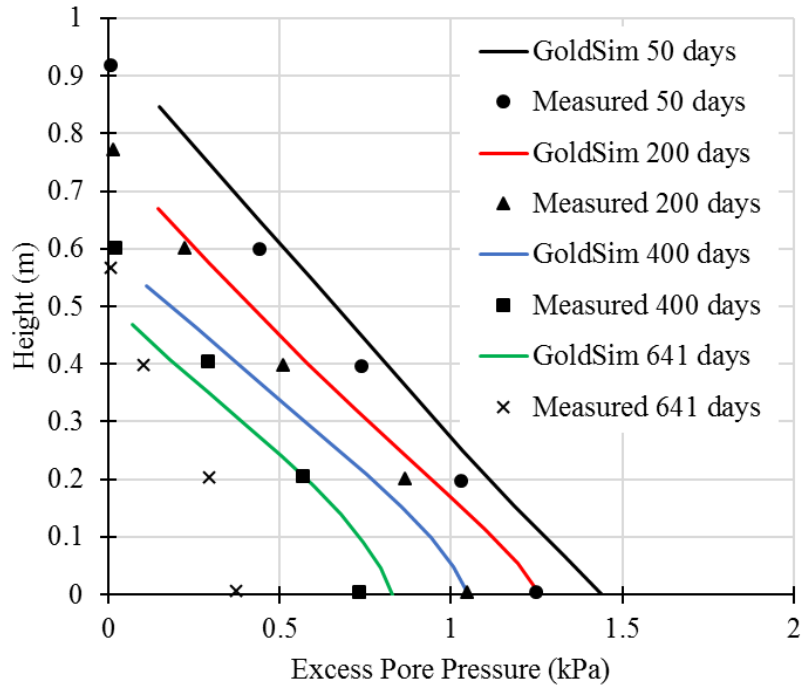
Figure 3-13 Profile comparison of excess pore pressure for caustic MFT.
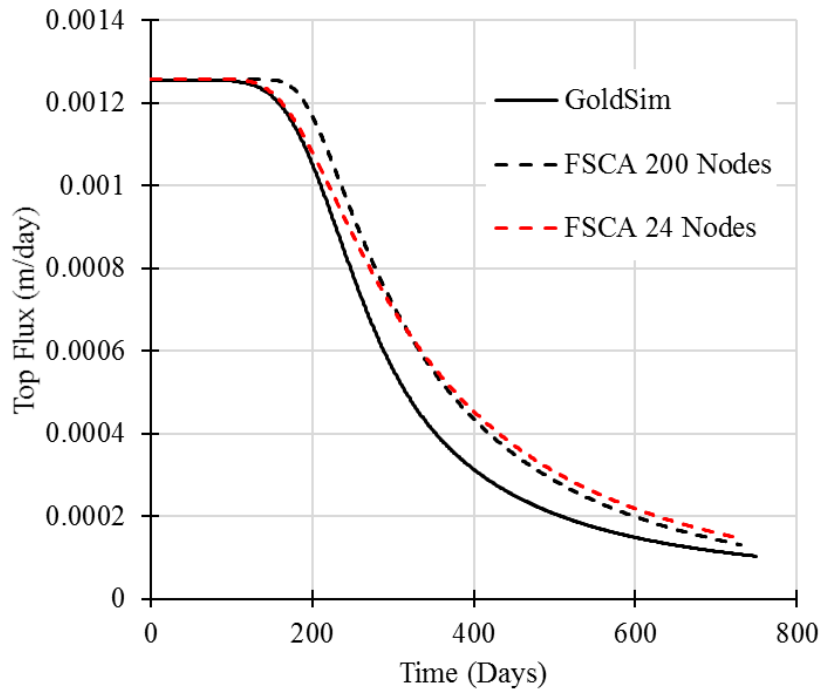
Figure 3-14 Upward flux comparison for caustic MFT.
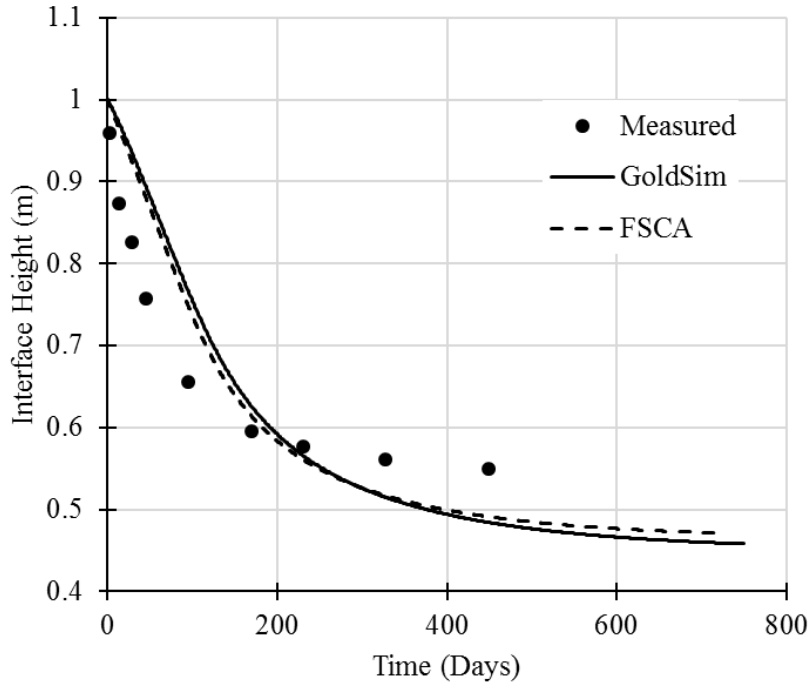
Figure 3-15 Interface height comparison for non-caustic MFT.
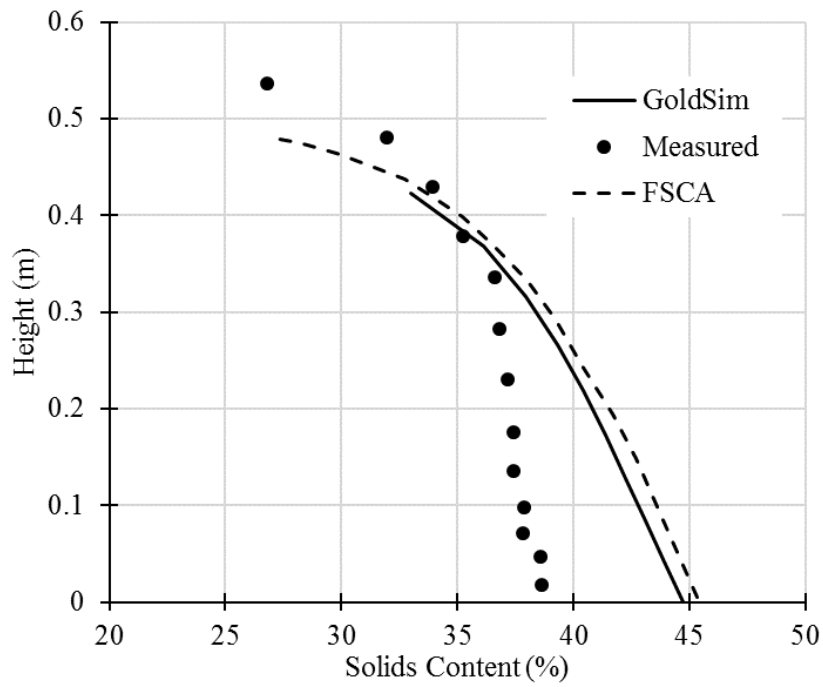
Figure 3-16 Comparison of solids content at 446-day for non-caustic MFT.
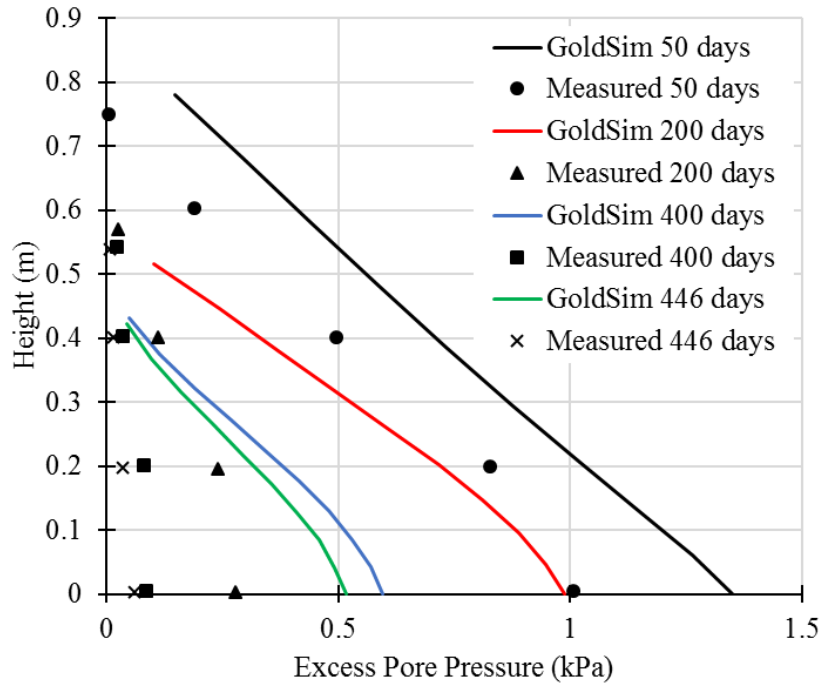
Figure 3-17 Comparison of excess pore pressure for non-caustic MFT.
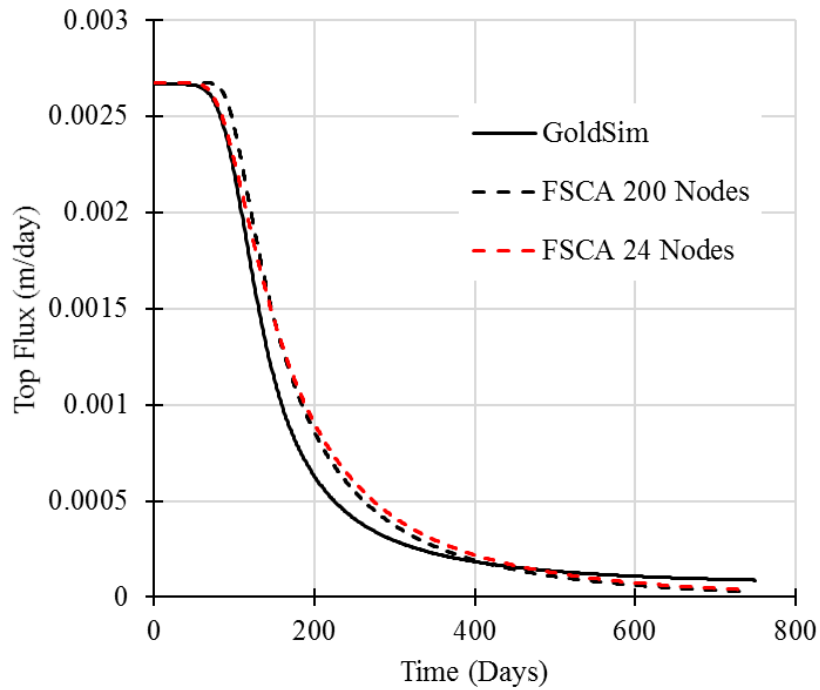
Figure 3-18 Upward flux comparison for non-caustic MFT.
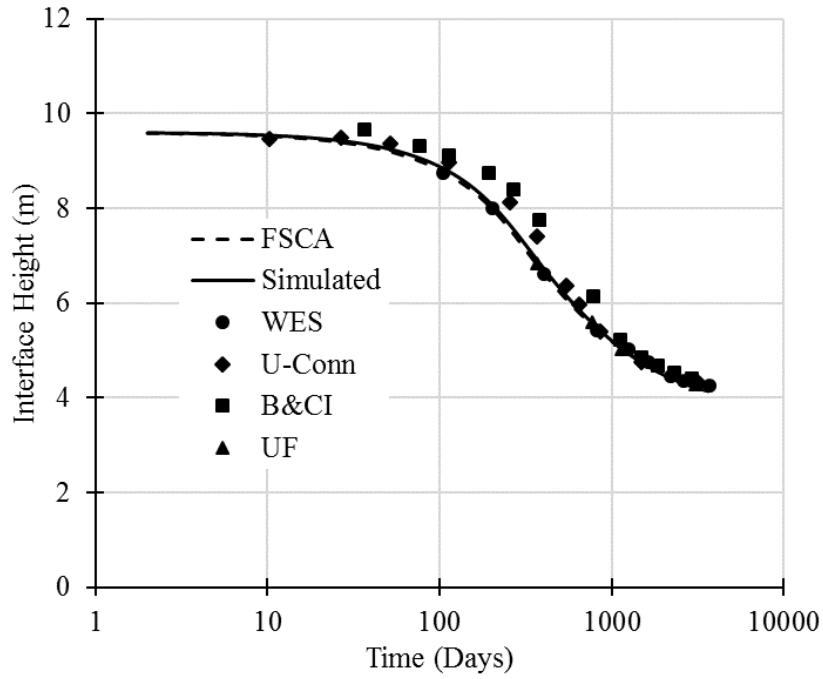
Figure 3-19 Inter-face height comparison for phosphate tailings
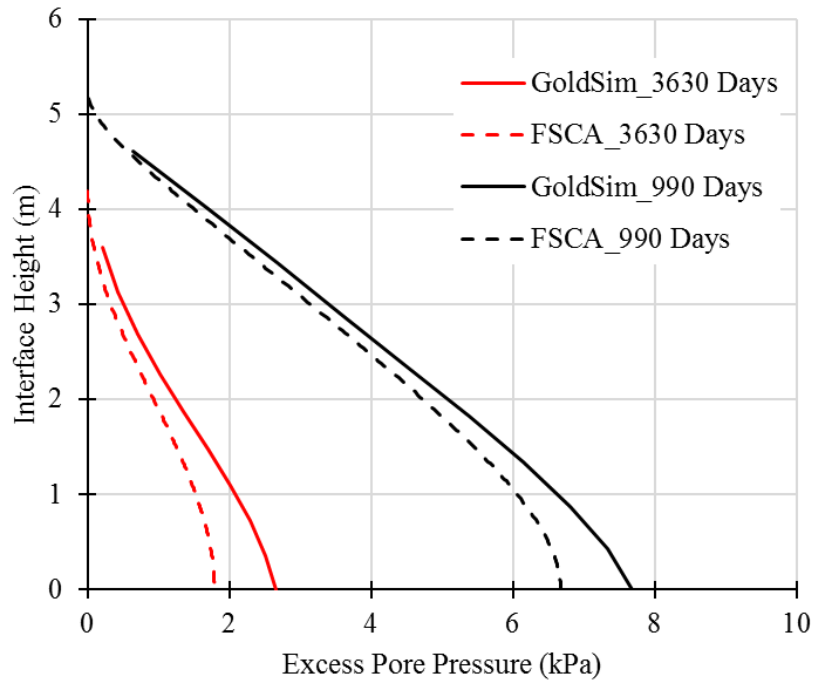
Figure 3-20 Excess pore pressure comparison for phosphate tailings
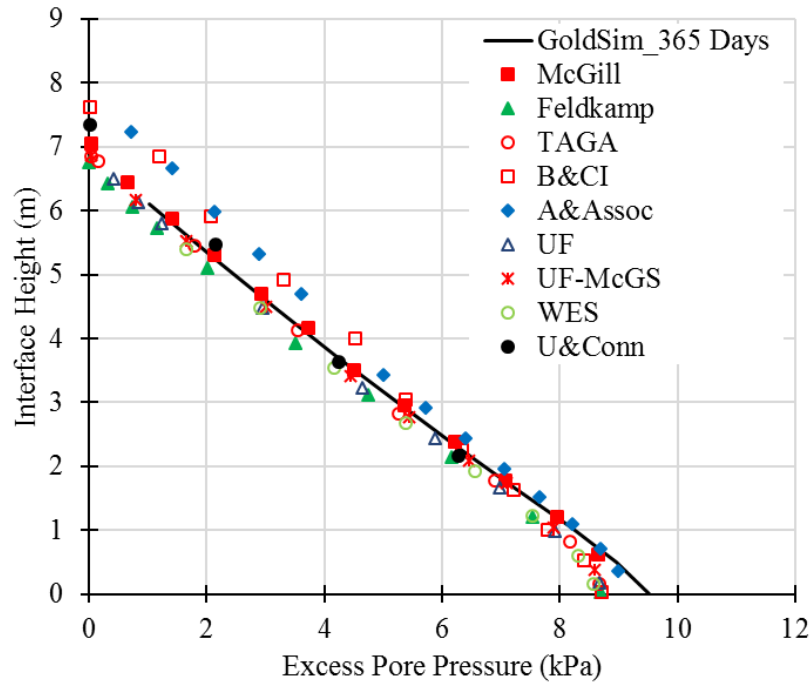
Figure 3-21. Comparison of excess pore pressure between the GoldSim model and various numerical methods summarized in Townsend and McVay (1990)
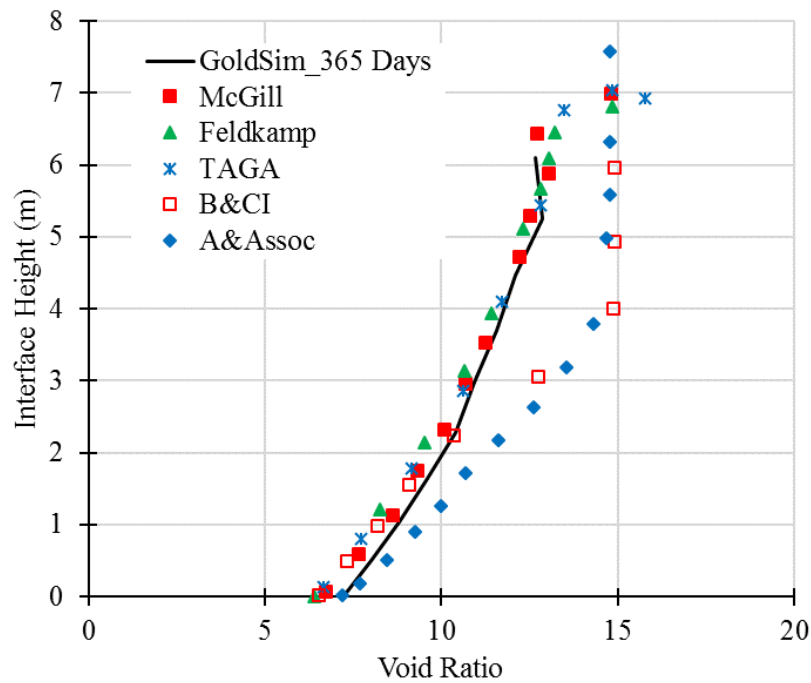
Figure 3-22. Comparison of void ratio between the GoldSim model and various numerical methods summarized in Townsend and McVay (1990)
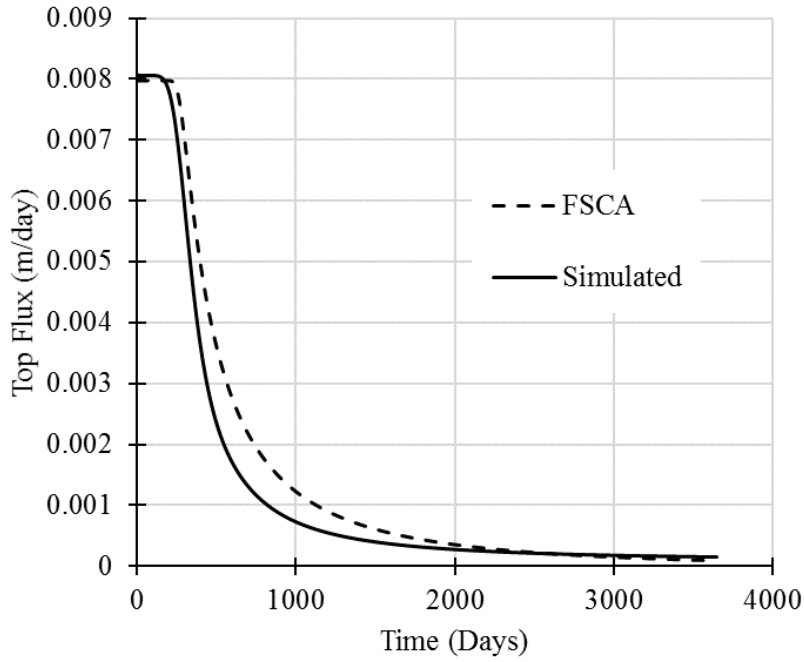
Figure 3-23 Upward consolidation flux comparison for phosphate tailings.
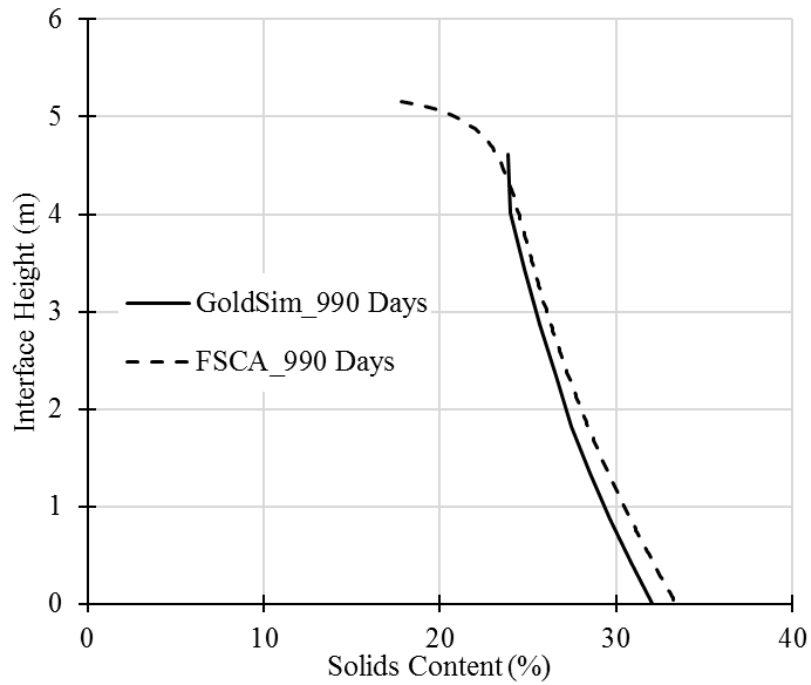
Figure 3-24 Solids content comparison for phosphate tailings.
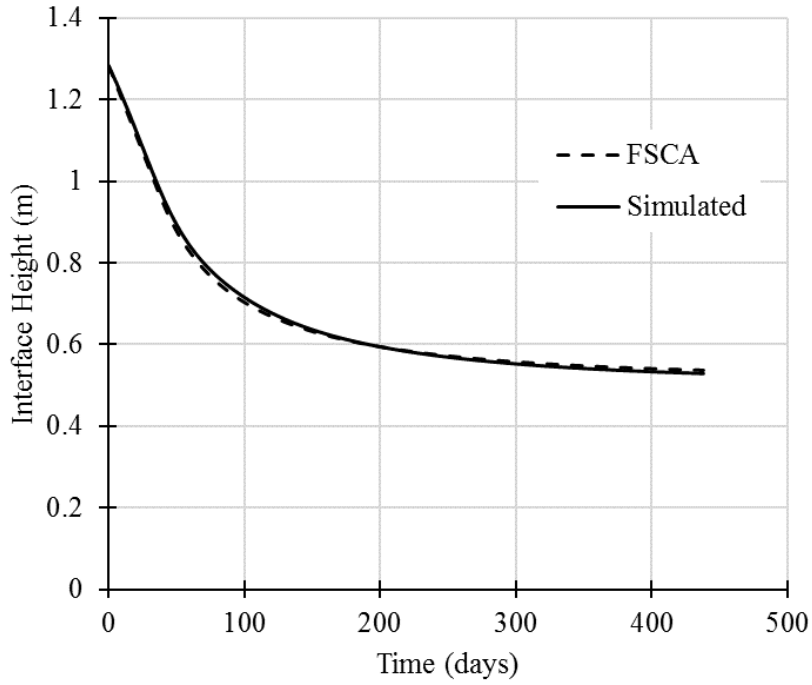
Figure 3-25 Interface height comparison for COF tailings.
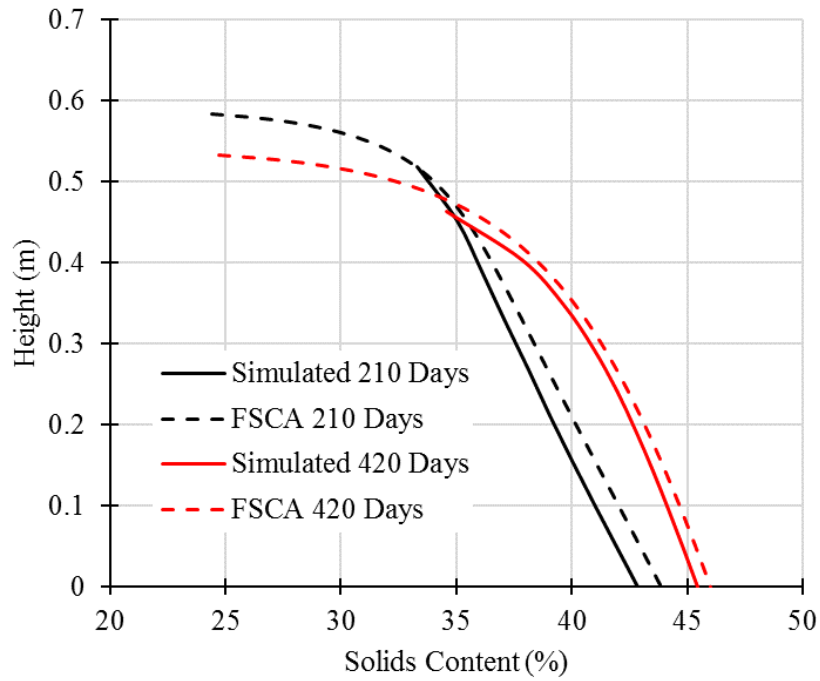
Figure 3-26 Solids content comparison for COF tailings
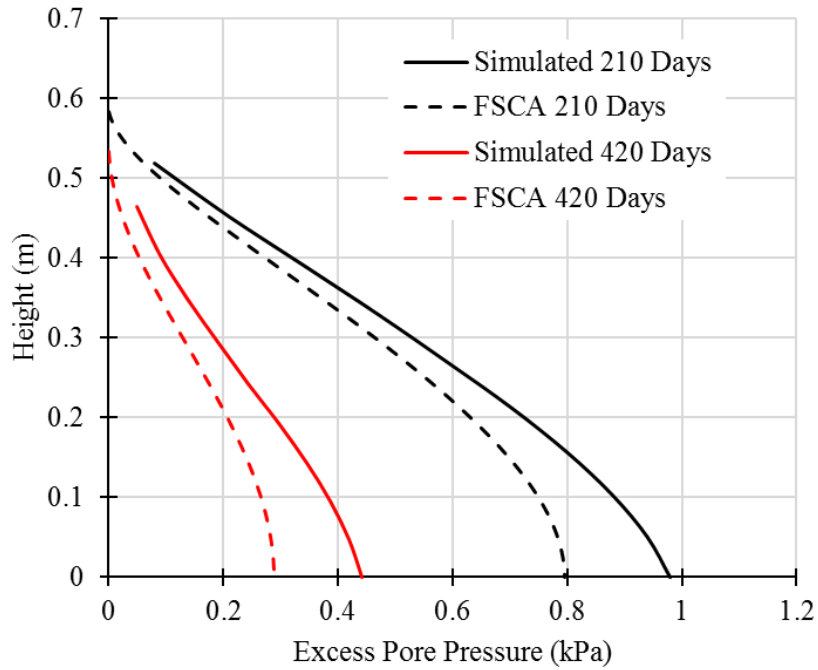
Figure 3-27 Excess pore pressure comparison for COF tailings.
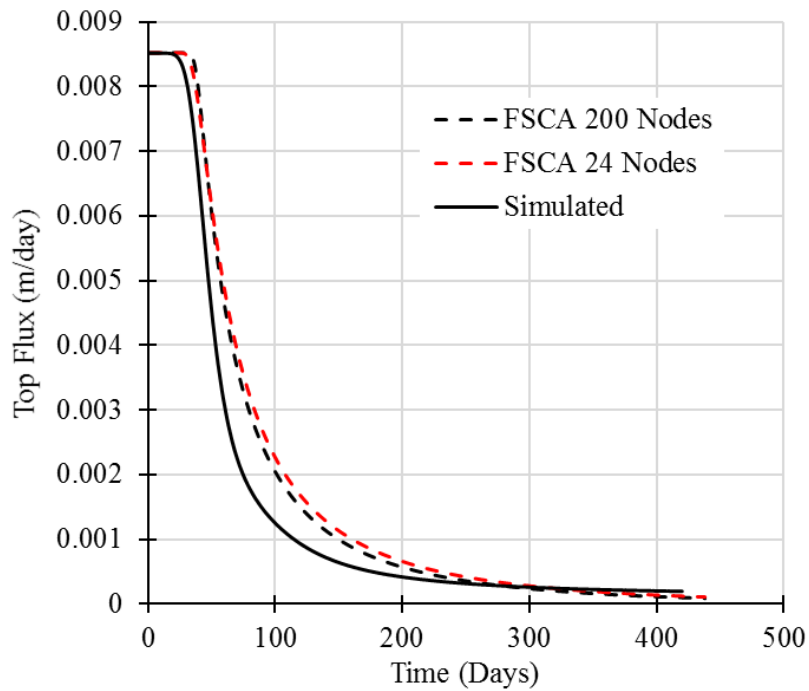
Figure 3-28 Upward flux comparison for COF tailings.
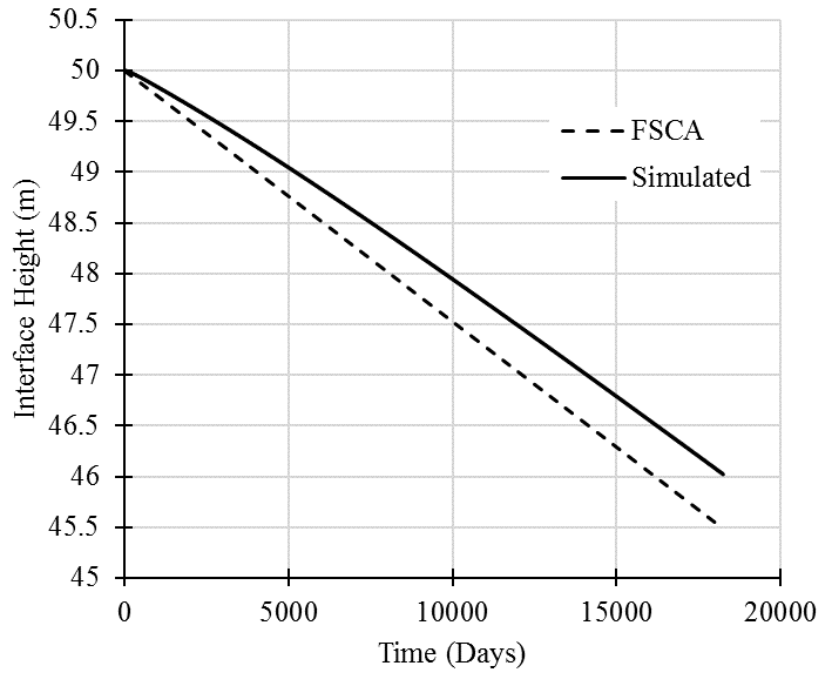
Figure 3-29 Interface height comparison for TT
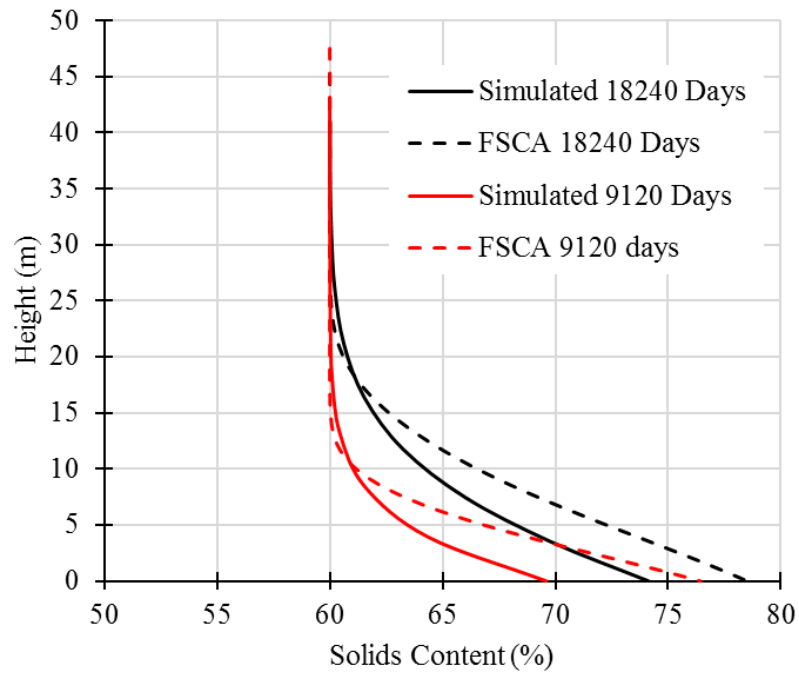
Figure 3-30 Solids content profile comparison for TT
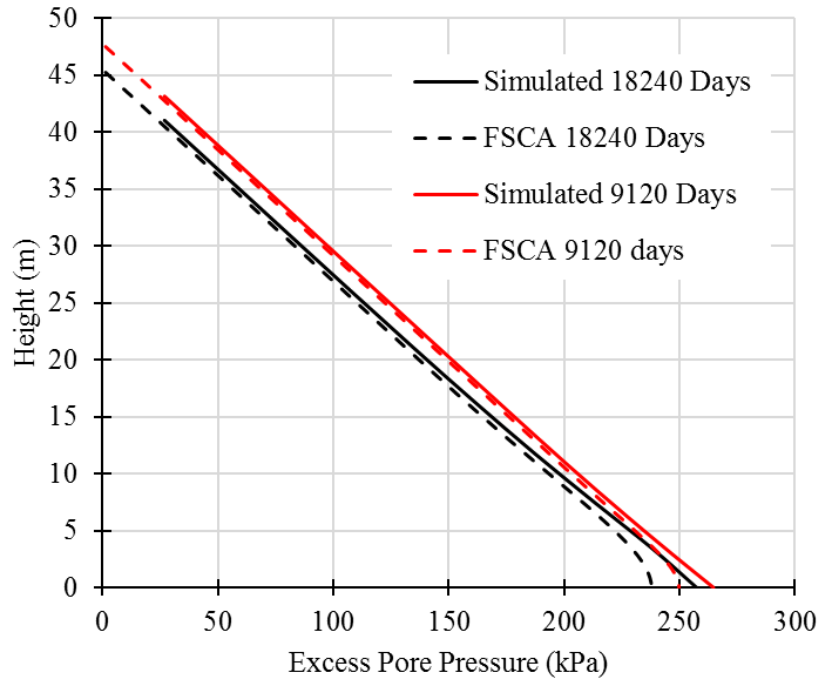
Figure 3-31 Excess pore pressure comparison for TT
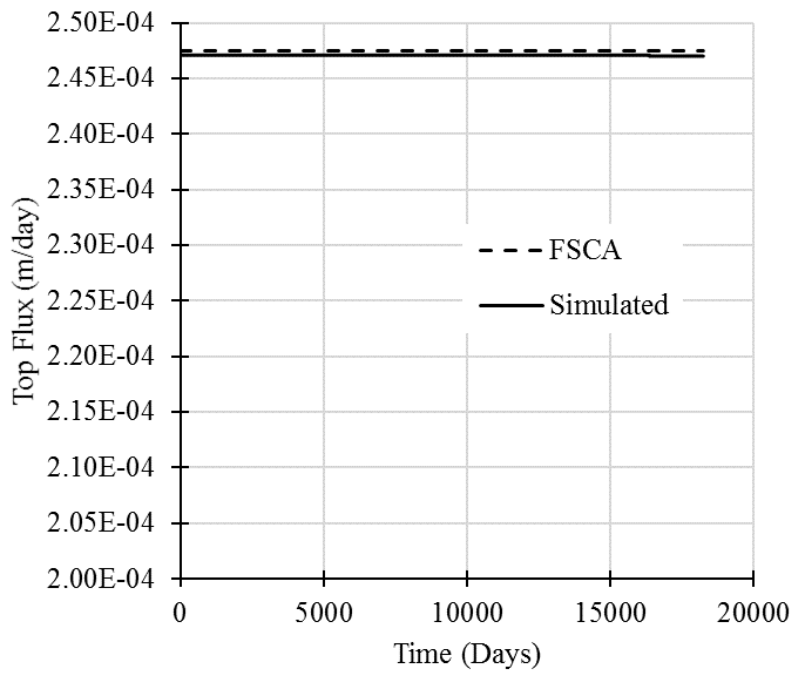
Figure 3-32 Upward flux comparison for TT

3.3 STOCHASTIC MODEL SETUP IN GOLDSIM

Recently, risk-based approaches in tailings management have been gaining acceptance and popularity in the industry (Mining Association of Canada 2017). A SD-based modeling approach provides a cost-effective platform to qualitatively and quantitatively capture the probability of occurrence, which is one of the components in any risk assessments (Vick 2002). SD-based models can be easily switched to stochastic models by converting deterministic input to probabilistic input and setting up Monte Carlo simulation parameters.

One of the main advantages in adopting SD-based approach is the ability to simulate multiple scenarios using Monte Carlo techniques. Once the deterministic model has been calibrated and validated, a stochastic simulation can be easily set up by assigning probabilistic distributions to controlling parameters and slightly modifying the model structure.

To demonstrate the capability of SD models to propagate input uncertainties to output values, the objective of the stochastic model is to evaluate uncertainties in the magnitude of consolidation settlement at the end of 10-year period. A case study involving quiescent consolidation of the phosphate tailings is described below.

3.3.1 Monte Carlo Simulation Techniques

The Monte Carlo technique uses randomly generated values from probabilistic input to create multiple simulation runs or realizations. Since the input is in the form of a probability distribution, the output is also in the form of a probability distribution, as part of descriptive statistics of the propagated realization output. The accuracy of Monte Carlo simulation depends on the number of realizations with larger number of realizations leading to better accuracy and more complete representation of the output probability distribution. More detailed coverage of Monte Carlo techniques as applied in geotechnical engineering can be found in Baecher and Christian (2003) and Macciotta (2013).

3.3.2 Epistemic vs Aleatory Uncertainty

In stochastic simulation models, it is sometimes useful to separately model uncertain or epistemic parameters as well as variable or aleatory parameters (Baecher 2016). Uncertainty in epistemic parameters represents lack of knowledge that can be reduced through additional investigation or research. This lack of knowledge can come from insufficient laboratory and field investigation, theoretical simplifications and assumptions. On the other hand, aleatory parameters represent inherent randomness or uncertainties that cannot be reduced or eliminated.

3.3.3 Nested Monte Carlo Setup

Input parameters controlling the quiescent consolidation process can be divided into epistemic and aleatory category. This can be accomplished by using a nested Monte Carlo technique (Baecher 2016). In a nested or two-dimensional Monte Carlo set-up, probabilistic input in the outer model represents epistemic uncertainty due to lack of knowledge while those in the inner model represents aleatory uncertainty due to inherent uncertainties in the system.

In the simulation, the inner model represents variation of compressibility (A1 and B1) and permeability (C1 and D1) due to aleatory uncertainty which, by definition, cannot be reduced or eliminated. The outer model represents lack of experimental and field data. Figure 3-33 illustrates how the nested Monte Carlo can be set up by a Sub-Model element in GoldSim. The Sub-Model element represents a separate inner model within the outer model. The user can specify its own simulation setting just like in the outer model (GoldSim 2018). Af, Bf, Cf, and Df in the outer model provide values to the mean values for A1, B1, C1 and D1 which are themselves probabilistic distributions in the inner model. Since both the inner and outer model carry out Monte Carlo simulation, running the outer model multiple times creates a distribution of distribution for any output from the inner model.

The model assumes the absence of natural or aleatory randomness in the material properties of the tailings deposit due to the following reasons: 1) the effect of geomorphology and climate on compressibility and hydraulic conductivity parameters are limited to the surface; 2) the stochastic model evaluates uncertainties during the closure phase when the deposition process has taken place and stopped; and 3) the stochastic model is not intended to simulate spatial uncertainties in solids content, fines distribution and beach slopes during the active deposition stage. Instead, the aleatory

uncertainty in this case is assumed to arise from the limitation of site characterization. In reality, financial and logistical constraints restrict borehole spacing and maximum coverage of the site investigation program. Irreducible limitations of testing equipment and site investigation tools also contribute to the aleatory uncertainty in site characterization. Thus, the probabilistic input for the inner model captures the aleatory uncertainty arising from irreducible financial and technical constraints.
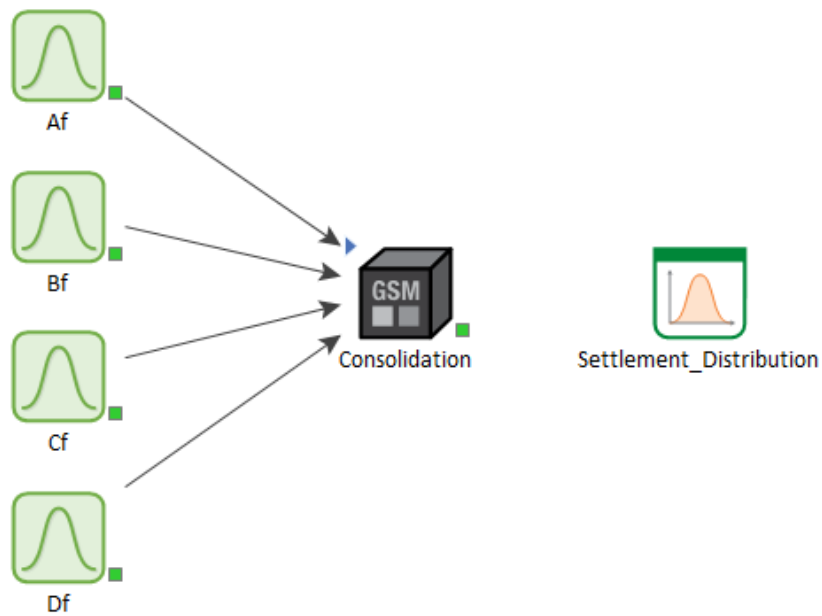
Figure 3-33 Nested Monte Carlo setup using a Sub-Model element "Consolidation" in GoldSim (viewed from the outer model).

3.3.4 Probabilistic Input

The 1 m caustic MFT in Table 3-1 is used as a case study to demonstrate the stochastic approach. Simulation duration, boundary and initial conditions remain the same as the deterministic case.

Figure 3-34 is a screenshot of GoldSim setup for the compressibility parameter A1 in the inner model. Probabilistic input for compressibility parameter A and permeability parameter C uses Beta-PERT distribution due to lack of statistical data and insufficient sample size from which statistically significant inference can be drawn. Parametrically, changes in compressibility

parameter A and permeability parameter D have less effect on the time to 90% consolidation T_{90} than B and D (Rourke and Hockley 2018). However, parameter A is more influential in terms of the magnitude of settlement height based on the sensitivity analysis (see Figure A1-10). Since the objective is to evaluate uncertainties in the magnitude of settlement instead of T_{90}, deterministic values are used for B and D.

Probabilistic distributions assigned to each input can be based on statistical summary of testing and field data or based on expert opinions (Vick 2002). In this case, the reducible epistemic uncertainty is assumed to deviate 30% from the most likely value (see Table 3-2). As mentioned before, aleatory or inherent uncertainty is assumed to be based on the irreducible financial, logistical and technical limitation of site investigation of the tailings deposit. Parameters in the inner model are assumed to deviate only 10% from values sampled from the outer distribution (see Table 3-3). Values in the "Most Likely" column of Table 3-2 come directly from the deterministic parameter input of phosphate tailings in Table 3-1. Both deviation values are chosen arbitrarily for demonstration purposes. In practice, the deviation values should be based on the range of values from elicitation of expert opinions, testing and field data.

In the nested Monte Carlo simulation, the outer model is set up as a static model without incorporating time duration and time stepping while the deterministic model is converted to a stochastic inner model. Special setup in GoldSim are required in order to properly display nested Monte Carlo results (see Figure A1-9). Latin Hypercube Sampling method was used due to its balanced sampling of probability space. (McKay et al. 1979). Three scenarios, consisting of increasing number of nested Monte Carlo runs, were simulated (see Table 3-4).

Table 3-2 Probabilistic input for the outer model (epistemic uncertainty or reducible uncertainty).

Parameter	Distribution	Most Likely	Minimum	Maximum
Af (kPa)	Beta-PERT	7.72	5.40	10.04
Bf	Deterministic	-0.22	-0.22	-0.22
Cf (m/day)	Beta-PERT	2.53E-07	1.77E-07	3.29E-07
Df	Deterministic	4.65	4.65	4.65

Table 3-3 Probabilistic input for the inner model (aleatory uncertainty or inherent uncertainty due to technical, financial and logistical limitation).

Parameter	Distribution	Most Likely	Minimum	Maximum
A1 (kPa)	Beta-PERT	Af	0.9*Af	1.1*Af
B1	Deterministic	Bf	Bf	Bf
C1 (m/day)	Beta-PERT	Cf	0.9*Cf	1.1*Cf
D1	Deterministic	Df	Df	Df
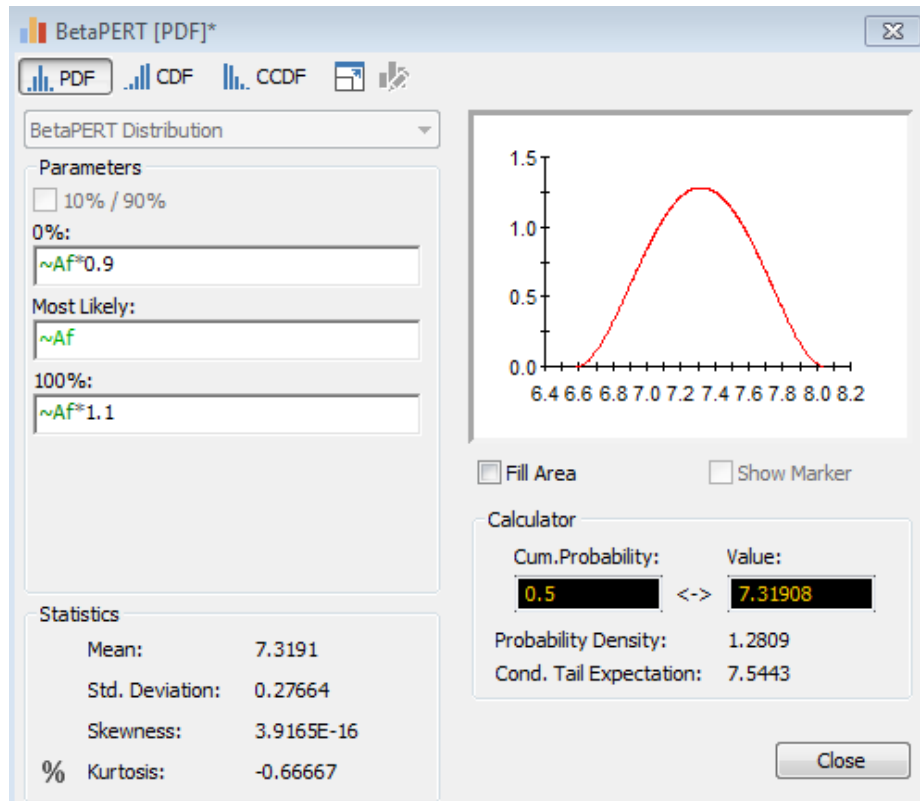
Figure 3-34 Sample input setup for compressibility parameter A1 in the inner model

3.3.5 Results and Discussion

A probability-based settlement prediction will provide further input to future risk assessment exercises. By creating a distribution result element in the outer model, the probability of not exceeding certain magnitude of settlement is known. Each realization simulated from the outer model produces a distribution type of result. As an example of how a distribution of distributions is presented, Figure 3-35 shows multiple Complementary Cumulative Distribution Functions (CCDFs) viewed from the outer model as the result of epistemic uncertainty. The most commonly used output is the CCDF in Figure 3-36, which incorporates both epistemic and aleatory uncertainty. In this case, three scenarios were constructed from aggregating a total of 25, 100 and 400 Monte Carlo runs. The 25 Monte Carlo runs consisted of 5 realizations in the outer model for each of the 5 realizations in the inner model. The 100 Monte Carlo runs consisted of 10 realizations in the outer model for each of the 10 realizations in the inner model. Similarly, the 400 Monte

Carlo runs consisted of 20 realizations in the outer model for each of the 20 realizations in the inner model.

The total model run-time increased substantially with increasing number of realizations (Table 3-4). Fewer realizations may save time but will compromise the adequacy of sample coverage as evident in the 25-realization case. Higher number of realizations provide sufficient sampling resolution of the distribution function but may not be efficient in terms of model run-time. Modelers and users need to strike the right balance between sampling resolution and model run-time.

From visual inspection, the shape of the CCDF curve changed dramatically when the number of realizations is increased from 25 to 100, as evident in Figure 3-36. The conclusion drawn from the CCDF also changed as a result. For example, under 25 realizations, the probability of exceeding a consolidation settlement of 5.5 m is approximately 30%. Under 100 realizations, the probability is now at approximately 47%, a significant increase that may affect the calculation of risks. However, under 400 realizations, the probability is reduced slightly to approximately 45%, a change that may have little effect on the calculation of risks.

Table 3-4 Summary of Monte Carlo scenarios

Total Number of Realizations	Inner Model Realizations	Outer Model Realizations	Model Run-Time*
25	5	5	48 minutes 55 seconds
100	10	10	3 hours 22 minutes 41 seconds
400	20	20	13 hours 26 minutes 16 seconds

*Using an Intel i7 CPU duo core M620 at 2.67 GHz
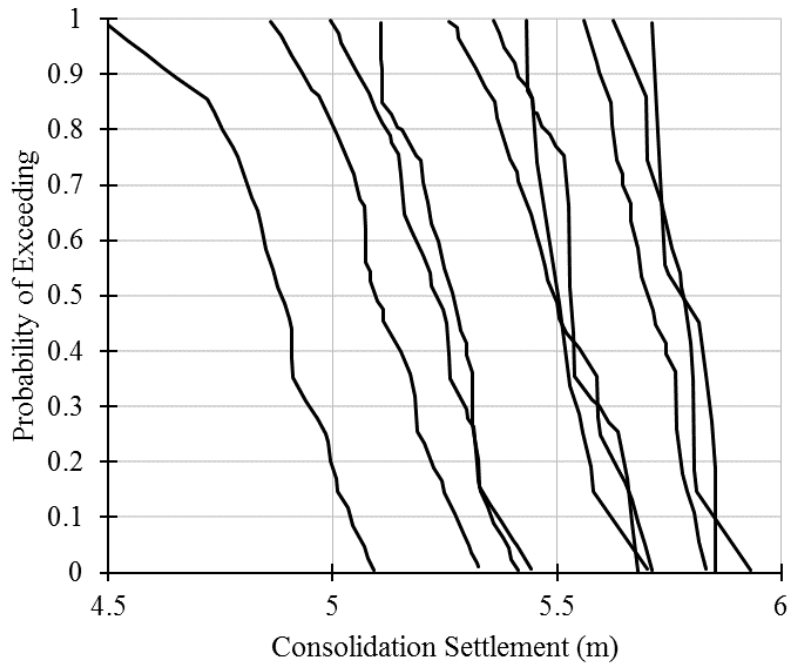
Figure 3-35 Examples of "Distributions of Distributions" as viewed from the outer model after a total of 100 realizations; each solid line represents a CCDF sampled from the inner model.
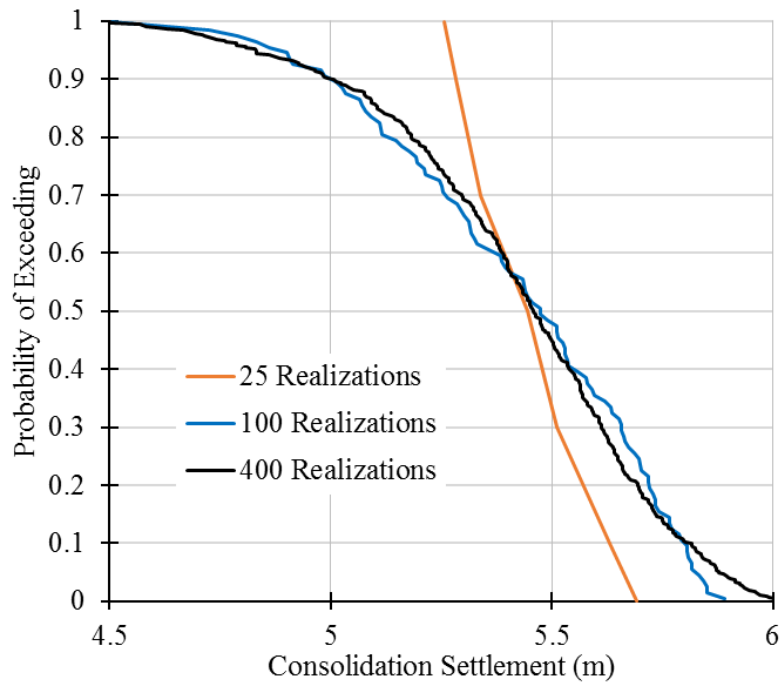
Figure 3-36 Aggregated CCDF incorporating both epistemic (outer model) and aleatory uncertainty (inner model)

3.4 Conclusions

Consolidation of tailings deposit plays an important role in closure planning. A SD model was developed and tested as the foundation for further stochastic simulation of tailings consolidation process. SD-based methods make all components of the numerical solution visible and easy to modify. This transparency also makes SD-based tools an ideal platform for communication and education. The developed model shows that system-dynamics is a viable approach provided that spatial variability and constitutive relationship can be reasonably simplified. The SD-based consolidation model demonstrated successful simulation of various types of tailings under different settings. Despite the discrepancies observed between simulated and experimental values, the behaviour and trend generated by the model are consistent with experiment data and predictions made by commercial software. Therefore, the consolidation model should only be used as a high-level comparison and predictive tool. Any detailed design or further analyses should be handled by more rigorous tools based on the large strain consolidation theory. Additional modification is required to extend the model's applicability in partially-drained and unsaturated conditions. The calibration process can also be automated to reduce computing time and increase numerical stability.

4 DEVELOPMENT OF UNSATURATED FLOW SUB-MODEL FOR COARSE SAND TAILINGS CAP-SUBSTRATE INTERACTION

4.1 PROBLEM DEFINITION

In Alberta, there have been no successful precedents in capping deep fines-dominated tailings deposits. Tailings storage facilities at some oil sands mines are due for closure in the next decade. Using coarse sand tailings (CST) as the intermediate cap material between tailings substrate and vegetation cover has been proposed in several regulatory applications (Imperial, 2016; Shell, 2016 and Suncor, 2017). Most studies in the past have focused on the interaction between overburden waste and soil cover. Therefore, the importance of developing a simulation tool to understand the interaction between tailings substrate and soil cover cannot be understated.

The unsaturated flow sub-model will focus on the tailings cap layer, specifically fluid transport and interaction between climatic flux at surface and upward consolidation flux from the underlying tailings. The final model consists of the consolidation model from Chapter 3 and the unsaturated flow sub-model based on an earlier SD infiltration and drainage model developed by Huang et al (2011a). SD algorithms and functional relationships are implemented in the GoldSim simulation environment with further modifications and improvements of the original Huang et al (2011a) model. The following sections describe the development and validation of the unsaturated flow sub-model.

4.2 KEY ASSUMPTIONS

Simplification and assumptions are required due to lack of field data in capping deep soft tailings in Alberta. The simulation model assumes that the tailings cap layer is in a vadose zone where Darcy's Law describes the water transport processes, both saturated and un-saturated. In this study, except for surface evaporation, only advection-based water transport process is simulated within the soil layers since the influence of diffusion-based mechanism is limited to the tailings-cap interface where high concentration gradient may exist (Kessler et al. 2010). Typically, vertical pressure gradient and the force of gravity control the dynamics of the water transport processes. Ellsworth and Jury (1991) also concluded that laboratory column experiment, where one-dimensional vertical flow is the dominant process, can adequately describe field-scale solute transport processes for structureless loamy sand. Butters et al (1989), Kessler et al (2010) and

Romano et al (1998) expressed similar views that lateral water flow can be generally neglected, and that vertical gradient controls the flow process. Therefore, the model is one-dimensional without considerations for lateral flow and anisotropy.

To address spatial variations in material properties, the model employs a finite difference approach. The capping layer is discretized into 18 sub-layers (see Section 4.3.1). For numerical expediency, each discretized sub-layer is assumed to be homogenous throughout the user-defined thickness.

Zero volume change may be an adequate assumption for coarse-grained material (Zhang 2017). Since the scope of modelling is limited to the coarse sand tailings (CST) cap, volume change due to suction can be neglected for the capping layer. The validation cases and case study assume the absence of load-induced volume change (i.e. no surcharge load on top of the CST cap). Likewise, the effect of unloading due to erosion is also neglected.

In the GoldSim model, the hysteresis effect is ignored. Hysteresis in the Soil Water Characteristic Curves (SWCC) refers to the non-unique relationship between water content and matric suction and its dependency on the sequence of wetting and drying (Fredlund et al, 2012). Since volumetric water contents from the drying curve corresponds to maximum suction values, the actual soil water storage and movement during wetting events may be inaccurate using the non-hysteresis SWCC (Bashir et al. 2015). Huang et al (2011a) and Huang et al (2013) used the non-hysteresis SWCC of sand to simulate infiltration and drainage process and produced satisfactory matches with measured data. To account for the hysteresis effect, the wetting curve of SWCC is typically assumed to be a lateral, parallel shift of the drying curve (Fredlund et al. 2012). Though this lateral shift can be empirically derived, it is the smallest for sand when compared to clay and silt (Fredlund et al. 2012). The GoldSim model aims to simulate water movement in the CST material which consists of primarily fine sand. Furthermore, studies have shown that hysteresis has limited influence on hydraulic conductivities (Huang et al. 2011a). For these reasons, the drying curve of the SWCC is used to simulate water movement in the CST layer.

The combined model is intended as a high-level screening tool. The main objective is to examine behaviours at a macroscopic, system level, not focus on numerical values produced by those behaviours. Therefore, the top boundary conditions use simple water balances and water

accounting. Precipitation is a lumped parameter that include both rainfall and snowmelt. Evaporation is dependent on mean air temperature, surficial suction and potential evaporation. For the surficial Layer 1, the maximum allowable infiltration rate is controlled by the saturated hydraulic conductivity of the layer. It is assumed that there is no water ponding at the surface. No surface run-off will be produced unless the infiltration rate exceeds the saturated hydraulic conductivity of the surficial layer.

Finally, the suction pressure in the model refers to the matric suction pressure as $u_a - u_w$. The air pressure is typically assumed to be atmospheric thus u_a is zero (Fredlund 2012). Osmotic suction and osmotic flow due to concentration gradient of dissolved solids are not included in the model.

4.3 MODEL SELECTION AND SETUP

The following SD models developed for simulating soil water storage are evaluated as the candidate for integration with the consolidation sub-model from Chapter 3. Lee (1993) proposed using CLD and SFD to conceptualize hydrological processes. Elshorbagy et al (2005) and Julta (2006) used a combination of empirical and physically-based formulation in their waste cover model with greater emphasis on the empirical formulation. The model needs at least 7 parameters to be calibrated (Julta 2006). Furthermore, the calibration process requires site-specific data. Nguyen (2014) used the water balance approach to model soil moisture content in his integrated modelling of an agricultural production system. In comparison, the saturated-unsaturated flow model by Huang et al (2011a) adopted a primarily physically-based approach. The model requires only one parameter, saturated hydraulic conductivity K_s of the soil cover, to be calibrated against field data. The physics-based approach is less site-specific and more flexible especially when there is a lack of field data. Therefore, the SD model based on Huang et al (2011a) is chosen as the basis for further development. Additional details on the field program which Huang et al (2011a) used for calibration can be found in the companion papers: Huang et al (2011b and 2015) and Zettl et al (2011). For detailed model setup in the GoldSim software, refer to Appendix 2.

4.3.1 Model Conceptualization

The unsaturated flow sub-model follows the same set up in the SV60 scenario of the original model. Figure 4-1 and Figure 4-2 illustrates the model setup at a conceptual level. The reclamation cover is discretized into 18 layers each with identical model structures except the top and bottom layer where various boundary conditions apply. The model uses the same level of discretization as site SV60 in the original model for ease of verification against the simulated and experimental results from Huang at al (2011a). In addition to external water input from boundary conditions, the water transfer mechanism within the reclamation cover is dependent on the inter-layer hydraulic gradient and the inter-layer hydraulic conductivities.
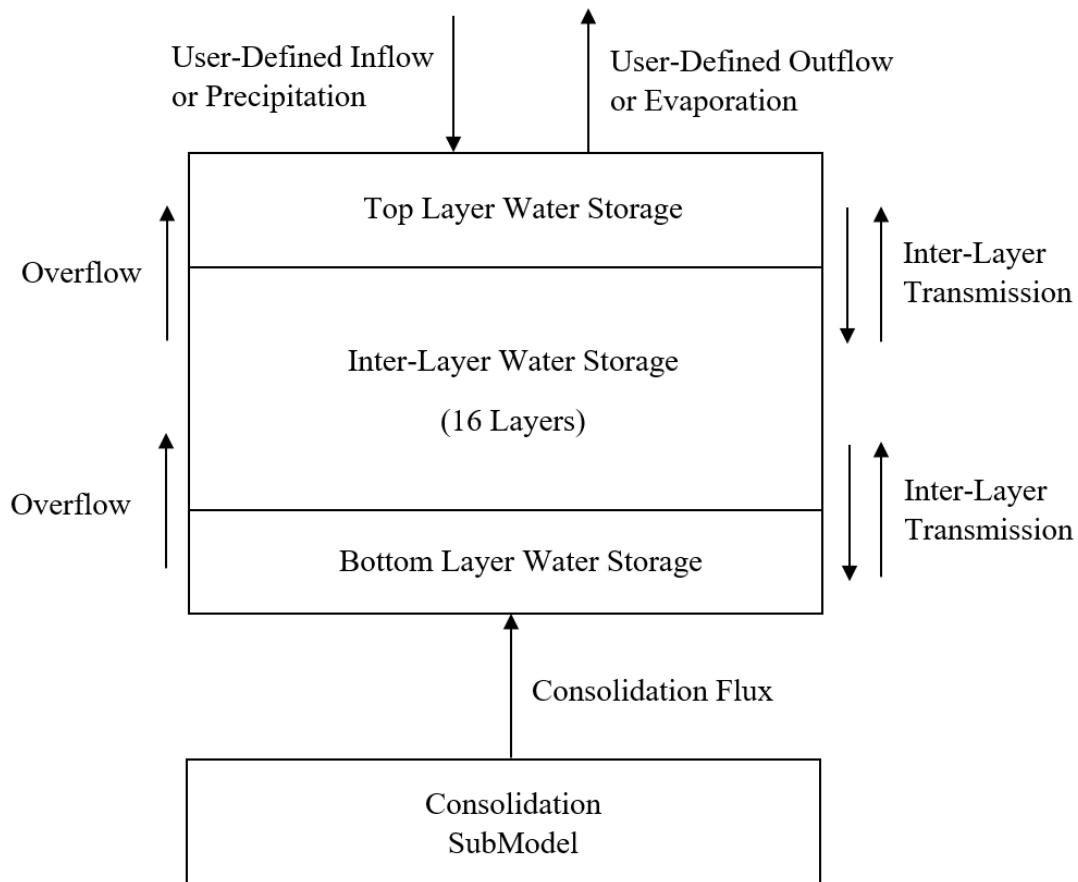
Figure 4-1 Conceptual setup of the unsaturated flow sub-model
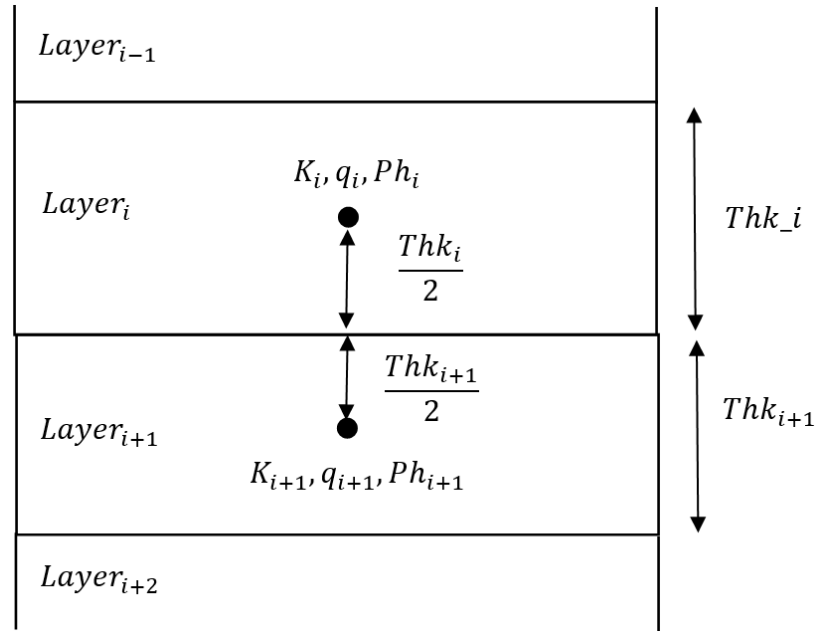
Figure 4-2 Geometric Setup of the GoldSim model

4.3.1.1 Model Variables

The stock variables track water storages in all layers. There are 18 stock variables with one stock variable representing the water storage in each of the 18 layers. Upper and lower limit of the stock variables are determined by the layer storage capacity at full saturation and at residual water content respectively. The flow variables, consisting of inflow and outflow elements, track the rate of water moving in and out of stock variables (water storage) in each layer. For the top layer, the inflow elements are infiltration rate from climatic or user-defined input and overflow rate from the underlying layer. The outflow elements are evaporation rate, surface run-off and transmission rate to the underlying layer. For the bottom layer, the inflow elements are transmission rate from overlying layer and upward consolidation flux. The outflow element is percolation drainage rate to the underlying foundation or user-defined withdrawal rate. For the intermediate layers in between, the inflow and outflow elements are the transmission rate from the overlying and underlying layers. Stock and flow variables are described in Table 4-1.

Converters are auxiliary variables that explain and are used to calculate the stock and flow variables. Input data and boundary conditions are manipulated through the converter elements and turned into flow rate. In another words, except stock variables, any variables in the equation for

flow rate are considered as converters. Table 4-2 highlighted converters that require direct user input. The description of mathematical relationships between converters and flow variables can be found in Section 4.3.2 and will not be repeated here.

Table 4-1 Stock and flow variables in the SD model.

Stock and flow variables	Definition	Default Unit
Water Storage	Stock variable that tracks the cumulative amount of water in each layer.	mm
Infiltration_Rate	Inflow variable that describes the rate of inflow to the surface layer; in the form of a Selector element in Goldsim, it can be based on climatic input, a constant rate or user-defined flow function.	cm/min
Overflow	Inflow variables that describe the rate of overflow from fully saturated underlying layers to the layer above. There is no overflow when the layer is un-saturated.	cm/min
Surface_Runoff	Outflow variable that describe the rate of surface runoff when monthly precipitation rate exceeds the saturated hydraulic conductivity of the top layer	cm/min
Evaporative_Flux	Outflow variable that describe the actual evaporation rate driven by surficial suction and potential evaporation rate	cm/min
Transmission Rate_i*	Inflow and outflow variables that describe the inter-layer transmission rate from Layer (i-1) to Layer (i); rate driven by gravity, suction head gradient and hydraulic conductivities.	cm/min
Upper_BC_Inflow	Inflow selector element that describes the downward flux into the top layer; see Section 4.3.4.4.	cm/min
Upper_BC_Outflow	Outflow selector element that describes the upward flux out of the top layer; see Section 4.3.4.5.	cm/min
Lower_BC_Inflow	Inflow selector elements that describe the upward flux into the bottom layer; see Section 4.3.4.6	cm/min
Lower_BC_Outflow	Outflow options that describe the downward flux out of the bottom layer; see Section 4.3.4.7	cm/min

*i varies from 2 to 18

Table 4-2 Converters in the SD model.

Converters	Definition	Default Unit
alpha_i	Van Ganutchen-Maulem fitting parameter for SWCC in Layer (i); this is a user input.	1/cm
n_i	Van Ganutchen-Maulem fitting parameter for SWCC in Layer (i); this is a user input.	Dimensionless
m_i	Van Ganutchen-Maulem fitting parameter for SWCC in Layer (i); this is a user input.	Dimensionless
Ks_i	Saturated hydraulic conductivity for the layer i material; this is a user input.	cm/min
K_i	Unsaturated hydraulic conductivity for Layer (i)	cm/min
Thk_i	Thickness of Layer (i); this is a user input	cm
Ph_i	Suction water pressure head within the Layer (i); negative water pressure head taken as positive	cm
Qs	Saturated volumetric water content for layer i material; this is a user input	Dimensionless
Qr	Residual volumetric water content for layer i material; this is a user input.	Dimensionless
Qini	Initial volumetric water content; this is a user input.	Dimensionless
q	Volumetric water content in Layer (i)	Dimensionless
Hr	Relative humidity in the soil voids	Dimensionless
Ha	Relative humidity of the air immediately above the soil surface; this is a user input.	Dimensionless
Ta	Mean air temperature immediately above the soil surface; this is a user input.	Celsius and Kelvin
PE_Rate	Monthly potential evaporation rate from field measurement; see Section 4.3.2.3	mm/day
C	Calibration factor for the saturated hydraulic conductivity; this is a user input.	Dimensionless

*i varies from 1 to 18

4.3.1.2 The Causal Loop Diagram (CLD)

CLD can help users and modelers understand the dynamic processes in an intuitive, non-mathematical manner. The dynamics of water storage in each discretized layer can be described by feedback loops. Figures 4-3 to 4-5 show the three steps the modeler can take to construct a quantifiable CLD.

Traditionally, CLD does not contain symbols for stock variables. However, Binder et al (2004) recommended the inclusion of at least some form of stock and flow symbols in the CLD to facilitate the process of converting CLDs to Stock and Flow Diagrams (SFD). Ford (2010) suggested identifying the stock and flow variables from the listed variables in Figure 4-3 as the first step in creating the CLD. The second step typically involves the drawing of one-way influence arrows from the flow variables to the stock variables. In this case, the actual evaporation rate and infiltration rate are the flow rates into the stock variable which is called "Layer 1 water storage". The transmission rate to Layer 2 is the flow rate out of the stock variable. Once the stock and flow variables are identified, the rest of the variables are classified as converters or auxiliary variables.

The second step involves connecting the rest of the variables with one-way influence links but without adding the plus and minus signs and the feedback symbols (see Figure 4-4). It is the easiest to start the influence arrow from the relevant converters to the flow variables. Then influence arrows are drawn between converters based on the chosen governing relationships in Section 4.3.2. Finally, feedback structures will be identified and completed once the influence arrows are traced back to the stock variable.

The third and final step involves adding the positive and negative signs to determine the polarity of each influence arrow. Inside a feedback loop, odd number of negative signs indicates a negative or balancing loop while even number of negative signs indicates a positive or reinforcing loop. Detailed procedures for classifying feedback loops are described in Chapter 2.

Figure 4-5 shows a partial CLD covering the top layer and its two underlying layers. The complete CLD with additional layers underneath follows the same structure. Stock variables are put inside solid rectangular text boxes. It should be noted that in the CLD from Huang et al (2011a), $Infiltration\_Rate$ is part of a feedback loop controlled by the volumetric water content and un-saturated hydraulic conductivity of the surficial layer. In this study, the surficial layer is assumed

to become saturated immediately upon wetting. Therefore, the infiltration rate is an external variable controlled by climatic input, the upper limit of which is controlled by the saturated hydraulic conductivity (see Section 4.3.4.2).

Examination of the CLD in Figure 4-5 revealed the following insights. Loop #1 describe the suction-driven evaporation process in which the evaporation rate will reduce as Layer 1 becomes drier. The balancing nature of Loop #1 indicates that the evaporation rate is the greatest at the beginning when there is little suction and exponentially decreases as suction is increased by more evaporation. For Layer 1, the primary driver of changes in the water storage is the infiltration rate which is an exogenous variable dependent on user-defined or climatic input. Exogenous variables are defined as variables outside any feedback structures. Loop #5 and Loop #8 describe the reinforcing effect of hydraulic conductivity on inter-layer transmission rate. The increase in volumetric water content increases hydraulic conductivity and the transmission rate, which then increases Layer 3 water storage. The rest of the feedback loops are negative or balancing in nature. Suction gradient is the main driver in Loop #3, #4, #6 and #7. Increased suction gradient results in higher outflow transmission rate, the effect of which is amplified by decreases in water storage and further increases in suction head of the layer. At the same time, when high suction gradient is present between two layers, any increase in transmission rate is balanced by decreasing hydraulic conductivity in the layer of higher suction head.

Behaviour of a multi-feedback, first order non-linear system is controlled by the dominance of either positive or negative feedback loop at any given time (Sterman, 2004). When there is a net inflow (i.e. precipitation > evaporation), positive feedback loops will dominate. When there is a net outflow (i.e. evaporation > precipitation), negative feedback loops will dominate.

After the CLD has been completed, the modelling process should be paused to allow time for discussion over the assumptions, key variables, scope and boundary of the model. This discussion can be facilitated by the Bull's Eye Diagram as suggested by Ford (2010). As an alternative to the CLD, the Bull's Eye Diagram offers an effective and compact way of communicating the boundary of the model to users and modelers (Trimble, 2014). Model variables in the CLD from Figure 4-5 are grouped into two categories as shown in the Bull's Eye Diagram (see Figure 4-6): endogenous and exogenous. Endogenous variables are any variables inside a feedback loop while exogenous variables are any variables outside feedback loop. The Bull's Eye Diagram resembles a dart board

in which key areas of interests are close to the centre ring of the diagram. The endogenous variables are placed in the inner ring while the exogenous variables are placed in the middle ring. It is the endogenous variables and processes that give rise to the dynamic behaviour during simulation (Ford 2010). A quick glance at the content of the endogenous ring in Figure 4-6 intuitively shows the focus of the model.

Also shown in Figure 4-6 are the excluded variables in the outer ring which describe the model's assumptions. The user does not have to list every excluded variable and process as there are too many to fit inside the diagram. As suggested by Ford (2010), the excluded variables and processes in the Bull's Eye Diagram were selected based on their relevance to the modelling objective and their potential for inclusion in future versions of the model.

An iterative process of model revision and expansion may move some of the excluded variables to the inner rings or some of those exogenous variables to the endogenous ring as part of feedback structures. For example, void ratio and saturated hydraulic conductivity can be categorized as endogenous if the effect of volume change is incorporated into a feedback loop. Therefore, the Bull's Eye Diagram should serve as a platform for future model revisions and discussions.
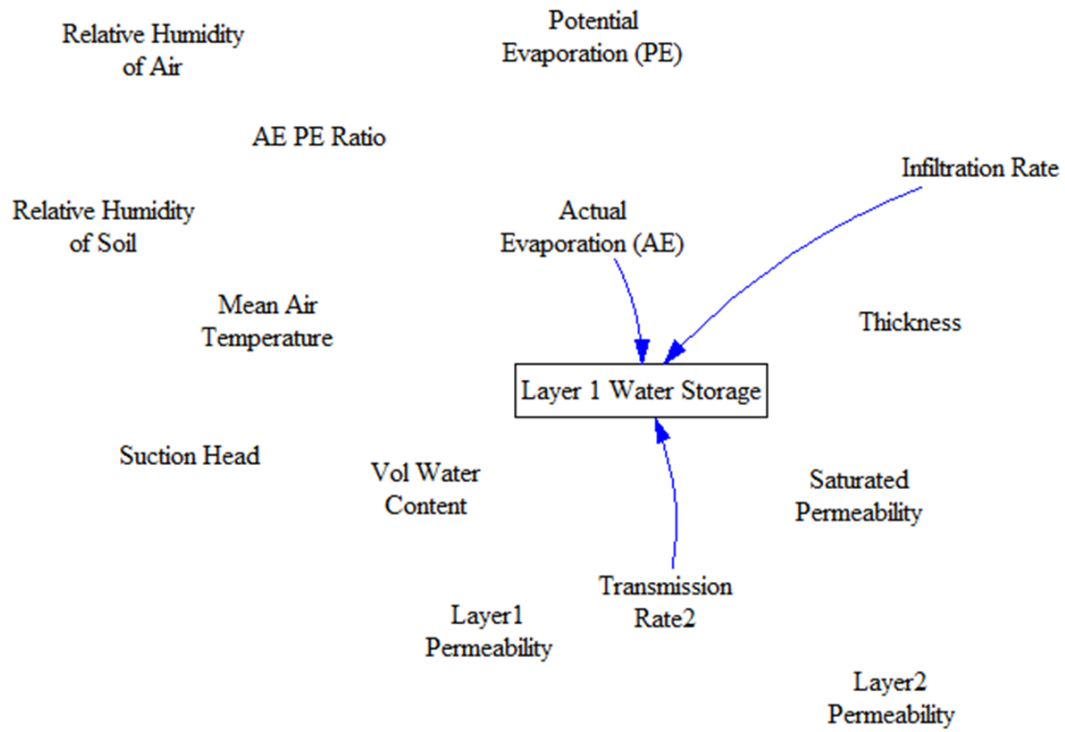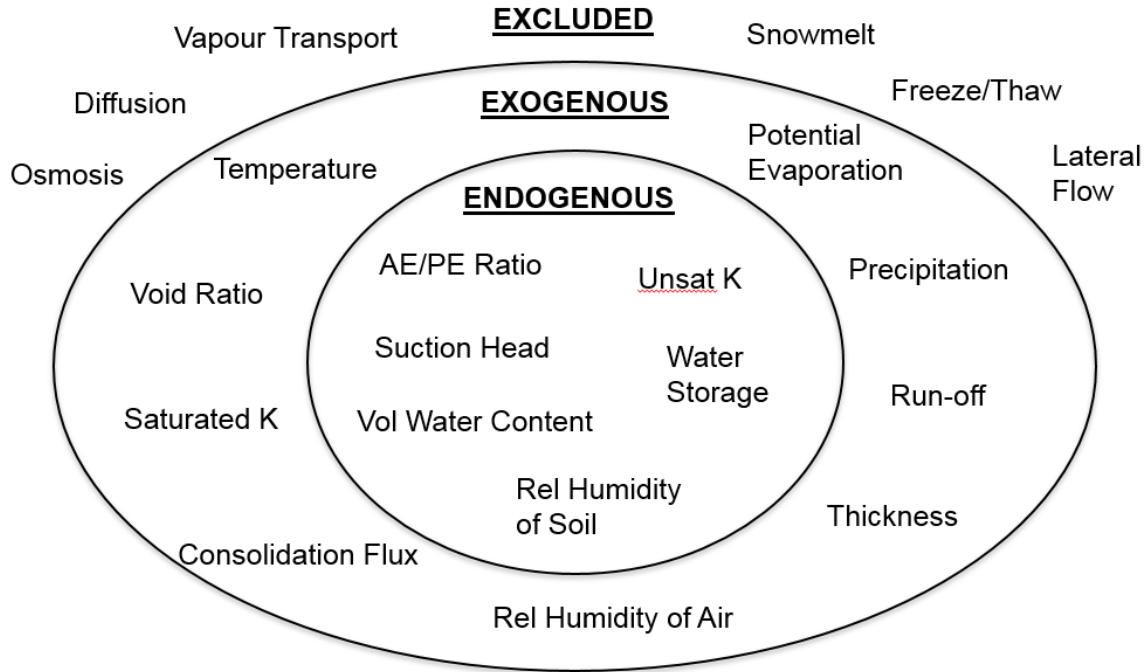
Figure 4-3 Identification of stock, flow and auxiliary variables
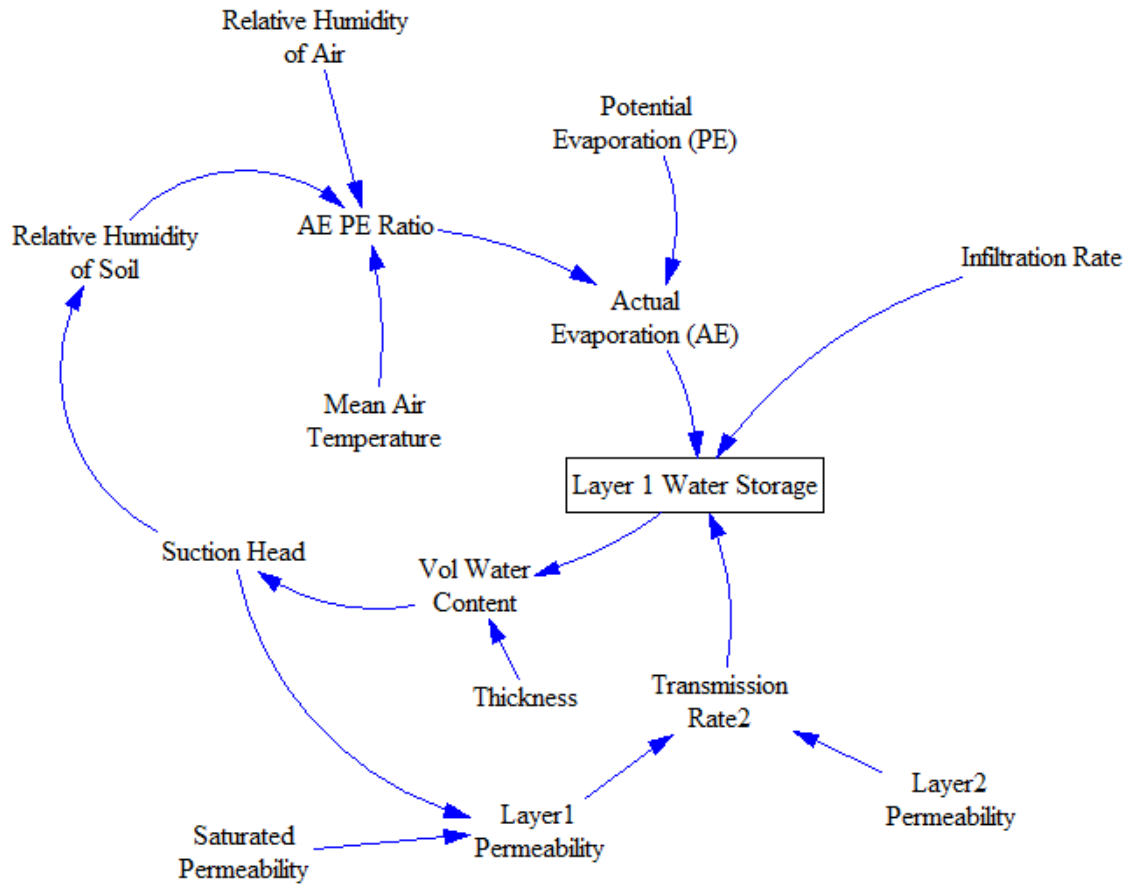
Figure 4-4 Construction of a preliminary CLD by connecting variables with influence arrows

Figure 4-5 Partial causal loop diagrams for the GoldSim model.

Figure 4-6 The Bull's Eye Diagram for the partial CLD in Figure 4-5

4.3.2 Model Formulation

This section describes the mathematical formulation between the variables listed in Table 4-1 and Table 4-2. Calculation of hydraulic conductivity, volumetric water content, suction head, and inter-layer transmission rate follows the procedure from the original model. This model added an overflow function described by Equation 4.9 to 4.11.

The total head gradient drives the water transport process from one layer to the adjacent layers. Each layer is modelled as a one-dimensional vertical column. The relationship between pressure head gradient and water flow rate can be described by a re-arranged, simplified version of Darcy's equation (Hillel 1998):

$$f = K(\theta)\left(\frac{h_{top} - h_{bot}}{L} + 1\right) \qquad (4.1)$$

where f is water flux in cm/min, θ is the volumetric content (cm³/cm³); $K(\theta)$ is the hydraulic conductivity (cm/min) as a function of the volumetric content θ; h_{top} is the water pressure head at the top of the column in cm; h_{bot} is the water pressure head at the bottom of the column in cm; L is the length of the column in cm. Note that in the software implementation of Equation 4.1, $(h_{top}-h_{bot})$ becomes $(h_{bot} - h_{top})$ in Equation 4.8 due to the assumption of positive sign for negative suction pressure.

The van Genutchen equations (van Genutchen, 1980 and Maulem, 1976) describe the inter-layer transmission rate, hydraulic conductivity as a function of volumetric water content and suction pressure head in each layer. Only the drying SWCC is used to derive the fitting parameters as the effect of hysteresis is ignored. The van Genutchen equations are re-arranged in GoldSim as follows:

$$Ph = \frac{\left[\left(\frac{1}{S_e}\right)^{\frac{1}{m}} - 1\right]^{\frac{1}{n}}}{a} \tag{4.2}$$

$$q = \frac{Wate\ Storage}{Thk_i} \tag{4.3}$$

$$K = K_s S_e^{\frac{1}{2}}\left[1 - \left(1 - S_e^{\frac{1}{m}}\right)^m\right]^2 \quad for\ S_e < 1 \tag{4.4}$$

$$K = K_s \quad for\ S_e = 1 \tag{4.5}$$

$$S_e = \frac{q - Q_r}{Q_s - Q_r} \tag{4.6}$$

$$m = 1 - \frac{1}{n} \tag{4.7}$$

where a in 1/cm, n and m are van Genuchten model fitting parameters; S_e is the normalized effective volumetric water content; q is the volumetric water content of the layer; Thk is the thickness of Layer (i) in cm; $Water\ Storage$ is the cumulative amount of water stored in the layer

in mm; Q_r and Q_s are residual and saturated volumetric water contents respectively; K_s is the saturated hydraulic conductivity in cm/min; Ph is the suction pressure head of the layer in cm. Note that for ease of computation, Ph is taken as positive under un-saturated condition.

The inter-layer hydraulic conductivity is assumed to be the average of the two layers. Hydraulic conductivities in both layers affect the transmission rate. (Romano et al, 1998). The inter-layer transmission rate between adjacent layers f_i is calculated by re-arranging and modifying the Darcy's equation in Equation 4.1, as follows:

$$f_i = \left(\frac{1}{2}\right)(K_{i-1} + K_i)\left[\frac{Ph_i - Ph_{i-1}}{\frac{Thk_i}{2} + \frac{Thk_{i-1}}{2}} + 1\right] \tag{4.8}$$

where i varies from 2 to 18; f_i is interpreted as the rate of water movement from Layer (i-1) to Layer (i) in cm/min; f_i can be positive or negative depending on the suction pressure head gradient between the two layers. K is the unsaturated hydraulic conductivity calculated by Equation 4.4.

Changes in water storage of each layer depend on the transmission rate to the underlying layer, the transmission rate from the overlying layer and the overflow rate from the underlying layer if soil water storage capacity is full or in another words, if the soil becomes fully saturated. The equation for changes in water storage in cm/min is as follow:

$$\frac{dS_i}{dt} = f_i + Overflow_{i+1} - f_{i-1} \tag{4.9}$$

$$If \ \frac{dS_{i+1}}{dt} > 0 \ cm/min \ and \ S_e = 1 \quad then \ Overflow_{i+1} = \frac{dS_{i+1}}{dt} \tag{4.10}$$

$$If \ S_e < 1 \quad then \ Overflow_{i+1} = 0 \ cm/min \ , \tag{4.11}$$

where the subscript i varies from 2 to 17; $Overflow_{i+1}$ is the rate of overflow from Layer (i+1) to Layer (i). Note that there is no overflow into Layer 18, which is the bottom layer.

The total soil water storage S_T is calculated by summing water storages in each of the 18 layers S_i as below:

$$S_T = \sum_{i=1}^{18} S_i \qquad (4.12)$$

4.3.3   Initial Volumetric Water Contents

The user needs to specify the initial volumetric water contents and their corresponding depths, which are then interpolated to work out the initial water storage for each layer. The initial volumetric water contents typically come from field measurement. Alternatively, it can be derived based on empirical relationships and hypothetical field conditions. Initial water content input for the validation cases can be found in Appendix 2.

4.3.4   Model Time Step

Calculations of variables are carried out at each time interval with the current values computed based on some functions of the values at the previous time step. In GoldSim, the user needs to specify the total duration of the simulation and the value of basic time step, which is also the frequency of the software saving calculated values as output.

The choice of basic time step is primarily based on the resolution of input time-series data and numerical stability. Typically, resolution of climatic data is daily and sometimes hourly. It was also found during trial simulations that a daily basic time step works better than monthly in terms of quality of match with experimental data, which is often measured on a minutely or hourly basis. Therefore, for the infiltration and drainage validation cases, a minutely basic time step is found to

adequately represent the system behaviour. For all other validation cases and the subsequent case study, a daily basic time step is chosen.

The function of unscheduled update timestep in GoldSim allows for shorter time interval than the basic time step without the need to save those un-scheduled results during simulation. As long as the unscheduled update timestep is less than the difference between the current time and the scheduled update time, the un-scheduled update timestep will be used in model calculation. This way, the model size is kept at a manageable level while numerical stability and accuracy are improved due to smaller time steps between the basic time interval. GoldSim (2018) provided sample scenarios to demonstrate how un-scheduled updates work in Chapter 7 of the user manual.

The resolution of unscheduled update timestep should be carefully considered due to its importance in the accuracy and numerical stability of the finite difference equations and the level of stock at any given time. A time step too large may suddenly fill up or drain out the stock as the amount of inflow and outflow is integrated over a longer time interval. On the other hand, a time step too small may increase model run-time and reduce efficiency.

The choice of time step for unscheduled update was based on a trial-and-error approach. Smaller time steps were used if the simulation became numerically unstable and crashed using large time steps. After several iterations, an un-scheduled update timestep of 0.1 minutes is found to be a suitable value for all validation cases.

4.3.5   Boundary Conditions

This section details the improvements made to Huang et al (2011a)'s model capability in terms of the range of boundary conditions it can handle. The philosophy of the model is based on the concept of stock-flow and feedback structures. Only Neumann boundary conditions are applied to the top and bottom boundary conditions. Therefore, the user needs to specify the inflow and outflow flux for the top and bottom layer.

4.3.5.1   Surface Infiltration

Surface infiltration rate can be precipitation, a constant rate based on user-input, or a user-defined inflow function. Precipitation is a lumped parameter that includes both rainfall and snowmelt. In

GoldSim, precipitation is handled by a LookUp table element, Monthly_Precip(Month) where Month inside the bracket varies from 1 to 12. The user enters the value of monthly precipitation in mm/day. At a monthly time scale for precipitation rate, the daily precipitation rate remains constant during a given month. The model is not capable of simulating infiltration due to the snowmelt process, which is best described by a daily time scale. From an operational perspective, the monthly time scale is not suitable for short-term tactical planning and prediction of water movement on a daily basis. However, the user has the freedom to switch to a daily or finer time scale for precipitation if a higher resolution is warranted.

4.3.5.2 Surface Run-off

The dominant run-off mechanism is determined by following the selection flow chart in **Figure 4-7** from Schmocker-Fackel et al (2007). The original model (Huang et al. 2011a) and the proposed case study (Chapter 5) use coarse sandy material as the cap soil. The coarse sand tailings (CST) cap is assumed to receive some degrees of compaction from construction equipment. There is little to no rapid vertical flow in the compacted CST cap. The model also assumes the absence of any sub-surface lateral flow within the soil for reasons stated in Section 4.2. Following the flow chart in Figure 4-7 leads to the choice of the Saturation Overland Flow (SOF) mechanism as the dominant run-off process.

The model adopts a simple analytical solution based on the assumptions that the surficial soil layer becomes immediately saturated during precipitation events (Smith 2002) and that the overland flow is negligible for high permeable soils subject to low-intensity rainfall (Dunne and Black, 1970; Dingman, 2002). Jubinville (2013) provided additional field data and descriptions on the calibration of this method.

In GoldSim, the surface run-off calculation is analytically handled by the following if statements:

If precipitation rate is greater than the saturated hydraulic conductivity K_s of the surficial layer, then the rate of surface run-off will be produced as:

$$Surface\ Runoff\ Rate = Precipitation - K_s + Overflow_1 \qquad (4.13)$$

If precipitation rate is less than the saturated conductivity K_s of the surficial layer, then all surface run-off will come from the daylighted overflow from Layer 1 to the surface (see Equation 4.9 to 4.11).
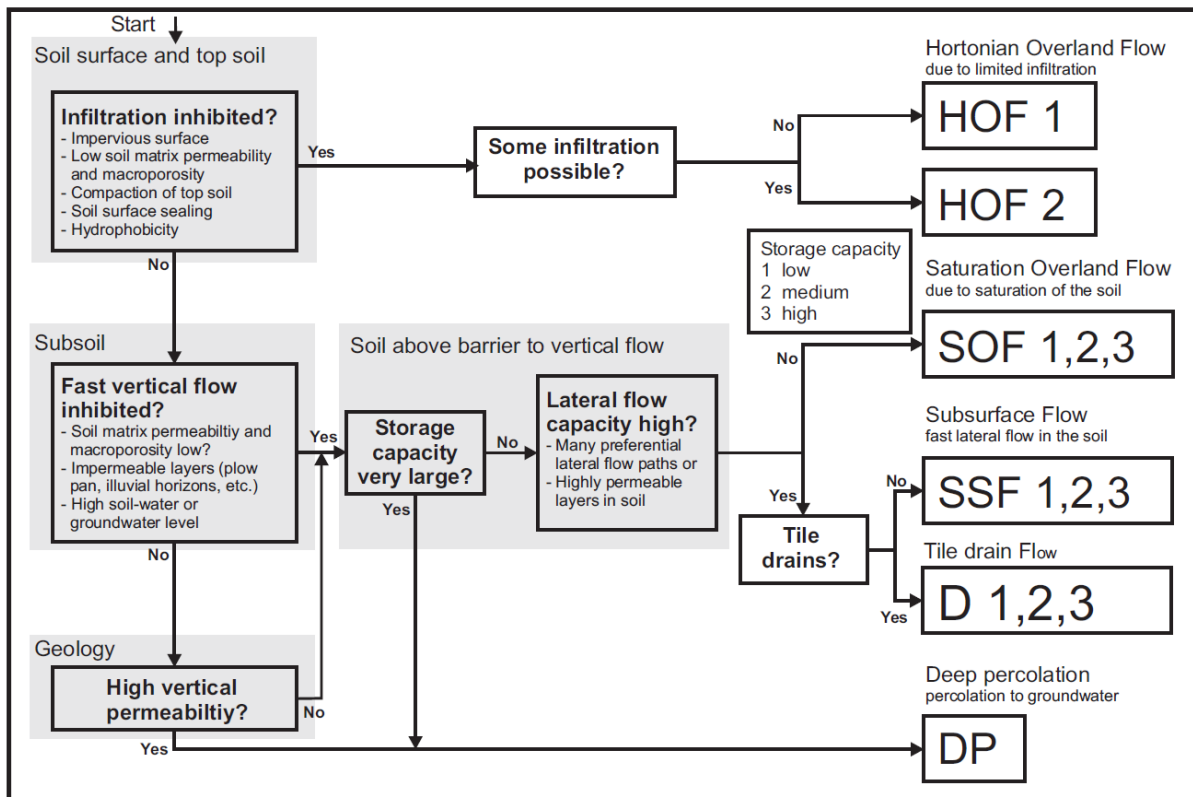
Figure 4-7 Selection flow chart for dominant run-off processes from Schmocker-Fackel et al (2007).

4.3.5.3 Surface Evaporation

For simplicity, the evaporation process is assumed to be isothermal and driven entirely by advective liquid-flow or hydraulic gradient potential (Stage I evaporation). Therefore, the characteristic length, which is described by Lehmann et al (2008) as the depth over which Stage I evaporation dominates, is ignored during spatial discretization of the surface layer. Under this assumption, resistance to evaporation within the unsaturated soil and in the atmosphere is ignored.

Following the end of Stage I evaporation, water transport during Stage II evaporation is driven by vapour diffusion. Stage II evaporation is also not considered in this model. Omission of Stage II evaporation will underestimate the amount of actual evaporation and depth of the drying front. As shown in the validation cases for sand and silt column, the effect of this omission is not significant in terms of total soil water storage (see **Figure 4-20** and **Figure 4-24**). However, if Stage II evaporation needs to be modelled, either the suction value or the relative humidity will have to be adjusted. Dunmola (2012), Fredlund et al (2015) and Tran et al (2016) provided a good summary of past studies and recent advances in numerical handling of Stage II evaporation.

The coupling of suction pressure head with evaporation rate is assumed to be limited to the surface layer (Layer 1). Thin lift deposition has been widely recognized as the method to take full advantage of the drying process (Li et al 2012 and Simms 2013). Typical recommended lift thickness is less than 0.5 m for paste and thickened tailings. (Simms et al. 2007 and Daliri et al. 2015). Limited experimental work on Fountainbleau sand shows that evaporation is limited to the surface layer and that surface evaporation does not significantly affect volumetric water content beyond the 0.3 m depth during 30 days of evaporation tests (Song et al. 2013). The typical thickness of the intermediate cap ranges from 2 m to 5 m, which translates to a thickness of less than 0.3 m for the surface layer based on a discretization scheme of 18 layers. Therefore, the assumption of limiting evaporation to the surface layer is reasonable provided that the thickness of the surface layer does not exceed 0.5 m for TT material and 0.3 m for sand material.

Based on Wilson et al (1997), actual evaporation rate at the soil surface is dependent on surface suction, measured potential evaporation rate, mean air temperature, relative humidity of the soil void and air. The calculation of relative humidity of soil voids is given by Equation 4.14 based on the thermodynamic equilibrium between relative humidity of soil voids and total soil suction head. (Edlefsen and Anderson 1943).

$$h_r = exp\left(\frac{\psi g W_v}{R T_a}\right) \qquad\qquad (4.14)$$

where h_r is the relative humidity of the un-saturated soil voids; T_a is the mean air temperature typically measured at weather stations; ψ is the total matric suction head taken as a positive value in metres; W_v is the molecular weight of water at 0.018 kg/mol, R is the universal gas constant at 8.314 J/(mol.K); and g is the gravitational acceleration at 9.81 m/s^2.

Assuming the same temperature applies to the air, water and soil, the calculation of actual evaporation rate is based on the formulation by Wilson et al (1997):

$$\frac{AE}{PE} = \frac{h_r - h_a}{1 - h_a} \qquad\qquad (4.15)$$

where AE/PE is the ratio of actual evaporation rate to potential evaporation rate; h_a is the relative humidity of the air immediately above the soil surface; and h_r is the relative humidity of the soil voids. Actual evaporation rate is given by multiplying the potential evaporation rate by the AE/PE ratio in Equation 4.15. Potential evaporation (PE) is typically measured at a daily or monthly interval at weather stations.

Figure 4-8 provides a high-level overview of the surface evaporation process, which is coupled to the suction pressure head Ph_1 and the volumetric water content q_1. The partial CLD in Figure 4.8 is derived from Equation 4.14 and Equation 4.15. The negative feedback loop shows that evaporation is a balancing process that brings the system to equilibrium. The amount of evaporative flux is kept in balance by increasing suction in a drying soil layer.

The user can also specify the maximum suction pressure at which the top layer approaches the residual volumetric water content, regardless of soil types. Soils near the ground surface typically have extremely high values of suction (Wilson et al. 1997). Experimental data suggested 1,000,000 kPa as the upper limit of allowable suction pressure corresponding to a water content of zero

(Fredlund and Xing, 1994). Based on experimental results from Wilson et al (1997), the AE/PE ratio of sand, silt and clay all fell to zero at 100,000 kPa suction pressure. Therefore, for simulation purposes, the default value for maximum allowable suction pressure is set to 100,000 kPa.
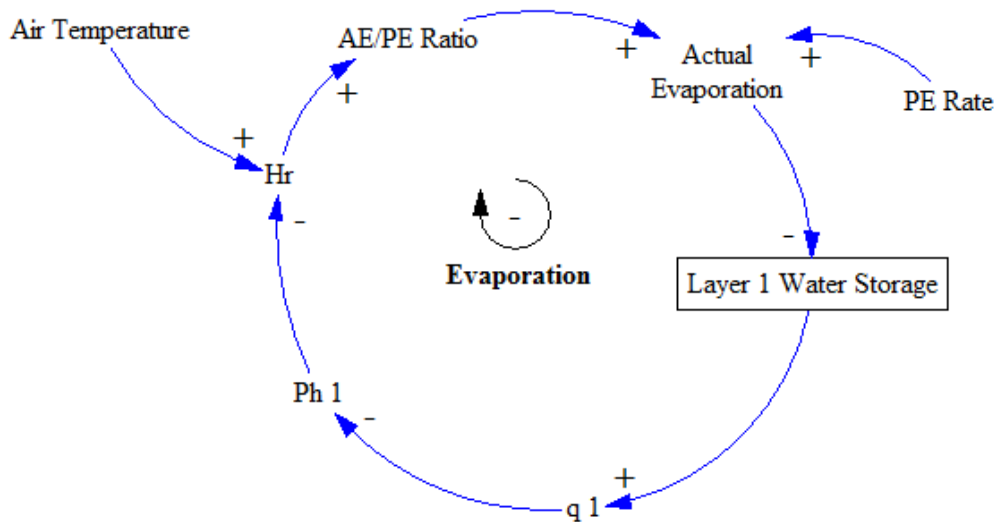
Figure 4-8 Partial causal loop diagram for surface evaporation.

4.3.5.4 Upper Boundary Condition (BC) – Inflow and Outflow Options

Surface infiltration and surface run-off described in Section 4.3.5.1 and 4.3.5.2 respectively are two of the options for the upper boundary inflow condition. Other options include a constant infiltration value specified by the user and a user-defined infiltration flux function.

Surface evaporation described in Section 4.3.5.3 is one of the options for the upper boundary outflow condition. Other options include a constant evaporative flux value specified by the user and a user-defined evaporative flux function.

4.3.5.5 Lower Boundary Condition (BC) – Inflow and Outflow Options

Options for water flux into the bottom layer include a constant value specified by the user, flux values from output of the consolidation model in Chapter 3 and a user-defined flux function.

Options for water flux out of the bottom layer include a constant value specified by the user, free drained at the rate of the hydraulic conductivity of the bottom layer, subject to seepage face condition or a user-defined flux function. For seepage face boundary condition, if the bottom layer is un-saturated, then there will be no flux coming out of the bottom. If the bottom layer is saturated, then the flux will be the saturated hydraulic conductivity at a pressure head of zero.

4.4 MODEL VALIDATION

The model is validated against a combination of past field data and simulated results by HYDRUS. Coefficient of Determination (R^2), Root Mean Square Error (RMSE) and Mean Relative Error (MRE) are used to assess the quality of match between historical data and simulated results. The equations for R^2, RMSE and MRE are as follows:

$$R^2 = 1 - \frac{\sum_{i=1}^{n}(M_i - S_i)^2}{\sum_{i=1}^{n}(M_i - \bar{S})^2} \qquad (4.16)$$

$$RMSE = \sqrt{\frac{\sum_{i=1}^{n}(M_i - S_i)^2}{n}} \qquad (4.17)$$

$$MRE = \frac{\sum_{i=1}^{n}\left|\frac{M_i - S_i}{S_i}\right|}{n} \qquad (4.18)$$

Where M_i is the measured daily values; S_i is the simulated daily values; $\bar{S}$ is the average simulated daily values during the simulation time; n is the duration of the simulation in days.

Three validation cases, at both field-scale and lab-scale, were selected. To establish the reference validity of the model, Case I repeated the same validation cases conducted by Huang et al (2011a). To check numerical stabilities, Case II in Section 4.4.2 tested extreme conditions of drying and wetting against results from HYDRUS-1D. Case III in Section 4.4.3 simulated the evaporation process by comparing simulated results with lab-scale column drying experiments performed by Huang et al (2013).

4.4.1   Validation Case I: Simple Infiltration and Drainage

Detailed description on the field experiments and soil sampling can be found in Zettl et al (2011) and Zettl (2014). Various infiltration and drainage experiments were conducted at seven reclamation trial sites located 50 km to 120 km north of Fort McMurray, Alberta, Canada. This validation exercise uses only the SV60 scenario since it is more complex in terms of soil texture and heterogeneity (Huang et al. 2011a). On average, soil at SV60 contains 98% sand, 1% silt and 0.5% clay based on a total number of 21 disturbed samples taken every 2 cm of depth. Heterogeneity is represented by assigning unique soil parameters to each of the 18 layer containers in GoldSim. In the field, the drainage test was conducted right after the infiltration test. After the drainage tests were completed, a soil pit was excavated to a depth of approximately 110 cm. Disturbed samples were collected at 2 cm to 10 cm depth interval for laboratory analysis in volumetric water contents, dry bulk density and grain size distributions. In GoldSim, thickness of each layer is derived from the depth of field sampling. For the parameter input of each layer, 18 unique SWCC fitting parameters and saturated hydraulic conductivities K_s were predicted using the Arya-Paris PTF and Kozeny-Carman equation respectively (Huang et al. 2011b). Hydraulic parameter input was listed in Figure 4-9. Detailed GoldSim setup for Validation Case I can be found in Appendix 2.

	(cm)	(cm)			(cm-1)		(cm/min)
	Depth	Thickness	Qr	Qs	alph	n	Ks
1	3.5	7	0	0.483	0.07	1.717	0.944
2	8.5	3	0.007	0.508	0.057	1.968	0.71
3	13.5	7	0.007	0.536	0.102	2.517	0.703
4	18.5	3	0.011	0.504	0.093	2.736	0.624
5	21.5	3	0	0.452	0.068	2.388	0.521
6	26.5	7	0	0.401	0.034	2.302	0.341
7	32.5	5	0.001	0.355	0.058	2.136	0.351
8	40	10	0	0.356	0.057	2.169	0.456
9	46.5	3	0	0.36	0.057	2.095	0.423
10	50.5	5	0	0.356	0.056	2.396	0.26
11	56	6	0	0.352	0.06	2.568	0.382
12	63.5	9	0	0.405	0.049	2.455	0.27
13	71	6	0	0.385	0.027	2.711	0.187
14	76	4	0	0.378	0.132	1.488	0.297
15	81	6	0	0.264	0.083	2.109	0.272
16	90.5	13	0.013	0.303	0.092	2.206	0.725
17	99.5	5	0	0.287	0.046	2.362	1.169
18	106	8	0	0.34	0.064	2.306	0.457

Figure 4-9 Screenshot of Validation Case I and II hydraulic parameter input in GoldSim.

4.4.1.1 Infiltration Validation

The field infiltration test consists of a PVC access pipe installed to a depth of 160 cm at SV60, a minimum 15 cm deep double-ring infiltrometer centered over the PVC pipe, and a string of multisensory capacitance probes (MCP) to measure volumetric water contents. The resolution of measurement by MCP is at every 10 cm of depth. The double-ring infiltrometer maintains a constant ponded water depth between 5 cm and 10 cm. The wetting front was monitored at 4-minute interval until the wetting front has reached 100 cm depth.

Layer parameter input for thickness, depth, Q_r, Q_s, Q_{ini}, a, n, and K_s can be found in Huang et al (2011b), and in Figure 4-9. The top boundary condition is a ponded water head kept at a near-constant depth. Therefore, the GoldSim model equivalence uses a constant surface infiltration rate of 0.944 cm/min which is equal to the K_s of the top layer. The bottom boundary condition is free drainage which is equivalent to setting the bottom outflow rate equal to the hydraulic conductivity of the bottom layer in GoldSim. Total simulation time in GoldSim is set at 120 minutes with a basic time step of one minute. The maximum allowable unscheduled updates between the minutely time step is specified to be 0.1 minutes (See Section 4.3.4).

The performance of the GoldSim model is dependent on the value of saturated hydraulic conductivity, K_s (Huang et al. 2011a). The infiltration process was first simulated using the original K_s then re-simulated using a calibrated value of K_s. Here, original K_s refers to values calibrated and validated in the HYDRUS model. The dotted line representing the original K_s in Figure 4-10 underestimated the cumulative soil water storage simulated while the solid line representing the calibrated K_s matched the measured values very well. As discussed by Huang et al (2011a), the underestimation of water storage was due to limited spatial discretization in the SD model. At a higher spatial resolution, additional water potential gradients increase water transport rate in the entire depth of the soil layer. Therefore, the K_s needs to be increased to better match the field measurement. The calibration process doubled the value of original K_s reducing RMSE and MRE of water storage from 16 mm and 1.3% to 5 mm and 0.4% respectively.

Using the calibrated K_s value, the volumetric water content at depth 52.5 cm and 82.5 cm matched well with field measured data, as shown in Figure 4-11 and Figure 4-12 respectively. The GoldSim model predicted a slightly later arrival of the wetting front at both depths, though this was more prominent at depth 52.5 cm (see Figure 4-11). Huang et al (2011a) and Gerke and van Genuchten (1996) argued that these discrepancies in wetting front may be due to limitation of the Darcy's equation to model preferential flow in the field.

In Figure 4-12, the GoldSim model showed decreases in water content prior to the arrival of the wetting front while the Huang et al (2011a)'s SD model showed a horizontal, near-constant volumetric water content until approximately at 33 minutes. One of the reasons behind this discrepancy is how initial pressure gradient is treated at the beginning of the simulation. The GoldSim model allows for gradient-driven movement of water between layers prior to the arrival of the wetting front. The SD model in Huang et al (2011a) seems to restrict downward movement of water until the arrival of the wetting front, even though some pressure gradient may have already been present at the very beginning of the simulation.

In SD models, behavioural consistency is more important than numerical accuracy, especially if the objective of modelling is reflective rather than predictive. Despite those discrepancies above, the GoldSim model is successful in replicating the behaviour of the infiltration test.
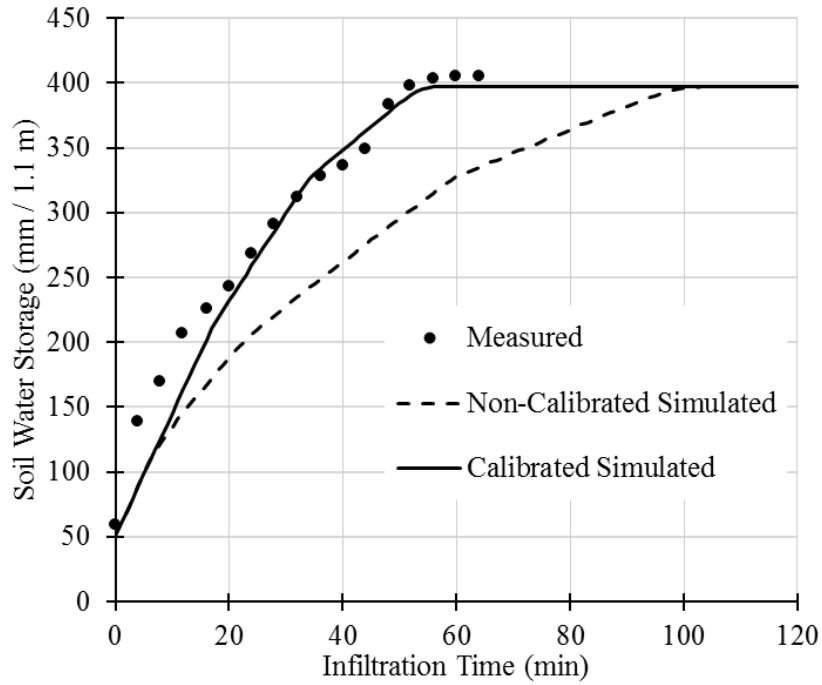
Figure 4-10 Water storage comparison of field measurement, HYDRUS and GoldSim
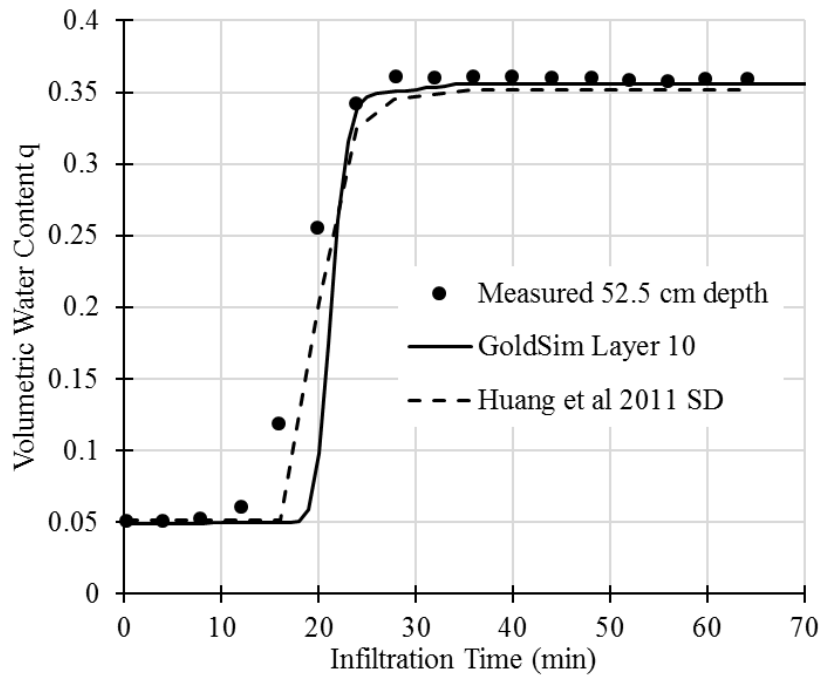
Figure 4-11 Volumetric water content comparison between measured and simulated results at depth 52.5 cm.
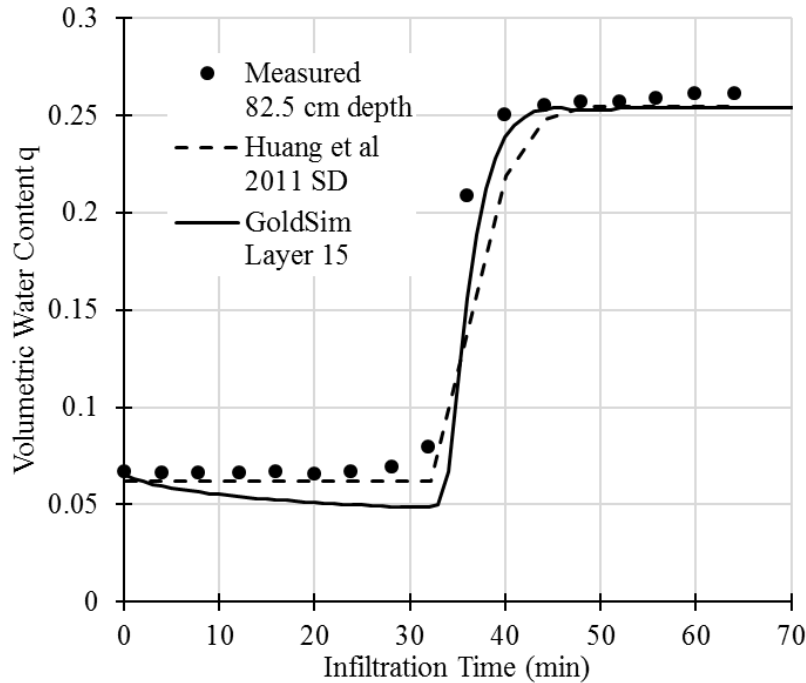
Figure 4-12 Volumetric water content comparison between measured and simulated results at depth 82.5 cm.

4.4.1.2 Drainage Validation

As described in Huang et al (2011a), during the infiltration test, once the wetting front has progressed past the 100 cm depth of the soil profile, water inflow at the surface was stopped. Evaporation was prevented by covering the area with plastic. Like the infiltration test, volumetric water contents at various depth were continuously monitored by the capacitance probes for 1200 minutes or 20 hours.

In GoldSim's drainage simulation, the top boundary condition was set to an infiltration rate of zero. The bottom boundary condition was free drainage. The simulation duration was set to 1100 minutes. Dynamic time step setting remains the same as in the infiltration simulation. The initial soil profile is assumed to be fully saturated ($Q_{ini} = Q_s$).

Using the original K_s value, the simulated water storage result by GoldSim agrees reasonably well with the original SD result and the measured data (Figure 4-13). The RMSE and MRE values between measured and simulated water storage are 4 mm and 1.3% respectively. Comparisons of

measured and simulated volumetric water contents were shown in Figure 4-14 and Figure 4-15 for depth at 52.5 cm and 82.5 cm respectively.

At 52.5 cm depth, Figure 4-14 shows that during the first 200 minutes, the GoldSim model still under-estimated the water contents but generated more accurate results than the original SD model. At later drainage time, the GoldSim model (solid line) slightly over-estimated the water contents while the original model (dotted line) slightly under-estimated the water contents.

At 82.5 cm depth, Figure 4-15 shows that the GoldSim model over-estimated the water contents during the first 600 minutes and slightly under-estimated the water contents after 600 minutes. The GoldSim model also delayed the arrival of distinct drainage period by approximately 30 minutes. This delay is likely due to the treatment of initial pressure gradient in GoldSim prior to the arrival of drying front, as described in Section 4.4.1.1.

In general, once the simulation passed the 600-minute mark, the GoldSim model is in good agreement with measured data at both depths. The discrepancies above are consistent with those from the original SD model in Huang et al (2011a). Huang et al (2011b) attributed those discrepancies to the absence of hysteresis. However, it can be inferred that the benefit of including hysteresis may be marginal as Huang et al (2011b) suggested that non-hysteresis models provide reasonable estimation of water storage and water contents.
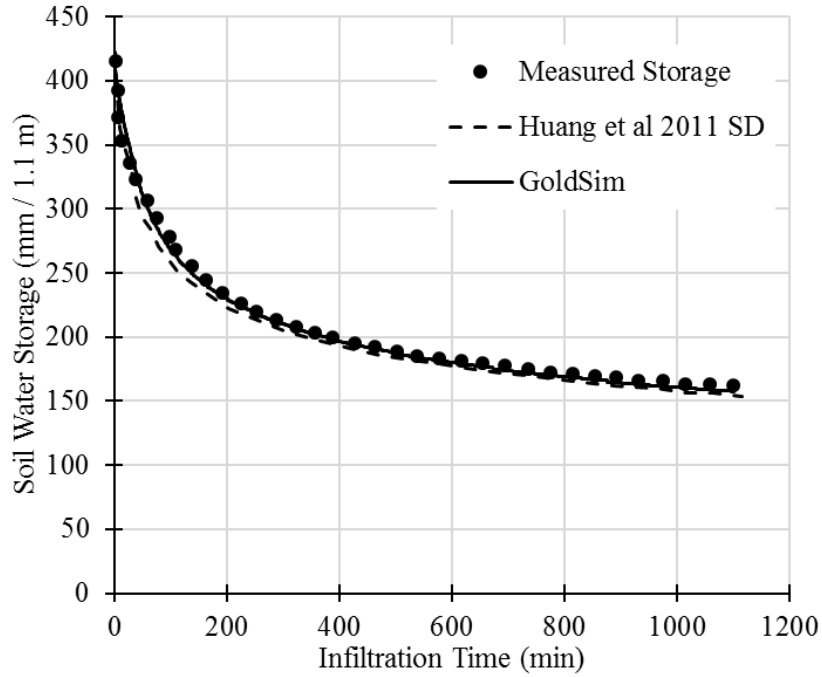
Figure 4-13 Comparison of total soil water storage during drainage.
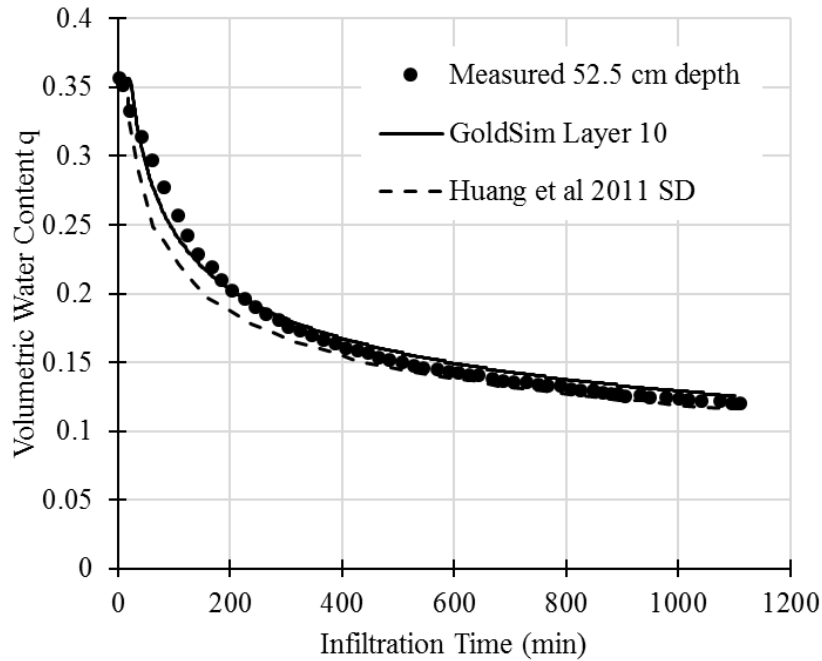
Figure 4-14 Comparison of water contents during drainage at 52.5 cm depth.
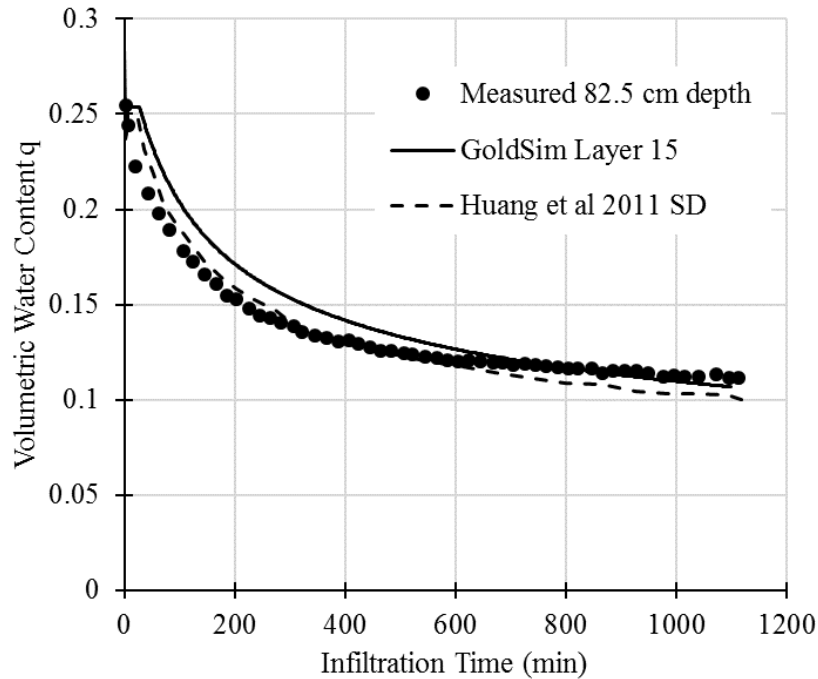
Figure 4-15 Comparison of water contents during drainage at 82.5 cm depth.

4.4.2 Validation Case II: Extreme Condition Testing

Greater user confidence of the model can be derived from the ability to properly simulate extreme conditions (Sterman 2004). In this case, extreme conditions were imposed on the exogenous boundary conditions, namely the net flux at the surface and the net flux at the bottom. Upper and lower limits of those boundary conditions were determined by climatic input (Figure 4-16), engineering judgement and simulation results from the consolidation model (see Chapter 3). Monthly mean temperature and monthly relative humidity in Fort McMurray can be found in Appendix 2. The GoldSim model is compared against results from a finite difference software package, HYDRUS 1D.
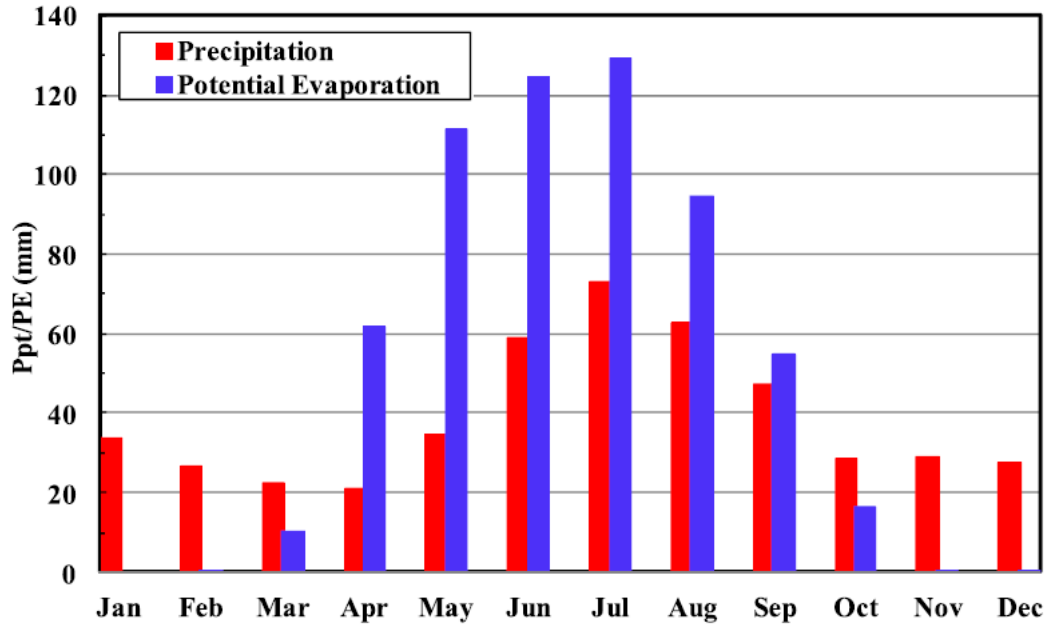
Figure 4-16 Average monthly precipitation and potential evaporation in Northern Alberta (after Song and O'Kane, 2013)

4.4.2.1 Extreme Wetting

The extreme wetting test uses the same geometry, soil property setup and initial moisture conditions as Section 4.4.1 (see Figure 4-9). Total simulation time is set at 290 days with a daily time step and maximum allowable time stepping of 0.1 minutes. The upper boundary condition is subject to seasonal precipitation normals in Fort McMurray, Alberta (Figure 4-16) without any evaporation during the simulation. The bottom boundary condition is subject to an upward flux of 4.78E-05 cm/min, which is equivalent to the consolidation release rate of a 60 m thick Thickened Tailings deposit with an initial solids content of 50%. Detailed setup in GoldSim can be found in Appendix 2.

Figure 4-17 shows that the GoldSim model is capable of handling extreme conditions of wetting due to the excellent match of results between GoldSim and HYDRUS. The GoldSim model correctly simulated the overflow mechanism once the water storage of the underlying layer became fully saturated. Surface run-off commenced at 194-day when the entire soil layer became saturated and water in excess of the soil water storage capacity started daylighting as surface run-off.
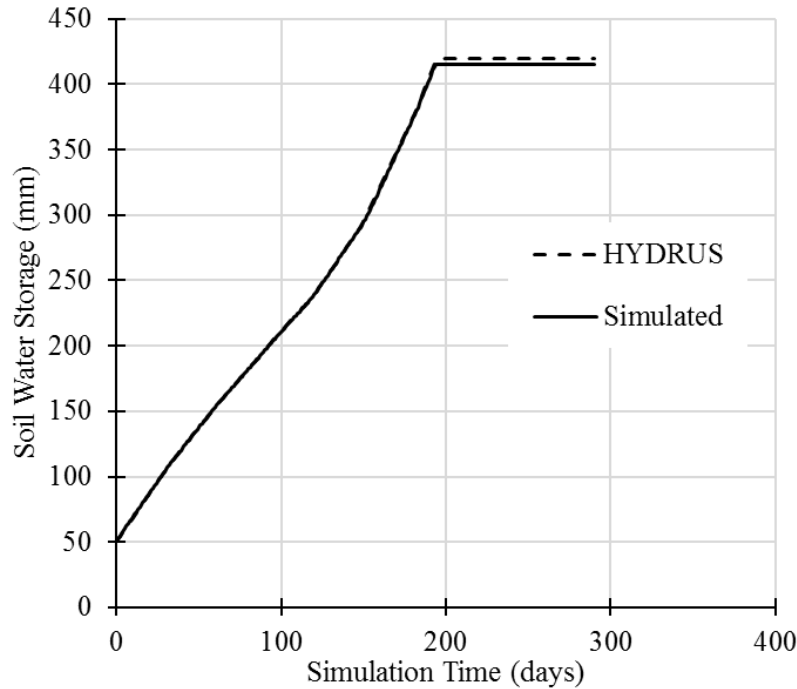
Figure 4-17 Comparison of extreme wetting tests between GoldSim and HYDRUS

4.4.2.2 Extreme Drying

The extreme drying test uses the same geometry and soil property setup as Figure 4-9 in Section 4.4.1 except the initial volumetric water content, which is set to fully saturated condition Q_s. Total simulation time is set at 365 days with a daily time step and maximum allowable time stepping of 0.1 minutes. The upper boundary condition is subject to seasonal evaporation normals in Fort McMurray, Alberta (Figure 4-16) without any precipitation during the simulation. The bottom boundary condition is subject to a free drainage condition. There is no upward flux at the bottom.

Figure 4-18 and Figure 4-19 show that the GoldSim is capable of handling extreme conditions of drying due to the excellent match of results between GoldSim and HYDRUS. The soil water storage decreased rapidly during the first 100 days of the simulation then slowed down afterward. Due to substantial decreases in hydraulic conductivities as matric suction was increased, water movement between layers and out of the bottom layer became negligible. The soil layer did not reach its residual water storage capacity at the end of the simulation since steep decreases in hydraulic conductivity prevented upward evaporative movement of water at the top and downward gravity drainage at the bottom (Figure 4-18).
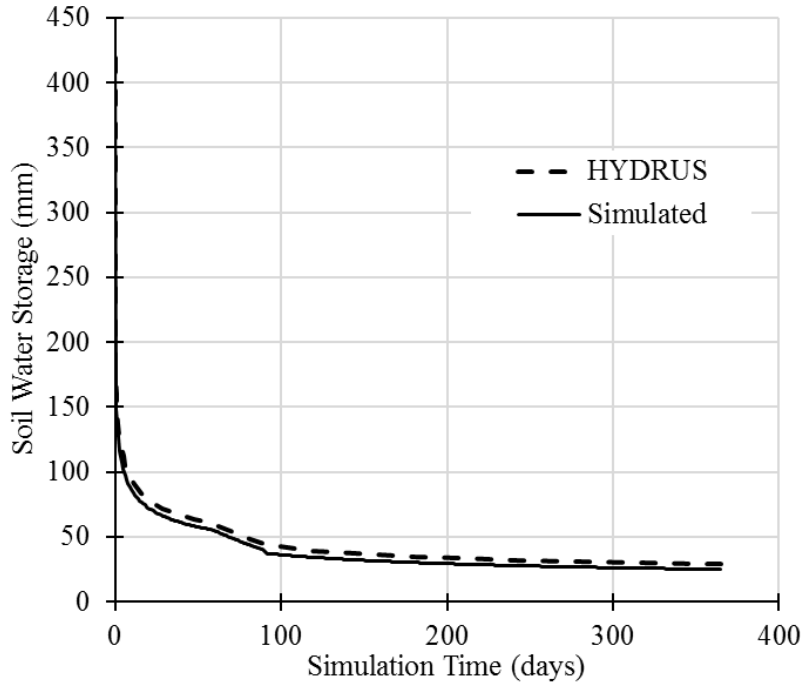
Figure 4-18 Comparison of water storage results under extreme drying
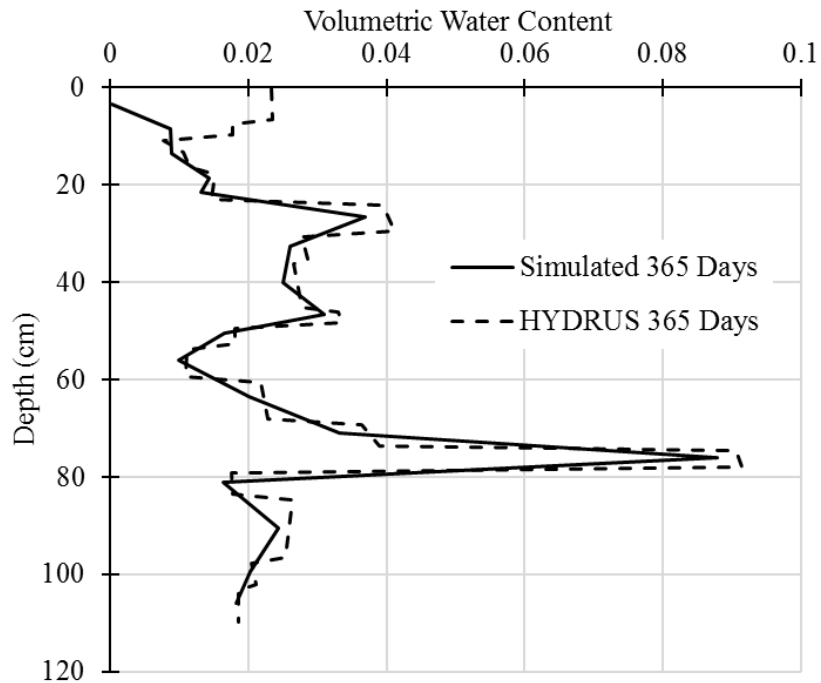
Figure 4-19 Comparison of water content profile under extreme drying

4.4.3   Validation Case III: Column Evaporation Experiment

The final validation case evaluates the model's ability to simulate changing boundary conditions and versatility in different soil material types. Two column drying experiments were used as the validation data. Huang et al (2013) provided detailed desriptions of the experiment program. Key model input parameters and high-level experimental procedures applicable to both sand and silt are summarized below.

The columns were 60 cm in height. In GoldSim, the 60 cm deep column is divided into 18 layers of equal thickness. Soil properties (Q_s, Q_r, a, n, and K_s) were assumed to be uniform in the entire 60 cm depth. Table 4-3 lists the numerical values for the soil property input. Both column tests in Section 4.4.3.1 and 4.4.3.2 were conducted in a controlled environmental chamber where relative humidity was kept at 11.1%. The potential evaporation (PE) rate was measured by water-filled evaporation pans. The bottom of the columns was controlled by a valve that allowed either free drainage or a constant head water table. Water content over time was measured at the sampling ports drilled on the side of the columns.

Table 4-3 Soil hydraulic parameters (after Huang et al, 2013).

Soil Properties	Beaver Creek sand	Processed silt
Q_s	0.347	0.408
Q_r	0.005	0.0095
Optimized a (1/cm)	0.0176	0.0027
Optimized n	3.838	3.082
Optimized K_s (cm/min)	6.12E-03	3.39E-05

4.4.3.1   Column Evaporation of Beaver Creek Sand

Soil properties of the Beaver Creek sand are listed in Table 4-3. The top boundary condition is subject to evaporative flux calculated by the suction-AE/PE ratio equation (Wilson et al, 1997). Average potential evaporation rate of 5.8 mm/day is used. Air temperature was kept at 35.3 degrees Celsius. The simulation adopted two stages of bottom boundary conditions. The first stage

involved maintaining a constant pressure head at the bottom for 31 days. In GoldSim, this constant pressure head was converted to an equivalent constant upward flux of 9.97E-05 cm/min based on a cumulative lower boundary inflow of 44.5 mm over 31 days. Then the second stage prescribed a zero flux lower boundary condition for another 30 days. The total simulation duration is therefore 61 days.

Figure 4-20 shows that the GoldSim model slightly underestimated changes in water storage. However, the behavioural trend in the GoldSim model is in good agreement with the measured data with a R^2 value of 0.99. The RMSE and MRE values for water storage are approximately 7 mm and 5% respectively. Change in water storage reached a plateau after 10 days (see Figure 4-20) as the surface layer (Layer 1) dried up to its residual water content (see Figure 4-21). The transmission rate from the surface layer (Layer 1) to its underlying layer (Layer 2) was the greatest at the start of the simulation but rapidly declined to almost zero after 10 days (see Figure 4-22). Evaporative flux is applied to Layer 1 only, resulting in an increased pressure gradient between Layer 1 and Layer 2. As water content in Layer 1 decreased due to evaporation, hydraulic conductivity also decreased. Eventually the reduction in hydraulic conductivity overwhelms the effect of increasing pressure gradient, restricting further upward water flow from the underlying layers.

For water content profile, the agreement is poor in the top 20 cm depth (see Figure 4-23). The following reasons likely contribute to the discrepancies as suggested by Huang et al (2013). The unsaturated hydraulic conductivity at low water contents or high suction pressure was under-estimated by the equations of van Genutchen (1980) and Maulem (1976). The lower hydraulic conductivity at the surface (Layer 1) would limit the evaporation process, resulting in lower water storage at the end of simulation. As mentioned in Section 4.4.1.1, limited spatial discretization reduces water transport between layers, especially near the surface where pressure gradient is the greatest due to evaporation-induced suction head. More accurate measurement of soil hydraulic parameters could improve simulation performance.

Additionally, it is important to note that the GoldSim model is isothermal, assuming no vapor transport under unsaturated condition. This assumption tends to overestimate the AE/PE ratio and evaporation rate, especially for the sand column since soil and air resistance to evaporation are ignored. The stock element in GoldSim allows the user to set a lower bound below which further

outflow is restricted. Therefore, from a validation perspective, the model seems to produce satisfactory results in water storage and water content profile despite this shortcoming. One way to numerically include vapour transport is to adjust either total suction approach or relative humidity. Dunmola (2012) and Fredlund et al (2015) summarized the adjustment approaches and provided additional experimental data for comparison. However, this is outside the scope of this model thus will not be implemented.
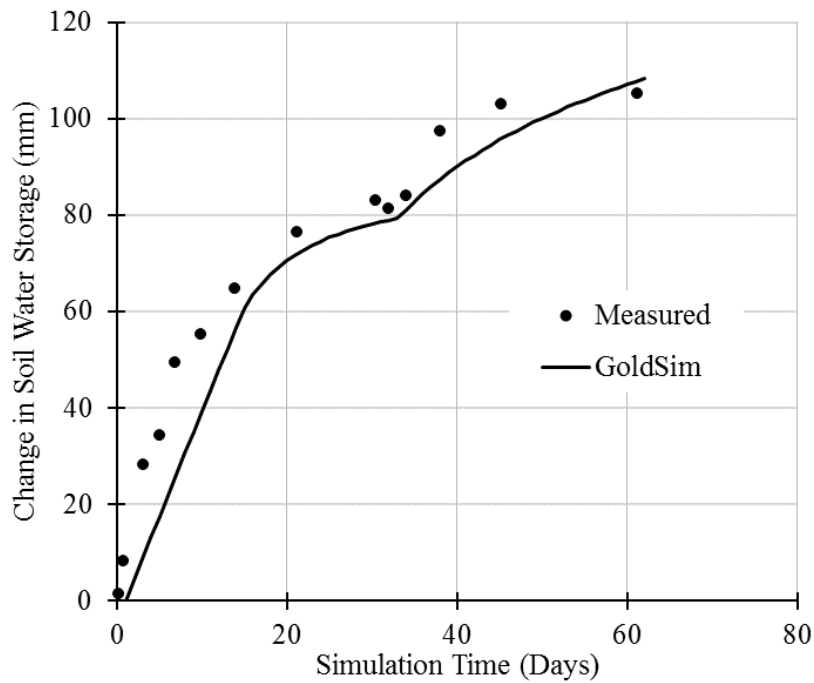
Figure 4-20 Comparison of cumulative changes in soil water storage between measured Beaver Creek sand and GoldSim simulation.
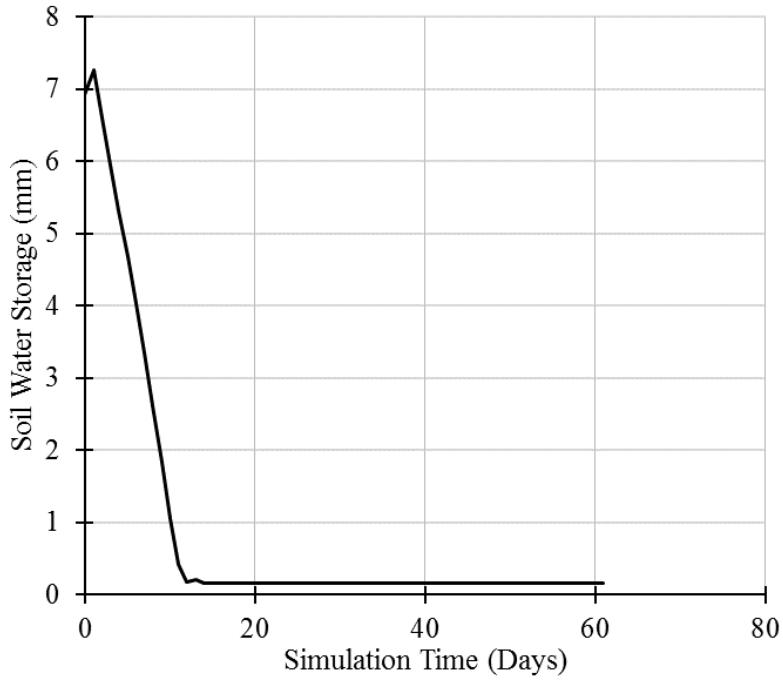
Figure 4-21 Water storage over time in the surface layer (Layer 1).
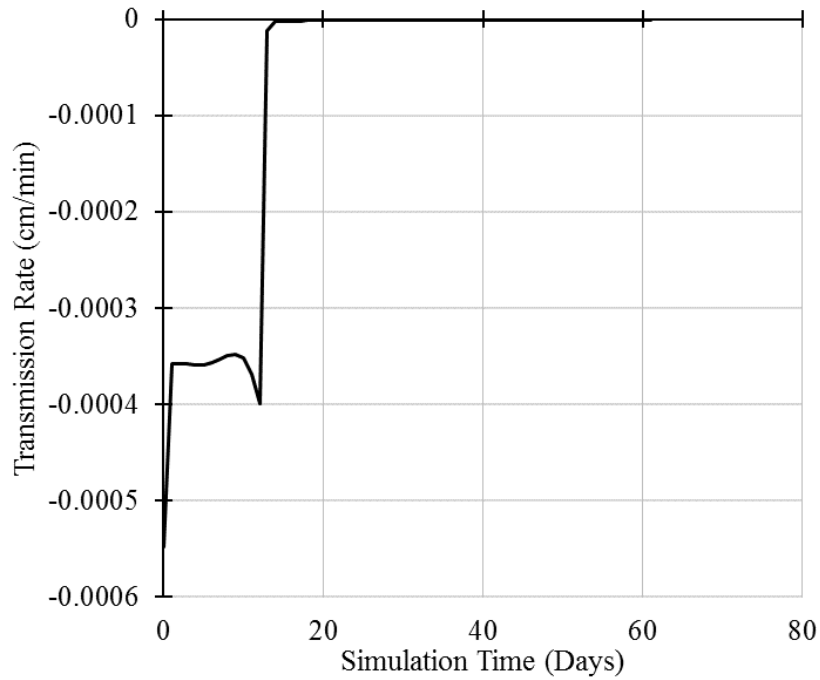
Figure 4-22 Transmission rate from Layer 2 to the surface layer (Layer 1); negative sign indicates an upward direction of water flow.
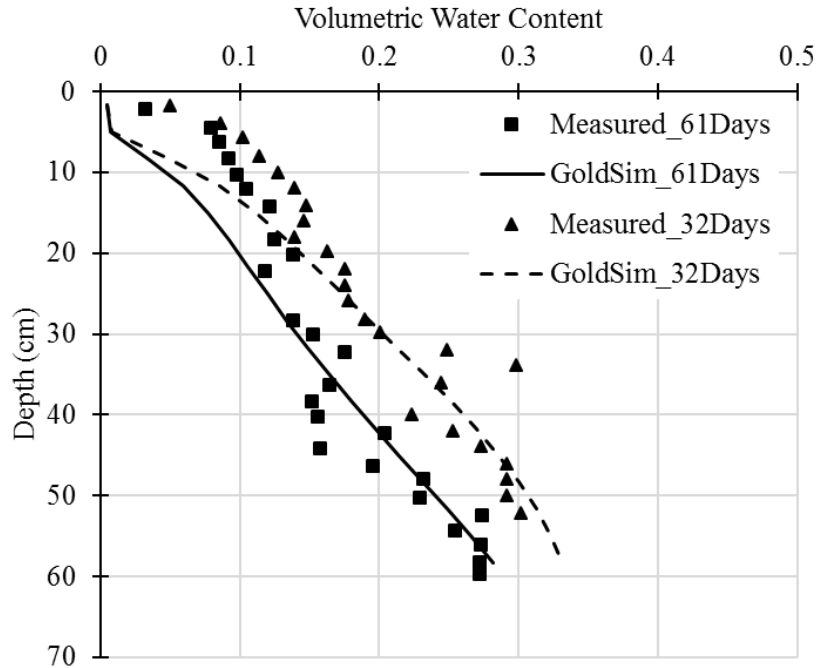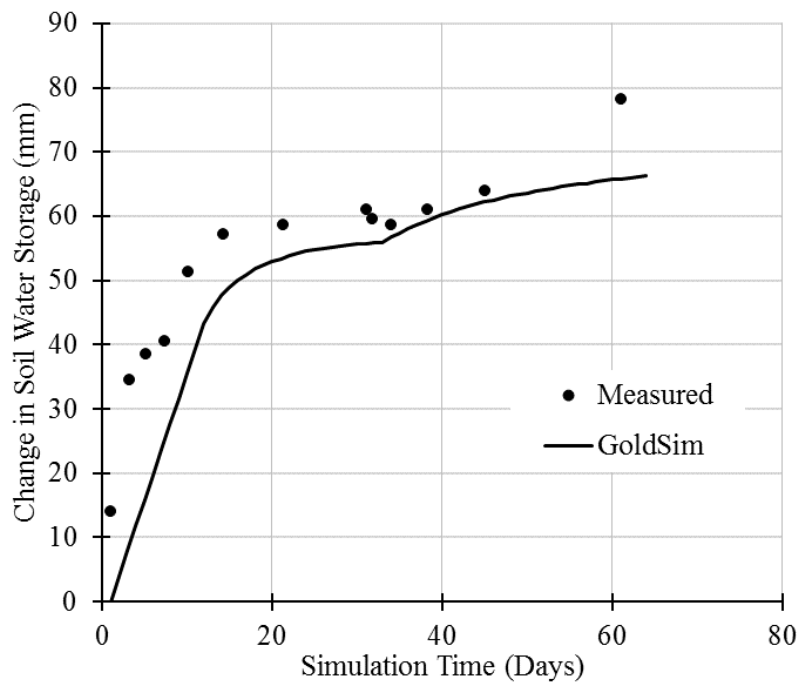
Figure 4-23 Comparison of water content profile at 32 days and 61 days between measured Beaver Creek sand and GoldSim simulation.

4.4.3.2 Column Evaporation of Silt

Soil properties of the processed silt are listed in Table 4-3. The top boundary condition is subject to evaporative flux calculated by the suction-AE/PE ratio equation (Wilson et al, 1997). Average potential evaporation rate of 5.6 mm/day is used throughout the simulation. Air temperature was kept at 36 degrees Celsius. Similar to the sand column, the simulation of silt column adopted two stages of bottom boundary conditions. The first stage involved maintaining a constant water head of 5 mm above the soil bottom. In GoldSim, this constant water head was converted to an equivalent constant flux of 1.29E-04 cm/min based on a cumulative lower boundary inflow of 57.5 mm over 30.92 days. Then the second stage sets a zero-flux, impermeable lower boundary condition for another 30.08 days. The total simulation duration is therefore 61 days.

Like the Beaver Creek sand case, a similar water transport mechanism is at work for silt. Using the K_s calibrated in HYDRUS, the GoldSim model produced a good behavioural match of water storage with a R^2 value of 0.99 (Figure 4-24). The RMSE and MRE values for total water storage

are 6 mm and 3% respectively. Like the measured data, the simulated surface layer (Layer 1) also reached its residual water content in about 8 days, restricting any further upward water movement from the underlying layer (Figure 4-25).

The GoldSim model overestimated changes in water storage during the first 31 days under a constant upward flux lower boundary (see the black line in Figure 4-24). The omission of vapour transport contributes to the over-estimation of water storage as the AE/PE ratio remains close to unity until after the first 31 days. Uncertainties in K_s also contributes to the over-estimation as a re-calibrated K_s half of the original value produced a better match of results during this period (see the red line in Figure 4-24).

However, the re-calibrated K_s scenario under-estimated changes in water storage during the zero-flux period after 31 days, as shown by the red line in Figure 4-24. This is mainly due to: 1) a lower K_s which increases water holding capacity and reduces inter-layer flow; and 2) the dry, near impermeable surface layer (Layer 1) which prevents upward transmission of water from the underlying layers to the surface.

In the top 20 cm depth, the discrepancy in water content profile is more pronounced at 32-day than at 61-day (Figure 4-26). The calibrated K_s, which was reduced by half from the original K_s, yielded better agreement in water content profile of the top 20 cm. However, below 20 cm, the match of water content is poorer than the scenario using the original K_s. This disagreement below 20 cm is caused by the assumed homogeneity in the material properties, limited spatial discretization and absence of vapour transport mechanism. Further calibration of K_s, finer spatial discretization and inclusion of vapour transport can certainly increase the numerical accuracy of the model (see Figure 4-26). However, the current validation effort is deemed sufficient for the purpose of establishing the behavioural validity of the model.
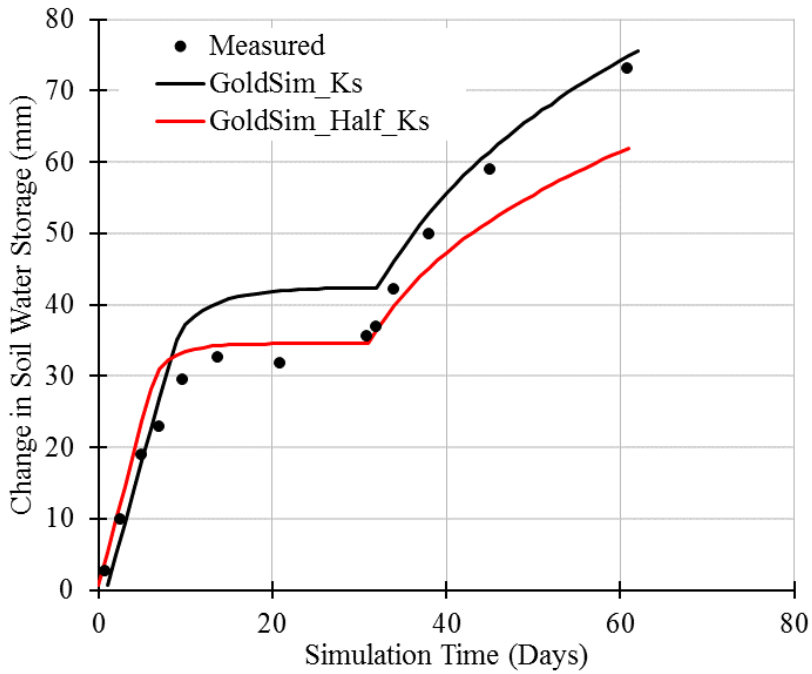
Figure 4-24 Comparison of changes in water storage between measured processed silt and GoldSim simulation.
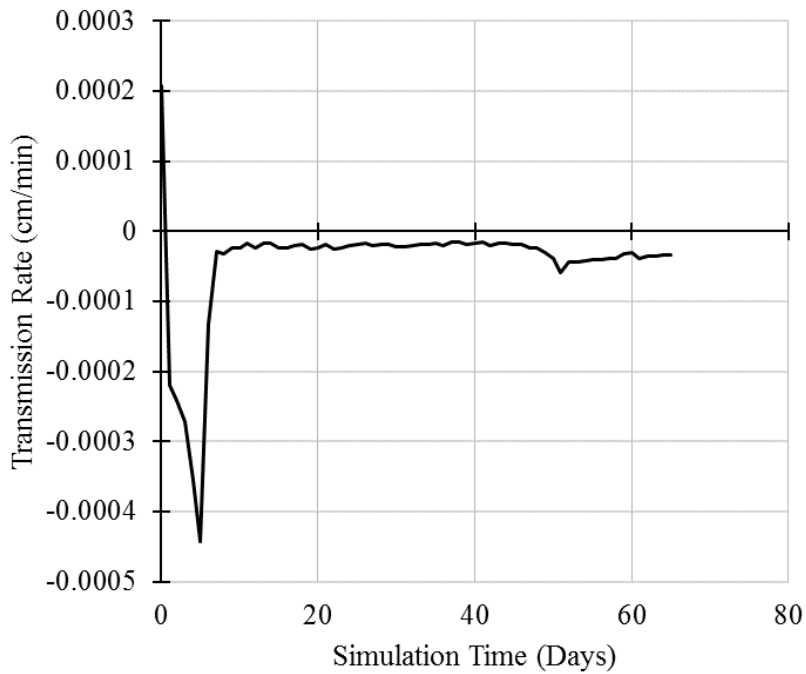
Figure 4-25 Transmission rate from Layer 2 to the surface layer (Layer 1) using optimized K_s; negative sign indicates an upward water flow.
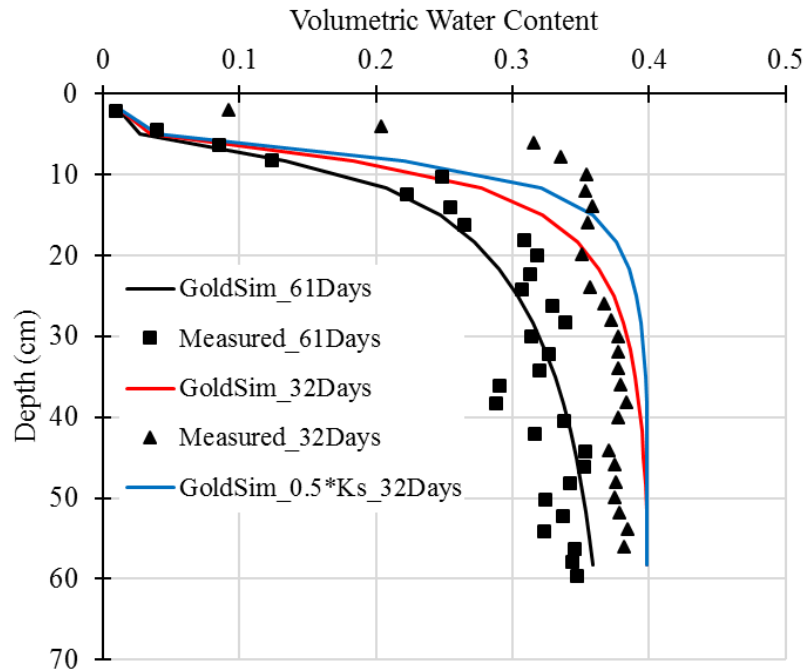
Figure 4-26 Comparison of water content profile at 32 days and 61 days between measured processed silt and GoldSim simulation.

4.4.3.3 Column Evaporation of Dual-Layer Systems

Additional validation runs were conducted on the sand-silt and silt-sand system from Huang et al (2013). The sand-silt system consisted of a 30 cm of sand layer overlying a 30 cm of silt layer. The order of sand and silt was reversed for the silt-sand system setup. In GoldSim, Layers 1 to 9 were assigned to the top material and Layers 10 to 18 were assigned to the bottom material. The same hydraulic properties from Section 4.4.3.1 and 4.4.3.2 were used. The sand-silt system received a cumulative lower boundary inflow of 20.6 mm, and the silt-sand system received a cumulative boundary inflow of 91.7 mm, both over 31.09 days after which the lower boundary was made impermeable. The daily bottom inflow was assumed to be constant during the first 31.09 days. The initial water contents for both systems were assumed to be the HYDRUS-simulated water contents on the 1st day from Huang et al (2013).

The simulated water contents and storage showed the same behaviour as the single-layer setup from Section 4.4.3.1 and 4.4.3.2. The model under-estimated the change in water storage in sand layers while overestimating it in silt layers (see Figure 4-27 and Figure 4-29). In terms of water

content profiles, discrepancies similar to those from Section 4.4.3.1 and 4.4.3.2 were observed near the surface (see Figure 4-28 and Figure 4-30). However, the model successfully represented water contents at the interface between sand and silt. In the silt-sand system (Figure 4-30), both sand and silt layers were un-saturated. In the sand-silt system (Figure 4-28), the lower silt layer remained fully saturated while the overlying sand layer was unsaturated. As discussed by Huang et al (2013), this demonstrated how the sand-silt system can restrict oxygen diffusion as the coarser sand layer acts as a capillary barrier on the top.

Figure 4-27. Comparison of changes in water storage between measured values from the sand-silt column and GoldSim simulation.
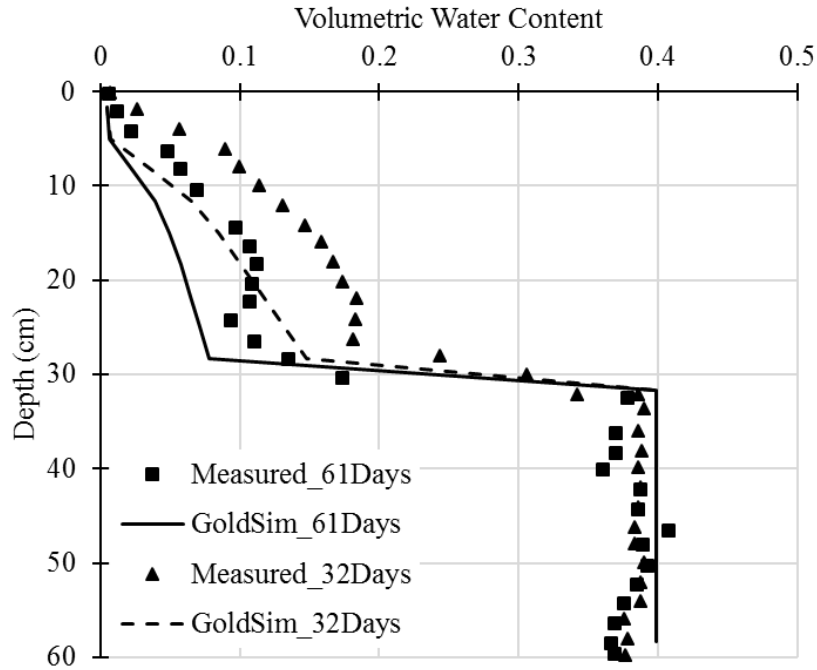
Figure 4-28 Comparison of water content profile at 32 days and 61 days between measured values from the sand-silt column and GoldSim simulation.
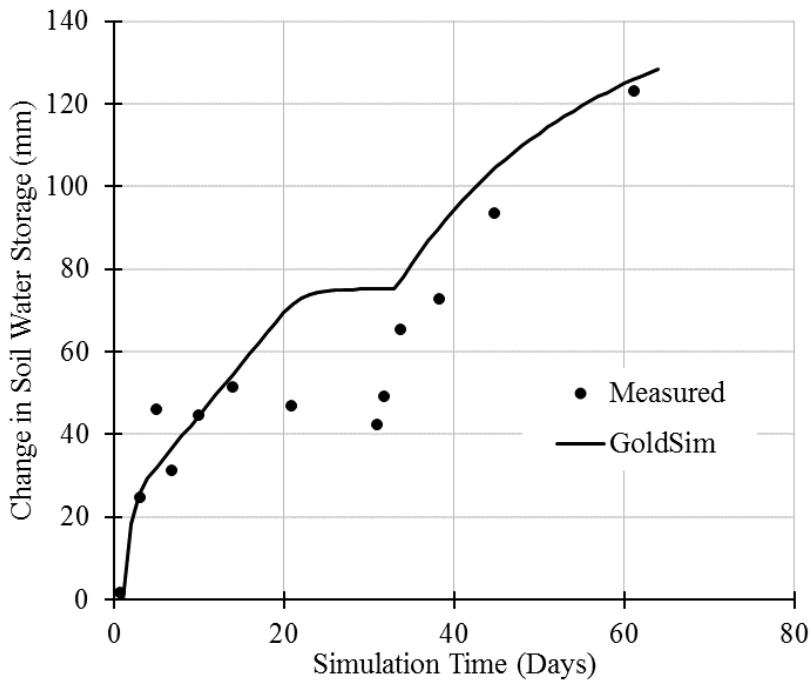
Figure 4-29 Comparison of changes in water storage between measured values from the silt-sand column and GoldSim simulation.
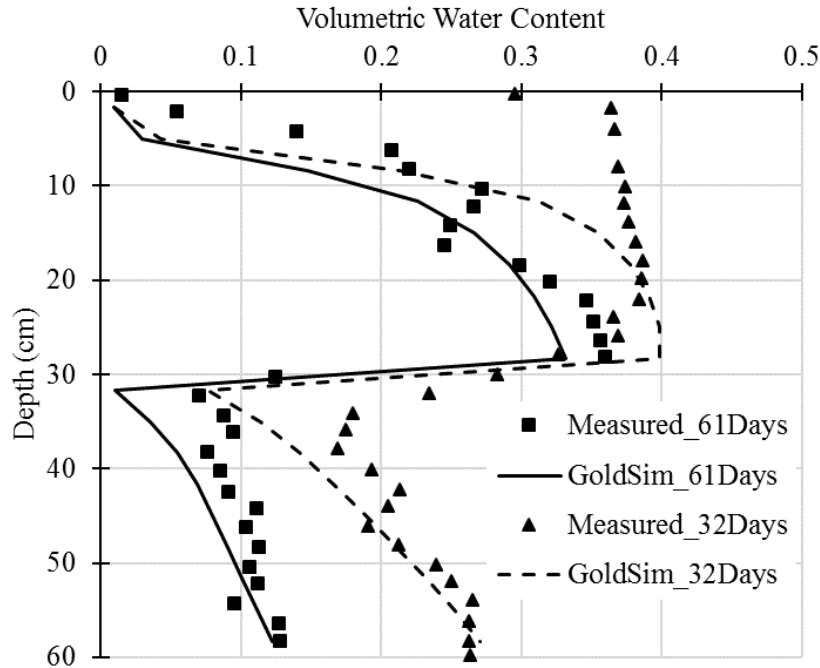
Figure 4-30 Comparison of water content profile at 32 days and 61 days between measured values from the silt-sand column and GoldSim simulation.

4.5 WATER BALANCE CHECK

A water balance calculation at the specified time step was carried out for all validation cases. The water balance calculation for the cap layer uses climatic input specified by the user, lower boundary conditions and changes in soil water storage. The equations for the water balance check, as implemented in GoldSim, are listed below:

$$WB = Inflow - Outflow - (\Delta S) \qquad (4.15)$$

$$Inflow = Cum\ Top\ Infil + Layer18.CumUpwardFlux \qquad (4.16)$$

$$Outflow = Layer1.Cum\ Evap + Layer1.Cum\ Runoff$$
$$+ Layer18.CumBotFlux \qquad (4.17)$$

Where ΔS is the change in total water storage with respect to the initial water storage at any given time; $Inflow$ is the cumulative amount of water flowing into the cap layer; $Inflow$ consists of the cumulative amount of surface infiltration from precipitation ($Cum\ Top\ Infil$) and of upward flux

into the bottom layer due to consolidation or user-specified flux function ($Layer18. CumUpwardFlux$); $Outflow$ is the cumulative amount of water leaving the cap layer at any given time; $Outflow$ consists of cumulative amount of evaporative flux at the surface ($Layer1. Cum\,Evap$), cumulative surface runoff due to precipitation or overflow ($Layer1. Cum\,Runoff$), and cumulative downward flux from the bottom layer ($Layer18. CumBotFlux$); WB is the water balance check component, which should be as close to zero as possible.

For all validation cases, WB results are close to zero and less than 1 mm. Therefore, the model has taken into consideration of all components of the water mass movement.

4.6 USER INTERFACE AND VISUAL DESIGN

The gaming approach advocated by Elsawah et al (2015) is adopted as the guiding principle in the visual design part of the GoldSim model. The user interface and dash boards for the integrated model are carefully designed to facilitate transparency and functionality for the less technical or non-technical users. As shown in Figure 4-31, the sequence of parameter input is partitioned into different areas and clearly labelled such that the set-up process is less prone to omissions and errors. The user can monitor real-time results during an ongoing simulation without having to wait until the end of the simulation. The user can also see, open and examine every variable in the model the same way the creator of the model did during the development process.

Figure 4-32 shows how select links are bolded to emphasize the feedback structure. The arrows and elements are strategically placed to minimize unnecessary crossing of each other. The container element in GoldSim is a useful feature to group and organize variables according to their functions and categories, minimizing visual congestion.

Figure 4-31 Parameter input user interface
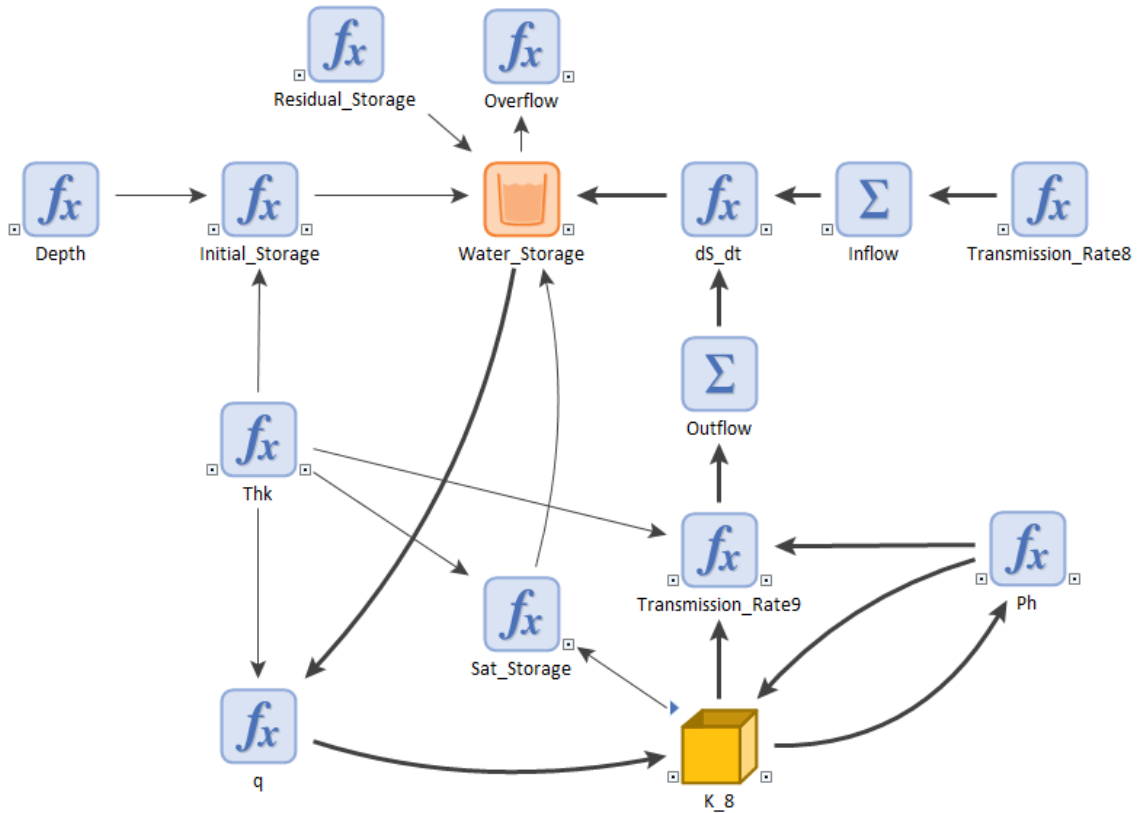
Figure 4-32 Typical layer setup inside one of the 18 containers

4.7 INTEGRATION WITH CONSOLIDATION SUB-MODEL

A Sub-Model element is a self-contained system that represents a model within a model. The main outer model embeds a separate, inner Sub-Model element with its own independent simulation settings (GoldSim 2018). A Sub-Model element called "Consolidation" in Figure 4-33 stores the entire consolidation model developed in Chapter 3. The unsaturated flow model developed in previous sections is designated as the main outer model. One-way influence arrows were bolded to emphasize the spatial feedback structures. Activation of the Sub-Model element requires a triggering condition, without which the sub-model will not run. In this case, the consolidation sub-model will be activated if the user selects the "Consolidation Upward Flux" option in the "Lower Boundary Inflow Condition" drop-down menu, as shown in Figure 4-31.

In order for the consolidation sub-model to provide a flux output to the main model, the user has to open the interface tab of the Sub-Model element and specify the output type as "Time History" and the output definition as "Final Value" in the "Output Interface Definition" panel. Doing so will enable the main, outer model to access output generated by the sub-model.

To avoid missing and mismatch of time series output between the sub-model and the main model, the user must specify identical start date and time for both. Both models use a daily basic time step. For unscheduled updates, the consolidation sub-model adopts an hourly time step while the un-saturated flow model adopts a 0.1-minute time step.
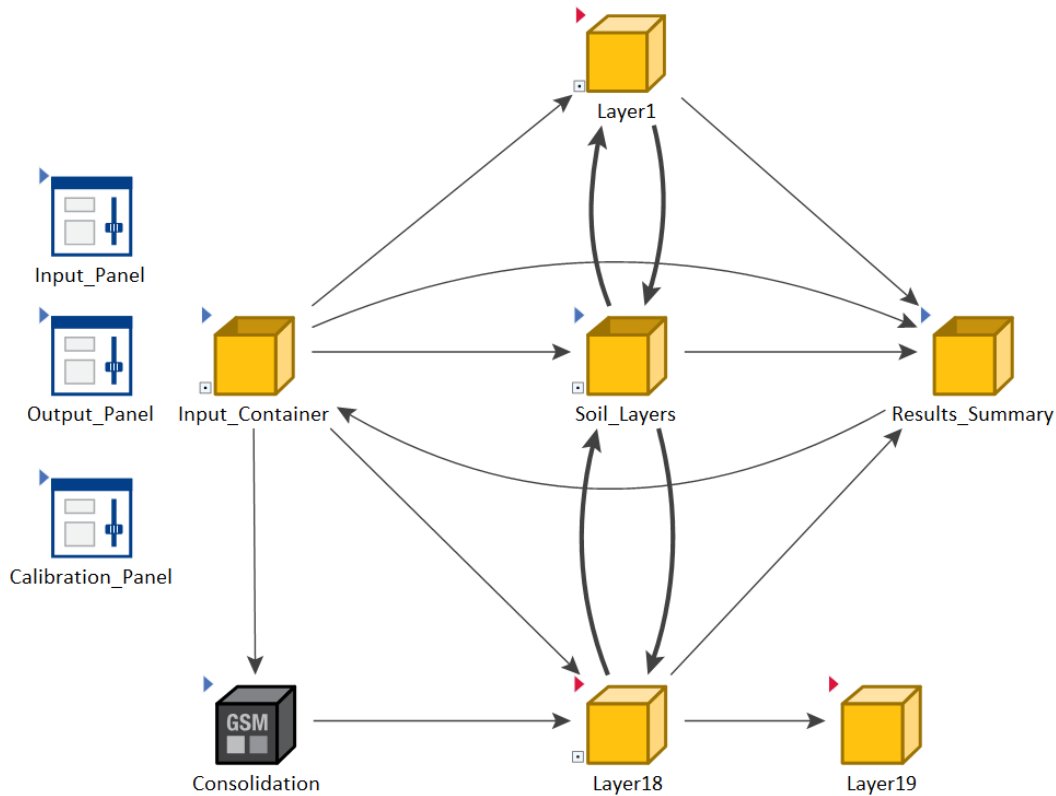
Figure 4-33 Overview of the integrated model

4.8 CONCLUSION

An earlier SD model, developed by Huang et al (2011a), was modified, validated and implemented in the GoldSim software to become the unsaturated flow model in this thesis. The model development added capabilities of handling surface evaporation, precipitation and consolidation flux. Then the unsaturated flow model and the consolidation model were combined into a single model through the sub-model element function in GoldSim. The integrated model was intended to simulate fluid transport and soil water dynamics between the CST cap and the tailings substrate.

The validation process adopted multiple approaches to build confidence in the model. Measured data from simple infiltration and drainage tests were used to establish reference validity of the model. Numerical data from HYDRUS 1D were used to assess model stability under hypothetical extreme drying and wetting conditions. Measured data from column drying experiments were used

to test the model's flexibility and ability to handle different material types and dynamic boundary conditions.

The predicted behaviour of soil water storage and water content profile over time agreed well with the measured and simulation data. In case of discrepancies with field data, calibration of K_s is required prior to applying the model to other data sets. Additional spatial discretization (i.e. adding more layers) will increase the level of agreement in terms of numeric values. However, the objectives of the GoldSim model are to foster interdisciplinary understanding, build transparency and facilitate linkages to sub-models. While further increasing spatial resolution is technically feasible in the software, doing so will hamper efficiency and create an overly complex model. As a result, the GoldSim model may not be a suitable tool for detailed assessment of layer geometry and thickness options.

Despite those limitations, the GoldSim model developed under a SD framework has demonstrated its suitability as a high-level simulation tool for assessing long-term soil water dynamics. The SD modelling process promotes shared understanding of key physical processes through the use of CLD, SFD, visual design in GoldSim, and simplification of differential equations. All functional relationships and variables are explicitly expressed in a SD simulation environment. For example, the user is able to examine and sometimes alter the model structure and details of calculation in Figure 4-32 and Figure 4-33 in the same way a modeler did during the development process. The transparency and participatory nature of the SD modelling process aims to eliminate the boundary between modeler and the end-user and to bring together technical and non-technical stakeholders. Therefore, SD modelling can be a useful tool in tailings management and mine closure studies.

5 CASE STUDY – COARSE SAND TAILINGS (CST) CAP OVER THICKENED TAILINGS (TT)

5.1 PROBLEM DEFINITION AND OBJECTIVES

The overall guiding philosophy of tailings closure in the Oil Sands rests on the condition that the reclaimed landscapes will have equivalent or better capability to sustain the a-priori ecological system native to the site (Kessler et al. 2010). To achieve the goal of non-disturbance, two broad categories of ecosites are typically planned: terrestrial ecosite (i.e. upland) and aquatic ecosite (i.e. end-pit lake, wetland).

This case study will focus on the first step of creating an upland landform: capping deep fines-dominated deposits (i.e. Thickened Tailings) prior to vegetation placement. There are many environmental challenges associated with upland landform, one of which is the negative effect of high salinity in the future vegetation root zone due to upward migration of consolidation-release water from tailings substrate (Cilia 2017; Rima and Beier 2018). High soil salinity near the surface can impose additional stresses to future vegetation cover and forest growth (Renault et al. 1999 and Vessey et al. 2018). Kessler et al (2010) summarized three key driving mechanisms by which salt can migrate upward: 1) diffusion-driven salinity gradient; 2) advection-driven water movement and 3) restricted downward flushing of salt due to low hydraulic conductivity of saline-sodic material.

The first step toward understanding the salt migration process is to understand the long-term soil water dynamics in the capping layer during the transition period between end of tailings deposition and placement of vegetation cover (Zettl et al. 2011). One of the objectives in this thesis is to develop and use the SD methodology to bring transparency and shared understanding to the modelling process. The SD models developed in Chapter 3 and 4 promote this objective by explicitly expressing all variables in the numerical solution and empowering both users and modelers with the ability to view and modify functional relationships between the variables. Therefore, the case study will use the integrated model developed in Chapter 3 and Chapter 4 to gain insights on key drivers of soil water dynamics in the capping layer.

The objectives of this case study are to examine the impact of lower boundary conditions and saturated hydraulic conductivity on the scheduling of future vegetation placement and maturity. Planners and stakeholders are often interested in the financial impacts of reclamation and closure, one of which is knowing the amount of time the underlying flux will reach and potentially daylight the surface of the capping layer. These objectives entail asking and answering the following questions:

Question 1: when and under what conditions will the upward flux "daylight" or reach near the cap surface?

Question 2: what are the major factors that influence the time to reach a quasi- equilibrium state in the capping layer?

For Question 2, major factors under investigation are limited to endogenous parameters within the system, that is within the active control of construction operators, engineers and planners. For example, void ratio and hydraulic conductivity of the capping layer can be varied by degree of compaction and placement method. Solids content of the underlying tailings layer can be controlled by dewatering technologies. Exogenous variables outside human control such as climatic input and groundwater recharge are not included.

5.2   MODEL FORMULATION

Several oil sands operators have proposed sand capping as part of their closure strategy for deep fines-dominated tailings deposits as in the case of Thickened Tailings (TT). (Imperial 2016; Shell 2016; and Syncrude 2017). The basic conceptual setup of the model can be found in Figure 4-1 from Section 4.3.1. The geometry essentially involves a generic 3 m thick CST cap on top of a 50 m thick TT deposit. The thickness values of CST cap and TT deposit are chosen based on reasonably worst-case capping requirement and average expected heights of deep deposits respectively.

Two sub-models, the consolidation sub-model and the flow sub-model, form the backbone of the integrated model. The consolidation sub-model will supply time-dependent upward flux to the bottom water storage in the flow sub-model. In GoldSim, the consolidation sub-model is

represented by a sub-model element while the flow model is the main umbrella model. Detailed setup in the software is described in Appendix 3. Chapter 3 and Chapter 4 described the development and validation of the consolidation and flow model respectively. The same information will not be repeated here.

5.3 PARAMETER INPUT

5.3.1 Unsaturated Flow Model for Coarse Sand Tailings (CST)

Kouakou (2014) conducted a comprehensive laboratory program on flume deposits from Total's beaching studies. The van Ganutchen parameters and saturated hydraulic conductivity K_s are based on results from the beach sand and A3 flume deposits. Water content and void ratio input are based on the CST field trials from McKenna et al (2010). Table 5-1 lists values of parameter input for GoldSim.

McKenna et al (2010) observed that there is no distinct trend of K_s variation over depth at two trial pads of CST placement. The unsaturated hydraulic parameters, initial volumetric water contents and K_s are assumed to be the same over the entire depth of the cap layer. The entire cap layer is assumed to be homogenous.

Proposed CST cap thickness generally ranges from 1 m to 5 m (Imperial 2016 and COSIA 2012). As a compromise, a 3 m thick CST cap is assumed for this case study. The 3 m thick cap layer is equally divided into 18 layers with each layer 16.7 cm thick.

The CST cap is assumed to be placed mechanically and thus expected to receive some degree of compaction. McKenna et al (2010) analyzed field compaction data on tailings beach sand from two trial pads that are mechanically placed. 40T articulated dump trucks mechanically placed the tailings sand after which D8 and D9 dozers spread and compacted the fill. The average Troxler-measured field dry density is about 1754.5 kg/m³ with an average gravimetric water content of 3.5%. Using Equation 5.1 and Equation 5.2, the average field dry density translates to a void ratio of approximately 0.51 and degree of saturation at 18%. Therefore, the mechanically placed CST can be considered initially unsaturated. The initial volumetric water content Q_{ini} is calculated by Equation 5.3 below:

$$e = \frac{G_s \rho_w}{\rho_d} - 1 \qquad\qquad (5.1)$$

$$Sat = \frac{w G_s}{e} \qquad\qquad (5.2)$$

$$Q_{ini} = \frac{Se}{1 + e} \qquad\qquad (5.3)$$

where e is the void ratio of the soil; ρ_w and ρ_d are the density of water and dry density of soil respectively; G_s is the specific gravity of the soil solids; w is the gravimetric water content; Sat is the degree of saturation.

Unsaturated soil properties were derived from soil water characteristic curve (SWCC) measurements up to a suction pressure of 100 kPa. The van Ganutchen-Maulem fitting parameters $(a, n,$ and $m)$ were estimated by the data fitting function in SoilVision's SVFlux software. The unit of a was converted from the default 1/kPa in SVFlux to 1/cm in GoldSim.

Table 5-1 CST hydraulic parameter input in GoldSim.

Parameter Type	Value	Description	Default Unit
a	0.023	van Genuchten-Maulem fitting parameter	1/cm
n	5.48	van Genuchten-Maulem fitting parameter	Dimensionless
m	0.82	van Genuchten-Maulem fitting parameter (m=1-1/n)	Dimensionless
K_s	1.2E-04	Reference saturated hydraulic conductivity	cm / s
e	0.51	Void ratio	Dimensionless
Q_{ini}	0.061	Initial vol. water content	Dimensionless
Q_s	0.428	Saturated vol. water content	Dimensionless
Q_r	0.012	Residual vol. water content	Dimensionless

5.3.2   Consolidation Model for Thickened Tailings (TT)

Various operators have conducted laboratory and field trials on thickened tailings technology. Shaw et al (2010) and COSIA (2012) provides a good summary of available results from large-strain consolidation experiments performed on TT. It is important to note that the consolidation parameters of TT are dependent on a multitude of factors, such as flocculant types and dosage, thickener design, rheology, pipeline transport, depositional environment, and post-deposition treatment. The scope of this case study is limited to examining the effect of different end-product consolidation properties (i.e. initial solids content). The causes behind those different properties will not be investigated here.

For this modelling exercise, GoldSim input for large-strain consolidation parameters (A, B, C and D) was derived from Total's TT trial studies (Table 5-2). Specific gravity of solids G_s for TT is 2.44 (Scott et al. 2008). Initial solids content (SC) of TT is assumed to be uniform throughout the entire deposit. Compressibility or effective stress-void ratio fitting parameters were taken from

COSIA (2012). Permeability-void ratio fitting parameters were taken from Zhang et al (2017). The parametric relationships of A, B, C and D follow those described in Chapter 3. Equation 5.4 and 5.5 converted fines void ratio e_{fines} used in COSIA (2012) to void ratio e assuming a Sands-to-Fines Ratio (SFR) of 0.9, which is equivalent to a fines content (FC) of 53%.

$$FC = \frac{1}{1 + SFR} \tag{5.4}$$

$$e = e_{fines} * FC * \left(\frac{G_{coarse}}{G_{fines}}\right) \tag{5.5}$$

where G_{coarse} and G_{fines} are the specific gravity of coarse mineral grains and fines mineral grains respectively.

Table 5-2 TT parameter input for GoldSim consolidation model.

TT Parameter	Value	Description	Default Unit
A	1.6231	Compressibility curve fitting parameter	kPa
B	-0.256	Compressibility curve fitting parameter	Dimensionless
C	1.09E-04	Permeability curve fitting parameter	m/day
D	3.042	Permeability curve fitting parameter	Dimensionless
SC_0	0.40 to 0.65	Initial solids content	Dimensionless
G_s	2.44	Specific gravity of solids	Dimensionless
e0_fictitious	0.1	Initial void ratio for the bottom fictitious layer	Dimensionless
deposit_h	50	Total height of the TT deposit	m
Min_DT	0.1	Maximum dynamic time step	days

5.3.3 Upper Boundary Condition

The upper boundary is subject to monthly normal climatic input in Fort McMurray, Alberta (Figure 4-16). Input for relative humidity and mean temperature can be found in Table A2-1 and Table A2-2 in Appendix 2 respectively. Evaporation setting remains the same as in Section 4.3.4.3 and Section 4.4.2. This model adopts a monthly resolution of climatic input. For higher resolution (i.e. daily precipitation instead of monthly), the user has the option of using the daily stochastic Fort McMurray weather generator developed by Shahin et al (2013).

5.3.4 Lower Boundary Condition

The flux output element Consolidation.v from the consolidation model provides the upward inflow rate (cm/min) through a time series element in the main flow model. No downward flux into the

TT layer is permitted for the bottom layer of the cap. No lateral drainage out of the CST layer is permitted as the problem is restricted to modelling one dimensional vertical flow.

5.4 SCENARIO ANALYSIS

From earlier studies, the value of saturated hydraulic conductivity K_s controls the accuracy and behaviour of the flow model (Huang et al. 2011a and 2011b) since the GoldSim model has limited spatial discretization. Solids content (SC) has been designated by the regulator and operators as one of the key performance indicators for thick fines-dominated deposits (AER, 2015). The magnitude of upward flux from the TT deposits is dependent on the initial SC of the deposited tailings. Therefore, the scenario analysis involves five scenarios in which the magnitudes of K_s and initial SC are varied while climatic input and boundary conditions remain the same.

For K_s sensitivity scenarios, the initial SC is assumed to be at 60% while the value of K_s will be varied up to one order of magnitude from the reference value (Table 5-3). For initial SC scenarios, K_s of the CST cap is assumed to be 1.2E-04 cm/s while the value of initial SC will be varied from a minimum of 40% to a maximum of 65%, which covers the full range of expected behaviour upon deposition (Table 5-4). All sensitivity simulations will run for a period of 10 years or 3650 days at a daily time step. Maximum dynamic time stepping of 0.1 minutes and 0.1 day are prescribed for the main flow model and the consolidation model respectively.

Table 5-3 Ks scenario summary

Scenario	CST K_s (cm/s)	Initial SC of TT (%)	Description
1a	1.2E-04	60	Reference
2a	2.4E-04	60	$2*K_s$
3a	1.2E-03	60	One Order More
4a	6.0E-05	60	Half K_s
5a	1.2E-05	60	One Order Less

Table 5-4 TT initial SC scenario summary

Scenario	CST K_s (cm/s)	Initial SC of TT (%)	Description
1b	1.2E-04	N/A	No Consolidation Flux
2b	1.2E-04	40	Lower Limit
3b	1.2E-04	50	Resonably Worst Case
4b	1.2E-04	60	Reference
5b	1.2E-04	65	Upper Limit

5.5 CST K_s SCENARIO RESULTS AND DISCUSSION

This section discusses the results from simulation scenarios in Table 5-3. Given a TT deposit with an initial SC of 60%, Figure 5-1 indicates that the value of K_s in the capping layer has very little influence on the amount of time the total water storage takes to reach a quasi-equilibrium behaviour, which is characterized by the sustained oscillatory pattern past about 2000 days. This sustained oscillatory pattern in total water storage during the quasi-equilibrium stage was caused primarily by the seasonal variations in temperature, precipitation and relative humidity as evident in the dashed lines from Figure 5-2 and Figure 5-3.

From the "global" perspective of the entire layer, K_s appears to influence how total water storage reaches the quasi-equilibrium phase. The low hydraulic conductivity of the surface layer limits the peak water storage during the summer months. In Figure 5-1, Scenario 5a "One Order Less K_s" sustained a rising trend approximately one year longer than Scenario 3a "One Order More K_s" case. Scenario 5a also maintained a peak value about 80 mm greater than Scenario 3a during the quasi-equilibrium phase.

From the "local" perspective of each individual layer, water storage dynamics can be divided into two distinct phases: 1) the unsaturated phase during the early period of simulation; and 2) the quasi-saturated phase after the arrival of wetting front. The duration of each phase and arrival time of the wetting front depends on the net inflow, upward consolidation flux, and to a lesser extent, the magnitude of K_s. The transition from the unsaturated to the quasi-saturated phase is characterized by a steady rise of water storage toward the fully saturated level of the layer. This

steady rise of water storage is more dramatic in deeper layers (Figure 5-3) than shallower layers (Figure 5-2) since the deeper layers receive the consolidating flux earlier and are less influenced by the climate.

As shown in Figure 5-2, K_s in Layer 4 appears to regulate the extent of climatic influence on the water storage. During the unsaturated phase, reduction of K_s by one order of magnitude increased the amplitude of oscillation in water storage by approximately 50%. However, simulated behaviour during the quasi-saturated phase were completely different from and opposite to those observed during the unsaturated phase. In the lower K_s case, amplitude of fluctuation in water storage was dampened by the arrival of wetting front and during the quasi-saturated phase. In the higher or the reference K_s case, amplitude of fluctuation in water storage was amplified by the arrival of wetting front.

One possible explanation of the dampening and amplifying behaviour is that during the quasi-saturated phase, the higher K_s amplifies the dominance of positive or reinforcing feedback loops, which facilitate water transfer between layers. In comparison, the lower K_s dampens the influence of positive feedback loops and instead makes room for the dominance of negative or balancing feedback loops, which restrict water transfer between layers. In the deeper Layer 6 (see Figure 5-3), the aforementioned dampening and amplifying behaviours disappeared when the consolidation flux overwhelmed the evaporative flux and kept the layer fully saturated during the quasi-saturated phase.

The effect of K_s on water storage behaviour appear to be partially supported by field observations at two re-constructed watershed research stations near Fort McMurray. Detailed information on the field instrumentation setup and soil hydraulic parameters can be found in Meiers (2002), Boesce (2003) and Julta (2006). The prototype covers consist of a peat layer ranging from 15 cm to 20 cm in thickness underlain by a till layer ranging from 20 cm to 80 cm in thickness. The Bill's Lake (BL) cover consists of a 100 cm thick, relatively homogenous peat-till mix layer. The hydraulic conductivity of the peat is approximately one order of magnitude higher than that of the till material or the peat-till mix based on testing results from Meiers (2002). The monitoring results from the field showed that the peat layer in the prototype covers is more responsive to fluctuations in major rainfall events than the peat-till matrix at BL, according to Meiers (2002) and Boesce (2003).

Major rainstorms and snowmelt at the watersheds are analogous to the arrival of wetting front from the simulated consolidation flux in GoldSim. Therefore, a similar argument can be made: the peat layer tends to amplify the effect of major rainfall events on water storage while the peat-till matrix tends to dampen the effect. However, it is unclear whether the dampening and amplification effect can be attributed solely to K_s since lateral flow and topography are not included in the GoldSim simulation model. Therefore, experiments conducted in a more controlled environment are required to isolate and study the effect of varying K_s on soil water storage.

The magnitude and duration of fluctuation in soil water storage may be significant as some vegetation can be highly sensitive to even the smallest amount of disturbance and oscillation in soil water storage (Alberta Environment, 2010).
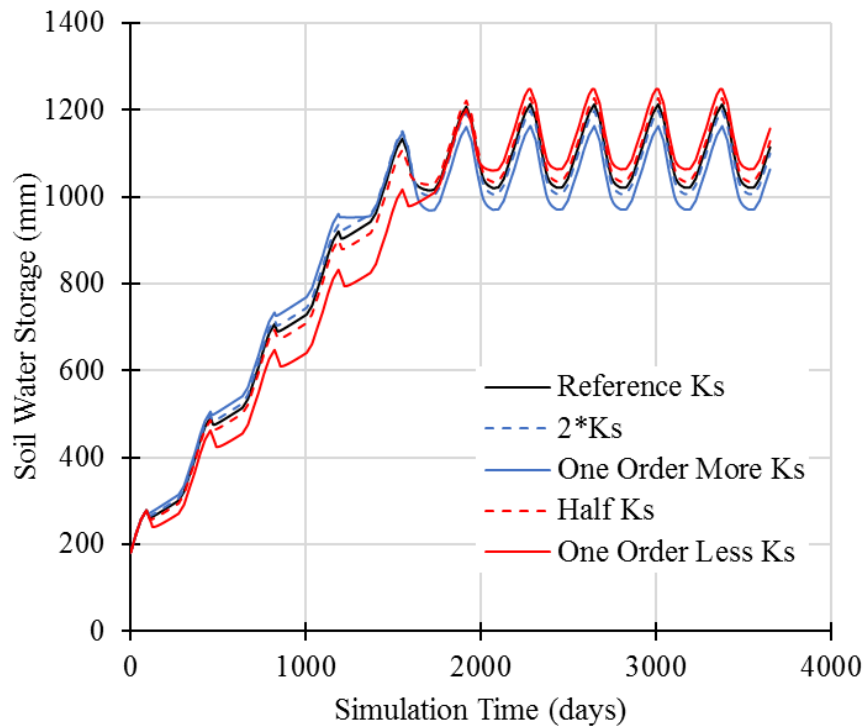

Figure 5-1 Effect of different K_s on total soil water storage
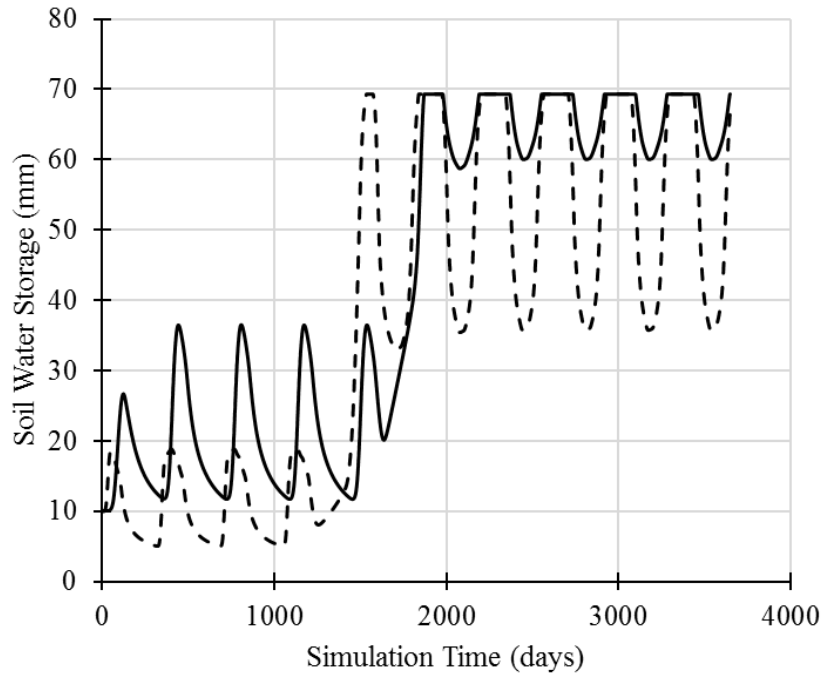
Figure 5-2 Climatic influence on the water storage at depth 58 cm (Layer 4); solid line is Scenario 5a ("One Order Less Ks" case); dashed line is Scenario 1a (Reference Ks case).
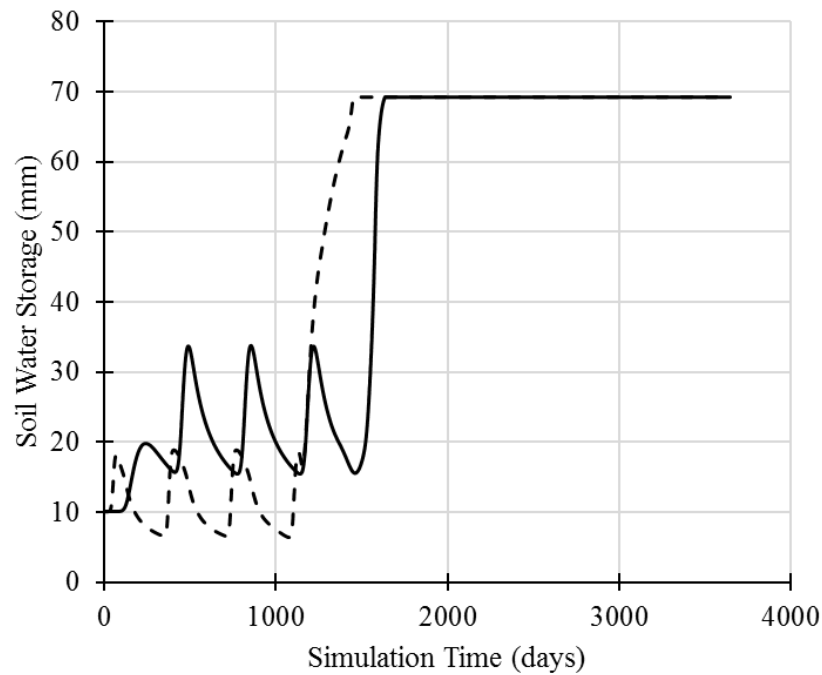
Figure 5-3 Climatic influence on the water storage at depth 92 cm (Layer 6); solid line is Scenario 5a ("One Order Less Ks" case); dashed line is Scenario 1a (Reference Ks case)

5.6 INITIAL SC OF TT SCENARIO RESULTS AND DISCUSSION

This section discusses results from simulation scenarios in Table 5-4. Under the same reference K_s for the cap layer, Figure 5-4 indicated that the behaviour of soil water storage is highly sensitive to the initial SC of the consolidating TT. An increase of 10% in the initial SC of TT delayed the amount of time the flux takes to reach near the CST cap surface by 1 to 2 years (see Table 5-5). The same delay was evident in the time gap between the solid and dashed line at 58 cm depth (Layer 4). As shown in Figure 5-5 and Figure 5-6, the wetting front under the zero-consolidation scenario reached both Layer 4 and Layer 6 at about 1000 days or almost two years later than the scenario with consolidation.

The sensitivity of water storage behaviour to consolidation flux is also supported by the rest of simulated scenarios. Flux from TT with initial SC of 40% and 50% (Scenario 2b and 3b in Table 5-4) reached near the cap surface in as few as two to three years. The upward consolidation flux overwhelmed the evaporative flux at the surface. From the perspective of feedback structures, the positive feedback loop brought by precipitation and consolidation flux dominated over the negative feedback loop from the process of evaporation, causing the consolidation release water from TT to daylight at the cap surface. At the end of the 10-year simulation, the cumulative release water in the form of surface run-off was 4170 mm for TT with initial SC of 40% and 744 mm for TT with initial SC of 50% (see Figure 5-8). There is no precipitation-induced run-off since all the water at the surface was absorbed by the CST cap whose K_s is higher than the peak precipitation rate. All surface run-offs are induced by overflow from the underlying layers.   Increasing the initial SC of TT from 40% to 50% reduced the surface run-off by more than 80%. In practical terms, a 10% increase in the initial SC of each layer of TT deposited during the operational phase will have significant benefits and cost-savings during the closure phase.

Furthermore, if the initial SC of TT falls below 60%, operators have 2 to 3 years to implement remediation measures before the consolidation release water from TT reaches the surface, as shown in Table 5-5. Increasing the CST cap thickness can delay but cannot prevent the daylighting of TT-affected water at the surface. Therefore, any improvement in the initial SC, especially for TT at the lower end of solids content spectrum, will significantly reduce the amount of release water at the surface.

The cumulative run-off results in Figure 5-8 may be under-estimated due to the absence of the snowmelt process in the model and assumption of a flat topography. During the snowmelt process, free water may accumulate on the surface of a layer that is still frozen (Julta, 2006). Given an inclined topography, the accumulated water will then flow down and contribute to the total surface run-off in addition to the contribution from the TT flux that daylighted at the surface.

On the other hand, consolidation release water from TT with initial SC of 60% and of 65% will not reach the cap surface as shown in Figure 5-8 where the cumulative surface run-off and overflow rate are zero for both initial SCs. Under these scenarios, the top 50 cm of the CST cap remains at an un-saturated state most of the time, as shown in Figure 5-7. When the initial SC of the underlying TT is above 60%, the evaporative flux is able to remove any consolidation flux that migrated into the surficial layer. Advective flux from TT with initial SC above 60% is not sufficient to permeate the CST cap with consolidation release water. The evaporative flux also created a low permeability barrier at the surface that significantly slowed down the upward movement of the consolidation release water from TT.

Based on the observation above, in order to prevent daylighting of the release water from TT, the initial SC requirement for this type of TT needs to be at least 60%. The initial SC requirement will change for different types of TT as consolidation properties are dependent on chemical dosage, polymer type, pore fluid chemistry, etc. From a general point of view, the implication of TT with low solids content (i.e. <50%) may be significant in terms of both physical and chemical stability for the reclamation cover. Numerical studies conducted by Cilia (2017) on coke-over-centrifuged-tailings setup supported the same view that salinity migration is sensitive to the rate of settlement in tailings substrate. Therefore, further studies are warranted in this aspect.

Table 5-5 Comparison of time-to-quasi-equilibrium under different initial SC of TT

Initial SC of TT (%)	Time (days)	Time (years)
40	680	2
50	1141	3
60	1917	5
65	2285	6
No Consolidation	3000	8
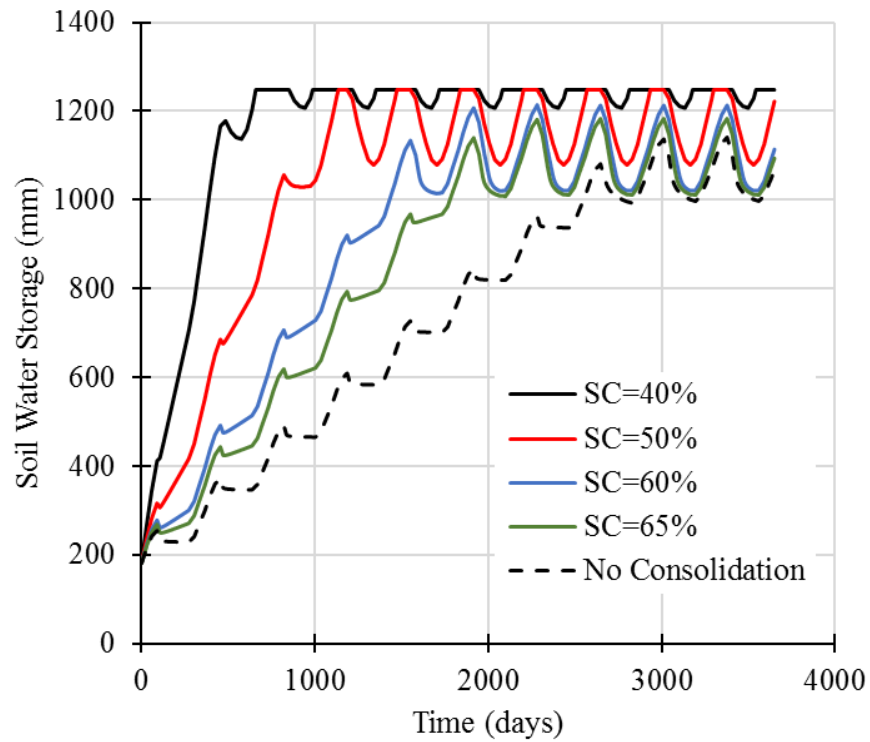
Figure 5-4 Sensitivity of initial SC of TT on total soil water storage
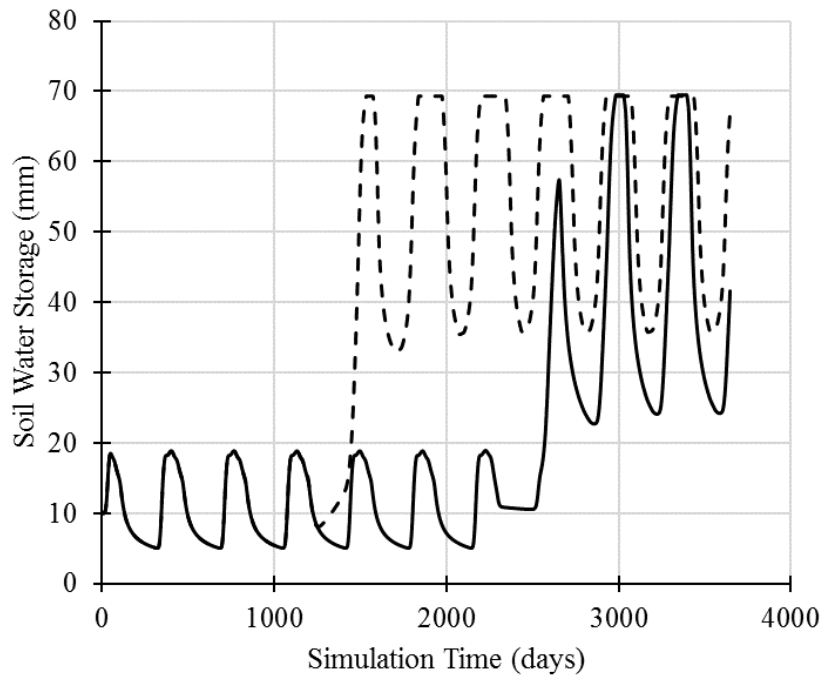
Figure 5-5 Climatic influence on the water storage at depth 58 cm (Layer 4); solid line is Scenario 4b (Reference Ks without consolidation case); dashed line is Scenario 1b (Reference Ks with consolidation case)
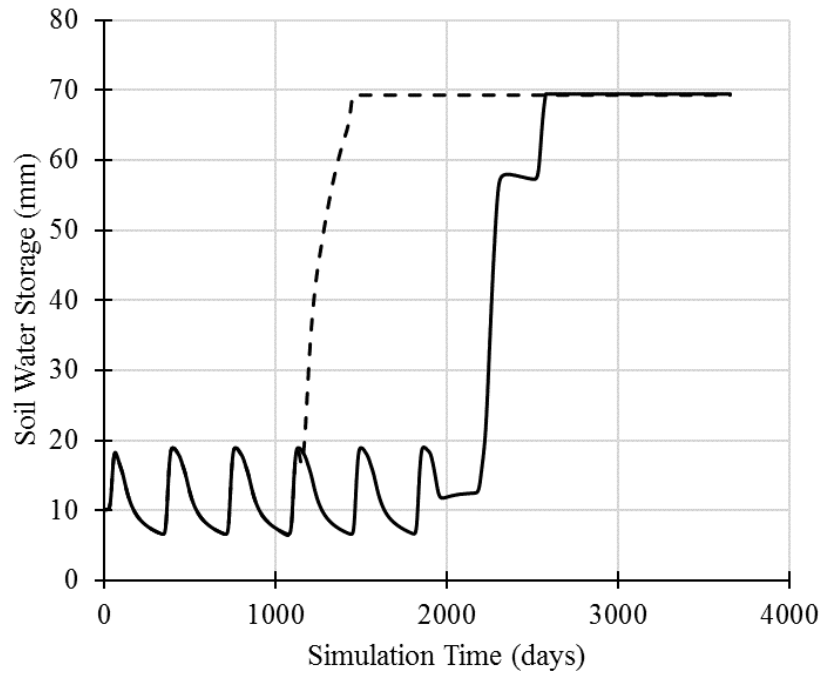
Figure 5-6 Climatic influence on the water storage at depth 92 cm (Layer 6); solid line is Scenario 4b (Reference Ks without consolidation case); dashed line is Scenario 1b (Reference Ks with consolidation case)
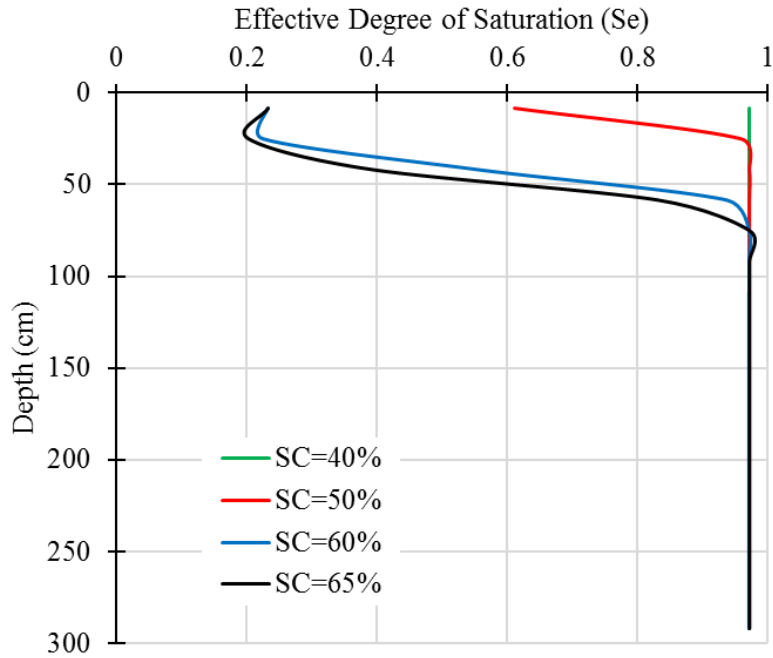
Figure 5-7 Effective degree of saturation profile at the end of the 10-year simulation for various TT initial SC under the reference Ks
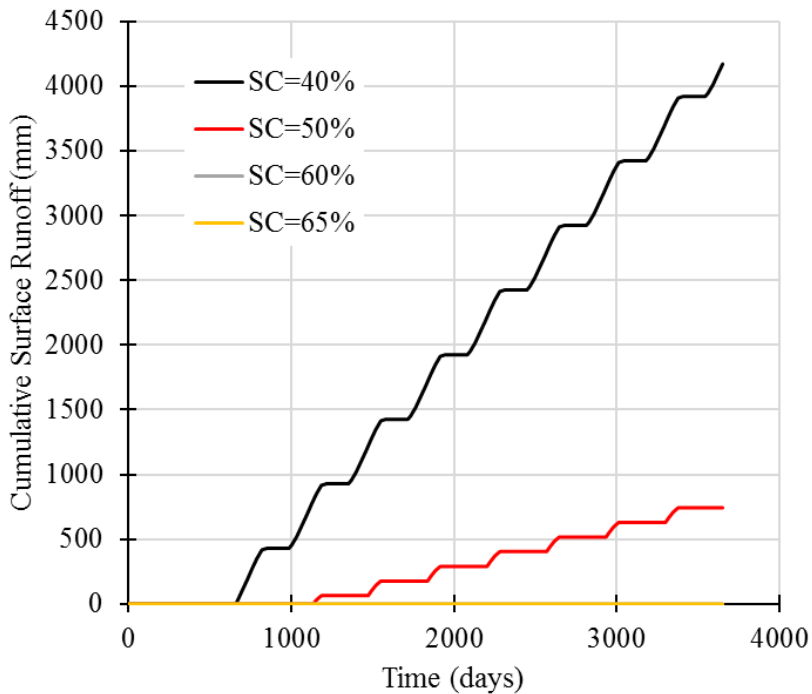
Figure 5-8 Cumulative surface run-off during the 10-year simulation for different initial SC of TT.

5.7 CONCLUSIONS

The integrated GoldSim model incorporating sub-models developed in Chapter 3 and Chapter 4 was successfully applied on a case study simulating real world scenarios in capping deep fines-dominated TT deposits. Concepts of CLD and feedback loops described in Chapter 2 were used to explain some of the observations on the dynamics of soil water storage over time. For Question 1 in Section 5.1, the amount of time for the consolidation flux to reach near or daylight at the surface is highly sensitive to the initial SC of underlying TT, varying from 2 to 8 years. In this case, the ability of climatic forces to remove release water from TT can only be utilized when the initial SC of TT exceeds 60%. Increasing the initial SC of TT from 40% to 50% could result in substantial reduction of the release water to the surface by as much as 80%.

For Question 2 in Section 5.1, the K_s of the capping layer has little influence on the time to reach a quasi-equilibrium state in soil water storage. However, K_s does influence the magnitude of peak soil water storage in the long term and the growth behaviour leading to the quasi-equilibrium state. The water storage under the lower K_s scenario is more susceptible to climatic fluctuations during the un-saturated phase than it is during the quasi-saturated phase. For the reference or higher K_s scenario, the opposite behaviours were observed. The water storage is more susceptible to climatic fluctuation during the quasi-saturated phase than it is during the un-saturated phase. For vegetation that is sensitive to large fluctuations in soil water storage or abrupt increases in water salinity, the ecological impact of these behavioural changes in the dynamics of soil water storage require further experimental and numerical studies.

6 CONCLUDING REMARKS

6.1 SUMMARY CONCLUSION

The thesis adopts System Dynamics (SD) as the modeling philosophy for simulating interaction of soil water dynamics between the CST capping layer and tailings substrate. The GoldSim software is used as the simulation engine for the consolidation sub-model and the un-saturated flow sub-model. Physical processes can be expressed by the process of creating causal loop diagrams (CLD) and subsequent conversion of CLDs into quantitative models. Underlying assumptions of the model are made explicit by identification of feedback structures through CLD and categorization of variables through the Bull's Eye Diagram.

The SD-based consolidation sub-model provides input to the un-saturated flow sub-model, which describes the water movement in the CST layer. Based on RMSE, MRE and visual inspection, the consolidation sub-model successfully simulated settlement and consolidation flux of various types of tailings under different material properties and thicknesses. The simulated behaviour are consistent with trends from experimental data and predictions made by commercial tools. Due to simplification of the numerical scheme and assumptions in the physical process, the consolidation sub-mdoel should only be used as a high-level screening tool. Analyses requiring high degrees of numerical accuracy should be handled by numerical tools that use implicit scheme to solve the governing equation of large-strain consolidation. Nested Monte Carlo simulations of both epistemic and aleatory uncertainty also demonstrate the feasibility and flexibility of SD models to carry out stochastic simulations and produce aggregated probabilistic input to future risk assessment.

The unsaturated flow sub-model is based on a previously developed SD-based infiltration-drainage model. This thesis improves the original model by enhancing the visualization design, simulating additional validation cases and adding capabilities to handle surface evaporation, inter-layer overflow and surface run-off under climatic influence. Confidence in the improved model is further demonstrated by the successful validation of extreme conditions and dynamic boundary conditions against experimental and numerical results.

The combined model incorporating the consolidation and un-saturated flow sub-model is then used to simulate water movement within the CST cap at a generic closed oil sands tailings storage

facility near Fort McMurray. Simulation results show that upward movement of consolidation release water from the tailings substrate plays a dominant role in the soil water dynamics of the CST capping layer during the early stage of reclamation. The amount of time for the consolidation flux to daylight at the CST surface is highly sensitive to the initial SC of underlying TT. The ability of climatic forces to remove release water from TT is limited. Increasing the initial SC of TT from 40% to 50% could result in substantial reduction of the release water to the surface by as much as 80%. There is no daylighting of release water at the CST surface if the initial SC of TT exceeds 60%.

The global dynamics of soil water storage is little affected by changes in the K_s of the CST layer whereas the local dynamics is highly influenced by K_s. Soil water storage under the lower K_s scenario is more susceptible to climatic fluctuations during the un-saturated phase than it is during the quasi-saturated phase. In the reference or higher K_s scenario, dynamic behaviours of soil water storage are more susceptible to climatic fluctuation during the quasi-saturated phase than during the un-saturated phase. For vegetation plants that are sensitive to large fluctuations in soil water storage or abrupt increases in water salinity, the ecological impact of these behavioural changes in the dynamics of soil water storage require further experimental and numerical studies.

6.2 LIMITATIONS OF THE MODEL

The limitations listed below are applicable to both the consolidation and unsaturated flow sub-models, which are collectively referred to as "the model":

- The model has limited capabilities of representing variables at different spatial scales since SD models are not intended to model complex spatial relationships.
- The model is suitable for simulating physical processes described by first order non-linear ordinary differential equations; the model is not able to simulate partial differential equations that require iterative solutions of equations and matrices.
- Simulations with a duration longer than 10 years take more than an hour to complete, preventing the use of the model in a workshop setting where time is often limited.
- In GoldSim, graphical icons of model variables are different from symbols traditionally used in SD. Those differences could potentially hinder acceptance of the model in the larger SD community.

6.3 RECOMMENDATION FOR FUTURE WORK

To fully exploit the advantages of CLD and participatory modeling techniques in the SD methodology, it is recommended to host multi-disciplinary, industry-wide modeling workshops. It is important to involve non-technical stakeholders as active participants in model building exercises. A multi-phase approach is preferred. The first phase may include activities to define and formulate research questions and modeling objectives based on a spectrum of quantitative and qualitative input. Focusing on specific problems, the second phase can use a variety of qualitative tools (i.e. CLD and the Bull's Eye Diagram) to create preliminary, simple models and promote shared understanding of the problem across disciplinary boundaries. Future phases of workshops should adopt an iterative, dynamic approach where quantitative and qualitive models inform each other and evolve over time based on feedbacks and new information.

For the consolidation sub-model, potential areas of improvement include: 1) extending the sub-model's ability to handle spatially heterogenous and temporally dynamic material properties; 2) implementation of additional feedback process (i.e freeze and thaw) between the surface layer of the tailings substrate and the bottom layer of the capping layer; and 3) automation of setup for the fictitious boundary layer to enhance user friendliness and numerical stability.

For the un-saturated flow sub-model, potential areas of improvement include: 1) implementation of a contaminant transport and mixing model if the objective is to study the migration of solutes in the capping layer; 2) adding vapour diffusion mechanism to more accurately describe the evaporation process; 3) implementation of water uptake due to vegetation roots; and 4) modeling the effect of volume change on various material properties.

Opportunities to integrate SD models with business, geomorphology, ecology and public policy models should be explored. Additional insights from an integrated social-economic-environmental model would be valuable to oil sands operators, regulatory bodies, governments and the general public.

REFERENCES

AER 2015, Tailings regulatory management initiative: engagement summary, Alberta Energy Regulator, Calgary, Alberta.

Alberta Environment 2010, Guidelines for reclamation to forest vegetation in the Athabasca Oil Sands region, Terrestial Subgroup of the Reclamation Working Group of the Cumulative Environmental Management Association, Fort McMurray, Alberta.

Baecher, G.B. 2016, Uncertainty in dam safety risk analysis, Georisk: Assessment and Management of Risk for Engineered Systems and Geohazards, vol. 10, no. 2, pp. 92-108.

Baecher, G.B. & Christian, J.T. 2003, Reliability and Statistics in Geotechnical Engineering, Wiley, Chichester, West Sussex, England.

Beier, N.A. 2015, Development of a Tailings Management Simulation and Technology Evaluation Tool, PhD thesis, University of Alberta.

Beier, N., Sego, D. & Morgenstern, N. December,2014, Assessing a novel technology using a tailings management simulation model, International Oil Sands Tailings Conference, University of Alberta, Lake Louise, Alberta, December 7-10, 2014, pp. 113.

Beier, N., Sego, D. & Morgenstern, N. 2009, Dynamic simulation of tailings management options, Tailings and Mine Waste, University of Alberta Geotechnical Centre, Banff, Alberta, Canada, November 1-4, 2009, pp. 441.

BGC Engineering Inc 2010, Review of reclamation options for oil sands tailings substrates, Oil Sands Research Information Network (OSRIN), Edmonton, Alberta, Canada.

BGC Engineering Inc & Oil Sands Research and Information Network 2012, Oil sands tailings technology review, Oil Sands Research and Information Network, University of Alberta, School of Energy and the Environment, Edmonton.

Binder, T., Vox, A., Belyazid, S., Haraldsson, H.V., Svensson, M.G. 2004. Developing System Dynamics models from Causal Loop Diagrams. Available online: https://pdfs.semanticscholar.org/cf00/ b9084b05ba357bf0c5fa7a5b9cc1b5695015.pdf (accessed January 24, 2019).

Bromwell, L.G. October,1984, Consolidation of mining wastes, Sedimentation/Consolidation Models, San Francisco, California, October,1984, pp. 275.

Butters, G.L., Jury, W.A. & Ernst, F.F. 1989, Field scale transport of bromide in an unsaturated soil: 1. Experimental methodology and results, Water Resources Research, vol. 25, no. 7, pp. 1575-1581.

Cargill, K.W. 1982, Consolidation of soft layers by finite strain analysis, U.S. Army Engineer Waterways Experiment Station; Springfield, VA.: available from National Technical Information Service, 1982, Vicksburg, Mississippi.

Chorley, R.J., Schumm, S.A., & Sugden, D.E. 1984. *Geomorphology*, Methuen, London and New York.

Cilia, C.R.C. 2018, Characterizing the physical and chemical mass transport of dissolved salts in layered oil sands waste undergoing reclamation, University of Saskatchewan.

Cockerill, K., Tidwell, V.C., Passell, H.D. & Malczynski, L.A. 2007, Cooperative Modeling Lessons for Environmental Management, Environmental Practice, vol. 9, no. 1, pp. 28-41.

COSIA 2012, Technical guide for Fluid Fine Tailings management, Oil Sands Tailings Consortium.

Daliri, F. 2013, The influence of desiccation and stress history on monotonic and cyclic shear response of thickened gold tailings, PhD thesis, Carleton University.

Davies, E.G.R. & Simonovic, S.P. 2011, Global water resources modeling with an integrated model of the social–economic–environmental system, Advances in Water Resources, vol. 34, no. 6, pp. 684-700.

Dingman, S.L. 2002. Physical hydrology. 2nd Edition, Prentice Hall, New Jersy, USA.

Dunmola, A.S. 2012, Predicting evaporative fluxes in saline soil and surface-deposited thickened mine tailings, Carleton University.

Dunne, T. & Black, R.D. 1970, An Experimental Investigation of Runoff Production in Permeable Soils, Water Resources Research, vol. 6, no. 2, pp. 478-490.

Edlefsen, N. & Anderson, A. 1943, Thermodynamics of soil moisture, Hilgardia, vol. 15, no.2, pp. 31-298.

Ellsworth, T.R. & Jury, W.A. 1991, A three-dimensional field study of solute transport through unsaturated, layered, porous media: 2. Characterization of vertical dispersion, Water Resources Research, vol. 27, no. 5, pp. 967-981.

ElSawah, S., McLucas, A. & Mazanov, J. 2015, Communicating About Water Issues in Australia, Simulation & Gaming, vol. 46, no. 6, pp. 713-741.

Elsawah, S., Pierce, S.A., Hamilton, S.H., van Delden, H., Haase, D., Elmahdi, A. & Jakeman, A.J. 2017, An overview of the system dynamics process for integrated modelling of socio-ecological systems: Lessons on good modelling practice from five case studies, Environmental Modelling and Software, vol. 93, pp. 127-145.

Elshorbagy, A., Jutla, A., Barbour, L. & Kells, J. 2005, System dynamics approach to assess the sustainability of reclamation of disturbed watersheds, Canadian Journal of Civil Engineering, vol. 32, no. 1, pp. 144-158.

Elshorbagy, A. & Ormsbee, L. 2006, Object-oriented modeling approach to surface water quality management, Environmental Modeling and Software, vol. 21, pp. 689-698.

Ford, A. 2010, Modeling the environment, 2nd edition, Island Press, c2010, Washington, D.C.

Forrester, J.W. 1994, System dynamics, systems thinking, and soft OR, System Dynamics Review, vol. 10, no. 2, pp. 245-256.

Forrester, J.W. 1987, Lessons from system dynamics modeling, System Dynamics Review, vol. 3, no. 2, pp. 136-149.

Fredlund, D.G., Rahardjo, H. & Fredlund, M.D. 2012, Unsaturated Soil Mechanics in Engineering Practice, John Wiley & Sons, Inc.

Fredlund, D.G. & Xing, A. 1994, Equations for the soil-water characteristic curve, Canadian Geotechnical Journal, vol. 31, no. 4, pp. 521-532.

Fredlund, M.D., Tran, D. & Fredlund, D.G. 2015, The calculation of actual evaporation from an unsaturated soil surface, 10th International Conference on Acid Rock Drainage & IMWA Annual Conference, MEND, Santiago, Chile, April 20-24, 2015.

Gerke, H.H. & van Genuchten, M.T. 1996, Macroscopic representation of structural geometry for simulating water and solute movement in dual-porosity media, Advances in Water Resources, vol. 19, no. 6, pp. 343-357.

Gibson, R.E., England, G.L. & Hussey, M.J.L. 1967, The Theory of One-Dimensional Consolidation of Saturated Clays, Géotechnique, vol. 17, no. 3, pp. 261-273.

GoldSim Technology 2018, GoldSim User Manual Version 12.1, Issaquah, Washington.

Hager, G.M., Kopainsky, B. & Nyanga, P.H. 2015, Learning as conceptual change during community-based group interventions: a case study with smallholder farmers in Zambia , International Conference of the System Dynamics Society, System Dynamics Society, Cambridge, MA, USA, July 19-23, 2015, pp. 1.

Haraldsson, H.V., Belyazid, S. & Sverdrup, H.U. June 1, 2006, Causal loop diagrams - promoting deep learning of complex systems in engineering education, 4th Pedagogical Inspiration Conference Lund University, Sweden, June 1, 2006, pp. 1.

Hillel, D., Warrick, A.W., Baker, R.S. & Rosenzweig, C. 1998, Environmental Soil Physics: Fundamentals, Applications, and Environmental Considerations, Academic Press, San Diego, CA.

Homer, J.B. 1996, Why we iterate: scientific modeling in theory and practice, System Dynamics Review, vol. 12, no. 1, pp. 1-19.

Hovmand, P.S. 2014, Community based system dynamics, Springer, New York, NY.

Huang, M., Elshorbagy, A., Barbour, S.L., Zettl, J. & Cheng Si, B. 2011a, System dynamics modeling of infiltration and drainage in layered coarse soil, Canadian Journal of Soil Science, vol. 91, no. 2, pp. 185-197.

Huang, M., Barbour, S.L., Elshorbagy, A., Zettl, J.D. & Cheng Si, B. 2011b, Infiltration and drainage processes in multi-layered coarse soils, Canadian Journal of Soil Science, vol. 91, no. 2, pp. 169-183.

Huang, M., Bruch, P.G. & Barbour, S.L. 2013, Evaporation and water redistribution in layered unsaturated soil profiles, Vadose Zone Journal, vol. 12, no. 1, pp. 1-14.

Hyndman, A. & Dawson, R. 2016, Capping and closing deep tailings fines deposits, International Oil Sands Tailings Conference, University of Alberta Geotechnical Centre, Edmonton, Alberta, Canada, December 4-7, 2016, pp. 154.

Imperial Oil Ventures Limited 2016, Kearl Oil Sands Tailings Management Plan

Jeeravipoolvarn, S. 2010, Geotechnical behaviour of in-line thickened oil sands tailings, PhD thesis, University of Alberta.

Jeeravipoolvarn, S., Gidley, I., Moore, T. & Tran, D. 2013, A finite strain consolidation model with evaporation: actual evaporation and un-saturation correction approach, Tailings and Mine Waste, University of Alberta Geotechnical Centre, Edmonton, Alberta, November 3-6, 2013, pp. 277.

Jeeravipoolvarn, S., Miller, W., Scott, D., Kabwe, L. & Wilson, W. 2017, Modeling Effect of Bitumen Extraction Processes on Oil Sands Tailings Ponds, Journal of Civil Engineering and Architecture, no. 11, pp. 48-59.

Jeeravipoolvarn, S., Scott, J.D. & Chalaturnyk, R.J. 2009, 10 m Standpipe Tests on Oil Sands Tailings: Long-Term Experimental Results and Prediction, Canadian Geotechnical Journal, vol. 46, no. 8, pp. 875-888.

Jubinville, S.K. 2013, Prediction of rainfall runoff for soil cover modelling, University of Alberta.

Jutla, A.S. 2006, Hydrologic modeling of reconstructed watersheds using a System Dynamics approach, M.Sc. thesis, University of Saskatchewan.

Kelly, R.A., Jakeman, A.J., Van Delden, H., Voidnov, A.A., Barreteau, O., Borsuk, M.E., Elsawah, S., Hamilton, S.H., Henrisksen, H.J., Kuikka, S., Maer, H.R. & Rizzoli, A.E. 2013, Selecting among five common modelling approaches for integrated environmental assessment and management, Environmental Modelling & Software, vol. 47, pp. 159-181.

Kessler, S., Barbour, S.L., Van Rees, K. C. J. & Dobchuk, B.S. 2010, Salinization of soil over saline-sodic overburden from the oil sands in Alberta, Canadian Journal of Soil Science, vol. 90, no. 4, pp. 637-647.

King, C.A.M. 1970, Feedback Relationships in Geomorphology, Geografiska Annaler.Series A, Physical Geography, vol. 52, no. 3, pp. 147-159.

King, L.M., Simonovic, S.P. & Hartford, D.N.D. 2017, Using system dynamics simulation for assessment of hydropower system safety, Water Resources Research, vol. 53, no. 8, pp. 7148-7174.

Kouakou, W.A. 2014, Geotechnical Characterisation of Oil Sand Tailings Beach Deposits in Flume Tests, M.Sc. thesis, University of Alberta.

Koul, S., Falebita, O.A., Akinbami, J.K. & Akarakiri, J.B. 2016, System dynamics, uncertainty and hydrocarbon resources modelling: a systematic review, Renewable and Sustainable Energy Reviews, vol. 59, pp. 199-205.

Kupper, A. M. A. G. 1991, Design of hydraulic fill, PhD thesis, University of Alberta.

Lane, D.C. 2007, The power of the bond between cause and effect: Jay Wright Forrester and the field of system dynamics, System Dynamics Review, vol. 23, no. 2, pp. 95-118.

Lane, D.C. & Sterman, J.D. 2017, A model simulator: The lives of Jay W Forrester, Journal of Simulation, vol. 12, no. 2, pp. 90-97.

Lee, J. 1993, A formal approach to hydrological model conceptualization, Hydrological Sciences Journal, vol. 38, no. 5, pp. 391-401.

Lehmann, P., Assouline, S. & Or, D. 2008, Characteristic lengths affecting evaporative drying of porous media, Physical Review E, vol. 77, no. 5, pp. 056309.

Li, A.L., Been, K., Wislesky, I., Eldridge, T. & Williams, D. 2012, Tailings initial consolidation and evaporative drying after deposition, Paste, eds. R.J. Jewell, A.B. Fourie & A. Paterson, Australian Center for Geomechanics, Sun City, South Africa, 2012, pp. 25.

Li, L. & Simonovic, S.P. 2002, System dynamics model for predicting floods from snowmelt in North American prairie watersheds, Hydrological Processes, vol. 16, no. 13, pp. 2645-2666.

Liu, R., Welfert, B. & Houston, S.L. 2017, Comparison of Averaging Methods for Interface Conductivities in One-Dimensional Unsaturated Flow in Layered Unsaturated Soils, Geotechnical Frontiers 2017American Society of Civil Engineers (ASCE), March 12-15, 2017.

Maani, K.E. & Cavana, R.Y. 2007, System Thinking, System Dynamics, 2nd Edition, Pearson Canada.

Macciotta, R. 2013, Quantitative risk assessment of natural and cut slopes: measuring uncertainty in the estimated risks and proposed framework for developing risk evaluation criteria, University of Alberta.

McKay, M.D., Beckman, R.J. & Conover, W.J. 1979, Comparison of Three Methods for Selecting Values of Input Variables in the Analysis of Output from a Computer Code, Technometrics, vol. 21, no. 2, pp. 239-245.

McKenna, G., Biggar, K., Kywa Win, S.M. & Journault, J. 2010, Oil sands tailings sand hydraulic conductivity, International Oil Sands Tailings Conference, University of Alberta Geotechnical Centre, Edmonton, Alberta, Canada, December 5-8, 2010, pp. 21.

McVay, M., Townsend, F. & Bloomquist, D. 1986, Quiescent Consolidation of Phosphatic Waste Clays, Journal of Geotechnical Engineering, vol. 112, no. 11, pp. 1033-1049.

Meadows, D.H. & Wright, D. 2008, Thinking in systems: a primer, Chelsea Green Pub., c2008, White River Junction, VT.

Mining Association of Canada 2017, A guide to the management of tailings facilities.

Monte, J.L. & Krizek, R.J. 1976, One-dimensional mathematical model for large-strain consolidation, Géotechnique, vol. 26, no. 3, pp. 495-510.

Mualem, Y. 1976, A new model for predicting the hydraulic conductivity of unsaturated porous media, Water Resources Research, vol. 12, no. 3, pp. 513-522.

Nguyen, H.T. 2014, A Systems Model for Short-Rotation Coppices: A Case Study of the Whitecourt, Alberta, Trial Site, M.Sc. thesis, University of Alberta

Nicolson, C.R., Starfield, A.M., Kofinas, G.P. & Kruse, J.A. 2002, Ten Heuristics for Interdisciplinary Modeling Projects, Ecosystems, vol. 5, no. 4, pp. 376-384.

Pollock, G.W. 1988, Large strain consolidation of oil sand tailings sludge, M.Sc. thesis, University of Alberta.

Renault, S., Paton, E., Nilsson, G., Zwiazek, J.J. & MacKinnon, M.D. 1999, Responses of Boreal Plants to High Salinity Oil Sands Tailings Water, Journal of Environmental Quality, vol. 28, no. 6, pp. 1957-1962.

Richardson, G.P. 2011, Reflections on the foundations of system dynamics, System Dynamics Review (Wiley), vol. 27, no. 3, pp. 219-243.

Richardson, G.P. 1997, Problems in causal loop diagrams revisited, System Dynamics Review, vol. 13, no. 3, pp. 247-252.

Rima, U.S. & Beier, N.A. 2018, Evaluation of temperature and multiple freeze-thaw effects on the strength properties of centrifuged tailings, 71st Canadian Geotechnical Conference Edmonton, Alberta, September 23-26, 2018.

Romano, N., Brunone, B. & Santini, A. 1998, Numerical analysis of one-dimensional unsaturated flow in layered soils, Advances in Water Resources, vol. 21, no. 4, pp. 315-324.

Rourke, H. & Hockley, D. 2018, Assessing Oil Sands tailings consolidation parameters relative to long-term reclamation, Tailings and Mine Waste, Colorado State University, Keystone, Colorado, September 30 - October 2, 2018, pp. 127.

Schmocker-Fackel, P., Naef, F. & Scherrer, S. 2007, Identifying runoff processes on the plot and catchment scale, Hydrology Earth System Science., vol. 11, no. 2, pp. 891-906.

Scott, J.D., Jeeravipoolvarn, S., Donahue, R. & Ozum, B. 2008, Characterization of oil sands thickened tailings, International Oil Sands Tailings Conference, University of Alberta Geotechnical Centre, Edmonton, Alberta, December 7-10, 2008.

Shahin, A., AbouRizk, S.M. & Mohamed, Y. 2013, A weather generator for use in construction simulation models, International Journal of Architecture, Engineering and Construction, vol. 2, no. 2, pp. 73-87.

Shaw, B., Hyndman, A. & Sobkowicz, J. 2010, Consolidation projections for thickened tailings, International Oil Sands Tailings Conference, University of Alberta Geotechnical Centre, Lake Louise, Alberta, Canada, December 5-8, 2010, pp. 253.

Shell Canada Energy 2016a, Jackpine Mine Fluid Tailings Management Plan, Alberta Energy Regulator.

Shell Canada Energy 2016b, Muskeg River Mine Fluid Tailings Management Plan, Alberta Energy Regulator.

Simms, P. 2017, 2013 Colloquium of the Canadian Geotechnical Society: Geotechnical and geoenvironmental behaviour of high-density tailings, Canadian Geotechnical Journal, vol. 54, no. 4, pp. 455-468.

Simms, P., Grabinsky, M. & Zhan, G. 2007, Modelling evaporation of paste tailings from the Bulyanhulu mine, Canadian Geotechnical Journal, vol. 44, no. 12, pp. 1417-1432.

Slingerland, N., Sommerville, A., O'Leary, D. & Beier, N.A. 2018, Identification and quantification of erosion on a sand tailings dam, Geosystem Engineering, pp. 1-15.

Smith, R.E. 2002, Infiltration theory for hydrologic applications, American Geophysical Union, Washington, D.C.

Song, Q. & Kane, M.O. 2013, Evaluation of evaporation and under-drainage in dewatering oil sands tailings in northern Alberta, Tailings and Mine Waste. University of Alberta Geotechnical Centre, Edmonton, Alberta, November 3-6, 2013, pp. 167.

Sterman, J. 2004, Business dynamics: systems thinking and modeling for a complex world, McGraw-Hill, 2004; International ed, Boston, M.A.

Sternman, J.D. 1994, Learning in and about complex systems, System Dynamics Review, vol. 10, no. 2, pp. 291-330.

Suncor 2017, Fort Hills Oil Sands Project Tailings Directive Application, Alberta Energy Regulator.

Syncrude Canada Limited 2017, Application for Approval of the Syncrude Mildred Lake Extension Project, Alberta Energy Regulator.

Townsend, F.C. & McVay, M.C. 1990, SOA: Large Strain Consolidation Predictions, Journal of Geotechnical Engineering, vol. 116, no. 2, pp. 222-243.

Tran, D.T.Q., Fredlund, D.G. & Chan, D.H. 2016, Improvements to the calculation of actual evaporation from bare soil surfaces, Canadian Geotechnical Journal, vol. 53, no. 1, pp. 118-133.

Trimble, J. 2014, Boundary concepts in system dynamics, 32nd International Conference of the System Dynamics Society, Delft, the Netherlands, July 20-24, 2014.

Van Genutchen, M.T. 1980, A closed-form equation for predicting the hydraulic conductivity of unsaturated soils, Journal of the Soil Science Society of America, vol. 44, no. 5, pp. 892.

Vessey, C.J., Lindsay, M.B.J. & Barbour, S.L. 2018, Sodium transport and attenuation in soil cover materials for oil sands mine reclamation, Applied Geochemistry, vol. 100, pp. 42-54.

Vick, S.G. 2002, Degrees of belief: subjective probability and engineering judgment, American Society of Civil Engineers.

Wilson, G.W., Fredlund, D.G. & Barbour, S.L. 1997, The effect of soil suction on evaporative fluxes from soil surfaces, Canadian Geotechnical Journal, vol. 34, no. 1, pp. 145-155.

Wilson, G.W., Fredlund, D.G. & Barbour, S.L. 1994, Coupled soil-atmosphere modelling for soil evaporation, Canadian Geotechnical Journal, vol. 31, no. 2, pp. 151-161.

Zettl, J. 2014, Infiltration and drainage through coarse layered soil: a study of natural and reclaimed soil profiles in the Oil Sands Region, Alberta, Canada, MSc thesis, University of Saskatchewan.

Zettl, J., Lee Barbour, S., Huang, M., Si, B. & Leskiw, L.A. 2011, Influence of textural layering on field capacity of coarse soils, Canadian Journal of Soil Science, vol. 91, no. 2, pp. 133-147.

Zhang, F. 2017, Unsaturated soil property functions for high volume change materials, PhD thesis, University of Alberta.

Zhang, F., Wilson, G.W. & Fredlund, D.G. 2017, Permeability function for oil sands tailings undergoing volume change during drying, Canadian Geotechnical Journal, vol. 55, no. 2, pp. 191-207.

APPENDIX 1 – CONSOLIDATION SUB-MODEL

A1-1. Additional GoldSim Setup Detail
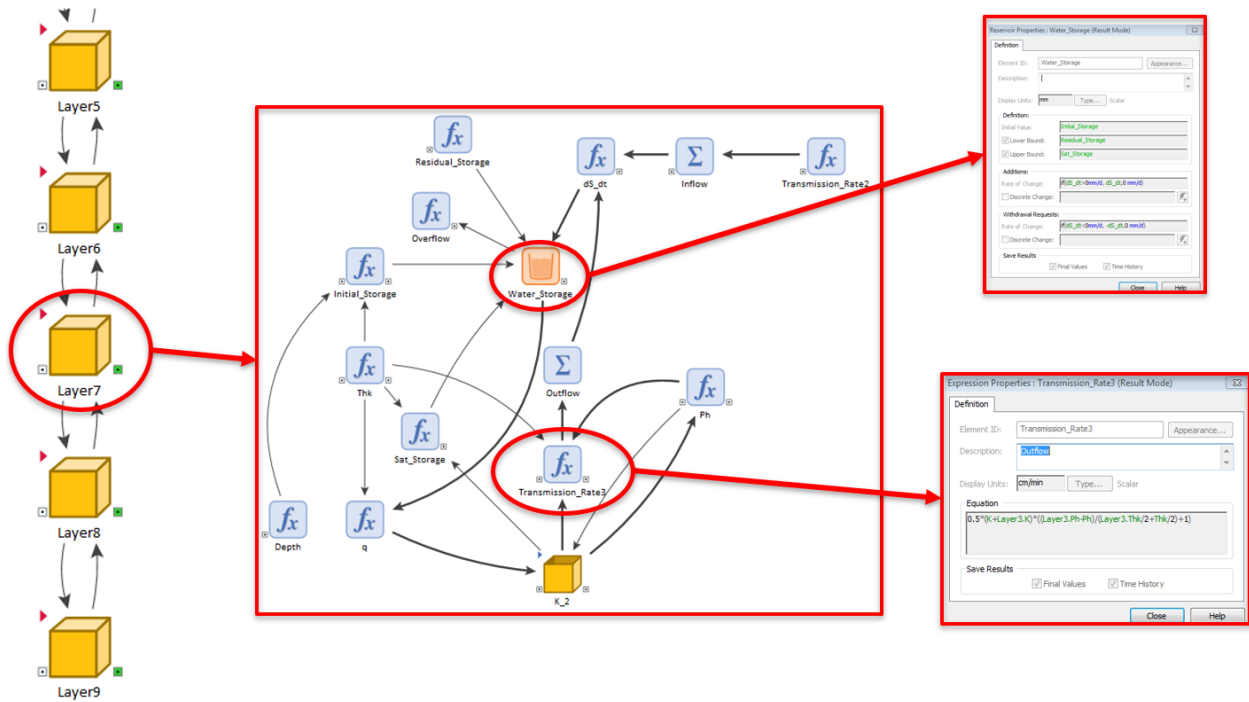
Figure A1-1. Overview of consolidation submodel in GoldSim
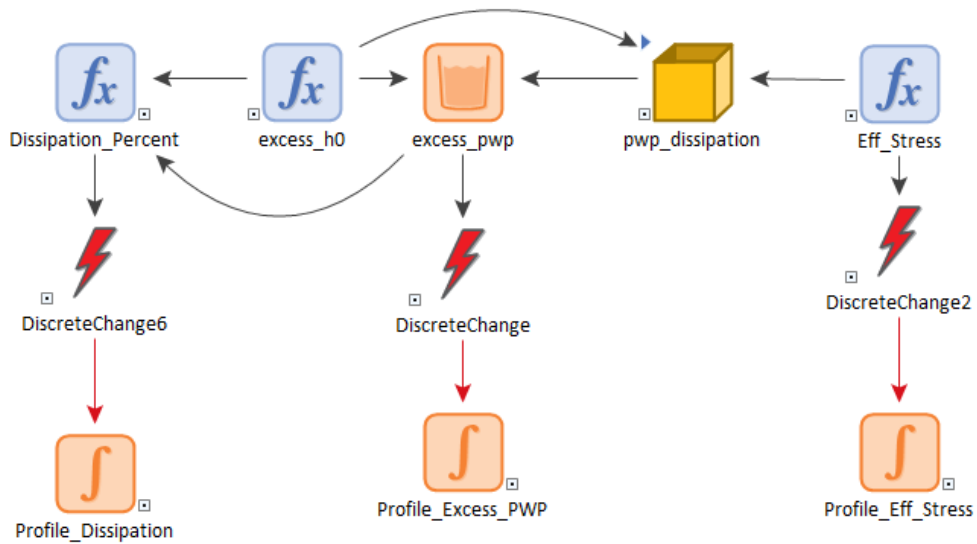
Figure A1-2. Calculation of excess pore pressure

Figure A1-3. Change in effective stress inside the pore-pressure dissipation container from Figure A1-2.
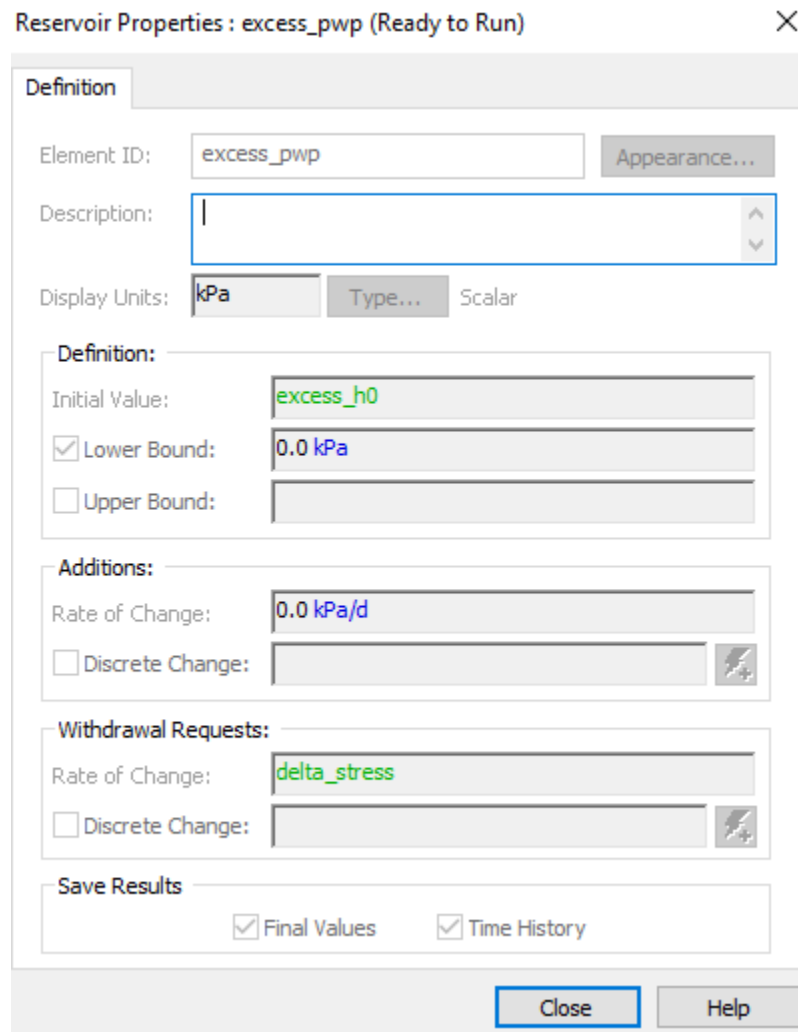
Figure A1-4. Screenshot of the reservoir element "excess_pwp"
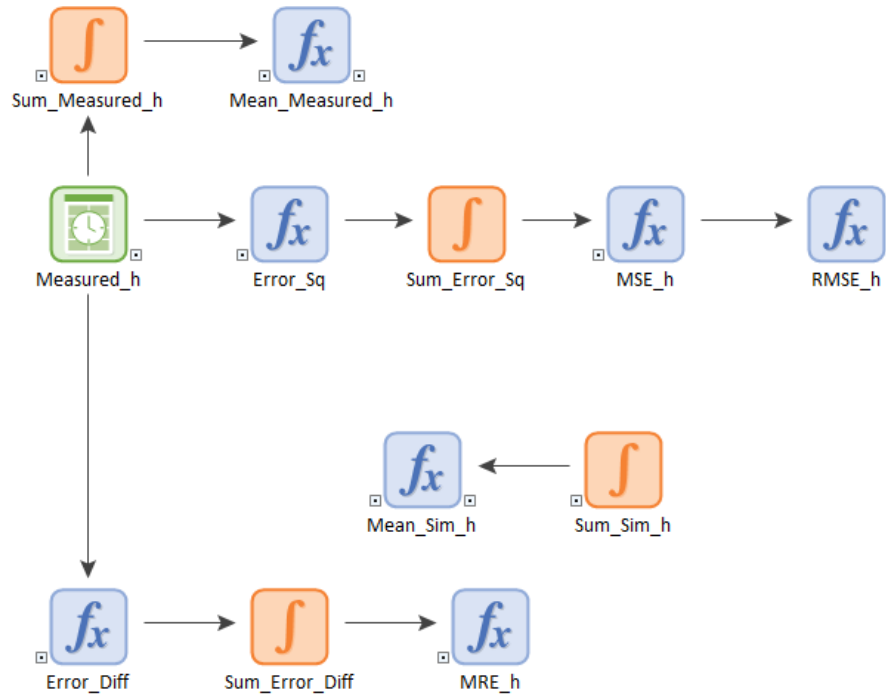
Figure A1-5. Calibration container for interface heights
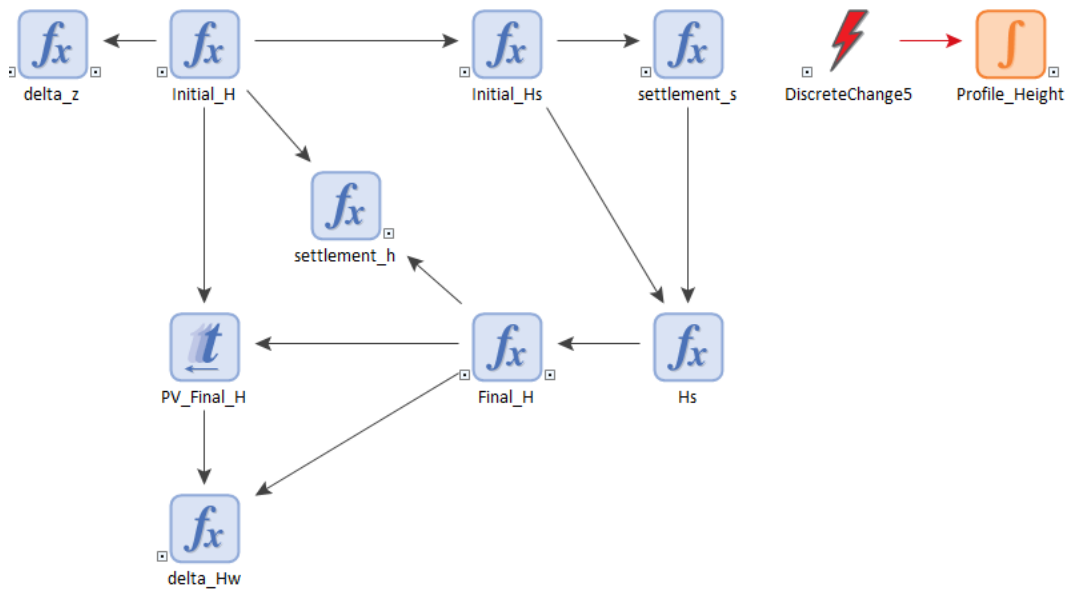
Figure A1-6. Calculation of interface height from void ratio
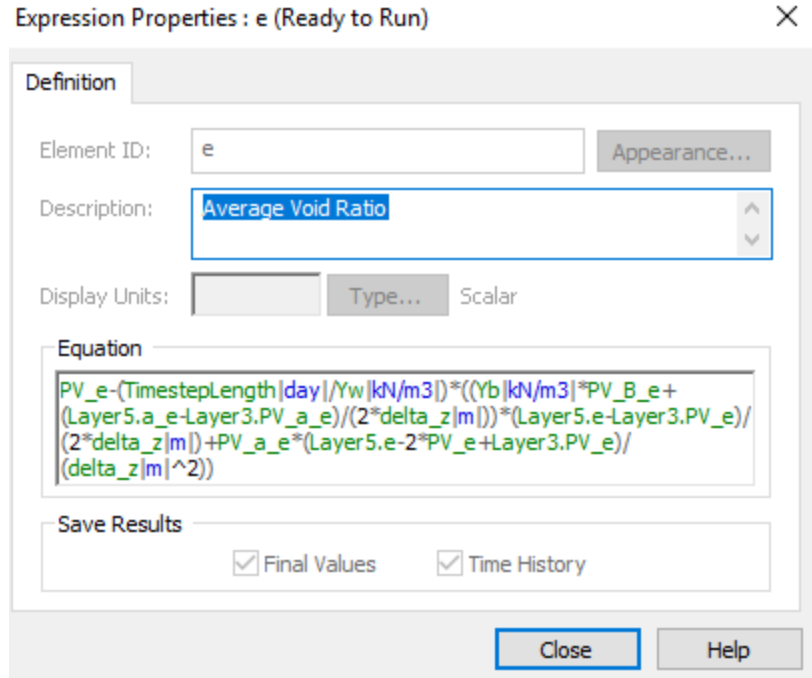
Figure A1-7. GoldSim codes for the void ratio based on Equation 3.4. This figure shows the setup in Layer 4.
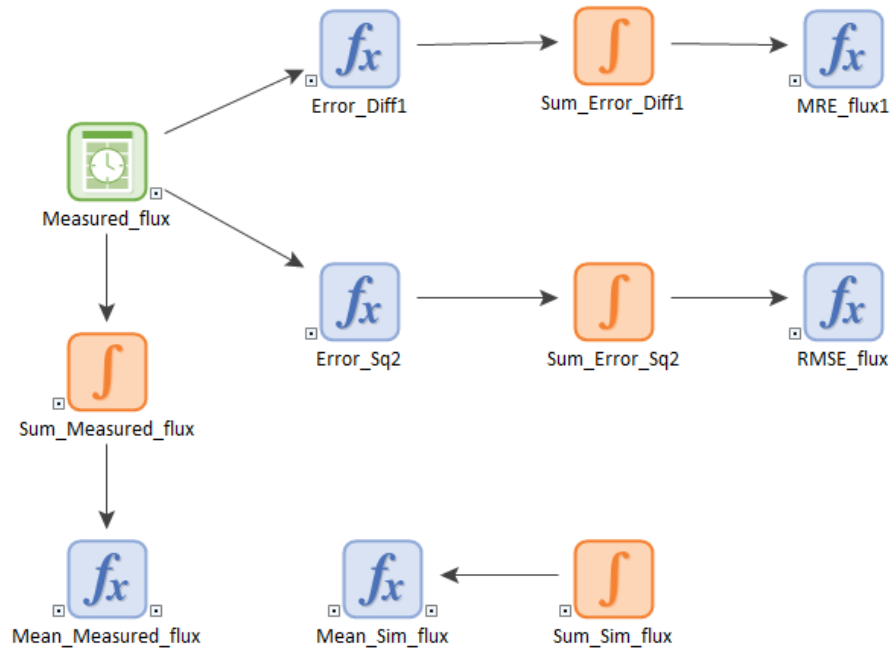
Figure A1-8. Calibration container for upward flux.
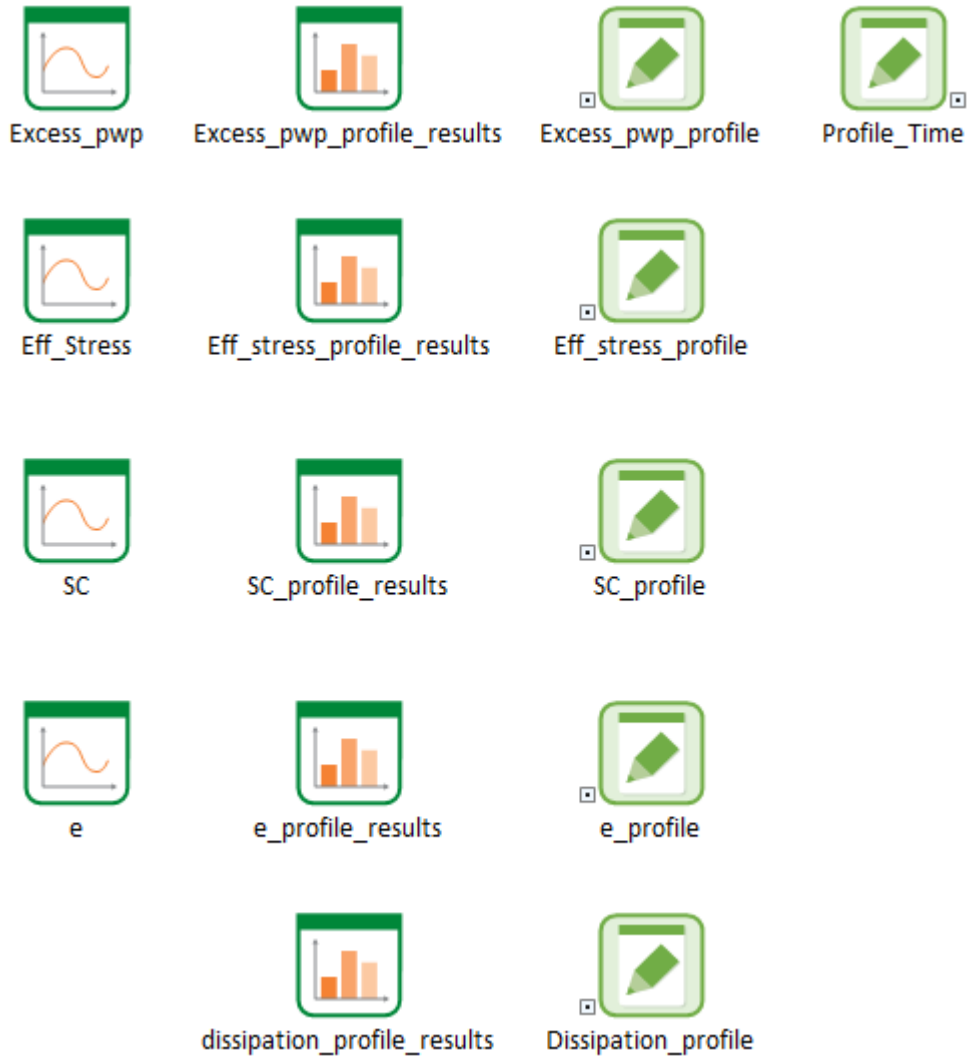
Figure A1-9. Results container for various result elements.
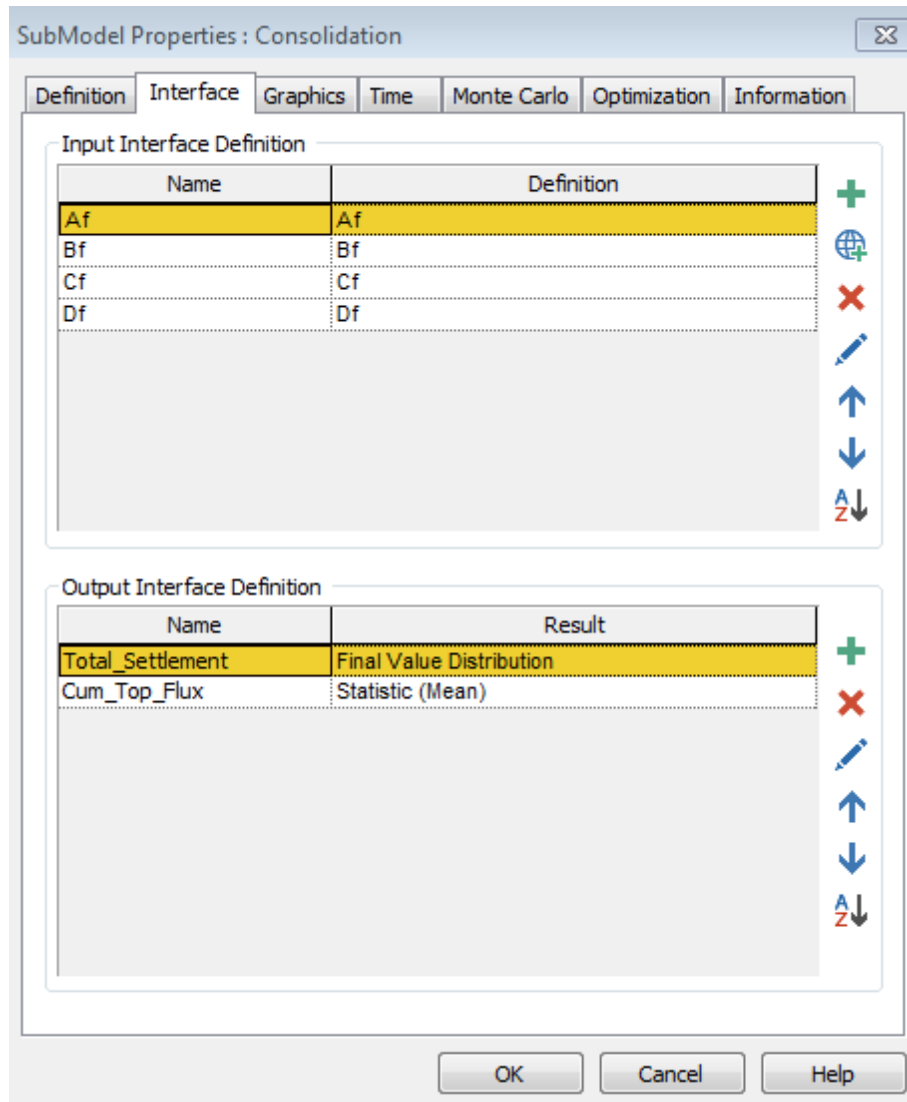
Figure A1-10. Interface setup of the outer model for nested Monte Carlo simulation.
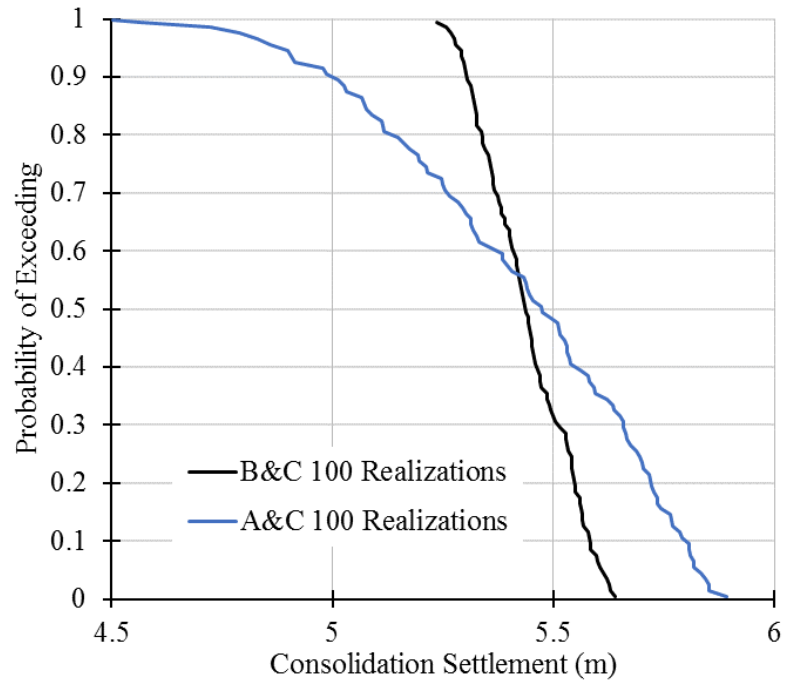
Figure A1-11. Comparison of CCDF; blue line represents CCDF generated by probabilistic input to parameter A and C; black line represents CCDF generated by probabilistic input to parameter B and C.

APPENDIX 2 – UNSATURATED FLOW SUB-MODEL

A2-1 Additional Climate Data

Table A2-1. Monthly average temperature in Fort McMurray, Alberta based on 1971-2000 Environment Canada climate normals station data.

Month	Temperature (Celcius)
January	-18.8
February	-13.7
March	-6.5
April	3.4
May	10.4
June	14.7
July	16.8
August	15.3
September	9.4
October	2.8
November	-8.5
December	-16.5

Table A2-2. Monthly average relative humidity in Fort McMurray, Alberta based on 1971-2000 Environment Canada climate normal station data.

Month	Relative Humidity
January	0.721
February	0.684
March	0.639
April	0.579
May	0.565
June	0.629
July	0.679
August	0.695
September	0.704
October	0.710
November	0.769
December	0.748

Table A2-3. Monthly average precipitation input based on Song and O'Kane, 2013

Month	Precipitation (mm/day)
January	1.1
February	0.9
March	0.8
April	0.7
May	1.2
June	2.0
July	2.4
August	2.1
September	1.6
October	1.0
November	1.0
December	0.9

Table A2-4. Monthly average potential evaporation (PE) input based on Song and O'Kane, 2013

Month	Potential Evaporation (mm/day)
January	0
February	0
March	0.3
April	2.1
May	3.7
June	4.1
July	4.3
August	3.2
September	1.8
October	0.6
November	0
December	0

A2-2 GoldSim Setup
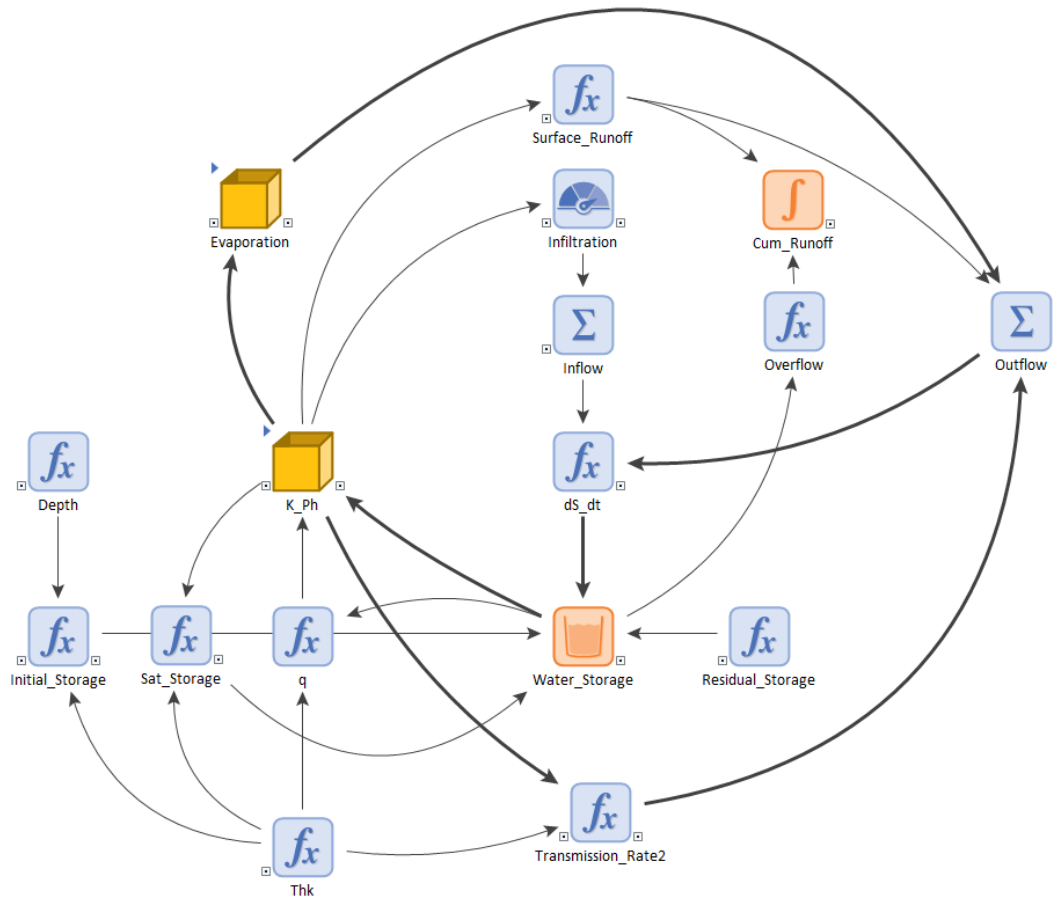
Figure A2-1. Top layer (Layer 1) setup.
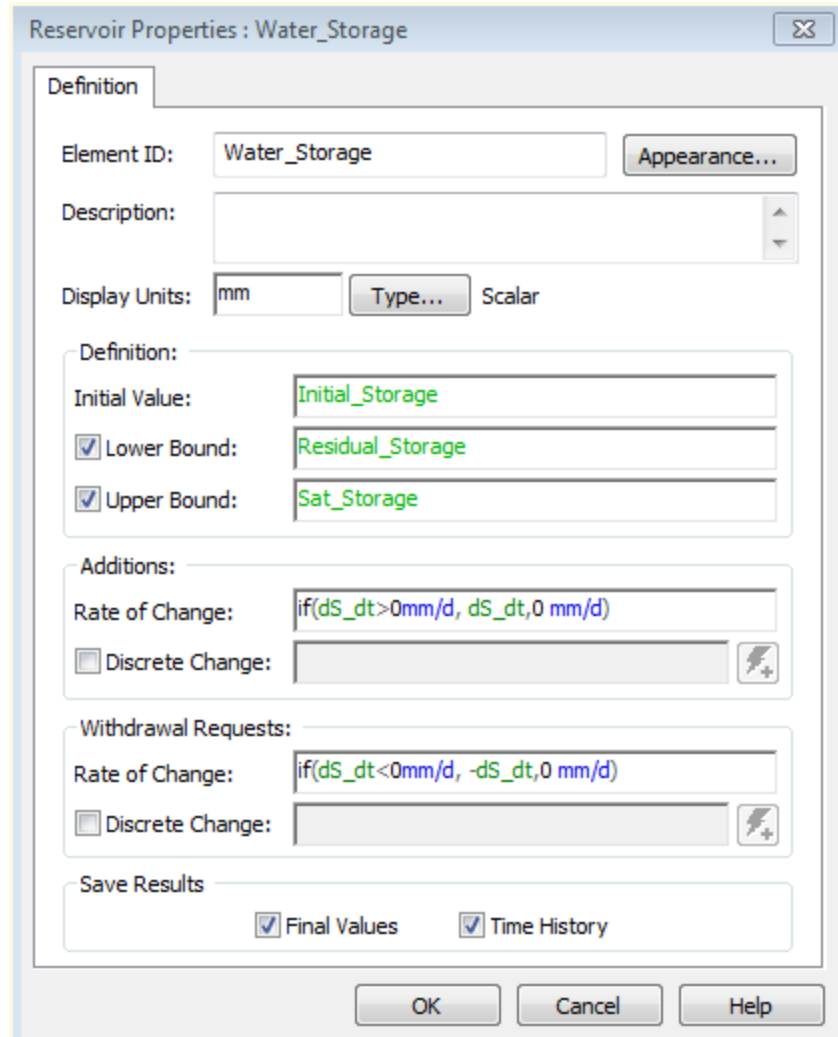
Figure A2-2. Typical set up for the Reservoir element "Water_Storage".
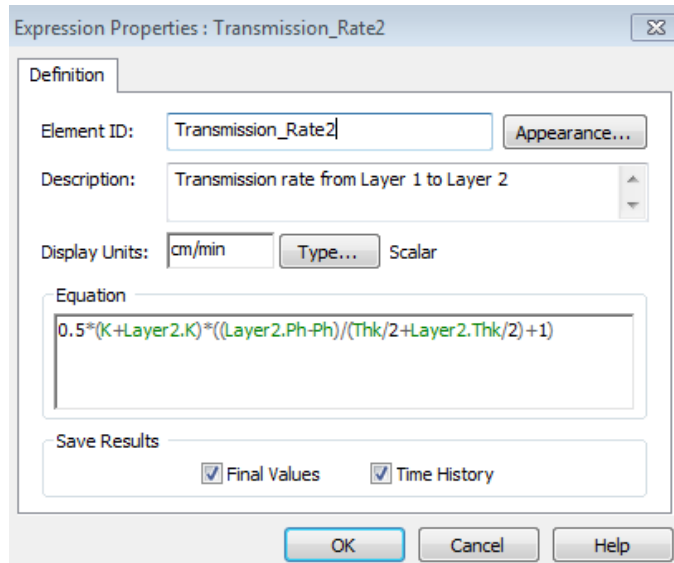
Figure A2-3. Calculation of transmission rate from Layer 1 to Layer 2 as viewed from the Layer 1 container.
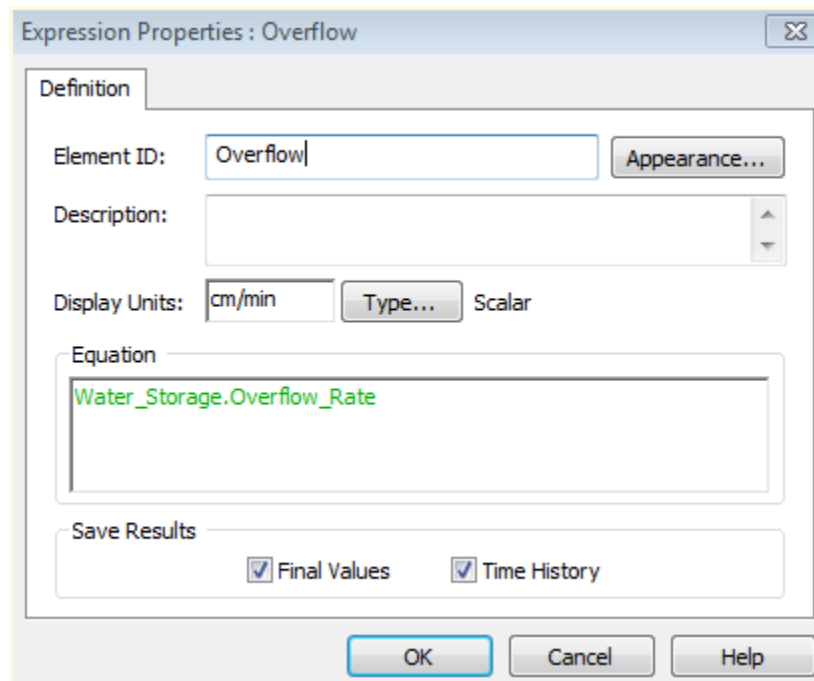
Figure A2-4. Calculation of overflow rate after the Reservoir element reaches its capacity.
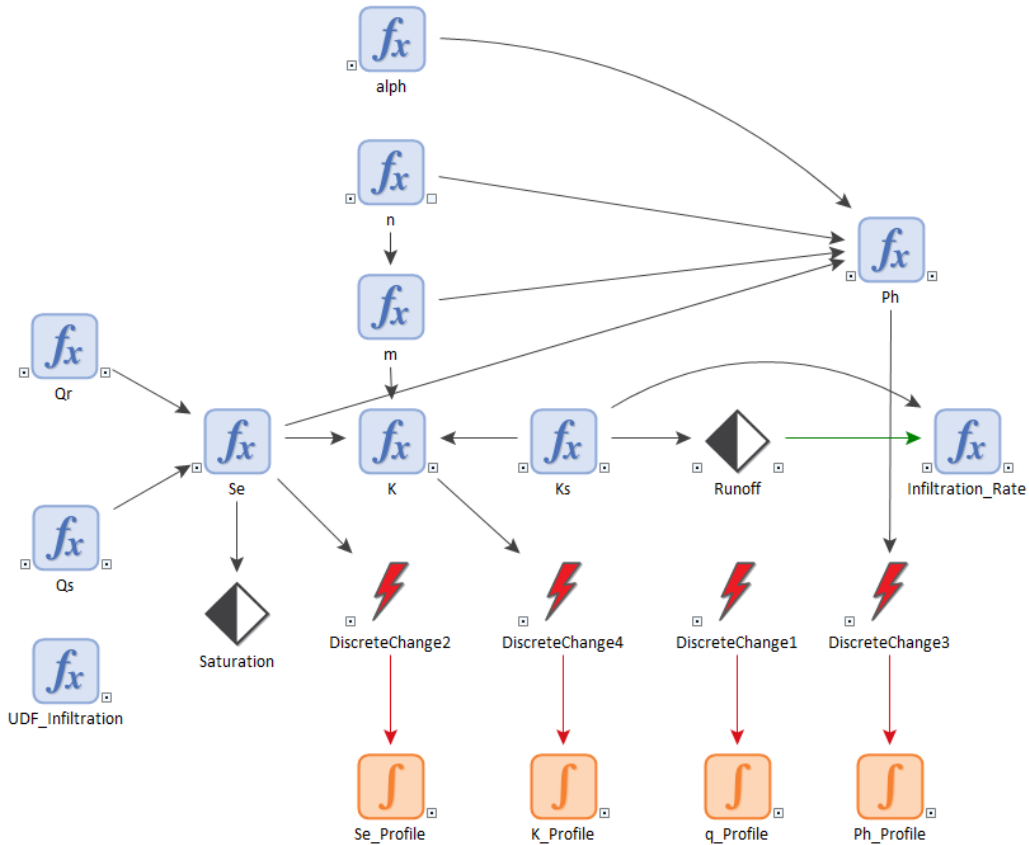
Figure A2-5. K_Ph container setup.
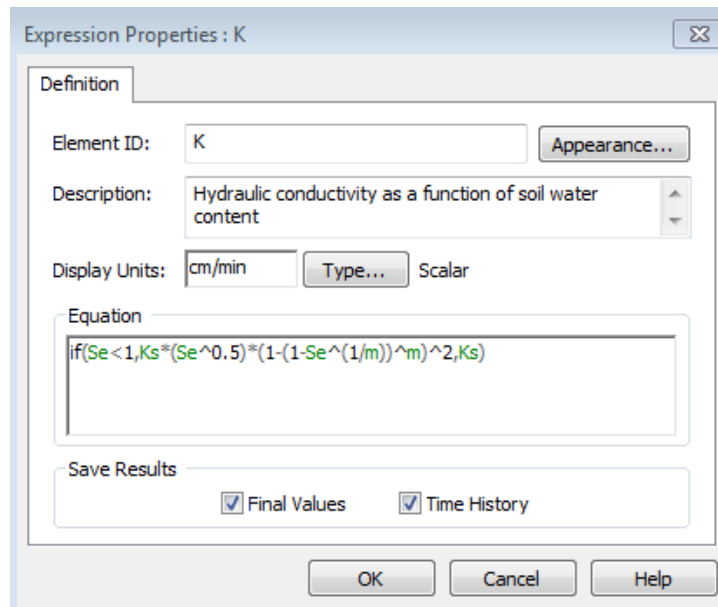
Figure A2-6. Calculation of hydraulic conductivity K in the K_Ph container.
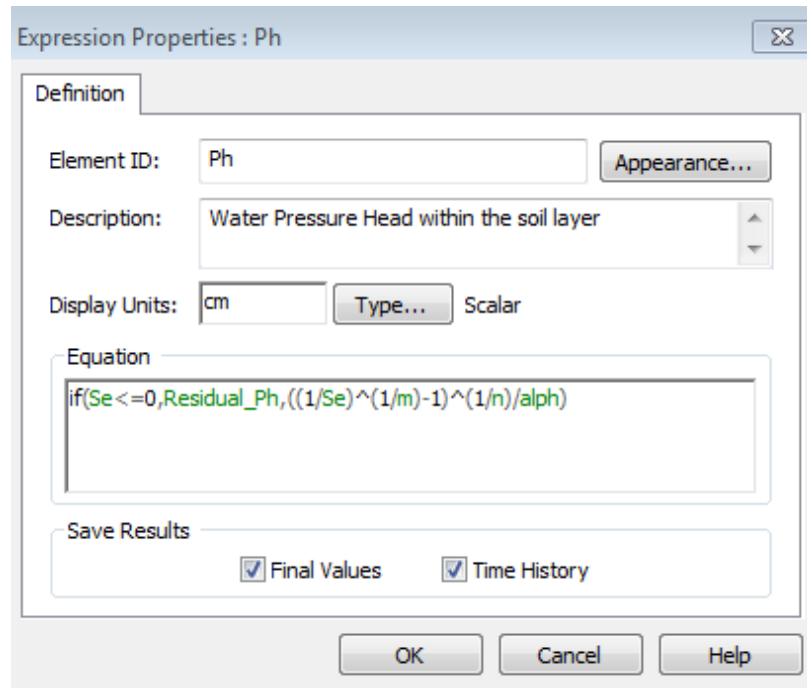
Figure A2-7. Calculation of suction pressure head Ph.
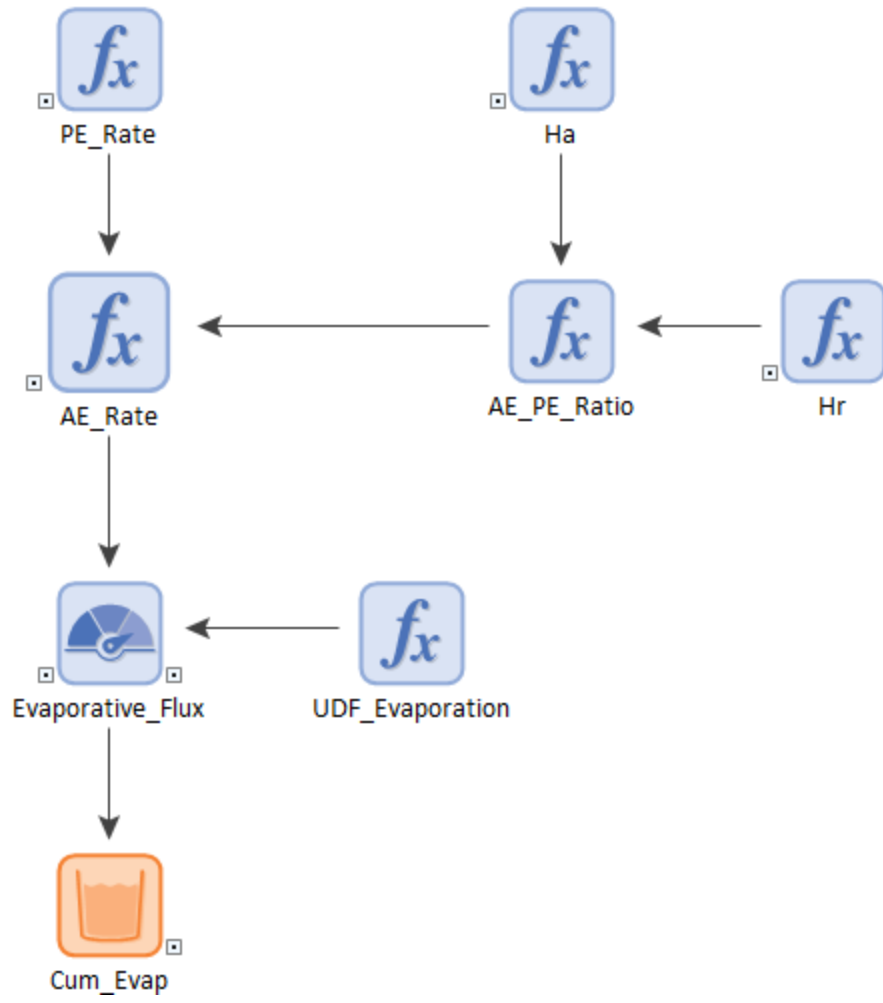
Figure A2-8. Evaporation container setup in Layer 1.
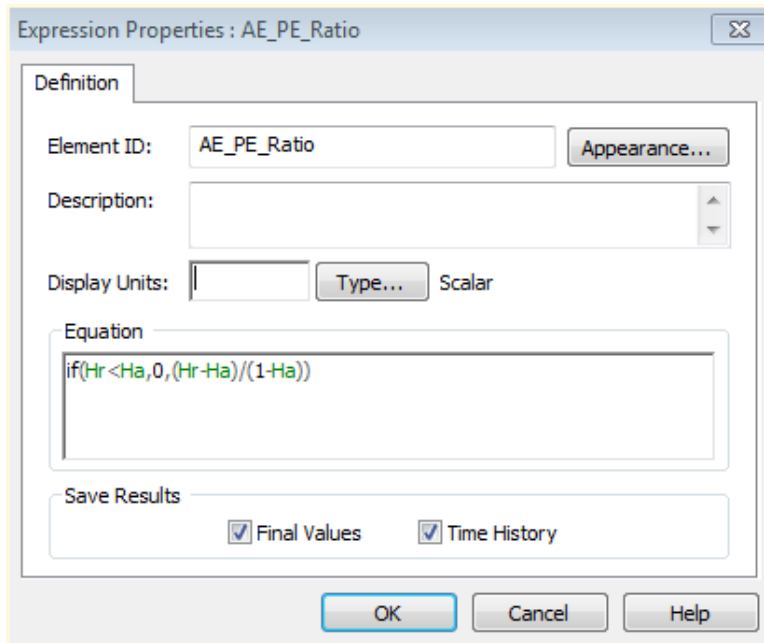
Figure A2-9. Calculation of AE/PE ratio in Layer 1.
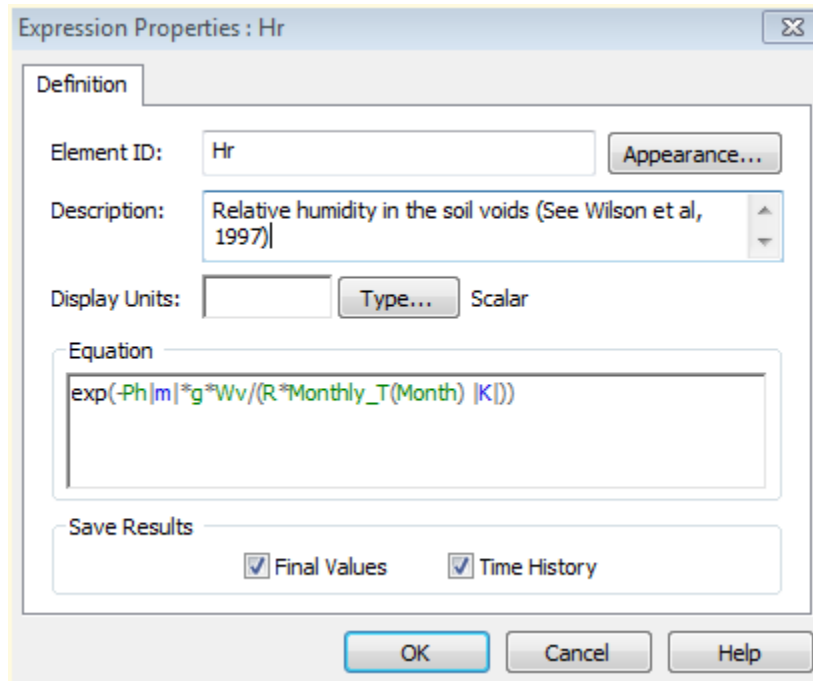
Figure A2-10. Calculation of relative humidity (Hr) in Layer 1.
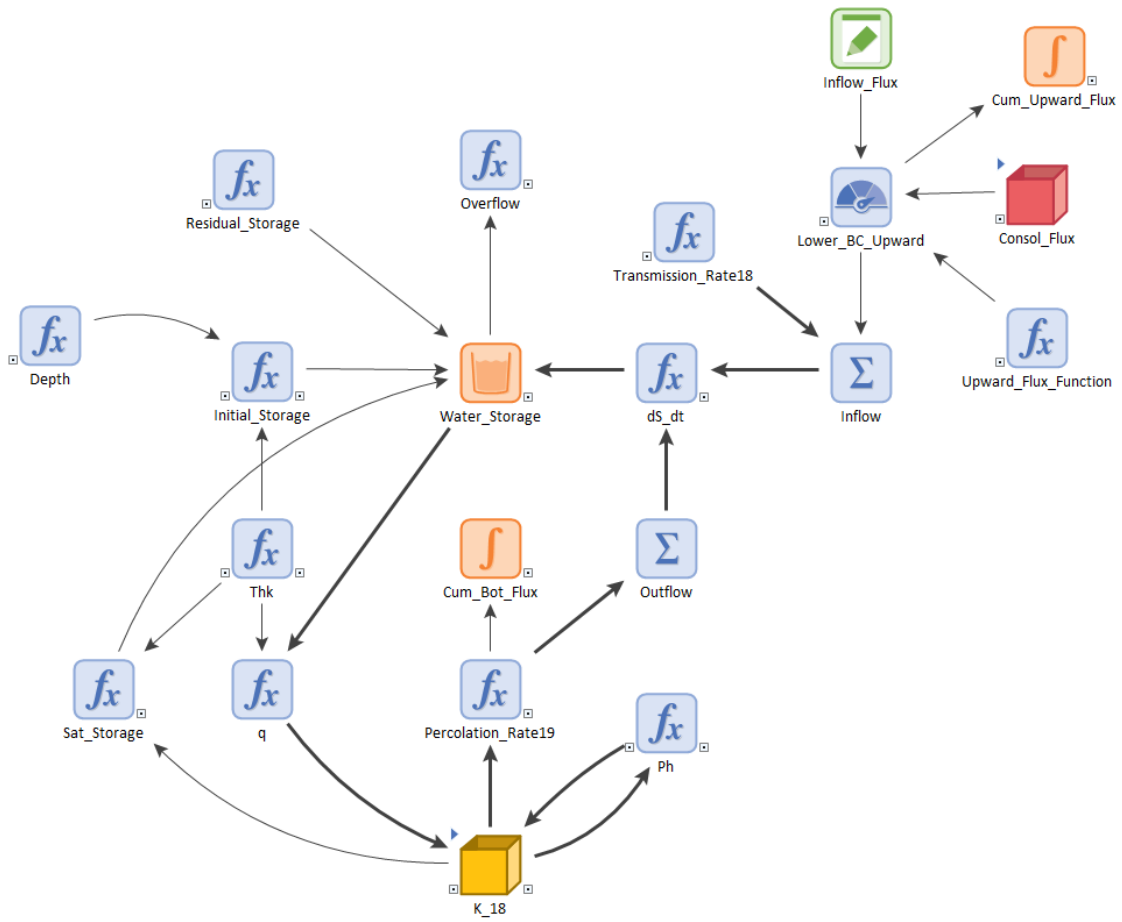
Figure A2-11. Setup in the bottom layer (Layer 18).
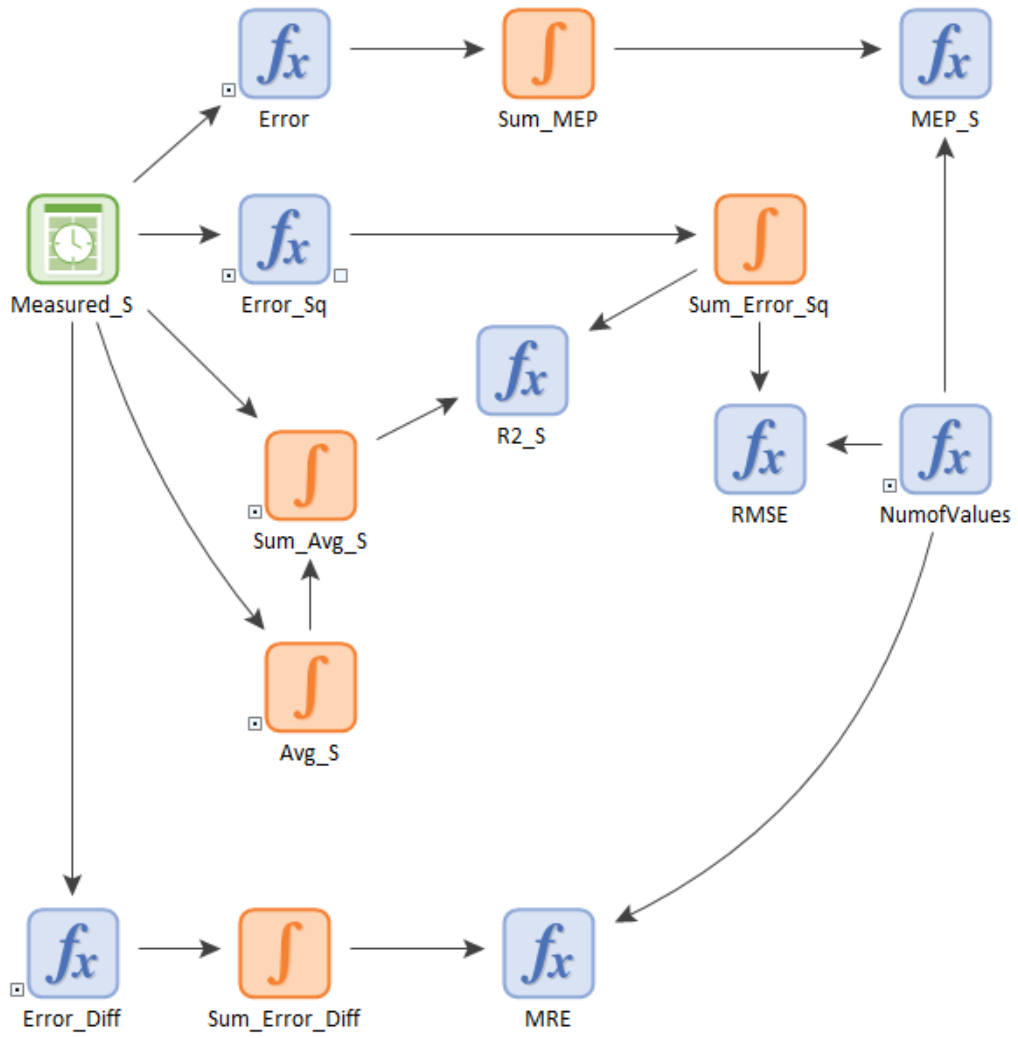
Figure A2-12. Calibration container setup.

Table A2-5. Initial volumetric water content for Section 4.4.1: Simple Infiltration and Section 4.4.2: Extreme Wetting.

Depth (cm)	Initial Volumetric Water Content
0	0.026
7	0.026
10	0.026
17	0.026
20	0.045
23	0.050
30	0.055
35	0.058
45	0.053
48	0.049
53	0.062
59	0.076
68	0.103
74	0.084
78	0.065
84	0.016
97	0.017
102	0.017

Table A2-6. Initial volumetric water content for Section 4.4.3.1: Column Evaporation of Sand.

Depth (cm)	Initial Volumetric Water Content
0.40	0.20
1.93	0.21
3.89	0.24
5.87	0.23
8.07	0.22
10.09	0.25
11.98	0.25
14.10	0.23
16.01	0.24
18.08	0.31
19.89	0.28
21.86	0.31
24.06	0.31
25.97	0.31
28.00	0.33
29.82	0.32
32.05	0.33
33.82	0.35
35.98	0.41
37.99	0.36
39.85	0.36
41.99	0.36
43.90	0.41
45.99	0.38
47.93	0.38
49.90	0.39
52.05	0.38
53.87	0.43
56.01	0.41
57.76	0.41
59.73	0.41

Table A2-7. Initial volumetric water content for Section 4.4.3.2: Column Evaporation of Silt.

Depth (cm)	Initial Volumetric Water Content
1.88	0.40
4.05	0.38
6.05	0.39
7.94	0.38
10.12	0.37
14.00	0.39
16.10	0.42
17.99	0.41
19.98	0.40
22.07	0.40
23.97	0.42
26.05	0.41
29.94	0.41
34.11	0.41
36.00	0.41
38.08	0.39
40.26	0.39
42.07	0.40
44.15	0.39
45.99	0.38
46.04	0.38
47.93	0.38
49.90	0.39
50.22	0.41
52.05	0.38
53.87	0.43
54.10	0.40
56.01	0.41
56.19	0.40
57.76	0.41
59.73	0.41

Table A2-8. Initial volumetric water content for Section 4.4.3.3: Column Evaporation of Silt-Sand System.

Depth (cm)	Initial Volumetric Water Content
0.31	0.32
2.00	0.34
3.63	0.36
5.76	0.37
7.70	0.38
10.14	0.39
12.64	0.39
14.89	0.40
17.14	0.40
20.20	0.40
23.83	0.40
28.26	0.41
30.26	0.40
31.37	0.32
31.99	0.28
35.12	0.30
37.31	0.30
39.12	0.31
41.31	0.32
43.94	0.33
47.37	0.33
49.94	0.34
52.63	0.34
55.75	0.34
57.63	0.34
59.75	0.34

Table A2-9. Initial volumetric water content for Section 4.4.3.3: Column Evaporation of Sand-Silt System.

Depth (cm)	Initial Volumetric Water Content
0.22	0.18
2.77	0.19
4.66	0.21
6.64	0.22
9.57	0.23
11.46	0.24
13.26	0.25
15.90	0.27
18.35	0.28
21.47	0.29
23.45	0.30
25.62	0.31
30.16	0.32
32.15	0.41
39.42	0.41
59.89	0.41

APPENDIX 3 – CASE STUDY ADDITIONAL RESULTS

A3-1 Ks Sensitivity Analysis

Step 1: Geometry and Soil Properties

	(cm)	(cm)			(cm-1)	
	Depth	Thickness	Qr	Qs	alph	n
1	8.33335	16.66666667	0.012	0.428	0.02259243	5.4848
2	25.00003333	16.66666667	0.012	0.428	0.02259243	5.4848
3	41.6667	16.66666667	0.012	0.428	0.02259243	5.4848
4	58.33336667	16.66666667	0.012	0.428	0.02259243	5.4848
5	75.00003333	16.66666667	0.012	0.428	0.02259243	5.4848
6	91.6667	16.66666667	0.012	0.428	0.02259243	5.4848
7	108.3333667	16.66666667	0.012	0.428	0.02259243	5.4848
8	125.0000333	16.66666667	0.012	0.428	0.02259243	5.4848
9	141.6667	16.66666667	0.012	0.428	0.02259243	5.4848
10	158.3333667	16.66666667	0.012	0.428	0.02259243	5.4848
11	175.0000333	16.66666667	0.012	0.428	0.02259243	5.4848
12	191.6667	16.66666667	0.012	0.428	0.02259243	5.4848
13	208.3333667	16.66666667	0.012	0.428	0.02259243	5.4848
14	225.0000333	16.66666667	0.012	0.428	0.02259243	5.4848
15	241.6667	16.66666667	0.012	0.428	0.02259243	5.4848
16	258.3333667	16.66666667	0.012	0.428	0.02259243	5.4848
17	275.0000333	16.66666667	0.012	0.428	0.02259243	5.4848
18	291.6667	16.66666667	0.012	0.428	0.02259243	5.4848

Figure A3-1. Geometry and soil property input in GoldSim
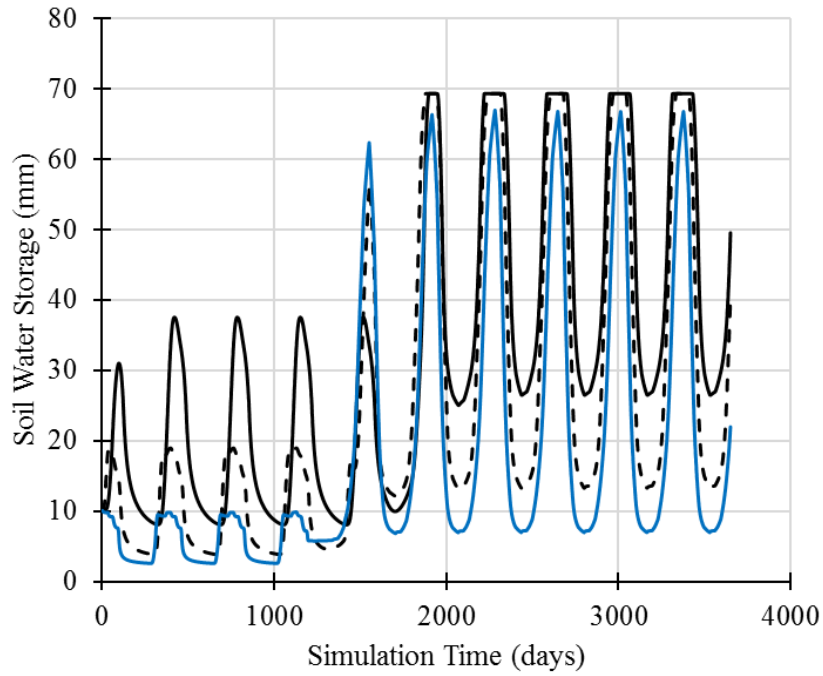
Figure A3-2. Soil water storage in Layer 3 at depth 41.67 cm; black solid line is the "One Order Less Ks" case; dashed line is the reference Ks case; blue solid line is the "One Order More Ks" case.
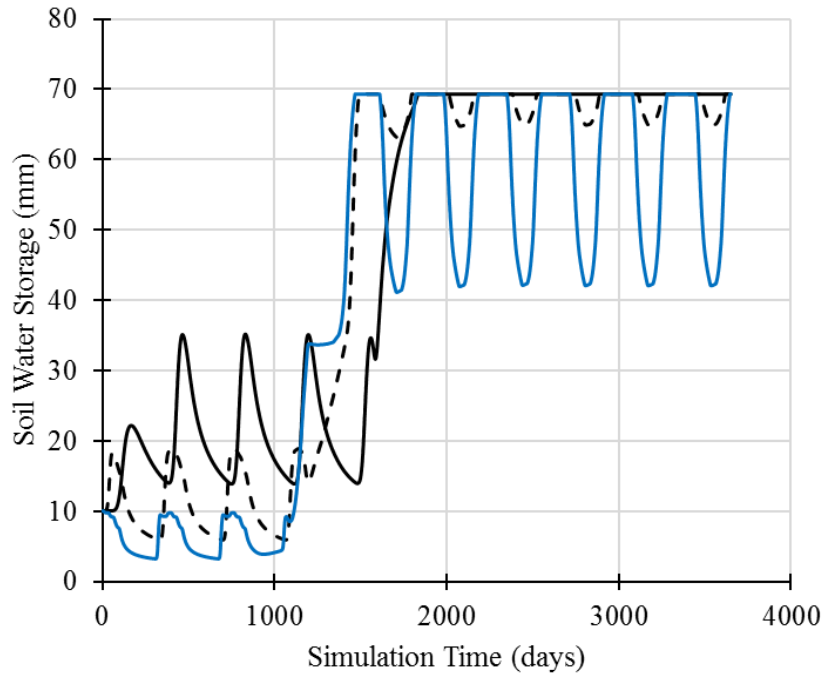
Figure A3-3. Soil water storage in Layer 5 at depth 75 cm; black solid line is the "One Order Less Ks" case; dashed line is the reference Ks case; blue solid line is the "One Order More Ks" case.
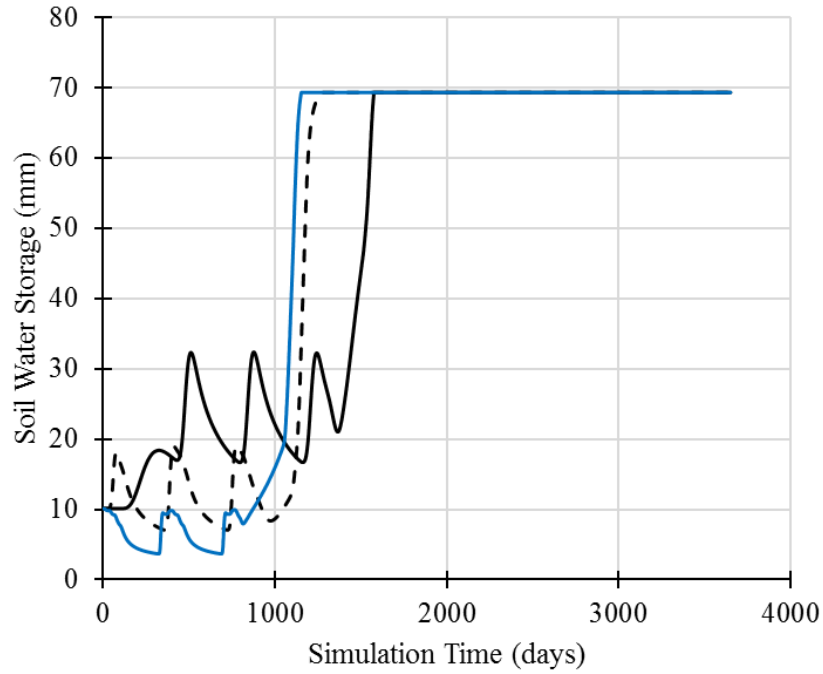
Figure A3-4. Soil water storage in Layer 7 at depth 108.33 cm; black solid line is the "One Order Less Ks" case; dashed line is the reference Ks case; blue solid line is the "One Order More Ks" case.
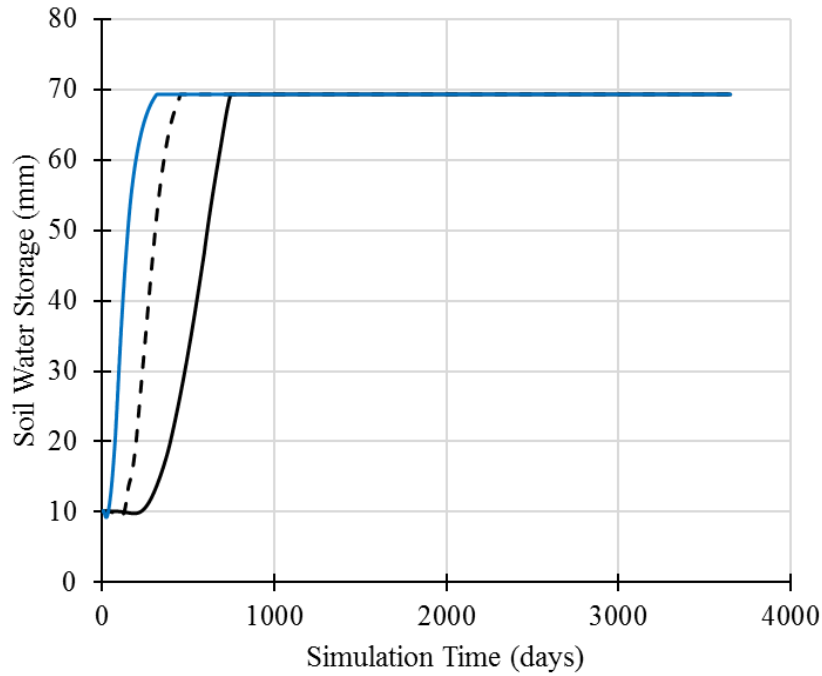
Figure A3-5. Soil water storage in Layer 16 at depth 258.33 cm; black solid line is the "One Order Less Ks" case; dashed line is the reference Ks case; blue solid line is the "One Order More Ks" case.

A3-2 TT Initial SC Sensitivity Analysis
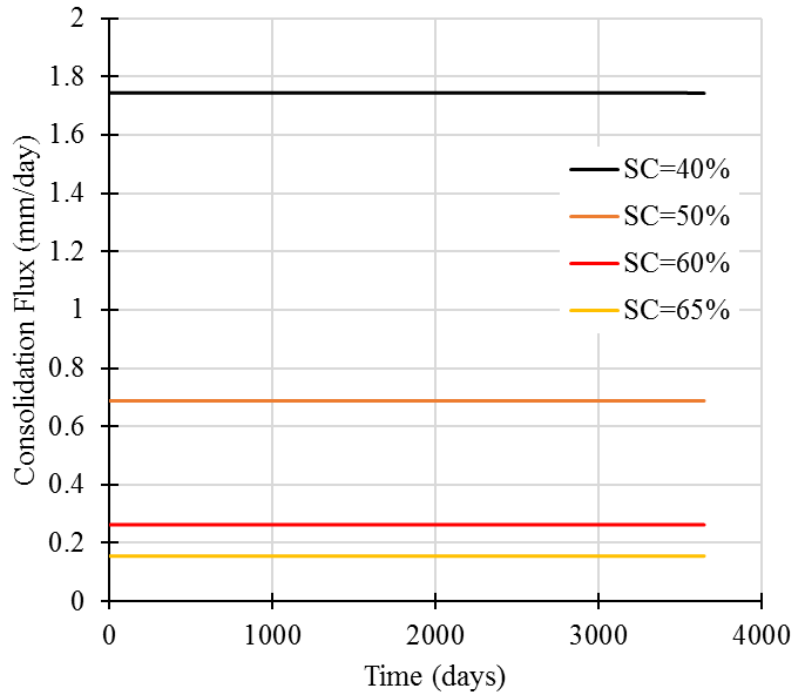
Figure A3-6. Consolidation flux for various initial SC of TT.
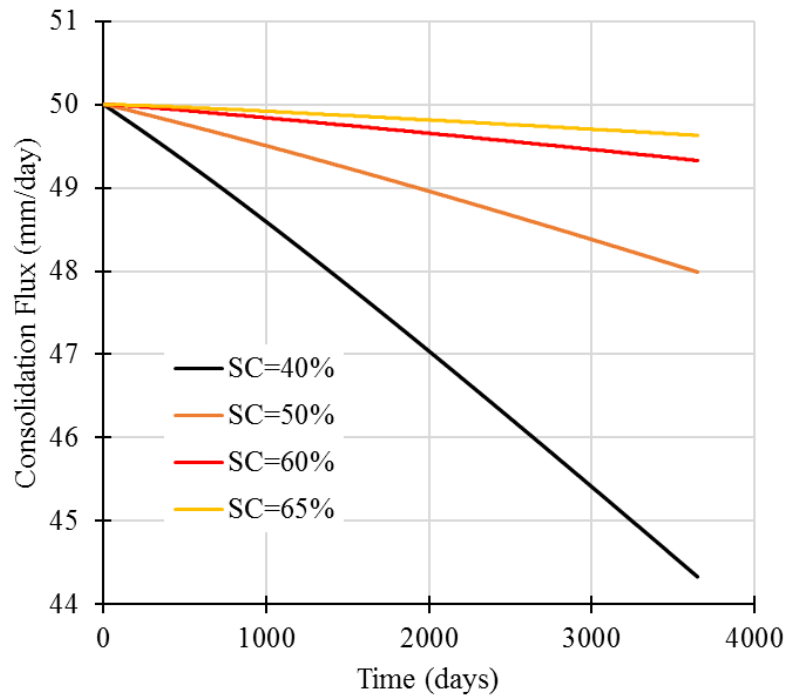
Figure A3-7. Inter-face heights for various initial SC of TT.
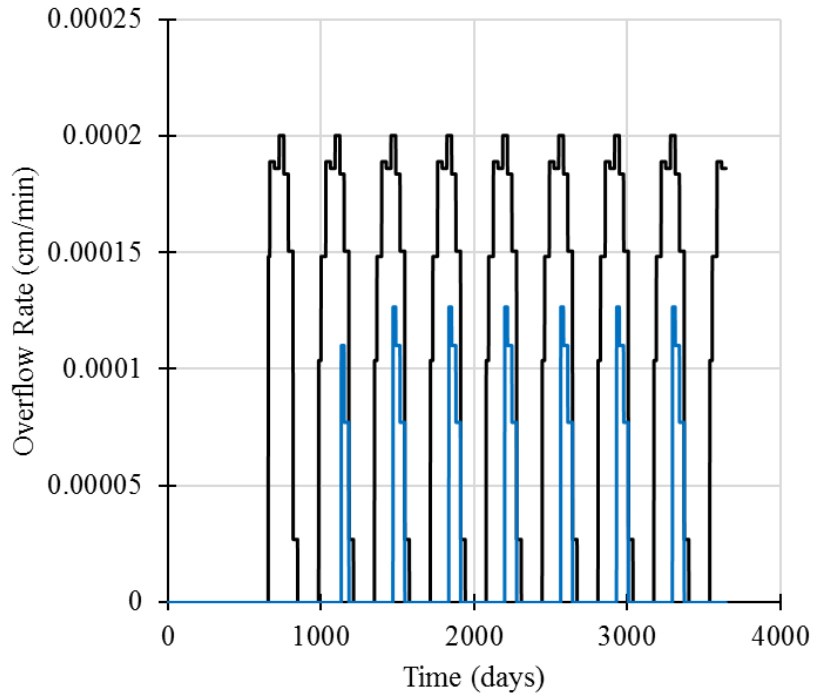
Figure A3-8. Comparison of surface overflow rates from Layer 1 between initial SC of 40% (black solid line) and initial SC of 50% (blue solid line).

APPENDIX 4 – GOLDSIM ELEMENTS AND FUNCTIONS

Tables below describe commonly used GoldSim elements and functions based on GoldSim's user manual (GoldSim, 2018).

Table A4-1. Stock elements in GoldSim

Element	Default Symbol	Browser Icon	Function
Integrator		∫	Integrates values. Also can compute moving average of a specified input.
Reservoir			Integrates (and conserves) flows of materials, allowing for upper and lower bounds to be specified.
Pool			More complex version of Reservoir, making it easier to model multiple ifnlows and outflows.

Table A4-2. Function elements in GoldSim

Element	Default Symbol	Browser Icon	Function
Expression		f_x	Defines mathematical or logical expressions.
Script		</>	Allows you to create your own custom element using a simple procedural language.
Previous Value		t	Returns the value of its input from the previous model update.
Extrema			Computes the highest (peak) or lowest (valley) value achieved by its input.

Table A4-3. Logic elements in GoldSim

Element	Default Symbol	Browser Icon	Function
Selector			Defines expressions with nested if…then logic.
Splitter			Splits an incoming signal into multiple outputs based on specified fractions.
Allocator			Allocates an incoming signal into multiple outputs given specified demands and priorities.
Sum		Σ	Facilities the addition of multiple values.
Convolution			Solves a convolution integral.
And			Combines multiple conditions using logical AND.
Or			Combines multiple conditions using logical OR.
Not			Logical NOT.
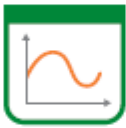
Table A4-4. Event elements in GoldSim

Element	Default Symbol	Browser Icon	Function
Timed Event			Generates discrete event signals based on a specified rate of occurrence, regularly or according to a specified distribution (i.e., randomly).
Triggered Event			Generates discrete event signals based on one or more specified conditions.
Decision			Generates one of up to three defined discrete event signals based on specified conditions.
Random Choice			Generates a user defined discrete event signal based on specified probabilities.
Milestone			Records the time at which a particular event or specified condition(s) occurs.
Status			Generates a condition (True/False) in response to particular events or specified conditions.
Discrete Change			Generates a discrete change signal (a value) that can subsequently discretely modify the values of other elements (e.g., Integrators and Reservoirs).
Interrupt			Interrupts a simulation when a specified event or condition occurs and displays a user-defined message and/or writes a message to the run log.

Table A4-5. Delay elements in GoldSim

Element	Default Symbol	Browser Icon	Function
Material Delay			Delays (and optionally disperses) material flows.
Information Delay			Delays (and optionally disperses) a signal.
Event Delay			Delays a discrete event signal. Can also be used to simulate queues.
Discrete Change Delay			Delays a discrete change signal. Can also be used to simulate queues.

Table A4-6. Result elements in GoldSim

Element	Default Symbol	Browser Icon	Function
Time History Result			Displays time history results.
Distribution Result			Displays probability distributions.
Multi-Variate Result			Displays multi-variate results (scatter plots, correlation tables, raw data).
Array Result			Displays vectors and matrices of results.

APPENDIX 5 –MODEL USER GUIDE

This appendix complements the descriptions of user interface in Chapter 3 and Chapter 4 on the set up and input procedures of the simulation. Below is a step-by-step guide for the unsaturated flow model. As shown in Figure 3-10, the user interface and input procedure of the consolidation model follow the same principles as those in the unsaturated flow model. Therefore, the steps below are focused on the unsaturated flow model only. The setup procedure for the consolidation model is similar thus will not be repeated here. Detailed descriptions of the GoldSim software can be found in its user manual available for download online.

Step 1: Geometry Setup

The first step is to set up the geometry of the tailings cap (Figure A5-1). By default, the tailings cap is discretized into 18 layers, each layer with their own input of depth, thickness, and unsaturated material properties. In order to run the model, all entries are mandatory in the Geometry and Soil Properties panel (Figure A5-1). The depth entry refers to the depth of the layer measured from the top of the cap in cm. The unsaturated material property entries (Qr, Qs, alph, n and Ks) are applicable to the entire thickness specified for that layer.

Figure A5-1. Geometry and soil properties entry in the user interface.

Step 2a: Boundary Conditions Setup

The second step is divided into 2a and 2b. Step 2a involves setting up the upper and lower boundary conditions. The model provides a range of options through a drop-down style menu (Figure A5-2). Essentially, the user needs to specify the rate of water flow into and out of the tailings cap at the top and bottom boundary. For the top boundary, the user can specify constant, climatic or customized water flow equation. The same options are available for the bottom boundary except the climate option. The user must also specify the initial water content of the tailings cap by clicking on the Initial Water Content button on top of the drop-down menus (Figure A5-2).
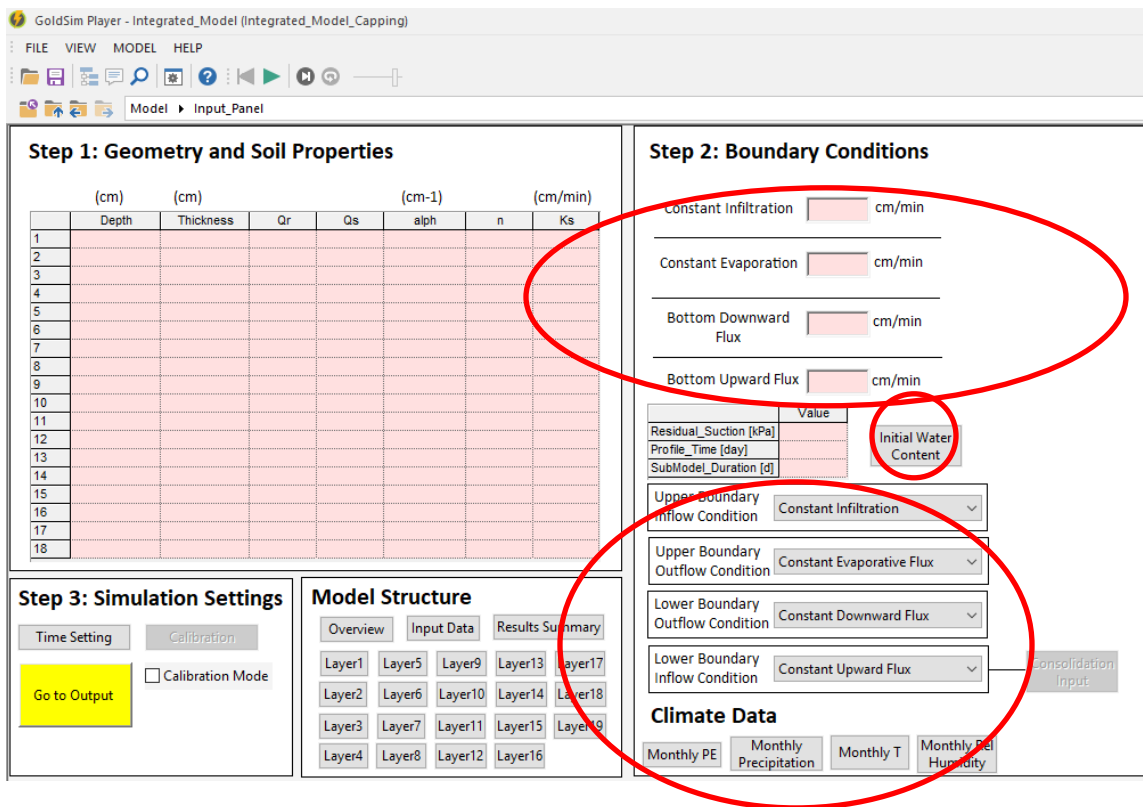
Figure A5-2. Boundary condition setup in the user interface.

Step 2b: Residual Suction, Profile Time and SubModel Duration

Options in Step 2b are in the Boundary Conditions panel. In order to run the model, the user must specify the residual suction or the lowest allowable suction value at which the model will

automatically switch to the residual soil water content. Profile_Time (day) refers to the user-specified time at which a profile of soil properties over depth is captured and saved.
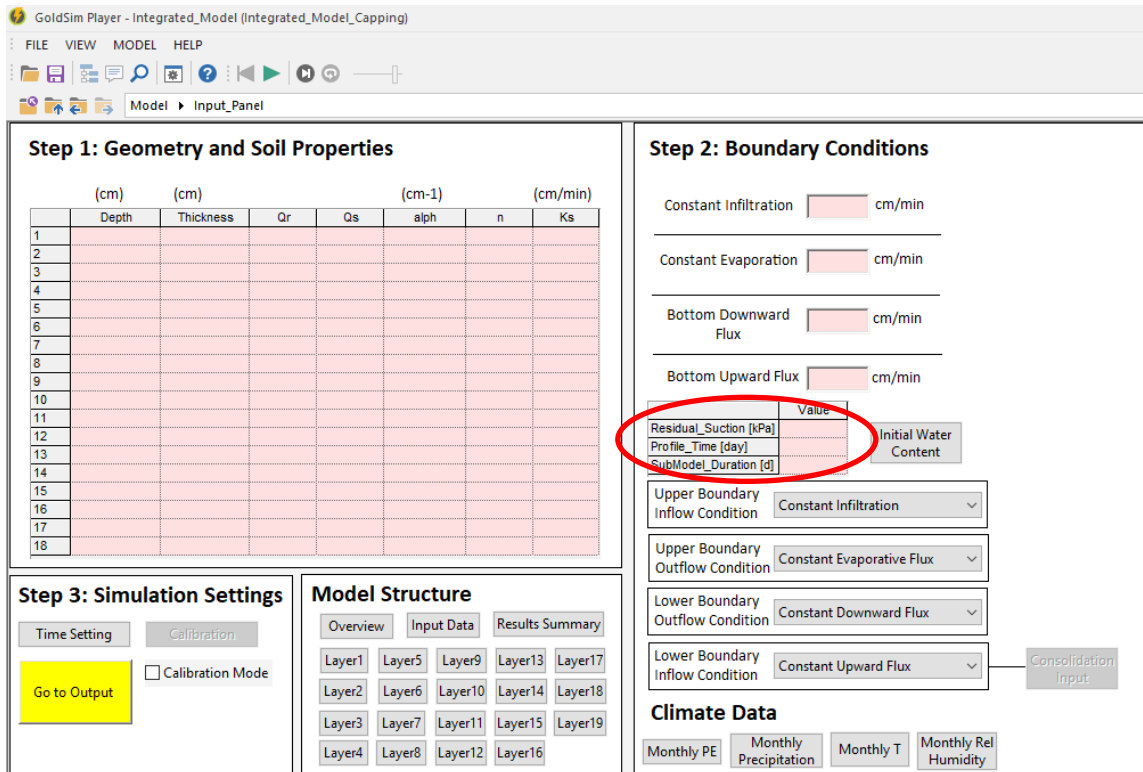

Figure A5-3. Miscellaneous setup in the user interface.

Step 3: Simulation Settings

The final step is to set up the global simulation setting. Clicking on the Time Setting button allows the user to specify the duration of the simulation, start and end time, time step, and realization parameters for the stochastic simulation (Figure A5-4). Detailed descriptions on simulation setting can be found in the GoldSim user manual.

The user can also access the calibration interface by checking the Calibration Mode box on the right side of the Time Setting button (Figure A5-5). The model applies a user-specified calibration factor C on the Ks value. The user must enter measured soil water storage over time in the Storage Calibration button and adjust element setting in the Calibration Element button (Figure A5-5).
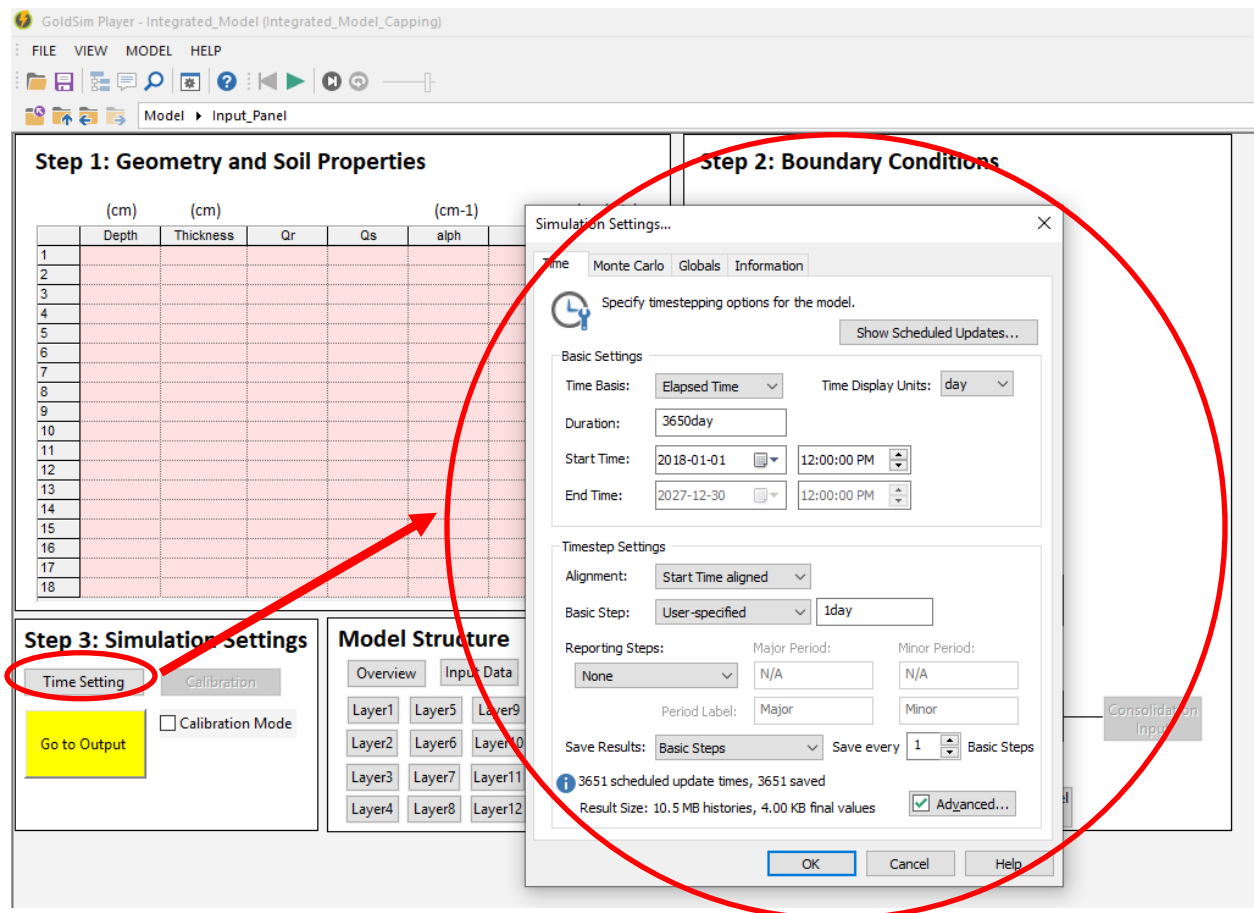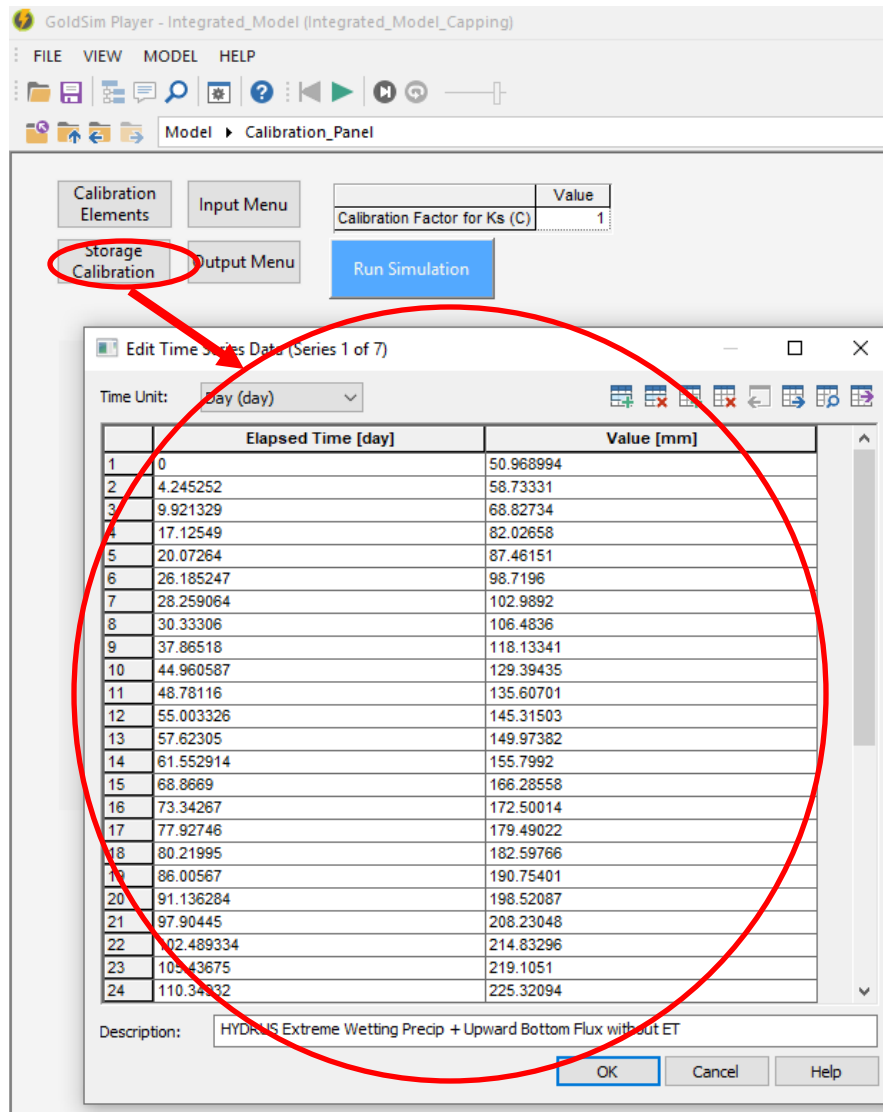

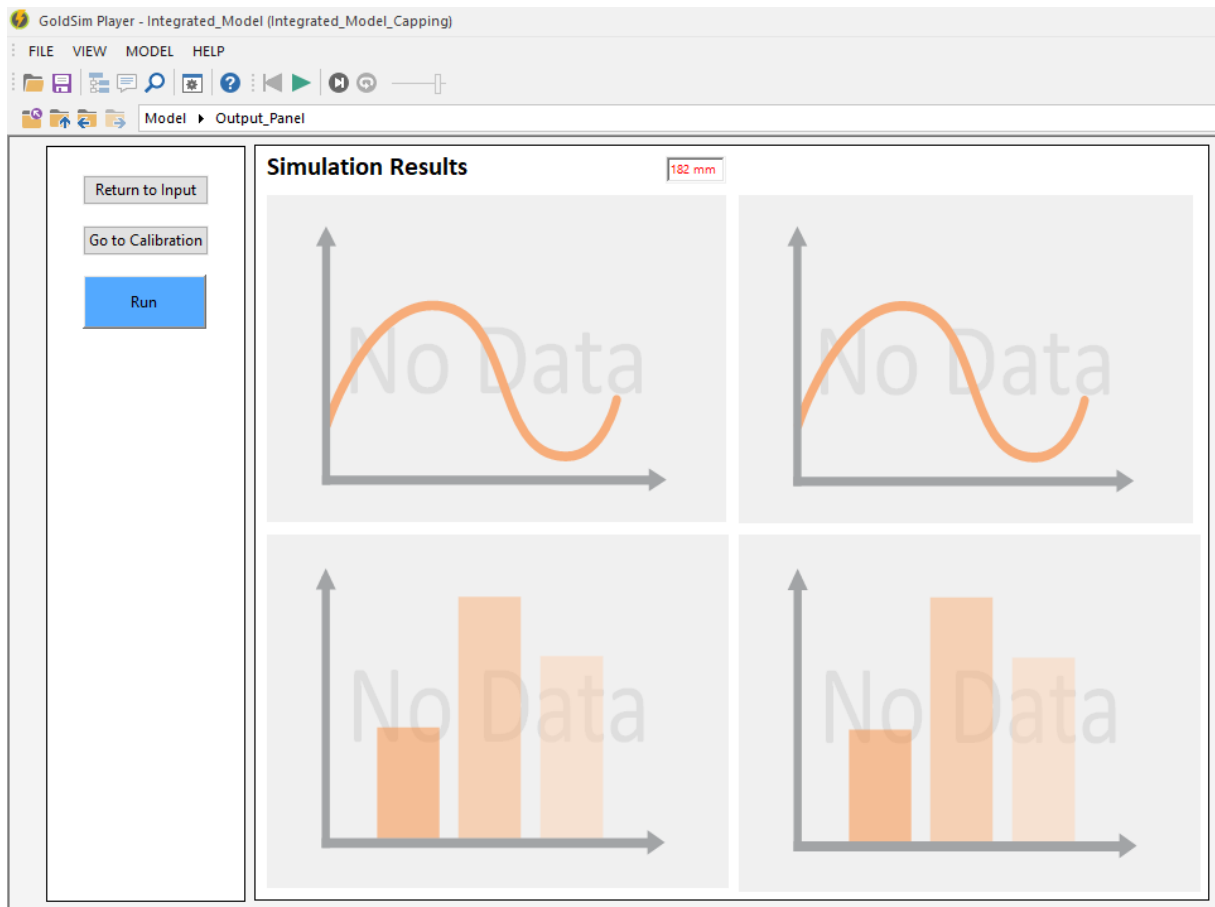**Figure A5-4. Simulation setting in the user interface.**

Figure A5-5. Overview of the calibration panel.

Step 4: Model Output

The final step is to run the simulation. Real time results in soil water storage, water balance check and snapshots of water contents over depth can be viewed in the Simulation Results Panel (Figure A1-9 and Figure A5-6). Additional model output elements can be viewed in the Results_Summary

container, which can be accessed by clicking on the Results Summary button in the Model Structure panel in the main user interface (Figure A5-7).

Figure A5-6. Overview of the simulation output panel.

Step 5: Model Structure

The Model Structure panel in the main user interface allows the user to examine the structure of the model. The user can access model elements using the buttons under the heading "Model Structure" (Figure A5-7). Screenshots of the model elements can be found in Appendix I for both consolidation and unsaturated flow models. Note that if the model is opened by the GoldSim player, which is a free model viewing tool, the user will not be able to modify any elements or relationships in the model.
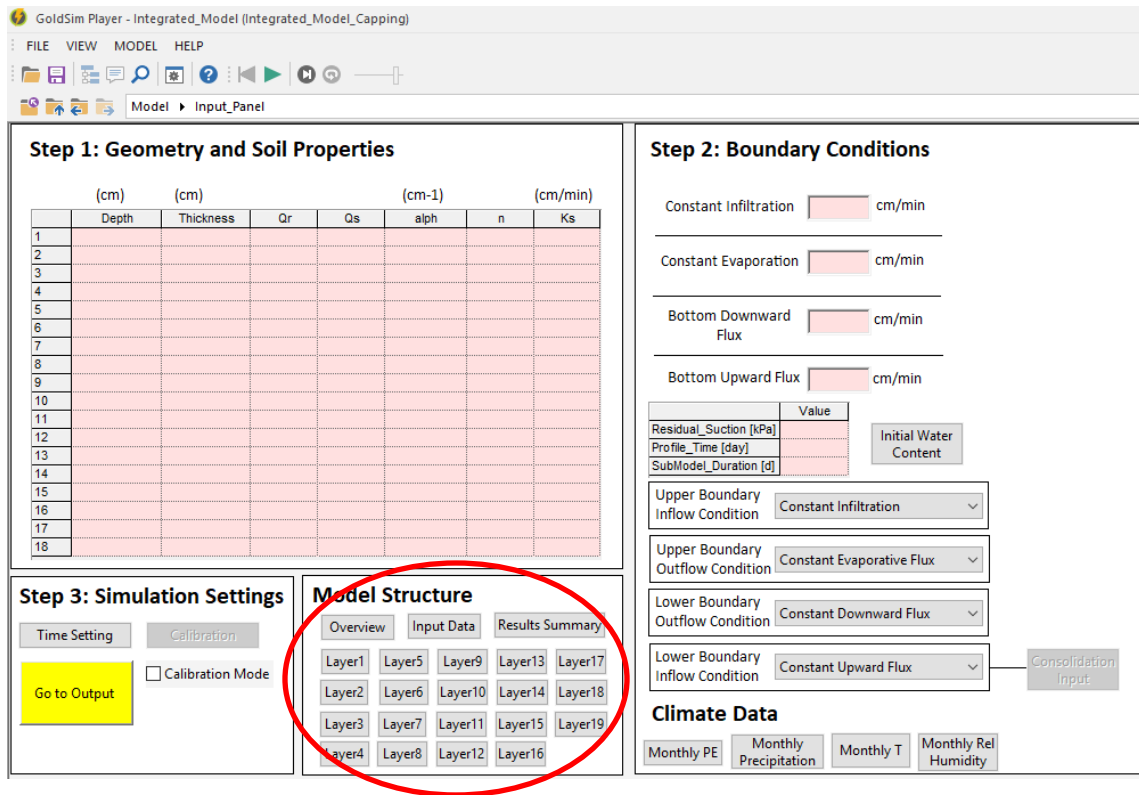
Figure A5-7. Model Structure panel in the main user interface.